Development of an efficient photovoltaic thermal collector

A Thesis

Submitted in Partial Fulfilment of the Requirements for

The Award of the Degree of

Doctor of Philosophy

by

DUDUL DAS
(Registration number: 156151011)

Centre for Energy
Indian Institute of Technology Guwahati
Guwahati-781039, Assam, India

December, 2020

DECLARATION

The work contained in this thesis entitled ***"Development of an efficient photovoltaic thermal collector"*** has been carried out by me under supervision of Dr. Pankaj Kalita, Assistant Professor, Centre for Energy, Indian Institute of Technology Guwahati, Assam, India. This thesis does not contain any materials previously submitted for the award of any degree or diploma.

Date:

Dudul Das

Registration number: 156151011

Centre for Energy

Indian Institute of Technology Guwahati

Centre for Energy

INDIAN INSTITUTE OF TECHNOLOGY GUWAHATI

भारतीय प्रौद्योगिकी संस्थान गुवाहाटी, गुवाहाटी- 781039

CERTIFICATE

This is to certify that ***Dudul Das*** has been working under my supervision since January 2016. We hereby forward his thesis entitled ***"Development of an efficient photovoltaic thermal collector"*** to be submitted for the award of the degree of Doctor of Philosophy to Indian Institute of Technology Guwahati. I certify that he has fulfilled all the requirements according to the rules of this institute and the investigations embodied in his thesis have not been submitted elsewhere for a degree or diploma.

Dr. Pankaj Kalita

Assistant Professor

Centre for Energy

Indian Institute of Technology Guwahati

Abstract

Due to the rise in greenhouse gas in earth atmosphere and global climate change, attention has been focused on harvesting energy from renewable resources such as solar, wind, hydro, biomass, geothermal tidal, wave, and ocean thermal energy. The global potential of solar energy is higher than the potential of all other renewable energy sources together. Solar energy is primarily harvested using two prominent conversion methods *viz.* solar thermal and solar photovoltaic (PV). In practice, solar PV conversion is quite common for power generation due to its inbuilt advantages like no moving parts, easy installation, availability of raw material and life of operation. However, PV system suffers from its lower conversion efficiency as well as a decrease in efficiency with the rise in cell temperature. PV cell converts only a small fraction (less than 20%) of irradiance into electrical energy. Infra-red radiation absorbed by the PV reduces the electrical efficiency of the cell. The influence of temperature on the electrical output is significant at higher cell temperature (>42 °C). To address this difficulty, solar photovoltaic-thermal (PV/T) collectors are proposed. PV/T is a promising technology where both electrical and thermal energy generation can be possible. Cooling uniformity and efficiency of the PV/T system are major challenges for its applicability. The present study is formulated to address the current challenges associated with the existing PV/T collectors. A novel thermal model of a PV/T system (tube and sheet type collector) by considering thermal contact resistance between the layers of a PV/T system, individual resistance of each layer and Ohmic heat generation in the PV layer has been carried out. The Root Mean Square Errors (RMSE) of 3.75 K, 1.36 K and 2.71 K were found for the water outlet temperature, glass surface temperature and cell temperature, respectively. The results illustrated that consideration of thermal contact resistance and Ohmic loss at the PV layer increases the accuracy of the model significantly. Based on the numerical investigation, initially two PV/T collectors *viz.* only tube absorber (M1) and sheet-tube (M2) configurations were developed. The cells in the PV/T collectors are made of Si-multicrystalline. Both the collectors have vertical oscillating tube assembly pattern. The performance of collectors are extensively studied under outdoor conditions. Higher thermal efficiency has been reported for the collector without absorber sheet. This is due to less resistance to the thermal energy transfer from the top surface of the PV/T collector to the flowing fluid in the tubes as compared to the module with sheet-tube configuration. Two more PV/T collectors namely rectangular spiral (M3) and horizontal oscillating (M4) transparent PV/T collectors without absorber sheet were developed and a comparative experimental investigation has been carried out. The performance of the M3 collector is found to be superior and hence considered for further investigation. Finally, a form-stable phase change biocomposite has been developed using water hyacinth biochar as matrix. The developed material is applied in the M3 collector for investigation of cooling uniformity. The results of the experiments demonstrate that the use of PCM- biocomposite improves the cooling uniformity, which further results in the enhancement of electrical output by 18.4%. Furthermore, this arrangement improves the thermal efficiency by 15.7% as compared to the M3 without the PCM- biocomposite. Based on the study M3 collector with PCM-biocomposite is found to be the best amongst all the developed collectors in terms of cooling uniformity, performance and cost.

Acknowledgement

First of all, I take this opportunity to express my profound gratitude and deep regards to my supervisor, Dr. Pankaj Kalita for his exemplary guidance, monitoring, constant support and encouragement throughout my doctoral research tenure. The blessing, help, guidance and advice given by him, are the key factors in shaping this work to its present form.

I would like to thank my doctoral committee members, Professor Pinakeswar Mahanta, Professor Kaustubha Mohanty and Professor Amaresh Dalal, for their valuable suggestions at different stages of my research. I would like to thank Professor V.S. Moholkar, Centre for Energy, Indian Institute of Technology Guwahati for his valuable help and guidance.

I would like to thank Professor Anupam Dewan, Department of Applied Mechanics, Indian Institute of Technology Delhi for his advice and allowing me an opportunity to work in his laboratory.

I am grateful to Department of Science and Technology, Govt. of India and the Indo-U.S. Science and Technology Forum (IUSSTF) for providing the platform to work at Centre for Energy Research, University of Nevada, Las Vegas (UNLV), United States as a Bhaskara Advanced Solar Energy intern. I would like to thank Professor Robert F. Boehm, who accepted my request to work in his laboratory, his valuable suggestions and guidance during the internship period at UNLV gave a new impetus to my research career.

I would also like to thank Dr. Sanjai Kumar Tyagi, Scientist - 'D', Department of Science & Technology, Govt. of India for his suggestions and providing his expert advice in various aspects related to my research. I would also like to thank Central Electronics Limited for allowing me to visit their manufacturing facility and getting me customized PV modules necessary for the research work. I would like to thank Dr. Akhil Garg, Associate Professor, Centre for Automotive Research and Tribology, Indian Institute of Technology Delhi for his advice and encouragement.

I would like to extend my gratitude to Dr. Lepakshi Barbora, Mr. Debarshi Baruah and Mr. Dhiren Huzuri, for their constant support and technical advice. I also thank Mr. Paragjyoti Sharma, Mr. Pranjal Bhuyan and all the staff of Centre for Energy, IIT Guwahati for their help.

I wish to thank Mr. Dilip Chetri, Mr. Mrinal Sarma and other staff members of Central Workshop for helping me in various stages of the experimental setup fabrication. Without their timely support, this work could not have been accomplished. I also extend my gratitude to Mr. Jiten Basumatary, Mr. Saiffuddin Ahmed and Mr. Chandan Banikya for their support.

I am thankful to Mr. Sartaj Tanweer for sharing his knowledge with me to accomplish my research goals. I would also like to thank Mr. Omkar Roy for his valuable inputs.

I would like to thank Mr. Dipankar Kalita and Mr. Kamal Das for their valuable help in setting up the experimental setup.

I am thankful to Miss Urbashi Bordoloi, Mr. Akash Dilip Kamble and Mr. Harrison Hihu Muigai who constantly helped me in my research and provided all necessary inputs. I would also like to take this opportunity thank Mr. Shayaram Basumatary, Mr. Samar Das and Mr. Rabindra Kangsha Banik, for their support and encouragement throughout the doctoral research tenure. I am thankful to Mrs. Firdausa Ahmed, Mr. Devarshi Kashyap, Mr. Kamal Basumatary and Mr. Hirak Basumatary for their help at various stages of my thesis work. I am thankful to Mr. Mukunda Madhav Khanikar for his encouragement and constant help. I also thank Miss Sudipta Bijoy Sarmah, Mr. Biraj Das and Mr. Debangsu Kashyap for their support in all ways possible.

Last but not the least I place a deep sense of gratitude to my parents and family, who have been a constant source of inspiration throughout this project.

Dudul

CONTENTS

Nomenclature

$A_{PV/T}$	:	Area of the PV/T module, m^2
A_p	:	Area of absorber plate, m^2
A_c	:	Area of photovoltaic cells, m^2
a	:	Effective accommodation parameter= $\frac{2-a_1}{a_1}+\frac{2-a_2}{a_2}$ where a_1, a_2 are the accommodation parameters for the surfaces in contact
B	:	Gas parameter= $\frac{2\gamma}{\Pr(\gamma+1)}$
C	:	Specific heat capacity of the fluid, J/kgK
C_{module}	:	Overall heat capacity of the module, J/kgK
c_p	:	Specific heat capacity of the PCM, J/kgK
E_g	:	Band gap Energy, eV
$\dot{E}_P$	:	Electrical power consumed by pump, W
$\dot{E}_{X_{PV}}$	:	Rate of exergy for PV system , W
$\dot{E}_{X_{PV/T}}$	:	Rate of exergy for PV/T system , W
f	:	Packing factor of the collector plate
F_R	:	Heat removal factor
F'	:	Collector efficiency factor
g	:	Acceleration due to gravity, m^2/s
G	:	Solar insolation, W/m^2
G_{ref}	:	Solar radiation flux at reference temperature T_{ref} , W/m^2
h_{ca}	:	Convective & radiative heat transfer coefficient from solar cell to ambient air, W/m^2K
$h_{c,g}$	:	Convective heat transfer coefficient at the inner glass surface, W/m^2K
$h_{c,solid}$	:	Solid contact conductance at junction interface, W/m^2K
h_{p1}	:	Penalty factor due to tedlar through glass, solar cell and EVA
h_{p2}	:	Penalty factor due to the interface between tedlar and the working fluid

$h_{r,a-g}$	:	Radiation heat transfer coefficient at the inner glass surface, W/m^2K
h_{wind}	:	Convective heat transfer coefficient at the outer glass surface , W/m^2K
$h_{r,g-a}$	:	Radiation heat transfer coefficient at the outside glass surface, W/m^2K
ΔH_m	:	Latent heat of fusion, J/kg
I_m	:	Current generated by PV module at maximum power point, A
J_0	:	Reverse saturation current density, A/m^2
J_{SC}	:	Short circuit current density, A/m^2
k	:	Thermal conductivity of a material, W/mK
ke	:	Molecular kinetic energy, J
k_g	:	Gas or filler material conductivity , W/mK
k_b	:	Boltzmann constant (1.38064852×10^{-23} J/K)
L	:	Characteristic length of the flat plate, m
M	:	Effective gas parameter= $\frac{aB\Lambda}{\sigma_r}$
m	:	Mass of PCM, kg
$\dot{m}_{air}$	:	Maas flow rate of air, kg/s
P_g	:	Gap pressure, atm
P_{PV}	:	Electrical power output from photovoltaic module, W
pe	:	Molecular potential energy, J
$Q_{Convection}$	:	Energy loss by convection from the module surface, W
$Q_{\text{Ref lection}}$	:	Energy loss by reflection from the PV module, W
Q_{Solar}	:	Energy received from the sun, W
Q_{Useful}	:	Part of thermal energy that can be recovered from PV module, W
T_a	:	Ambient temperature, K
$T_{air,in}$	:	Inlet temperature of air, K
T_c	:	Solar cell temperature, K
$T_{f,in}$	:	Inlet temperature of heat transfer fluid, K

$T_{f,out}$: Outlet temperature of heat transfer fluid, K

T_{PV} : PV module surface temperature, K

T_m : Surface temperature of PV module, K

T_{mp} : Melting point, K

T_{ref} : Reference Temperature, K

T_{sun} : Temperature of the sun, K

$T_{surface}$: Temperature of surface at which convection is taking place, K

t : Time of the day, hr.

$\dot{V}$: Volume flow rate of cooling fluid, m^3/s

V_f : Free stream wind velocity in the windward direction of the PV module, m/s

V_m : Voltage output at maximum power point, V

V_{OC} : Open circuit voltage, V

V_w : Magnitude of local wind velocity component parallel to the PV module surface, m/s

W : Width of the air duct, m

ΔT : Temperature difference between the outlet fluid and ambient temperature, K

$U_{t,ca}$: Overall heat transfer coefficient from PV cell to ambient through glass, W/m^2K

U_L : Overall heat transfer coefficient from solar cell to ambient, W/m^2K

U_p : Overall heat transfer coefficient from PV cells to absorber plate, W/m^2K

U_{tf} : Overall heat transfer coefficient from glass to cooling fluid through the PV cells, W/m^2K

b : Breadth of the channel for floe of fluid, m

α : Absorptivity

α_P : Short wave absorptivity of the absorber plate

α_T : Thermal diffusivity of a material defined as the ratio of thermal conductivity of specific heat capacity, m^2/s

$(\alpha\tau)_{eff}$: Product of effective absorptivity and transitivity

T_0 : Temperature at which $\eta_c = 0$, K

θ	:	Angle of inclination of the PV module with the vertical, Degrees (°), + and – signs denote facing downwards and upwards respectively
θ_{rib}	:	Rib angle
β_{ref}	:	Temperature coefficient at reference temperature (25 °C)
τ_g	:	Short wave transmittance of the glazing
ε	:	Emissivity of a material
ε_g	:	Emissivity of glazing
η_{el}	:	Electrical efficiency of PV, %
$\overline{\eta}_{el}$	:	Average electrical efficiency of PV, %
η_{ex}	:	Exergy efficiency, %
η_{oth}	:	Overall thermal efficiency, %
η_p	:	Absorber plate efficiency, %
$\eta_{PV/T}$	:	Efficiency of photovoltaic thermal system, %
$\eta_{T_{ref}}$	:	Cell electrical conversion efficiency under STC, %
η_{th}	:	Thermal efficiency of PV/T, %
$\eta_{overall}$	:	Overall efficiency of PV/T, %
η_I	:	First law efficiency, %
η_{II}	:	Second law efficiency, %
ρ	:	Density of the fluid, kg/m^3
σ	:	Stefan Boltzmann constant
μ	:	Dynamic viscosity, Ns/m^2
ν	:	Kinematic viscosity, m^2/s
γ	:	Efficiency correction coefficient for irradiance

LIST OF FIGURES

LIST OF TABLES

1

Introduction

1.1 Motivation

Energy use, its accessibility and affordability will continue to be the core ingredients of development, economic growth and poverty alleviation. With globalisation and improvement in the standard of living, the concept of development has transformed from mere development to sustainable development. The countries across the world are expected to provide not only the basic freedoms enshrined in their respective constitutions but also the most basic rights to clean air and the right to clean drinking water. The global energy agenda not only concerned with efficiency improvement but also considers the issues of climate change and global warming. Most of the energy projects need large capital investment and have long financial payback periods. However, the brighter side is that there has been a dramatic reduction in the cost of per unit generation from new and renewable energy sources, especially solar [1]. At the system level, the thermal and electrical energy generation costs are partly compensated by positive effects mainly from avoided emissions due to the use of renewable energy technologies [2]. With sufficient support from government policies, renewable energy has become financially viable with a shorter payback period. Renewable energy can supply two-thirds of the total global energy demand, and contribute to the bulk of the greenhouse gas emissions reduction that is needed between now and 2050 for limiting average global surface temperature increase below 2 °C.

The global energy consumption in the last century has almost increased eleven-fold [3], this can be seen from **Figure 1.1**. The largest increase in the rate of consumption has been in the coal, oil and gas divisions. Fossil fuels together constitute almost 87% of the total energy demand of the world [4]. Carbon dioxide emissions from burning fossil fuels are believed to be the main factor for an alarming rise in global temperatures. In 2004, the average atmospheric carbon dioxide concentration reached 377.4 parts per million (ppm) by volume. The safe level of carbon dioxide in the atmosphere is 350 ppm [5]. In recent times global levels of CO_2 concentration in the atmosphere have crossed 400 ppm [6]**.** The reported concentration of CO_2 in the atmosphere as reported on February 24, 2020, is 414.05 ppm [7]. The level of CO_2 increase can be observed from the Keeling curve as shown in **Figure 1.2**. The Keeling Curve is one of the most compelling pieces of scientific evidence that shows that carbon dioxide is accumulating in the earth's atmosphere. Already the harmful effects of climate change can be seen as rising seas, wildfires, killer cyclones, and extreme weather. Passing a 350 ppm mark of carbon dioxide concentration in our atmosphere is an ominous sign of what is waiting for human civilization.

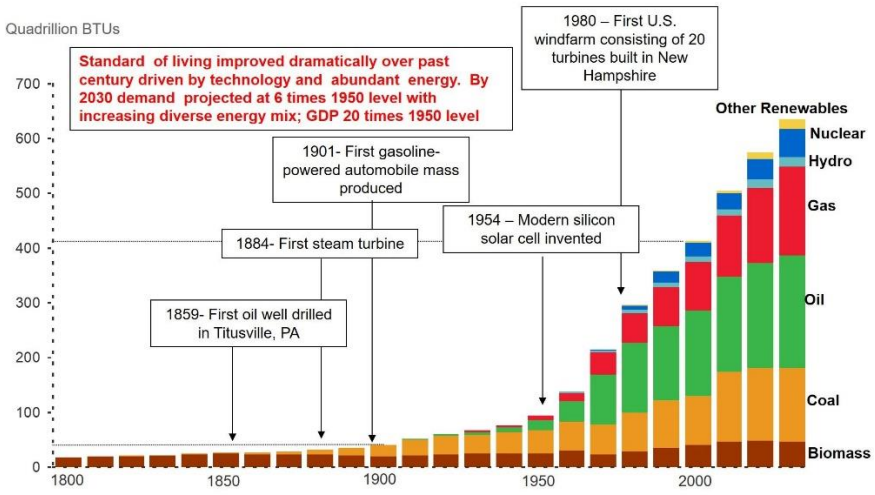

Figure 1.1. Source wise energy demand and evolution of various new sources [3]

The oil crisis in the 1970s and the global climate change concerns are alarming the need for alternative clean energy sources. Again, the 2008 oil crisis in the Arab region opened up the energy market to a new source the 'Shale Oil', but its sustainability is still a debate. This 2008 oil crisis leads to the adoption of renewable energy generation options in the Arab region [8]. Conference of the Parties, twenty-first sessions held at Paris in the year 2015 strictly warned and asked the nations to reduce their greenhouse gas emission level. Solar, wind and biomass are the major sources of renewable energy. Solar energy is the most prominent renewable energy source due to its availability around the globe. Two prominent solar energy conversion systems commonly used are the solar thermal and photovoltaic (PV). Usually, these two systems are used independently for the generation of thermal and electrical energy.

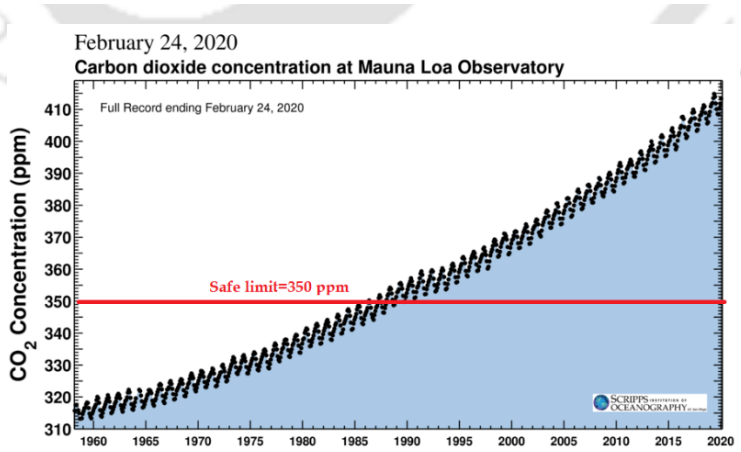

Figure 1.2. *Keeling curve:* CO_2 concentration measurements taken at the Mauna Loa Observatory in Hawaii [9]

In PV conversion electricity is generated from sunlight directly. The output of the PV system is highly dependent on climatic factors such as the solar irradiance, the ambient temperature, wind speed and the state of the PV module (cell material, ageing, frequency of cleaning etc.) [10,11]. Furthermore, it has been reported that the performance of the PV system is strongly dependent on operating temperature [12]. In general, PV cell temperature remains higher than the ambient temperature during the operating hours. Normal Operating Cell Temperature (NOCT) (T_a =20°C, G=800 W/m^2) considered for rating and testing of PV modules is usually in the range 42 °C – 46 °C [13,14]. It has been revealed that in silicon solar panels drop in power output is small between 30 and 42 °C. However, after 42 °C there was a consistent drop in power output of around 1.1% of peak power output per degree rise in temperature [15]. The reasons attributed for this decrease are an intensification of the thermal lattice vibrations leading to electron-phonon scattering, a decrease of charge carrier's mobility and reduction of the p–n junction built-in voltage and junction ability to separate electrons from holes [16]. Numerous correlations expressing the negative effect of temperature rise on the PV module's electrical conversion efficiency have been developed across the globe. Some of the prominent correlations are presented in **Table 1.1**.

Table 1.1 Correlations for estimation of solar cell efficiency

Authors	Correlations	Remarks
Evans and Florschuetz (1977)[17]	$\eta_{el} = \eta_{T_{ref}}[1-\beta_{ref}(T_c - T_{ref})]$	β_{ref} = 0.0041 °C^{-1}, $\eta_{T_{ref}}$ =0.15 for c-Si
Mohring *et al.* (2004)[18]	$\eta_{el} = \eta(G, 25^oC)\left[1+c_3(T_c - 25)\right]$	c_3 = % loss per °C **Type of cell** / **Value of c_3 in %** c-Si / -0.5 Polycrystalline-Si / -0.2 Thin film / -0.41
Notton *et al.* (2005)[19]	$\eta_{el} = \eta_{T_{ref}}[1-\beta_{ref}(T_c - T_{ref}) + \gamma \log_{10} G)$	β_{ref} = 0.0044 °C^{-1}, $\eta_{T_{ref}}$ =0.125

Photovoltaic (PV) cells convert photons received from the sun into electricity by exciting the electrons of semiconducting materials. PV cells have limited efficiency because only a narrow range of wavelengths of the solar spectrum has enough energy to excite the

electrons. The efficiency of well-designed silicon cells can exceed 50% for incoming light between 700 nm and 1100 nm, but is low or zero at shorter or longer wavelengths, respectively [20]. Absorbed light outside 1100 nm (i.e. infra-red) becomes heat, which could reduce the efficiency of the cell or, in the extreme, cause damage. Solar cell performance decreases with increasing temperature. It is evident from **Figure 1.3.** that the operating temperature plays a key role in the PV conversion process; the power output of a photovoltaic (PV) module depends linearly on the operating temperature [21]. In the last few decades, extensive work has been carried out to obtain a fundamental understanding of light-induced degradation in semiconductor materials and also to develop materials that are resistant to this degradation process. Staebler and Wronski (1977) [22] observed metastable changes in amorphous Si:H and also reported that the dark conductivity and photoconductivity of glow-discharge deposited amorphous silicon can be reduced significantly by prolonged illumination with intense light.

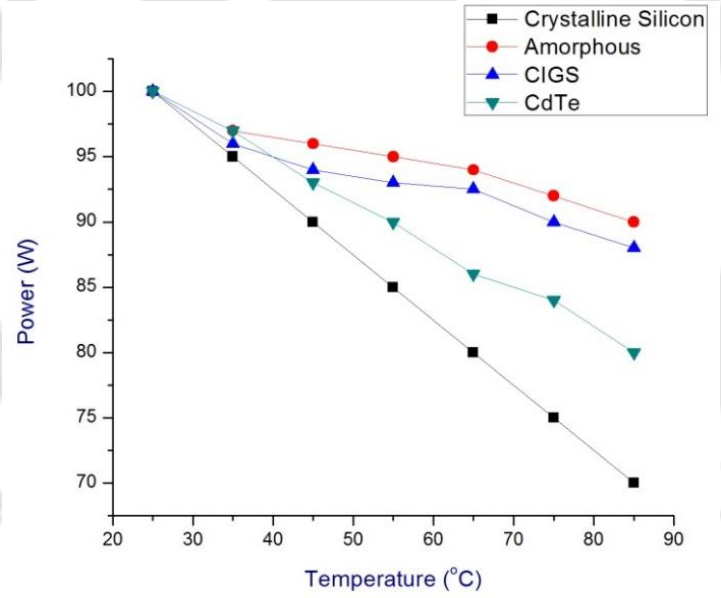

Figure 1.3. Effect of temperature on power output in various type of solar cell [21]

It is reported that open-circuit voltage decreases with increasing operating temperature whereas short circuit current density increases with increasing temperature, this decrease in open-circuit voltage results in efficiency degradation [23,24]. Reverse saturation current density (J_o) primarily controls the value of open-circuit voltage in the solar cells and measures the leakage or recombination of minority carriers across the p–n junction in reverse bias. Reverse saturation current density strongly dependent on temperature change and the bandgap of the material. The higher value of the bandgap will result in a lower value of

saturation current density. Reverse saturation current density (J_o) is given by the following equation:

$$J_o = CT^3 \exp\left(\frac{-E_g}{k_b T}\right) \tag{1.1}$$

In the above equation, solar cell material properties are combined in constant C. For an optimized solar cell design, a minimum value of C is desired. It has been reported that efficiency varies logarithmically with a variation of the magnitude of C [25].

In solar PV, photon energy received from the sun directly converted to electricity with the efficiency range of 5-25% based on the material used and radiation intensity. Further, the conversion efficiency is influenced by meteorological parameters. The major part of the incident solar energy is lost as low-grade thermal energy. Rawat *et al.* (2017) [26] developed the energy balance equation for a PV module and shows different losses associated with the PV module. The energy balance diagram for the PV module is shown in **Figure 1.4**.

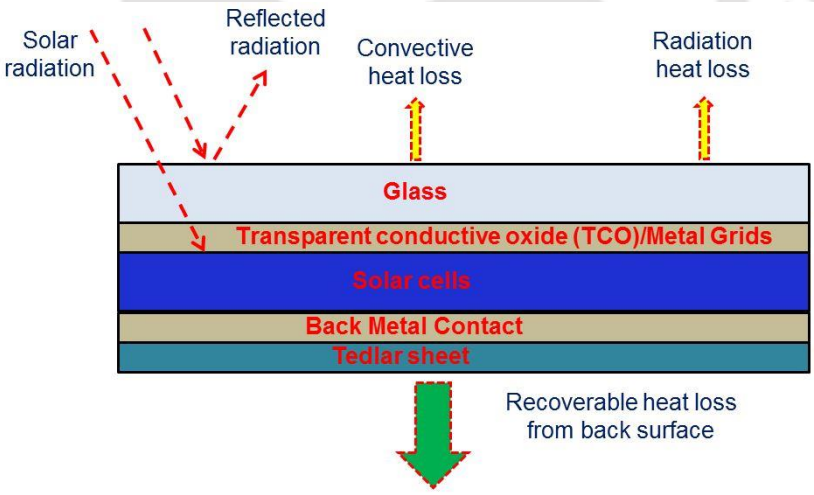

Figure 1.4. Energy balance diagram of a PV module [26]

It is desirable to recover the thermal energy which is generated in the PV module and allow the module to cool. This is beneficial in two ways first it checks the temperature induced electrical efficiency degradation and secondly, it allows to harvest thermal energy, which can be used for various other purposes like drying, water distillation, heat pump assisted air/water heating etc. If looked from an energy efficiency point of view it is recommended to use PV and thermal absorber together in a hybrid photovoltaic thermal (PV/T) energy system.

1.2 Global importance of PV/T

In 2018, newly installed renewable power capacity in the world has reached a net of 177 GW. Though this achievement needs to grow by over 300 GW on average each year between 2018 and 2030 to reach the goals of the Paris Agreement [27]. Solar PV capacity has shown a growth more than any other source of renewable electricity generation [28] and successfully compensated for slower increases in wind and hydropower, this can be seen from **Figure 1.5.** Due to an increase in the demand for power, large Gigawatt (GW) scale solar PV based plants are being installed worldwide [29]. **Figure 1.6.** shows the price trend of solar PV and the rise in the PV installation. It has been observed that, since 1975, costs of PV has decreased considerably while the installed PV capacity has gone up significantly [30]. Therefore, it is practical to analyze the influence of operating temperature on the electrical efficiency of the PV module. PV/T system is expected to provide significant energy recovery in comparison to traditional PV technology.

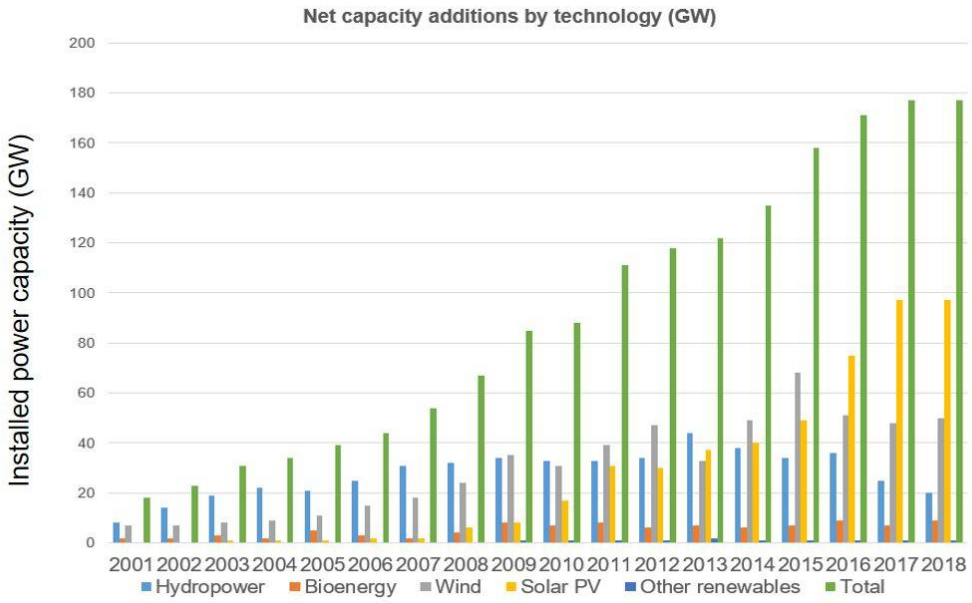

Figure 1.5. Net capacity additions by technology [27]

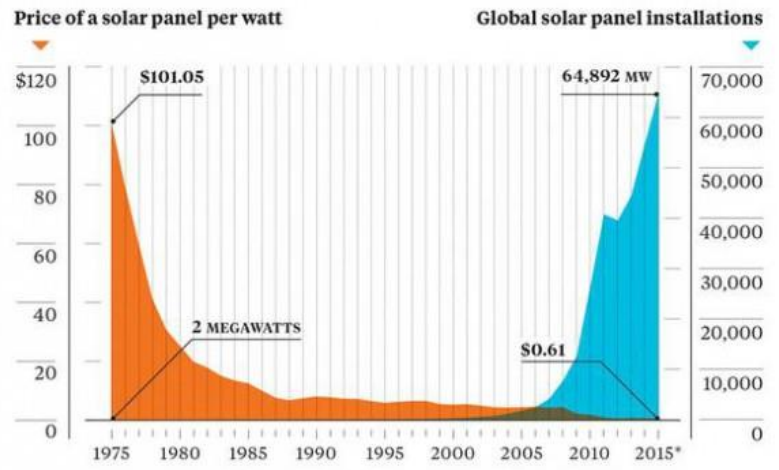

Figure 1.6. Trend of solar PV cell/module price and installation [31]

John Hollick, the inventor of Solarwall (Unglazed transpired PV/T collector) and chief executive officer of Canada based company, Conserval Engineering, asserted that PV/T systems can yield four times more energy from the same surface area for only a 25% increase in cost [32]**.** Vinod Khosla, the founder of Sun Microsystems and a renewable energy entrepreneur who also funded PVT Solar, has described Photovoltaic-thermal technology "a gargantuan leap in a field where engineers exult over the most incremental gains" [33].

Space heating and domestic hot water generation together constitute nearly 50% of global thermal energy consumption [34]. Most domestic and commercial applications fall in the low (20-80 °C) and medium (80-150 °C) temperature ranges making solar-thermal installations a suitable option. It has been estimated that 70% of the world's population projected to live in cities by 2060 [35], thus space crunch is expected to arise for the installation of separate electrical and thermal solar energy systems in the cities. PV/T technology provides encouraging arrangement when rooftop space is constrained and both heat and electricity are required simultaneously. The potential of PV/T has been confirmed with the aid of predictive simulations using computational tools, such as TRNSYS. PV/T systems have been estimated to cover ~60% of the heating demand. Applicability of PV/T for industrial usage is also reported to be economically attractive [36].

1.3 PV/T collector and its evolution

PV/T has been studied worldwide since 1974. The performance of various PV/T collector types had been studied theoretically, numerically and experimentally. Pioneering work on PV/T was carried out by Martin Wolf in 1976 and concluded that PV/T's were

technically and economically feasible [37]. First liquid-based PV/T collector was successfully demonstrated by Professor Böer, who installed it for his domestic applications in 1978 [38]. After these pioneering studies, several designs of PV/T collectors were constructed, tested and commercialised. Universities, research laboratories, research organizations and private companies have done several works on PV/T, few of them are listed in **Table 1.2**. A range of PV/T systems has been developed by researchers and private organizations. Numerical works have been carried out extensively on PV/T systems with the aid of modern analytical tools and CFD techniques. A detailed review of different types of PV/T's is presented in the next chapter. The energy scenario of the world is approaching to be solar dependent, more and more research and development intervention is required in thermal absorber design and fabrication, material and coating selection, energy conversion and effectiveness, performance testing, system optimization, control and reliability. These issues need to be addressed for future market expansion of PV/T and making it a competitive renewable energy technology with existing renewable energy generation options. To compete with other types of solar thermal collectors, PV/T collector must offer high performance. **Figure 1.7.** shows the gap between the efficiencies of the PV/T available today and desired PV/T to compete with other available solar collectors. This gap can be reduced through technological innovations and design improvement.

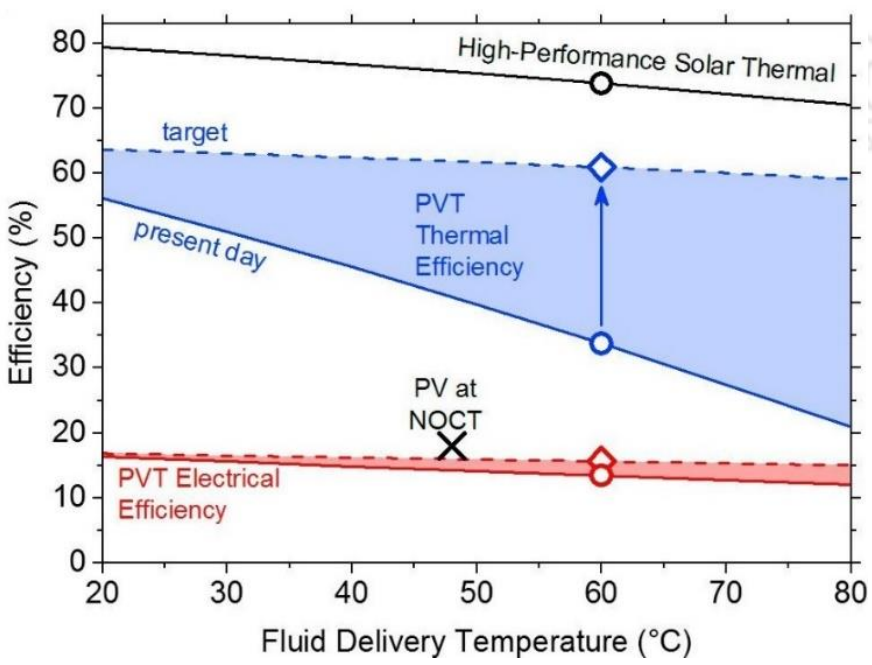

Figure 1.7. Target efficiencies for PV/T achievable with technical advances [37]

Table 1.2 Historical development of PV/T [38]

Year	Researcher and Place of work	Summary of the work
1974	Professor Böer, University of Delaware, USA	Building-integrated PV/T system called SolarOne
1976	Martin Wolf, USA	Developed liquid-based PV/T for residential heating.
1978	Professor Böer, University of Delaware, USA	Liquid-based PV/T called Solar Knoll for domestic use.
1978	Lincoln laboratory(MIT) and Sandia, USA	Full-size PV/T prototype development.
1978	SunWatt, USA	Low-concentrating PV/T
1980	Institut de Microtechnique, Switzerland	Thermal gradient test of PV/T
1991	Atlantis Energy, Switzerland	PV/T air roof
1996	Eindhoven University of Technology, Netherlands	PV/T for domestic hot water systems
2004	Millennium Electric and Technical University of Denmark	Building-integrated PV/T

In the past different techniques to manufacture PV/T collector are studied and applied worldwide. Few researchers tried glueing PV cells directly on the thermal absorber, while a few others tried to integrate commercially available PV modules to thermal absorber or heat extraction systems. The most popular and basic technique of manufacturing a PV/T collector is to place PV cells on the absorber of a thermal collector using thermal paste [39]. However, there are few issues in glueing PV cells directly to an absorber, such as the PV will not be protected from the environment and the system suffers from insufficient electrical insulation.

This drawback makes the technique unfit for commercial PV/T applications. The problem does not appear if a commercial PV module is integrated into a thermal absorber. The white Tedlar used as back sheet material for commercial silicon-based solar modules has relatively high reflection losses and thermal resistance. Tedlar is a transparent resin of ethylene-vinyl acetate (EVA) copolymer manufactured by Dupont. It is composed of vinyl acetate compounded with a curing agent, a UV absorber, a photo-antioxidant (Tinuvin 770) and a thermo antioxidant (Naugard P) [40]. Different layers of the PV and PV/T are shown in **Figures 1.8 and 1.9** respectively.

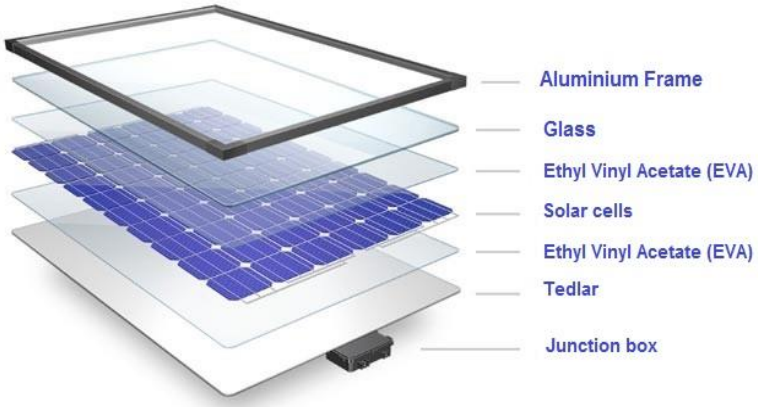

Figure 1.8. Different layers of a PV module

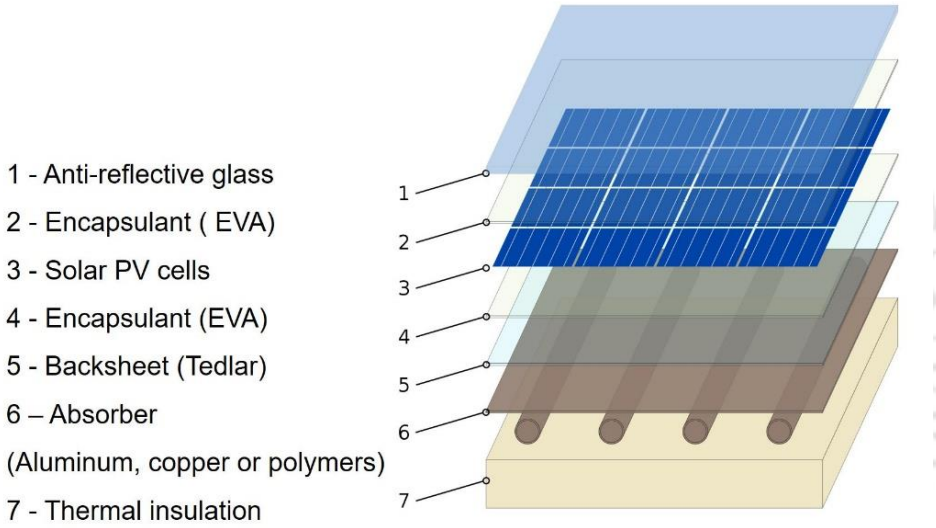

Figure 1.9. Cross-section of an uncovered PV/T collector with sheet-and-tube type absorber

1.4 Organization of the thesis

The entire thesis has been outlined in six chapters. Chapter 1 introduces the motivation, background and content of the thesis. In Chapter 2 detailed review of literature on different types of PV/T collectors developed around the globe, their performance parameters, the effect of operating parameters and methods of thermodynamic management have been presented. The summary of the literature survey, research gap and objectives of the thesis are also outlined in the Chapter. In Chapter 3, experimental setups, along with the experimental procedures, mathematical formulation and economic analysis, are discussed. The step by step derivation of the novel thermal model and its validation are presented in Chapter 4. Chapter 5 presents the results of the experiments carried out based on the experimental procedures

described in Chapter 3. Chapter 6 summarizes the research findings and scope for future work. Equipment used and uncertainty analysis in measuring collector efficiency are presented in appendices I and II respectively. Experimental data sheets for various absorber configurations are given in appendix III. Photographs of the developed experimental setup are given in appendix IV.

2

Literature review

2.1 Introduction

Research interest in PV/T has been gaining popularity since the 1970s. Several novel technologies had been developed, such as roll bond absorber, finned channels, wicks attached to the rear side of the PV, water jet cooling, use of phase change materials, heat pipes, nanofluid etc. In the following sections, research carried out in the last few years on different categories of PV/T's are discussed. For reviewing the broad area of PV/T research they are categorised into water-based PV/T[41], air-based PV/T [42], PV/T with phase change material (PCM) [43], PV/T with nanofluid as heat transfer medium [44], PV/T with heat pipes [45] and commercially available PV/T [46]**.** The chapter emphasised on the use of nanofluid and phase change material to harness maximum thermal energy from the system, also includes an insight into commercially available PV/T modules across the globe. It presents an enviro-economic evaluation of PV/T systems developed by various researchers and also enumerated thermodynamic methods for evaluating system efficiency, which includes both energy and exergy analysis. Finally, this chapter provides the necessary information about the requirement of future research in PV/T.

2.2 Categories of PV/Ts

2.2.1 Water-based PV/T systems

PV/T collectors utilizing water as heat transfer fluid are gaining more popularity because of higher overall efficiencies than air-based systems and more uniform cooling of the PV cells [47]. Water-based PV/T collectors can either have an external glass cover with an air gap between the cover and absorber or without external cover [41]. The covered PV/T has to compromise with electrical efficiency due to temperature rise while the other without cover suffers from lower thermal efficiency but better electrical efficiency [48]. The efficiency of PV/T collectors is related to the flow distribution of the coolants through the channel [49]. The design of the channels should be optimized to provide maximum heat transfer area and higher retention time for effective heat transfer from the collector to heat carrying fluid. Many researchers contributed to the field of increasing efficiency of PV/T water collectors. These novel cooling techniques are reviewed in this section.

Aste *et al.* (2015) [50] developed a PV/T collector which is shown in **Figure 2.1.** The PV collector was developed with amorphous silicon cell top layer and microcrystalline silicon bottom layer. The amorphous cell at the top absorb visible solar spectrum and convert it to electrical energy. While the bottom layer is sensitive to the near-infrared region of the solar

radiation spectrum. The PV/T collector was found to convert solar energy with an overall efficiency of 42%, which is given by 13.2% of electricity and 28.8% of thermal energy. He *et al.* (2006) [51] reported 40% daily thermal efficiency of the PV/T having aluminium-alloy channel with water as heat transfer fluid. Xu *et al.* (2011)[52] developed a novel low-concentrating solar PV/T assisted by heat pump system for water heating and reported that the average system Coefficient of Performance (COP) for heating water from 30 °C to 70 °C on a clear sunny day in summer was 4.8, with a reported electrical efficiency of 17.5%, which is 1.36 times higher than that of the same PV system without any cooling mechanism.

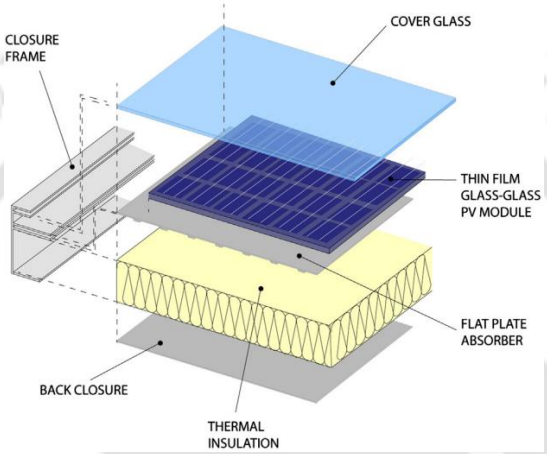

Figure 2.1. Isometric view of the PV/T collector developed by Aste *et al.* (2015) [50]

Table 2.1 provides a brief description of various works done during the last few years on water-based PV/T collector systems. Water-based PV/T collectors have the potential to remove conventional domestic hot water system. Researchers tried various modifications of PV/T collector to improve overall and electrical efficiency. Emphasis has been laid on discovering the most reasonable strategy of cooling. Water splash cooling is found to diminish the PV module temperature fundamentally. Application of synthetic clay layer on the backside of the PV with water sprayed on it also found to be useful in lowering the PV operating temperature and results in PV power gain. In the last decade different novel back panel configurations were developed to improve heat removal from the module. The sheet-and-tube is the most dominating thermal absorber fabrication technique. In the sheet-and-tube arrangement, a thin metal sheet glued to the PV back surface and metal tubes are welded on this sheet. Fluid flow pattern has a significant impact on the cooling of the PV panel and output temperature of the fluid. The web flow pattern is suitable to be used for better cooling of the PV module. In web-flow pattern maximum area is covered by the tubes carrying cooling fluid thus producing better cooling effect compared to other.

Table 2.1 Review on water-based PV/T collector systems

Author	Nature of study	Novelty of the study	Important findings
Kazem *et al.* (2020)[53]	Experimental & Numerical	Comparative study of three water cooling PV/T systems with variable flow channels (web type, direct type, spiral type)	The spiral flow collector found to produce the best efficiency among the compared PV/Ts.
Abdullah *et al.* (2020) [54]	Experimental & Numerical	Dual oscillating copper pipe absorber	The maximum experimental thermal efficiency reached 'optimum point' at a mass flow rate of 5 litre/min.
Yu *et al.* (2019)[55]	Experimental & Numerical	Grid-channel absorber and comparison with a conventional harp-channel configuration	Thermal and electrical efficiencies for grid-channel found to be higher as that of harp channel configuration. The thermal efficiencies at zero reduced temperature reached 70.5% for of harp channel and 74.5% for grid-channel absorber configuration. Pressure drop reported being twice in case of grid-channel as that of harp channel configuration.
Barone *et al.* (2019) [56]	Experimental & Numerical	Low cost plastic pipe absorber	Primary energy production of the proposed PV/T reported being only 20% lower than a standard commercial PV/T collector.
Hossain *et al.* (2019)[57]	Experimental	Double-serpentine sheet-tube absorber	Maximum thermal efficiency found to be as 76.58% at a flow rate of 2 litre/min. 5.7 % improvement in electrical efficiency as compared to PV.
Wu *et al.* (2018)[58]	Numerical	3-D model of water-cooled PV/T system with cooling channel above the PV panel.	The optimal mass flow rate and cooling channel height is 0.003 kg/s and 5 mm, and the corresponding exergy efficiency is 13.8%.
Aste *et al.* (2016)[59]	Experimental & Numerical	Monocrystalline Si PV sandwiched without any additional glass, bonded with a roll-bond aluminium absorber having the channel arrangement	The highest overall efficiency of 40.6% is reported for Athens while the highest electrical efficiency of 13.6% is reported for Milan.

		for fluid flow. The author's calculated overall efficiency and electrical efficiency in three places viz. Paris, Milan and Athens.	
Yazdanifard *et al.*(2016) [60]	Numerical	Effects of performance and geometrical parameters in laminar and turbulent regimes.	• The energy efficiency of the PV/T system with glazing is higher than the unglazed one. • The effects of various parameters on the output heat fluid temperature values are dominant in the laminar regime as that of the turbulent regime.
Qu *et al.* (2016)[52]	Experimental	PV/T integrated dual-source heat pump (DSHP).	• When the PV layer temperature is 69.2 °C, an electrical efficiency of 12.18 % has been reported. • Electrical efficiency can be increased by 10.3% as the top temperature of the PV/T panel decreased by ~45 °C.
Bombarda *et al.* (2016) [61]	Experimental	Roll-bond PV/T	• A newly established equation of thermal efficiency allows a fair comparison between PV/T and solar thermal collectors. $\eta_{th} = \frac{\dot{Q}_{th}}{GA - P_{el}} = \frac{\rho \dot{V} C (T_{f,out} - T_{f,in})}{GA - P_{el}} = \frac{\eta_{th}}{1 - \eta_{el}}$ • PV/T with roll-bond absorber can yield high thermal efficiency with proper insulation. • First and second law efficiencies for PV/T with roll-bond absorber is found to be 49% and 16.2% respectively.
Nižetić et al. (2016) [62]	Experimental	Water spray cooling	• PV layer temperature was reduced from 52 °°C up to 24 °C. • Simultaneous cooling of back and front of PV reported the highest electrical efficiency of 15.9% as compared to individual cooling of the back (15.6%) and front (15.4%) surface.
Yazdanpanahi *et al.* (2015) [63]	Experimental	Exergy efficiency of a solar PV/T water collector	• Exergy efficiency has a maximum value of 13.95% at a mass flow rate of 0.002 kg/s.

	& Numerical		
Aste *et al.* (2015) [50]	Experimental & Numerical	PV/T collector with thin-film PV with a roll-bond flat plate thermal absorber.	• $\eta_{overall} = 42\%$, $\eta_{el} = 13.2\%$, $\eta_{th} = 28.8\%$
Liang *et al.* (2015) [64]	Experimental	PV/T solar collector filled with graphite	$\overline{\eta}_{el}$: Without graphite 6.46%; With graphite 7.20% • The highest Primary Energy Saving efficiency is 48%.
Baloch *et al.*(2015) [65]	Experimental & Numerical	Converging channel cooling	• The experimental electrical efficiency increases from 9.8% to 12.5%.
Alami (2014)[66]	Experimental	Kera (Synthetic clay) layer applied to the backside of the PV module with water sprayed on the Kera layer	• At solar noon, T_{PV} (without clay) = 85 ˚C, T_{PV} (with clay) = 45 ˚C • Power output enhancement of 19.4% with clay.
Fudholi *et al.* (2014) [67]	Experimental & Numerical	Absorber with web, spiral and direct flow	• Web flow absorber reported the highest thermal and electrical efficiencies among the various configurations studied.

2.2.2 Air-based PV/T systems

Water can not be used as heat transfer fluid when the ambient temperature goes below zero degree Celsius, but under such condition, air can be used as heat transfer fluid in PV/T systems. PV/T with air as the heat transfer fluid is more extensively studied owing to its simplicity in construction, low operational cost and can be effectively integrated into existing buildings [68]. A typical PV/T air collector consists of an air duct directly below a photovoltaic array. However, several configurations for PV/T air collectors have been reported through both computation and experimentation. Attempts have been made to improve the heat transfer in solar air-based collectors. Some of the implemented designs of PV/T air systems are single-pass [69], double-pass [70], finned channel [69], impinging jets [71], ribbed wall [72] etc. Researchers used fins to enhance heat transfer area and other types of obstacles in the fluid flow path of a solar collector to increase turbulence [73,74]. Tonui and Tripanagnostopoulos (2007,2008) [75,76] investigated low-cost modifications of a PV/T air system to achieve higher overall efficiency and suggested the suspension of thin metal plate at the middle of the air channel. Belusko *et al.* (2008)[77] reported that jet impingement improved the thermal efficiency of the solar collector by 21% and observed that the flow distribution of jets plays a crucial role in determining the efficiency.

Table 2.2 presents a summary of work done by various researchers in the last decade on the air based PV/T system. Researchers tried with different absorber configurations to increase the outlet air temperature, thus enhancing the quality of air and the same can be put into some specific applications such as drying of fruits and spices [42]. The finned absorber is the most investigated configuration for the thermal absorber. The geometry of the fins including the orientation is a very important parameter in enhancing the heat removal from the PV module. Perforated fins are being used to facilitate the circulation of air across the back surface of the PV module. Double pass type PV/T are useful in increasing the air temperature. In some of double pass PV/T systems, the lower airflow channel is filled with porous media and found to be useful in enhancing both thermal and electrical efficiency of the system. In European countries, extensive work is done on air-based PV/T systems and the emphasis is laid on integrating such systems in buildings. The air-based collectors can be a useful system to be integrated into buildings for generating thermal energy necessary for space heating.

Table 2.2 Review of air based PV/T systems

Author	Nature of the study	Thrust of the study	System description	Concluding remarks
Özakin and Kaya (2019) [78]	Experimental and Numerical	Effect of fin addition to an air-cooled channel on exergy of monocrystal and polycrystal PV/Ts.	Fins on the absorber to circulate the forced air.	• The panel surface temperature decreased in the range of 10–15 °C. • The exergy efficiency of the monocrystal panel after the cooling process for cases of empty, sparse fins and frequent fins varied range 35–36%, 43–45% and 47–48%, respectively. These values are higher as that of polycrystal PV/T.
Fan *et al.* (2019) [79]	Numerical	A double pass PV/T solar air heater system integrated with heat pipes was developed to produce high-temperature air.	A dynamic model for performance prediction. The longitudinal fins are evenly inserted into the air channels	• Integration of heat pipes bring stronger cooling effects to the PV panel and has the potential to achieve a higher level of cooling uniformity in terms of the temperature distribution of the PV panel.
Gupta *et al.* (2019) [80]	Experimental	PV/T air dryer for chilli drying	Insulated drying cabin made of mild steel.	• Removes moisture at a 130% higher rate than the natural open sun drying process
Shahsavar and Rajabi (2018) [81]	Numerical	Performance study of a building integrated PV/T system from exergo-economic and enviro-economic points.	Air channel beneath the PV module.	• Covers 32.52% of the required heating load for ventilation air. • 4.51% improvement in the PV panel efficiency.
Amanlou *et al.* (2018) [82]	Experimental and	• Air cooling low concentrated PV/T.	A linear Fresnel reflector used as a concentrator.	• The efficiency of the PV/T collector is improved by 20%.

	Numerical	• Deflectors are used to achieve uniformity of air distribution on the PV panel.		
Slimani *et al.* (2017)[83]	Experimental and Numerical	• Investigations on the effect of adding a glass cover with a zone of steady air above the PV module. • An absorber plate is placed beneath the PV module, thus allowing double circulation of air.	There different PV/T systems were studied and compared with conventional PV module. System 1- Conventional air-based PV/T System 2- single-pass air-based PV/T System 3- Double pass glazed PV/T	• The overall efficiency of system 2 is reported to be 69.47% whereas for system 3 with the double circulation of air above and below the PV module is 74%. • It is found that the PV module efficiency increases with an increase in wind velocity and velocity of the coolant.
Assoa *et al.* (2017)[42]	Experimental	• Indoor testing and optimization of a prototype PV/T based fodder drying system. • Integration of the prototype to a building in Savoy, France.	PV panel integrated with an aluminium absorber. There is an insulated air gap below the absorber.	• The temperature of the PV panel reaches 81 ˚C at 800 W/m^2 and 93 ˚C when the radiation increases to 1000 W/m^2. • Backside insulation has a very low impact on the cooling of PV module; instead, an insulated air gap shows better results. • During July air temperature can be increased by 7.8 ˚C and the maximum outlet air temperature achieved is 32 ^{o}C
Ahmed and Mohammed (2017)[84]	Experimental	Role of a porous medium in enhancing the performance of a PV/T air system	The porous medium is inserted into the lower duct of the dual pass PV/T hybrid collector.	• The maximum thermal efficiency reported was 80.23% with the use of porous media and glass cover, 51.25 % thermal efficiency was reported without porous media and glass cover.

				• Use of porous media glass cover is recommended when the hybrid PV/T system is used solely for electricity generation.
Popovici *et al.*(2016) [72]	Numerical	Ribbed wall heat sink with highly conductive material for PV cooling.	Highly conductive ribbed wall heat sink attached to the PV panel. Ribs have holes to facilitate proper air circulation.	Maximum heat transfers at rib angle of 45°. $T_{PV} \propto h_{rib}$ $T_{PV} \propto 1/\theta_{rib}$
Mojumder *et al.* (2016)[69]	Experimental	Single-pass PV/T with thin rectangular fins.	Rectangular fins fixed longitudinally and integrated with a flat metallic sheet.	Thermal efficiency without fin and with four fins is 37.82% and 56.19% respectively at solar insolation of 700 W/m² and mass flow rate of 0.14 kg/s.
Hussain *et al.*(2015) [85]	Experimental	PV/T combined with honeycomb heat exchanger.	Honeycomb installed into the channel under the PV module as shown in **Figure 2.2.**	• Thermal efficiency (Without honeycomb) = 27%. • Thermal efficiency (With honeycomb) = 87%.
Brideau and Collins (2014) [71]	Experimental and Numerical	A predictive model of a PV/T with impinging jets and prototype development for outdoor experimentation.	Use of impinging jets of air on the plate instead of the traditional Parallel flow. It is shown in **Figure 2.3**.	• $\eta_{overall} = 54.5\%$
Bambrook and Sproul (2012) [86]	Experimental	Maximization of PV/T output by large ducts to minimize the pressure loss.	PV modules integrated into a rectangular insulated duct constructed using 50 mm thick polystyrene sandwiched between galvanized steel sheets.	• Thermal efficiency is in the range of 28 to 55% and the electrical efficiency in the range of 10.6 -12.2%. • At solar insolation of 800 W/m² and the ambient temperature of 17 °C, the maximum temperature of outlet air can reach 56 °C.

Teo *et al.* (2012) [87]	Experimental	Uniform airflow distribution for efficient PV cooling	A parallel array of air ducts with fins attached to the rear side of the PV panel.	Cooling reduced the PV temperature from 68 °C to 38°C. The electrical efficiency with cooling and without cooling is reported to be 12.5% and 8.6% respectively.
Kumar and Rosen (2011)[70]	Analytical	Investigation of double pass PV/T air heater with a vertical fins	The fins are arranged at the right angle to the direction of airflow	• PV temperature is found to be reduced from 82 °C to 66 °C.
Shahsavar and Ameri (2010) [88]	Experimental & Analytical	Modelling and design of a direct-coupled PV/T air collector at Kerman, Iran.	A thin aluminium sheet suspended at the middle of the air channel. The airflow channel casing is constructed using Medium Density Fibreboard wood	• $\eta_{th} \propto \dot{m}_{air}$ • Setting glass cover on PV panels leads to an increase in the thermal efficiency of PV/T and decrease in electrical efficiency of the module.
Joshi and Tiwari (2007) [89]	Experimental & Analytical	Exergy analysis of a parallel plate PV/T air collector	Two modules connected in series.	Instantaneous energy and exergy efficiencies are found to be in the range 55-65% and 12-15% respectively.

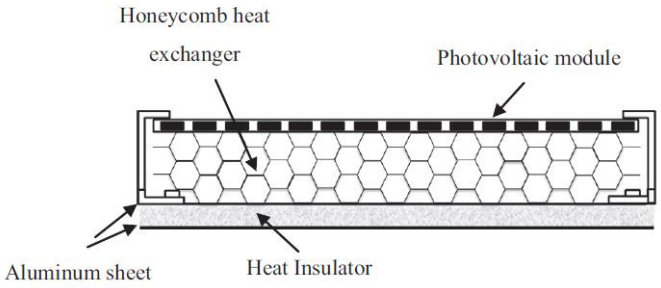

Figure 2.2. PV/T with Honeycomb heat exchanger [85]

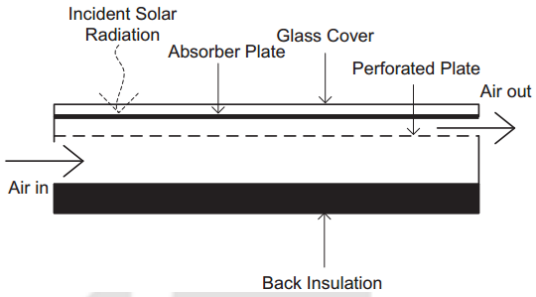

Figure 2.3. Impinging Jet Collector [71]

2.2.3 PV/T system with phase change material (PCM)

Phase change materials (PCMs) have been widely used in many of the applications including buildings and solar thermal systems. The use of PCMs in the solar thermal system increases the energy efficiency by storing heat and utilizing during off sun hours. The selection of PCM for a particular application is based on its cost, reliability, melting temperature and high latent heat of fusion. **Figure 2.4**. shows the classification of PCM.

When heat is supplied to PCMs, it undergoes sensible heating. Once it reaches the melting point, the PCM utilizes the latent heat of fusion and changes its phase from solid to liquid. When the thermal energy input is not available the liquid PCM releases the stored energy and converts to its original phase. Time and temperature requirement for melting depends on latent heat of fusion and thermal conductivity of the PCM. The thermal energy storage capacity of PCM is given by the following equation [90],

$$Q = \int_{T_i}^{T_m} mc_{ps}dT + ma_m\Delta H_m + \int_{T_m}^{T_f} mc_{pl}dT \qquad (2.1)$$

where m is the mass of PCM, a_m the fraction of PCM melted, ΔH_m the heat of fusion (J/kg). c_{ps} and c_{pl} represents the specific heat of PCM in solid and liquid phase respectively.

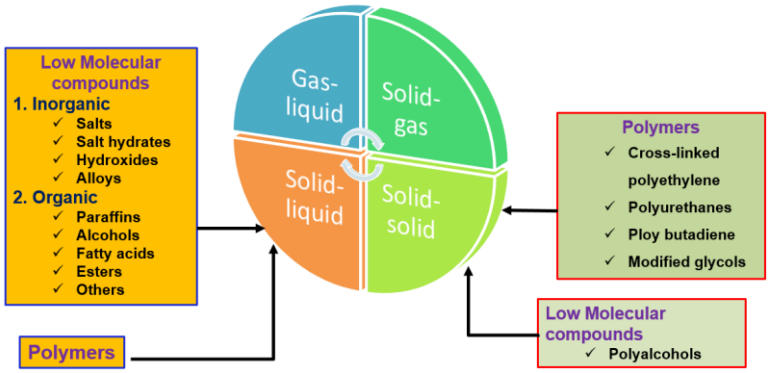

Figure 2.4. Classification of phase change materials [91]

Cooling of PV modules with PCM can be achieved with or without circulation of coolant. However, for effective cooling continuous removal of heat is necessary. A PCM for cooling of PV module should have high latent heat of fusion, high thermal conductivity, chemically stable, non-corrosive to construction materials, non-toxic, melting point lying in between the operating temperature of the PV panel and minimum sub cooling [92]. It has been reported that the organic compounds are promising as low-temperature PCMs for efficient cooling of PV modules [91]. An average value of 10.35 °C reduction in PV cell temperature has been reported by utilizing PCM. As a result, an improvement of electrical efficiency has been reported to be 2%. An increase of 30% electrical power has been reported in the case of PV-PCM (OM29) based panel [93]. PCM has been successfully used to regulate the temperature of the PV panel under hot climatic conditions. An approximate enhancement of 6% yearly electrical yield has been reported using a PCM having melting point in the range of 38-43 °C under the climatic condition of UAE [94]. Abdelrahman *et al.* (2019) [95] carried out experimental work to enhance the PV performance using PCM (RT35HC) containing a small volume fraction of Al_2O_3 with cylindrical fins. The results show the use of heat sinks with RT35HC enhances the performance by 20–46.3% when compared with the free surface configuration. This increase in efficiency is due to the enhancement of thermal conductivity. The addition of PCM can generate up to 30% more thermal output when used with roll bond absorber design [96]. The PCM is contained in metallic pouches to prevent possible leaks during the liquid state. This increases the additional cost to the system and reduces the efficiency of heat exchange between the PV and PCM. Hossain *et al.* (2019) [97] used Lauric acid as PCM which was contained in leak-proof aluminum foil packets for enhancing the thermal efficiency of two side serpentine PV/T collector. Luo *et al.* (2017) reported that by mainiatining PV panel temperature below 50 °C the PV power output increased by 7.28% [98].

One of the most challenging tasks is to ensure high thermal conductivity of PCM to maintain a high heat transfer coefficient. Attempts were made to enhance the thermal conductivity of PCM by applying fins and metal fillings. Waeli *et al.* (2017) [44] have used a mixture of paraffin wax as a PCM and SiC nanoparticle, placed inside a container which holds the heat transfer fluid-carrying copper tubes and integrated it to the PV module. The authors have reported that during peak sunshine hours (12.00 noon to 2.30 pm at Bangi, Selangor Malaysia), a reduction in the PV module temperature of 17 °C. As reported, this results in an increase of thermal energy by 37.84% in comparison with water in copper tube arrangement. Huang *et al.* (2011)[99] reported that fin spacing influence the PV surface temperature, which is shown in **Figure 2.5**. When the fin spacing is reduced, the fins inhibit the onset of natural convection in the molten PCM and the melting process is primarily determined by conductive heat transfer.

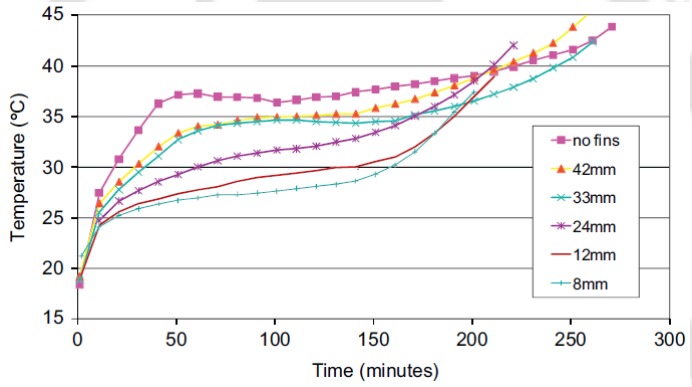

Figure 2.5. Average PV panel surface temperature with different fin spacing [99]

Kılkış (2020)[100] developed an integrated, multi-layered, composite PV/T module consisting of a multitude of standalone mini PV/T cartridges. Individual PV/T cartridge consists of several sandwiched layers with PV cells, Thermoelectric Generator (TEG) units, packed-bed PCM layer for thermal storage, and thermally controlled heat pipes with dynamic control. The developed system found to produce 25% more energy and 30% more electrical power output than a conventional PV/T system. Rajaee *et al.* (2020)[101] experimentally investigated a novel heat sink for a PV/T-TEG hybrid system. The effectiveness of simultaneous usage of the Co_3O_4/water nanofluid and enhanced PCM as a cooling method on the performance of the PV/T-TEG was thoroughly examined. The results revealed that using nanofluid with enhanced PCM, as a cooling method, improved the overall electrical efficiency by 12.28% compared to water cooling technique. Also, an increase of 11.6% in the exergy efficiency of the PV/T-TEG has been observed in comparison with PV/T-TEG with the water cooling method.

Cavity formation in PCM during heat exchange process causes an additional problem as it increases the thermal resistance. Moreover, the formation of cavity pushes the mass of PCM surrounding it and causes volumetric expansion, which finally results in leakage of PCM. Since PCM easily catches fire, fire prevention measures need to be adopted while using these materials. The use of fire retardants with PCM has also been reported [102]. Some of the literature where researchers used PCM in PV/T systems are presented in **Table 2.3.** The thermal properties of PCM are also presented in the same table.

The low heat conductivity and the problem of liquid leakage during phase transitions have become the two significant shortcomings while using PCM in PV/T systems. For instance, the solid-liquid transition must be suitably contained to prevent leakage. There are two ways to deal with pure PCMs to improve their stability and performance. The first one is to make form-stable PCMs, which is a network on micro or macroscale matrix where PCMs are trapped. Whereas encapsulation is applied in the second case. The use of encapsulation may incur additional cost and heat resistance caused by the capsule shell, thus reducing the effectiveness of heat transfer during operation. Low thermal conductivity of commonly used PCMs is another technological problem to be addressed.

Researchers have tried to address these issues in the recent past around the globe to develop a suitable latent energy storage material. Inaba and Tu (1997)[103] blended paraffin and high-density polyethylene to develop a form-stable PCM. In an attempt to decrease the oozing rate of the new material, the authors have added a small amount of the resin (ethylene-α olein). Hong and Ge (2000)[104] prepared a low-temperature heat storage compound consisting of paraffin as a dispersing medium with high-density polyethylene (HDPE) for improvement of the stability. Wan *et al.* (2019)[105] have manufactured form-stable phase change material by using pinecone biochar as a supporting matrix for Palmitic Acid. They conducted various characterization tests and concluded that Palmitic Acid was bonded with biochar due to capillary action and surface tension. No chemical reactions have been reported between the materials and hence the chemical properties of original biochar have not changed. According to their study, the composite with a mass ratio of 6:4 (Palmitic Acid: pinecone biochar) showed the best stability. The thermal conductivity of the composite material increased by 43.76% when compared with pure Palmitic Acid. Wen *et al.* (2018)[106] have studied the thermal properties of a form of stable composite from fatty acid (Capric-lauric acid/diatomite). The composite was made by vacuum impregnation method. Expanded Graphite was added to increase the thermal conductivity of the composite. Capric- lauric acid

was absorbed by the diatomite holes very effectively without any chemical bonds between the two. They observed that the composite has good thermal and chemical stability over 200 cycles of heating and freezing. Li *et al.* (2018)[107] prepared a composite material for thermal energy storage with polyethylene glycol and ZSM-5. The mesoporous ZSM-5 was taken as a supporting material and vacuum impregnation method was employed. The thermal conductivity was increased by 200% than that of pure polyethylene glycol. Exudation stability test results showed that the doping of PEG could reach up 50 wt% without any leakage when the composite was undergoing the melting process. Liang *et al.* (2018)[108] fabricated one noble phase change material by Fatty Acid and wood flour via direct impregnation method. Scanning electron microscope (SEM) images showed that the porous spaces of wood flour are occupied by the fatty acid without leakage. The prepared composite material has high latent heats and suitable phase change temperature. Sari *et al.* (2018)[109] designed one diatomite-carbon nanotubes and Polyethylene glycol (PEG) composite for thermal energy storage. The composite was made through vacuum impregnation method. Without exhibiting melt leakage, PEG was confined as 42.8, 44.5 and 51.7 wt% in the shape-stabilized composite phase change materials, including 0.57, 1.70 and 2.50 wt% of CNTs while it was absorbed by raw diatomite as 41.0 wt%. The composite had a melting temperature of 7-8 °C, latent heat of 51.4-62.9 J/g and thermal conductivity increased up to 93% compared to RD/PEG composite.

Investigations have been carried out to improve the thermal conductivity of PCM. PV/T with graphite infused PCM and finned thermal absorber is found to enhance the electrical efficiency significantly. Different types of PCM's are experimentally and numerically proven to be used in PV/T systems for thermodynamic management. Paraffin is the most suitable heat storage material for low-temperature applications due to its low cost and availability. A mixture of different kinds of paraffin with different melting points for temperature regulation of the PV panel is suitable for its surface temperature regulation. The use of PCM in PV/T is found to be useful for hot climatic zones. The addition of PCM found to be not significant in thermal efficiency improvements but can be helpful to generate additional thermal energy after sunshine hours. The issue of leakage of PCM during the melting process needs further investigation. This is because encapsulating the PCM may lead to additional cost and lower heat transfer. So, form-stable PCM with appropriate eco-friendly matrix could be a potential candidate for an efficient thermal storage medium in solar applications. This kinds of study have not been found in the open literature. PV/T systems incorporated with PCM has also immense potential to be integrated into building facades.

Table 2.3 Review on PV/T with PCM

Author	New technique used	PCM type/grade	Thermal properties of PCM used				Reported results
			T_{mp} (°C)	h_f (kJ kg^{-1})	k (W m^{-1} K^{-1})	C (kJkg^{-1} K^{-1})	
Simón-Allué *et al.* (2019) [96]	Roll-bond absorber. The face in contact with the PV is flat while the opposite one presents a wavy pattern with fluid channels. PCM is located beneath the channel.	C48, ClimSEL™	48	---	---	---	Addition of PCM results in a better distribution of heat production, reaching to generate up to 30% of maximum thermal values after removing sun exposure. The insertion of the PCM also contributed to cushion the maximum working temperature in the PV/T panel.
Hossain *et al.* (2019) [110]	Two-sided serpentine flow PV/T with PCM	Lauric acid	44-46	228.90	---	---	Maximum of 14% improvement reported with reference to PV module.
Preet *et al.* (2017)[111]	PV/T-PCM system with copper tubes having fins attached to the aluminium absorber plate.	RT-30 (Paraffin)	28	222	0.2	2.4	It has reported that there is 300% increase in electrical efficiency of PV/T-PCM system as compared to conventional PV module at 0.031 kg/sec of water flow rate.
Browne *et al.* (2016)[112]	PV/T with heat exchanger having PCM embedded and thermosyphon flow.	Capric: palmitic acid (75:25 weight)	17.7-22.8	189-191	0.143	1.65	With capric: palmitic acid PCM embedded beneath PV panel temperature of water at the outlet was 5.5 °C more as compared to PV/T system without PCM. Seven times improvement in thermal energy output from the PV/T system with PCM as compared to a system without PCM has been reported.
Stropnik and Stritih (2016)[43]	Modification of PV panel with PCM	RT28HC (Paraffin)	28	245	0.2	2	Use of RT28HC can reduce temperature of PV cells from 75.5 °C to 44 °C.

Park *et al.*(2014)[113]	PCM attached to the rear side of the PV module placed between aluminium plates.	Paraffin	25	184	0.2	2.1	It has been reported that electrical efficiency increased by 3% due to the use of PCM as compared to PV panel without PCM.
Atkin and Farid (2015)[114]	PCM infused graphite with external finned heat	RT40 (Paraffin)	40	180	0.25	2.5	Use of graphite infused PCM and fins reduces PV panel surface temperature by 19 °C. Heat sink (increases overall efficiency by 12%) is more effective in PCM infused graphite (increases overall efficiency by 4%).
Hasan *et al.* (2015)[115]	PV panels with PCM and internal fins on the backside with two different PCM tested at Vehari (Pakistan) and Dublin (Ireland)	Eutectic of capric–palmitic acid (PCM1)	22.5	173	0.14	2	More power can be saved in the hot climate of Vehari than the colder climate of Dublin.
		Calcium chloride hexahydrate $CaCl_2$. $6H_2O$ (PCM2)	29.8	191	1.08	1.4	
Maiti *et al.*(2011)[116]	Enhancement of solar insolation in V-trough limiting the temperature of the PV module.	Paraffin	57	255	0.3	2.73	The PV module temperature can be maintained at 60–65 °C for sustained periods and an overall power gain of 55% is achieved due to self-regulation of PV panel surface temperature by paraffin.

2.2.4 PV/T collector with nanofluid as heat transfer fluid

The use of nanofluids as coolants in PV/T systems also has been reported owing to its superior optical and thermal properties as that of pure fluids[20]**.** The lower heat transfer observed with traditionally used fluids has compelled researchers to use solid additives to the fluids. Size of the particle in the fluid plays a critical role in their application as heat transfer fluid in solar energy applications. Fluids with micron-sized particles are reported to cause erosion in heat transfer equipment and precipitate quickly out of suspension. Michael and Iniyan (2015)[117] reported that nano-particle size, chemical reactivity, hardness, geometry influence the tribological properties of the nanofluid. The frictional wear effect of nanofluids depends on the flow channel wall material. It has been reported that erosion in aluminium is more when compared to copper and almost negligible for stainless steel [118] .

In recent years, numerous investigations were carried out to study the applicability of different nanofluids as a coolant in solar PV/T collectors. Generally, PV/T systems apply nanofluid in two forms, either as coolant or as a spectral filter [119]. Waeli *et al.* (2017)[120] have studied the effect of increasing SiC nanoparticle weight fractions to water at different temperatures (25 °C to 60 °C) and reported that, the nanofluid density increases with increasing nanoparticle fraction in water and it reduces with temperature rise. The experimental setup developed by Waeli *et al.* (2017)[120] is shown in **Figure 2.6**, where the authors used an exchanger and a separate nanofluid tank. The techno-economic assessment of a grid-connected PV/T system revealed that the use of nanofluid is crucial in improving the system efficiency as well as the payback period [121]. Yazdanifard *et al. (*2017)[119] reported that the type of base fluid used to prepare the nanofluid is crucial for enhancing system performance. In the turbulent regime under constant mass flow rate condition, Al_2O_3/water nanofluid shows an enhancement of about 5% in electrical energy and exergy efficiency of the system more than Al_2O_3/Ethylene Glycol-water. The improvement in the performance parameter is resulted due to the enhanced thermal conductivity of the nanofluid [119].

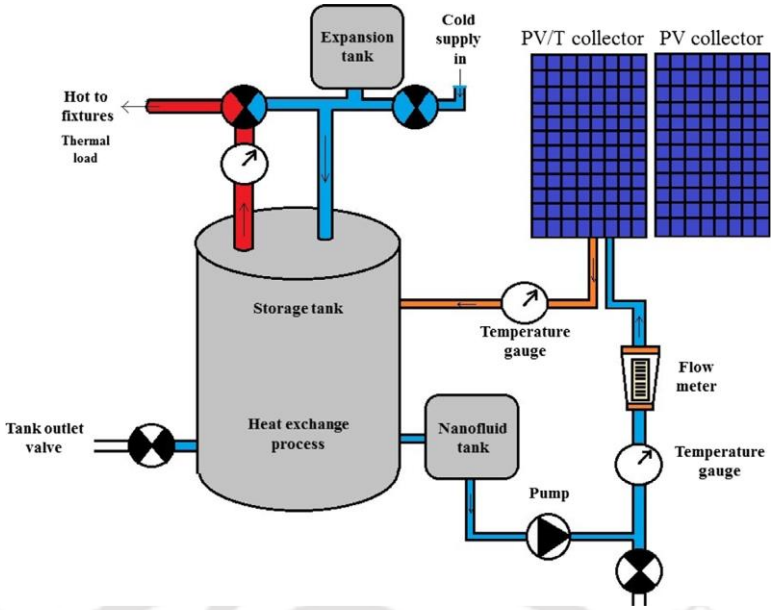

Figure 2.6. Schematic diagram of experimental setup developed by Waeli *et al.* (2017) [120]

Some filtering techniques of the solar spectrum promises to improve the efficiency and functioning of PV/T systems. Pure fluids may act as "selective" optical filters to check the IR radiation penetration to the PV cells if some nanoparticles are dispersed in it [122]. According to Hassani *et al.* (2016)[123], the simulation results show that nanofluid based optical filter and coolant outperform all other configurations in terms of high-grade exergy output. Hassani *et al.* (2017)[124] found that nanofluid (silica/water nanofluid 3% wt.) based optical filter absorbs both the IR and UV spectra, unlike the pure water-based optical filter which absorbs only the IR spectrum. Crisostomo *et al.* (2017)[125] employed core-shell Ag-SiO_2 nanoparticles in water as spectrum splitter to enhance PV output. The experimental results indicate 12% more energy output using Ag-SiO_2 –water nanofluid in a Fresnel lens concentrated PV/T prototype compared with a stand-alone PV system under the same level of illumination. One of the pioneering work in the filed of spectrally-tailorable, multi-particle nanofluid application in concentrated PV/T system was carried out by Hjerrild *et al.*(2016)[126]. The authors used a combination of suspended core-shell Ag-SiO_2 nanodiscs and multi-walled carbon nanotubes (CNTs) in water as nanofluid. The silver nanodiscs absorb visible light and the CNTs enhance the heating rate of the nanofluid.

Thermo-physical properties of nanofluids can be estimated from the expressions presented in **Table 2.4**. Selected research works on PV/T with nanofluids as heat transfer fluid are discussed in **Table 2.5**.

Table 2.4 Determination of properties of nanofluids

Author	Equation, Mathematical Relationships & Useful Information	Remarks
Drew *et al.*(1999)[127]	$\rho_{nf} = (1-\phi)\rho_f + \phi\rho_p$	Expressions for density, hydrodynamic viscosity, the specific heat of nanofluid, where ϕ is the particle volume fraction Subscripts p, n and nf corresponds to particle, fluid and nanofluid properties respectively
Brinkman H.C.(1952) [128]	$\mu_{nf} = \frac{1}{(1-\phi)^{2.5}}\mu_f$	
Yang *et al.*(1998)[129]	$(\rho C_p)_{nf} = (1-\phi)(\rho C_p)_f + \phi(\rho C_p)_p$	
Hamilton *et al.*(1962)[130]	$k_{nf} = \frac{k_p + (n-1)k_f - (n-1)\phi(k_f - k_p)}{k_p + (n-1)k_f + \phi(k_f - k_p)}k_f$	

Table 2.5 Selected research reported on PV/T with nanofluid as heat transfer fluid

Authors	Nature of work	New techniques used	Nanoparticle used	Important findings
Aberoumand *et al.* (2018)[131]	Experimental	Copper pipes pressed to the grooves made on a copper plate and attached to PV.	Ag	• With 4 wt% nanoparticles in the turbulent flow in pipes 35% increase in power output as compared to PVs was reported.
Hasan *et al.* (2017)[132]	Experimental (under indoor test conditions)	PV/T with jet impingement. It consists of four parallel tubes and 36 nozzles which directly injects the fluid to the backside of the PV/T collector.	SiO_2,SiC, TiO_2	• At an irradiance of 1000 W/m², a mass flow rate of 0.167 kg/s and the ambient temperature of 30 °C, the electrical, thermal and overall efficiencies were reported to be 12.75%, 85% and 97.75%, respectively. • The SiC/water nanofluid PV/T system reported the highest electrical and thermal efficiency. Additionally, the maximum power output of PV/T with SiC nanofluid found to be increased by 62.5% compared to the conventional PV module.
Waeli *et al.* (2017)[133]	Experimental	----	SiC	• The thermal conductivity of SiC nanofluid was measured at an interval of three months and it was to be reduced by 0.003 W/m K after six months.

				• Results showed negligible improvement in the thermal conductivity after 3 wt% of the nanofluid. • The use of SiC (3 wt%) nanofluid as heat transfer fluid in PV/T results enhancement of electrical efficiency by 24% as compared to PV.
Shamani *et al.* (2016)[134]	Experimental	PV/T having rectangular tube absorber tested with three different nanofluids	SiO_2, TiO_2 and SiC	• With SiC highest overall efficiency of 81.73% and electrical efficiency of 13.52% are reported.
Hassani *et al.*(2016)[123]	Numerical	Cascading nanofluid-based PV/T with separate channels one acts as a liquid optical bandpass filter above the PV cells while the other with thermal nanofluid recovers the waste heat from the back of the PV cells.		• PV/T with separate channels is more suitable than that with a double-pass channel. • Nanofluid-based coolant improved electrical efficiency for the GaAs and Si PV cells by 9% and 5.6%, and overall efficiency by 5.8% and 4.5%, respectively.
Michael and Iniyan (2015)[117]	Experimental	Copper sheet attached beneath the PV cells with thermally conductive adhesive eliminating Tedlar sheet.	Copper oxide – water (CuO/H_2O)	• Copper oxide – water nanofluid increased overall efficiency with glazing by 19.25% compared to water as heat transfer fluid. • η_{th} = 45.76%.
Karami and Rahimi(2014) [135]	Experimental	Straight and helical channels.	Water- Boehmite ($AlOOH.xH_2O$)	• η_{el} = 20.57% (Straight channel) • η_{el} = 37.67% (Helical channel) • The helical geometric channel allows better heat removal
Sardarabadi *et al.*(2014)[136]	Experimental	Comparison of pure water to a silica/water nanofluid in terms of energy and exergy efficiencies.	Silica/water	The pure water, silica (3 wt %)-water nanofluid and, silica (1 wt %)-water nanofluid reported thermal efficiencies of 66.8, 68.2 and 72.1%, respectively.
Ladjevardi *et al.* (2013) [137]	Numerical	Effect of graphite nanoparticles size is investigated on the efficiency of solar receivers in the absorption of solar energy.	Graphite nanofluid	• Thermal efficiency reported to be about 88% higher than pure water. • It will be possible to absorb 50% of incident irradiation energy with a solar collector having graphite nanofluids, while pure water solar collector can only absorb around 27%.

Attention has been paid in recent years to explore nanofluids with higher thermal conductivities. The thermal conductivity is directly proportional to the concentration of nanoparticle in the base fluid. The increase in the thermal conductivity of the nanofluid depends on the micro-convection process, which is caused by Brownian motion. For nanofluid to be successfully implemented for commercial use in heat transfer applications, the stability issue associated with the application of nanofluids needs to be resolved. When nanofluids are used in solar applications, it remains steady during the night time, which leads to the separation of both nanofluid and base fluid. This results in accumulation of nanoparticles at the bottom and reduces the thermal conductivity of the nanofluid as a whole. To avoid this situation an additional stirring unit is recommended whenever nanofluids are put into such applications. From the surveyed literature, it has been found that SiC-based nanofluids can be effectively used as heat transfer fluid in PV/T. There are nanofluids reported in the literature which can filter the wavelengths other than the visible wavelength region for enhancing the electrical efficiency of PV cells.

2.2.5 PV/T collector with heat pipe

A traditional water-type PV/T collector system is not recommended for use in cold climatic conditions because at very low-temperature freezing of water takes place and there is a considerable increase in volume, which results in damage to the system [138]. A heat pipe is a system with a very high thermal conductivity that allows quick transport of heat without any significant drop in temperature. Freezing can be avoided by carefully selecting the working fluid. Hence, a heat pipe and a solar collector can be integrated to form a heat pipe PV/T system. Several experimental and numerical studies on heat pipe-based solar thermal collectors have been conducted. A few of these studies are discussed here. Hammad (1995)[139] studied flat-plate heat pipe thermal collectors and reported that the thermal efficiency of a heat pipe collector is comparable to that of a water-cooled solar collector**.** The transient thermal performances of wickless heat pipe-based flat-plate solar collectors are dependent on various parameters such as solar insolation, the temperature of cooling water, material properties of the absorber plate, the thickness of absorber plate and the ratio of condenser-section length to the total length of wickless heat pipe [138]. Moradgholi *et al.* (2014)[140] have experimented on a heat pipe PV/T system using methanol as heat transfer fluid under different weather conditions and reported a substantial PV panel temperature (up to 15 °C).

Wu *et al.* (2011)[141] studied a PV/T system with heat pipe rows having equal diameter for both evaporator and condenser sections coupled with the PV module. The electrical, exergy and overall thermal efficiencies are reported to be 8.45% and 10.26%, 63.65% respectively. Hu *et al.* (2016)[45] reported that the angle of inclination affects the thermal efficiency of heat pipe equipped with PV/T system significantly and observed poor thermal performance when the inclination angle is kept below 20 °C, whereas the thermal performance of the wire-meshed heat pipe is not much affected by variation in the inclination angles.

Wang *et al.* (2016)[142] proposed a heat pipe-based building-integrated PV/T system with the metal wires filling into the gap between the finned heat pipes and the insulation layer. The experimental study reported that the temperature of water in the tank reaches 53.83 °C at simulated solar irradiance value of 900 W/m² and water flow rate of 200 l/h. The maximum thermal efficiency of 44.04% corresponds to the simulated solar irradiance of 300 W/m² and a water flow rate of 200 l/h has also been reported. Jouhara *et al.* (2016)[143] developed flat heat pipe solar PV/T in which the heat pipes were made from aluminium as the shell material and ammonia as the working fluid. They reported 15% increase in the electrical efficiency of the PV module as compared to that of without heat pipe coupling to the PV module due to homogenous cooling facilitated by heat pipes. Gang *et al* (2012)[138] developed a dynamic model of the heat pipe-based PV/T system and experimentally validated the proposed model. They reported energy and exergy efficiencies of 51.5% and 7.1%, respectively. The system developed by Gang *et al* (2012)[144] is shown in **Figure 2.7** and the side view of the system is also shown in **Figure 2.8**.

Chen *et al.* (2017)[145] reported that a combination of heat pipe based PV/T system with a heat pump could enhance the system performance significantly. The thermal energy output of the system increases with an increase in solar irradiance, while the exergy efficiency and overall energy efficiency decreases. The same effect is reported with the increase in the ambient temperature. But, with increasing the packing factor of the PV module results in a decrease in thermal efficiency, but electrical output increases. Researchers have concluded that the pitch of the heat pipe affects the system efficiency, increasing the pitch reduces all the performance parameters [145]. Khordehgah *et al.* (2019) have carried out a simulation study of a heat pipe-based PV/T system over a year. The authors reported that the average panel temperature could be reduced on an average by 25%, which resulted in 15% increase of the electrical power output.

Integration of heat pipe to PV/T collector is extensively studied in China. From the review, it is evident that heat pipe having wick is superior to that of wickless heat pipes for

application in PV/T collector. Wick gives structure and force to assist the condensate fluid back to the evaporator. The wick structure also guarantees equitable distribution of working liquid over the evaporator surface. It is also significant to note that the selection of working fluid in heat pipe plays a crucial role in its operation. For colder regions, fluids having a lower freezing point is preferred.

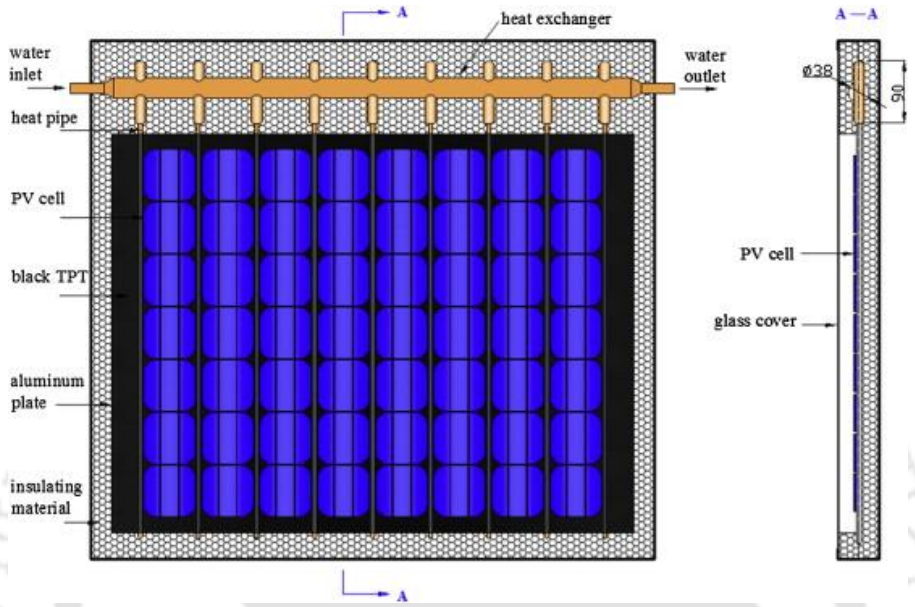

Figure 2.7. Heat pipe coupled PV/T collector [138]

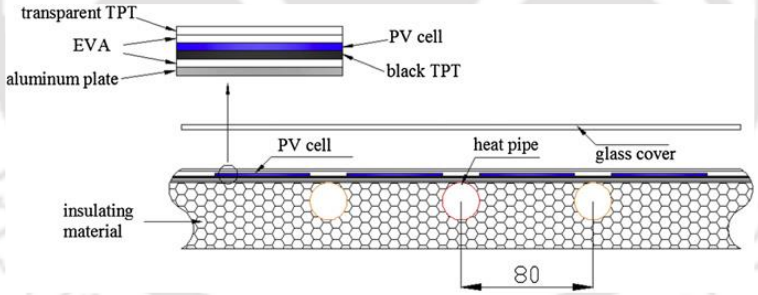

Figure 2.8. Side view of the heat pipe coupled PV/T collector [138]

2.3 Commercial PV/T collectors

PV/T's can be used in residential roof-top, commercial and industrial roof-top, solar power station and other on-grid applications. The thermal energy produced by a PV/T module can be used to satisfy different needs for example swimming pool heating, space heating, hot water generation, drying, industrial process heating etc. First PV/T was launched in 1991by an Israeli company named 'Millennium Electric'. Millennium Electric successfully tested their PV/T's in different locations of Israel for household hot water and electricity

before releasing commercially. PV/T developed by Millennium Electric can deliver 340 W of electrical energy and 1.5 kW of thermal energy [46].

SolarWall developed by the Canadian company Conserval Engineering was ranked as the 9th best energy inventions of the past 200 years by American Society of Mechanical Engineers (ASME). SolarWall is mainly integrated into buildings as shown in **Figure 2.9**, for space heating and improving the indoor air quality. When looking into SolarWall from its life cycle point of view, it is beneficial and with a lifespan longer than 30 years. SolarWall integrated air heating system was found to cut the GHG emission by 20-50% compared to traditional heating systems. SolarDuct PV/T collector, a variant of SolarWall is intended for roof mounting has already gained acceptance among solar energy users [46].

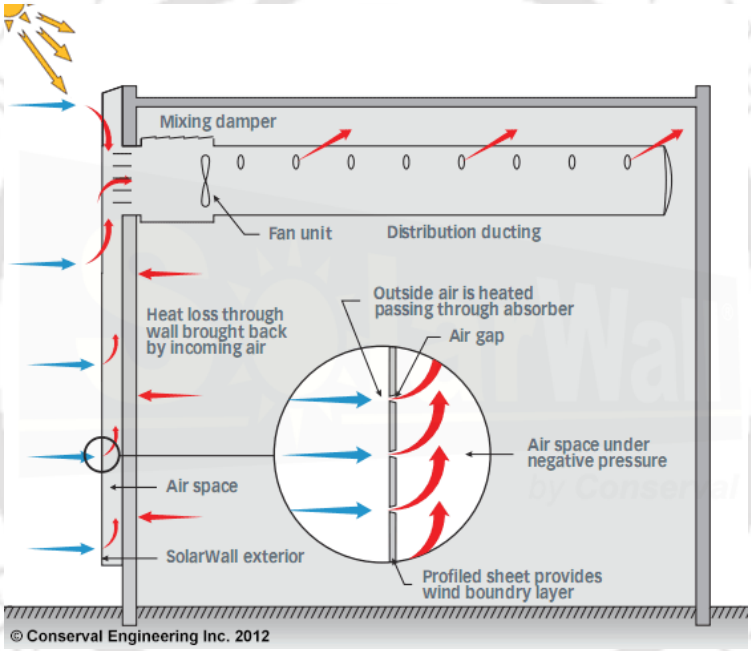

Figure 2.9. SolarWall air heating system [46]

SUNSYSTEM PVT240 developed in Bulgaria has a module electrical efficiency of 14.7% and thermal energy output of 900 W. It has thermal absorber made of copper and uses Propylene Glycol as heat transfer fluid [146]. Advanced hybrid solar (PV/T) panel produced by DualSun can produce 4 times more energy than a traditional PV module [147]. **Table 2.6** presents an overview of various commercial PV/T systems available around the globe considering parameters like electrical efficiency of the module, overall efficiency, type of absorber material, heat transfer fluid used, life, the quantity of thermal and electrical energy generated by the systems.

Table 2.6 Commercial PV/T modules available in different parts of the world

Product	Developer and Country	HTF	$\eta_{overall}$ (%)	η_{el} (%)	Thermal Output	Electrical output	Solar cell type	Absorber material	Life (years)
SolarWall [148]	Conserval Engineering, Canada	Air	50+	---	300-400 W/m²	100 W	---	---	30+
The Multi Solar System [46]	Millennium Electric T.O.U. Ltd., Israel	Water	85	15	8368 kJ/day	190 W	Mono-crystalline	---	25+
SolarVenti [149]	Aidt Miljo A/S, Denmark	Air	57-70	---	500 W/m²	6-18 W	---	---	10-20
Volther Powervolt [150]	Solimpeks Solar Energy Corporation, Turkey	Water		15	630 W	200 W	Mono-crystalline silicon	Copper	20+
SunDrum SDM100 [151]	SunDrum Solar, USA	Water	75	---	650 W	250 W	---	---	---
Sunsystem PVT240 [152]	New Energy System, Bulgaria	Propylene Glycol	---	14.7	900 W	240 W	Poly-crystalline silicon	Copper	---
DualSun Wave [147]	DualSun,	Water		15.4	912 W	240 W	Mono-crystalline Silicon	---	20+
TESZEUS 240P [153]	TESZEUS, China,	Water	---	14.6	651 W	240 W	Mono-crystalline silicon	Copper/ Aluminium	
FT220Cs [154]	FOTOTHERM, Italy	Water	---	13.7	888 W	220 W	Poly-crystalline silicon	---	25+
CoolPV [155]	FAFCO, USA	Water		16.4	996.44 W	275 W	Mono-crystalline silicon		30+
2Power [156]	PA-ID Process GmbH, Germany	Water	---	16	719 W	260 W	Mono-crystalline silicon	---	25+

SolarVenti, a PV/T air hybrid collector developed in Denmark has received satisfactory feedback from customers across the world. The system has a filter, which is stretched out across the inside surface of the back panel which makes SolarVenti maintenance-free in long run[149]. HYSOLAR, a revolutionary PV/T product developed by International Clean Energy Consortium, reduced the energy cost drastically and allowed better roof space

utilization[157]. Volther Powervolt developed by Solimpeks Solar Energy Corporation in Turkey reported an increase in electricity production of at least 25% per year with the cooling of PV cells. Volther Powervolt has a collector area of 1.427 m^2 and an electrical efficiency of 15.08%. It has an embossed aluminium backsheet with a thermal energy output of 630 W [150].

SunDrum's PV/T system which is a flat plate PV/T system reported an overall efficiency of 86% during peak hours in Massachusetts, USA, and its thermal analysis shows that the hybrid modules are 22 °C cooler compared to the conventional PV module. The payback period for SunDrum hybrid PV/solar water heating system is 5-10 years, which is longer than conventional domestic solar water heating system without the PV, but faster than a standalone PV system itself [158].

After reviewing various types of PV/T modules available in the global market, it has been observed that there are numerous areas which can be explored for further enhancement of commercially available PV/Ts. Most of the commercially available PV/Ts are used for space heating and hot water supply. Countries like Canada, the United States of America, and Germany etc. have exploited PV/T technology in the most efficient way possible, by employing them in building architecture as a wall or roof. SolarWall and SolarVenti are two of the most commercially successful product which is mainly used for space heating.

2.4 Thermodynamic analysis of PV/T system

Energy analysis is a conventional way of assessing the performance of an energy conversion system. However, exergy is a measure of the maximum available work obtainable from a process. Exergy analysis plays an important role in the study of the system which involves the conversion of low-grade energy into the high grade. Exergy analysis of energy conversion mechanisms such as PV/T may assist in optimization of electrical and thermal outputs.

According to Sahin *et al.* (2007)[159] the exergy efficiency in most of the instances gives a better comprehension of conversion than energy efficiency. The exergy efficiency emphasises that both external losses and internal irreversibility need to be dealt with to improve the system efficiency. Moreover, in some cases, internal irreversibility is more significant and more difficult to address than external losses. The energy efficiency of a PV system may vary between 7% and 12%, while the exergy efficiency of the system varies from 2% to 8%. The chemical exergy contributes to the system with a negative effect and provides

information about the unconsidered power of the system. Chow *et al.* (2009)[48] pointed that thermal performance of PV/T system is affected by six key parameters, of which three are internal, namely cell efficiency, packing factor, the ratio of water mass to aperture area and three are external namely, the ambient temperature, solar irradiance, and the wind velocity. It was observed that the energetic efficiency of the glazed PV/T collector was discovered constantly superior to unglazed collector yet exergetic efficiency of the unglazed PV/T collector was superior to the glazed one. Tiwari *et al.* (2009) [160] discussed the design aspects of an industrial PV/T integrated system to obtain hot water at a constant temperature by varying the flow rate and the number of collectors. Their investigation uncovered that the thermal and exergy efficiency had switched patterns concerning the collection of temperature hot outlet water. Vats *et al.* (2012**)** [161] compared heterojunction module comprising of thin amorphous silicon (a-Si) PV cell on top of a crystalline silicon (c-Si) cell with a traditional crystalline silicon-based module in terms of maximum electrical and thermal output. It was found that in case of heterojunction the annual electrical energy is highest (810 kWh) at the cost of lower value of thermal energy, whereas in case of a-Si the thermal energy is highest (464 kWh) at the cost of lower value of electrical energy. The crystalline silicon-based modules are preferred for construction of systems used in space heating applications. Koroneos *et al.* (2012) [162] reported that the exergy efficiency of solar heating or cooling system (only thermal collectors) is very low. Dubey *et al.* (2009)[162] evaluated monthly energy, exergy and electrical energy gain of PV/T air collector for five different Indian cities namely Srinagar, New Delhi, Jodhpur, Mumbai and Bangalore. Authors have studied two different configurations of PV/T air collector. In the first configuration, air flows over the absorber while in the second configuration air flows below the absorber. They have reported that the second configuration is beneficial both in terms of improving the electrical efficiency of the PV cells and the production of hot air. Evola and Marletta (2014)[163] showed that at a fluid inlet temperature (≈20 °C) the exergy efficiency is in the range of 0.5%- 2.5%. Exergy efficiency reaches the lowest value during the hottest month of the year when the energy efficiency would be at its maximum (around 60%). The findings of the investigation suggest that, when operating at low water inlet temperatures, the collector would reach a very high overall energy efficiency. However, the high value of overall energy efficiency is misleading. The thermal energy recovered by the PV/T collector, even in high quantities, is almost useless when available at low temperatures. Sobhnamayan *et al.* (2014)[164] performed exergetic optimization to determine the optimum operating mode of PV/T water collector by using Genetic algorithm. The maximum exergetic efficiency was found to be 11.36%, considering

the pressure drop losses in the flow pipes and studied the effect of climatic parameters. The researchers showed that increasing solar irradiance from 0 to 1000 W/m^2, exergetic efficiency increases from zero to 11.5%. Yazdanpanahi *et al.* (2015)[165] considered the observation and modelling by Tiwari *et al.* (2009) [166] and introduced losses accounting for pressure drop in the flow channels. They reported optimum exergy efficiency value of 13.95%. Gholampour *et al.* (2016)[167] reported in detail the effect of critical irradiance level and optimum PV coverage percentage as well as suction velocity on exergy and energy efficiency. Hazaml *et al.* (2016) [168] considered the exergy loss due to pressure drop in the coolant channel by considering the pump power input. Tiwari *et al.* (2017)[169] used the low-grade thermal energy for drying efficiently, the authors have connected a number of solar air heaters varies from 1 to 5 and a drying unit in series. Solar air heater was constructed using a semi-transparent PV module (glass to glass) and thermal flat plate collector.

The major advantages of exergy analysis are, (a) it provides a true measure of how nearly the actual performance of the system approaches the ideal, and (b) it identifies the causes and locations of losses[170]. Due to these reasons, exergy analysis is always preferred over energy analysis in energy conversion devices for its performance analysis. With respect to the solar energy collection devices, exergy analysis is found to be very useful in the improvement of conversion efficiency [171]. Mostly the focus is made on the thermal analysis under steady-state condition. Steady-state analysis of a process is feasible when appropriate control measures are implemented to achieve the desired setpoint value of the manipulated variable (Power output). An open-loop process subjected to frequent disturbances, thus such a process doesn't attain a steady-state condition. In operation, most of the PV/T modules may be considered as semi-batch type process rather than a continuous one. In practice, batch processes never attain a steady state. Therefore, the PV/T module should be modelled considering the transient behaviour. **Tables 2.7 and 2.8** show the mathematical expressions and formulations which are useful for energy and exergy analysis.

Table 2.7 Energy balance equations and relationships

Author	Equation, Mathematical Relationships & Useful Information	Comments
Tiwari *et al.* (2006)[172]	$Q_u = A_c F_R \left[h_{p1} h_{p2} (\alpha\tau)_{eff} G_T - U_L (T_{fi} - T_a) \right]$ $\eta_{overall} = \frac{\eta_{PV}}{\eta_p} + \eta_{th}$ η_p is the electrical conversion efficiency of a conventional thermal power plant which is approximately 38%	• This expression gives an example of available thermal energy for a PV/T system • The expression is used for the overall thermal efficiency of PV/T system.
Joshi *et al.* (2007)[89]	$\eta_{oth} = \frac{\eta_0 \{1 - f\Delta T\}}{0.38} + \eta_{th}$ $\dot{Q}_u = \frac{\dot{m}_a C_a}{U_L} \{h_{p1} h_{p2} (\alpha\tau)_{eff} G_T - U_L (T_{air,in} - T_a)\} \left(1 - \exp(\frac{-bU_L}{\dot{m}_a C_a} L) \right)$	• Overall thermal efficiency expression. • The useful heat harnessed from a PV/T module cooled by air
Chow *et al.* (2009)[48]	$\frac{dT_g}{dt} = \left[\frac{\{G_T \alpha_g + (h_{wind} + h_{r,g-a})(T_a - T_g) + (h_{c,g} + h_{r,c-g})(T_g - T_a)\}}{\rho_g \delta_g C_g} \right]$ $\frac{dT_c}{dt} = \left[\frac{\{G_T \tau_g \alpha_c - \dot{E}_{PV} + (h_{c,g} + h_{r,c-g})(T_g - T_c) + h_{c,f} A_f (T_f - T_c) + \frac{T_a - T_c}{R_{in}}\} + \frac{T_a - T_c}{R_{in}}\}}{\rho_g \delta_g C_g} \right]$ $\rho_f A_z C_f \frac{\partial T_f}{\partial t} = h_{c,f} A_f (T_c - T_f) - \rho_f u_f A_z C_f \frac{\partial T_f}{\partial y}$	• Expressions for glass cover temperature variation with time. Applicable for collectors with glass covering • Expression for solar energy collector cells temperature variation with time. Applicable for collectors with glass covering • Expression for temperature of fluid for the cooling system.

Joshi *et al.*

(2009)[173]

$$Q_{loss} = U_L bL\left[\lambda_1 G_T + (\lambda_2 - 1)T_a + \lambda_3 T_{fi}\right]$$

$$\lambda_1 = \frac{\tau_g f(\alpha_c - \eta_{PV})}{U_{t,ca} + U_p} + \frac{U_p(\alpha\tau)_{eff}}{h_{p2}(U_{tp} + U_f)(U_{t,ca} + U_p)} + \frac{U_p U_f(\alpha\tau)_{eff}}{U_L(U_{tp} + U_f)(U_{t,ca} + U_p)}(1 - \frac{F_R}{F'})$$

$$\lambda_2 = \frac{U_{t,ca}}{U_{t,ca} + U_p} + \frac{U_p}{(U_{tp} + U_f)(U_{t,ca} + U_p)}(U_{tp} + U_f(1 - \frac{F_R}{F'}))$$

$$\lambda_3 = \frac{U_p U_f F_R}{(U_{tp} + U_f)(U_{t,ca} + U_p)F'}$$

Expression for heat loss from PV/T to the surroundings

Tiwari *et al.*

(2009)[160]

$$G_T \geq \frac{U_L(T_{f,i} - T_a)}{h_{p1}h_{p2}(\alpha\tau)_{eff}}$$

$$\dot{M}(t) = \frac{\{F_g\{h_{p1}h_{p2}(\alpha\tau)_{eff} G_T\} - \{F_R U_L + (UA)_T + \varepsilon(UA)_p\}(T_0 - T_a)\}}{C_{p,w}(T_0 - T_a)}$$

- Threshold radiation intensity for PV/T system. This value is higher than the threshold intensity of a conventional flat plate collector
- Required mass flow rate for constant outlet temperature of the water

Vats and Tiwari (2012)[161]

$$\dot{Q}_{u,monthly} = \frac{\dot{E}_{electrical,monthly}}{0.38}$$

The conventional electrical output was converted to an equivalent thermal energy output by dividing it with the conversion factor of the thermal power plant. The conversion factor depends on the quality of the fuel.

Table 2.8 Exergy Analysis Equations and Relationship

Author	Equation, Mathematical Relationships & Useful Information
Fujisawa *et al.* (1997)[174]	Expression for overall exergic efficiency is given by considering initial fluid temperature equal to ambient temperature $\eta_{PV/T} = \eta_{PV} + \eta_{th} = \eta_c + \left(1 - \frac{T_a}{T_{f,out}}\right)\eta_T$
Bosanac *et al.*(2003)[175]	A correlation between available output heat and exergy $\dot{E}x^{Q_u} = \dot{Q}_u[1 - \frac{T_{ref}}{293 + \Delta T}]$
Tiwari *et al.* (2006)[172]	Overall exergic efficiency $\eta_{ex} = \eta_{PV} + \eta_{th}[1 - \frac{T_a}{T_w}]$
Sahin *et al.* (2007)[159]	$\sum_{in} ex_{in} m_{fi} - \sum_{ex} ex_{ex} m_{out} + \sum Ex^Q - Ex^W - I = 0$ For closed PV/T system there is no mass transfer between system and surrounding. $\sum_r Ex^Q - Ex^W - I = 0$ Expression for specific exergy $ex = [ke + pe + (\overline{H} - \overline{H_0}) - T_0(\overline{S} - \overline{S_0}) + [\sum_j (\mu_{j0} - \mu_{j00})x_j]$

$$Ex = E_{gen} + C_P(T_c - T_a) + T_a\left(C_p \ln\left(\frac{T_c}{T_a}\right) - \frac{Q_{loss}}{T_{cell}}\right)$$

Celik *et al.* (2007)[176]

Exergic solar input as a function of the surface temperature of the sun $(\approx 5777K)$ and ambient temperature.

$$\dot{E}x_{in} = \dot{E}x_{sun} = A_s \times G_T \times \left[1 - \frac{4}{3} \times \left(\frac{T_a}{T_{sun}}\right) + \frac{1}{3} \times \left(\frac{T_a}{T_{sun}}\right)^4\right]$$

Saloux *et al.* (2013)[177]

$$\bar{e}_{PV/T} = \frac{V_m I_m + Q_R \theta_R}{\left[1 - \frac{4}{3}\frac{T_0}{T_{sun}} + \frac{1}{3}\left(\frac{T_0}{T_{sun}}\right)^4\right] AG_T}$$

$Q_R\theta_R$ accounts for the product of heat recovered and Carnot factor.

Evola and Marletta (2014)[163]

Exergy interaction for heat interaction between the absorber plate and coolant fluid

$$\dot{E}x_Q = \dot{m}_w C_p \left[(T_{out} - T_{in}) - T_0 \ln\frac{T_{out}}{T_{in}}\right]$$

The subscripts in, out and 0 refer to the inlet, outlet water and reference temperature (dead state).

Sobhnamayan *et al.* (2014)[164]

Exergy efficiency of PV/T water collector considering the flow work done by pump

$$\eta_{ex} = \frac{\left[\dot{m}_w C_{p,w}(T_{W,out} - T_{W,in} - T_a \ln\left(\frac{T_{W,out}}{T_{W,in}}\right) - \dot{m}_w \frac{\Delta P_w}{\rho_w} + (V_{pump} I_{pump} - P_{pump})\right]}{G_T A\left[1 - \frac{4}{3}\left(\frac{T_a}{T_{sun}}\right) + \frac{1}{3}\left(\frac{T_a}{T_{sun}}\right)^4\right]}$$

Yazdanpanahi *et al.* (2015) [165]

Exergy efficiency for a flat plate water PV/T collector

$$\eta_{ex} = \frac{\dot{Q}_u\left(1-\frac{T_a}{T_{f,out}}\right)+\eta_{el,ref}\left[1-\beta_{ref}\left(T_c-T_{a,ref}\right)\right]GA_{PV/T}-\dot{E}_P}{GA_{PV/T}\left[1-\frac{4}{3}\left(\frac{T_a}{T_s}\right)+\frac{1}{3}\left(\frac{T_a}{T_s}\right)^4\right]}$$

Hassani *et al.* (2016)[123] In the case of PV/T with air-based optical filter and water and nano fluid-based coolant

$$\eta_{ex} = \eta_{el} + K\left(1-\frac{T_0}{T_{n,out}}\right)$$

In case of PV/T with water or nanofluid optical filter and nanofluid as coolant.

$$\eta_{ex} = \eta_{el} + K\sum_{i=1}^{2}\left(1-\frac{T_0}{T_{n,i}}\right)\eta_{th,i}$$

K is the fraction of work converted into electrical energy.

Hazami *et al.* (2016)[168] Exergy efficiency of a PV/T module considering the electrical power input to flow the coolant fluid.

$$\eta_{ex} = \frac{\dot{Q}_u\left(1-\frac{T_a}{T_{w,out}}\right)+\eta_{ref}\left[\left(1-\beta_{ref}\left(T_c-T_{a,ref}\right)\right]G_T A-\dot{E}_P\right.}{\left(1-\frac{T_a}{T_C}\right)G_T A}$$

2.5 Thermal modelling of PV/T collector

Lately, the development of thermal model for PV/T collectors has attracted significant attention. Jones and Underwood (2001)[178] developed a thermal model for PV modules considering the heat losses in detail. They considered heat loss by conduction, forced convection, free convection and the high and low wavelength radiation heat losses as well. A consideration of their module effective heat capacity led to the conclusion that the mean temperature throughout different layers of the module was uniform. Moreover, their study revealed that a dynamic model was required for the fluctuating solar irradiance instead of the steady-state approximation as the thermal response time of the module was significant compared to the period of measurement, necessitating the thermal mass of the system to be considered during the development of the thermal model. Raghuraman (2017)[179] developed two separate 1-D analyses for both liquid and air flat-plate PV/T collectors to predict the thermal and electrical performances. The author reported that the roll bond absorber plate can reduce the thermal resistance between the layer of a PV cell and tube for liquid collectors and enhance the performance of the collectors significantly. Chow (2003)[180] attempted to study the transient performance of a PV/T module and for this purpose, an explicit dynamic model was developed for a single-glazed flat-plate water-heating PV/T collector based on the control-volume approach. In India, the pioneering work in the field of numerical analysis of PV/T based water heating system was carried at Centre for Energy Studies, Indian Institute of Technology Delhi during the early years of 21st century. Tiwari *et al.* (2009)[160] analysed an integrated PV/T hot water system based on the energy balance approach. The analysis includes the derivation of an expression for water temperature underflow. The optimum hot water flow rate is 0.006 kg/s as reported in the study, based on overall exergy and thermal efficiency. Tiwari *et al.* (2011)[181] carried out an extensive review of thermal modelling of PV/T systems and provided valuable recommendations regarding the improvement of PV/Ts for better applicability. Numerical performance evaluation based on overall energy and exergy has been carried out for a hybrid PV/T array to optimize flow configurations for various climatic conditions of India. The entire study is based on the transient model, the authors recommended the use of thermal gain for space heating or drying and showed that PV/T helps reduce the peak demand on the grid by a reasonable quantity [182]. Mishra and Tiwari[183] analyzed PV/T water collectors under constant collection temperature mode and reported that collector fully covered by PV module is suitable for electricity generation. Shyam *et al.* (2015)[184] studied a series combination of PV/T water collectors partially covered with photovoltaic module numerically and proposed analytical

expressions for instantaneous thermal efficiency and temperature dependent electrical efficiency.

Dubey and Tiwari (2008)[185] designed and fabricated a PV/T solar water heater of capacity 200 litres and analysed it under varying atmospheric conditions. They neglected the heat capacity of the module in thermal modelling compared to the heat capacity of water in the storage tank. Additionally, they considered one-dimensional quasi-static heat conduction model without accounting for the Ohmic losses in their PV cell. Skoplaki and Palyvos (2009)[186] compiled different expressions for photovoltaic power output and efficiency according to the actual requirements. Torres-lobera and Valkealahti (2014)[187] considered finer details of radiation, including view factors for radiation heat transfer between surfaces to formulate a thermal model considering a mean invariant temperature throughout the module. Based on these observations researchers have developed a dynamic thermal model considering the mean temperature to be invariant throughout the module and took into account all the radiation losses with a proper view factor. Bambrook and Sproul (2016)[188] developed a steady-state model of PV/T air collector and proposed an expression for temperature variation of PV cells along the length of the collector neglecting heat losses due to radiation and free convection. One of the important works on numerical modelling of a PV/T cell was performed by Slimani *et al.* (2016)[189]. The authors developed a thermodynamic model considering all major and minor losses. According to Slimani *et al.* (2016) [189] the overall energy efficiency increased with the use of a glazing material above the PV cells and an absorber plate above the thermal insulator with the flow of coolant both over and beneath the PV cells.

Amori and Taqi Al-Najjar (2012)[190] developed a mathematical model and applied it to the climatic conditions of Iraq. This model was derived in terms of operating, climatic and design conditions. Their model incorporated some additions and corrections to the radiative and convective heat coefficients for losses at the top surface and the air duct with widely applicable sky temperature correlation. Khelifa *et al.* (2016)[191] developed a mathematical model for a PV/T water collector and studied temperatures of various layers of PV/T cell and predicted the cooling fluid outlet temperature. The authors also validated the model through an experimental study on a sheet and tube PV/T cell. They reported that coolant flow in the tubes reduced the PV module temperature by 15-20%. Huide *et al.* (2017)[192] studied three different solar energy systems, namely, PV/T, PV and thermal. They developed simulation models for all three systems. They reported that PV/T system was the most suitable for urban residential buildings and rural housing applications as well because of its high net electricity

output. The set of equations developed in the study considered the thermal resistance of each layer of the PV/T collector.

Simonetti *et al.* (2018)[193] developed and validated a thermal model for a PV/T cell under a transient regime based on the control volume approach. The PV/T collector considered in the study was an unglazed, sheet-and-tube PV/T cell consisting of a PV module and an aluminium absorber plate glued to the Tedlar layer with copper tubes soldered on the back of the absorber plate. Recently many researchers have attempted various approaches to improve the performance of PV/T cells. Paradis *et al.* (2018)[194] numerically investigated a new configuration of a PV/T collector used as an evaporator in a CO_2 trans-critical heat pump system. The solar absorber plate made of stainless steel was embedded to the back of the monocrystalline silicon PV cell, stainless steel tubes were arranged in a serpentine fashion and bonded to the solar absorber plate with two-phase CO_2 flow inside the tubes. Their results showed that heat dissipation and uniformity of temperature distribution across the wall was better for copper pipe compared to that for the stainless steel. It has been reported that cooling with CO_2 reduces the mean temperature from 320.6 K to 294 K and the overall collector efficiency reported reaching as high as 72.3%. Another important innovation in the field of PV/T collector performance enhancement is an integration of a micro-channel heat pipe array to the rear surface of the PV module. Modjinou *et al.* (2017)[195] proposed a PV/T module comprising of c-Si solar cells and wide microchannel heat pipes (MHP) filled with acetone as the heat transfer fluid. The MHP-PV/T module was investigated using both numerical (MATLAB) and experimental methods. The authors reported the daily thermal and electrical efficiencies to be 50.7% and 7.6%, respectively. Rejeb *et al.*(2020)[196] developed a transient two-dimension multi-physics model for the PV/T sheet-tube collector. The state variable variations were predicted by the finite volume method. The model has taken into consideration the impact of antireflective and low-emissivity coating and thermal resistance between the absorber plate and the cooling fluid. The addition of an anti-reflective coating on the photovoltaic module leads to an increase of both the electrical and thermal performances. Yu *et al.* (2020)[197] proposed a novel 2D irradiance - temperature coupling model that can predict the irradiance and temperature of every single PV cell. Results of the study indicate that the non-uniform distribution of irradiance exerted a significant effect on photovoltaic efficiency but a modest influence on thermal efficiency. The set of equations derived in the proposed model incorporated the thermal resistance of the individual layer of the PV/T collector.

The thermal models reviewed in this section could be suitable for the dynamic system simulation applications. However, the models did not consider the Ohmic heat generation in the PV layer and the role of therm contact resistance between different layers of the PV/T collector.

As evident from the literature studied, extensive numerical and experimental studies were carried out on PV/T systems. Although the literature can provide important tools for simulations of PV/T collectors, the deviations observed between experimental and numerical values are significant under outdoor conditions. Based on the study it has been found that the deviation in results of the experimental and numerical investigation may be due to non-consideration of the effect of thermal contact resistance and Ohmic loss at PV layer on the performance of a PV/T system in the developed models. Hence, it becomes essential to develop an accurate and comprehensive mathematical model to predict the performance of a PV/T system effectively.

2.6 Economic assessment and environmental analysis

Economic analysis of a newly developed system is a very important step to provide economic viability for its acceptance among the users. The three main parameters used in economic analysis are Cost Pay Back Time (CPBT), Internal Rate of Return (IRR), Net Present Value (NPV) and Cost of Energy (COE) generated by the developed system. CPBT is the time it takes for the system to generate enough revenue to recover the total investment cost. IRR is the discount rate above which the investment will no longer remain feasible. COE is the cost per unit of electricity generated by the system and it should be lower than the domestic electricity price of the region of interest. Majority of researchers had used these three methods for economic analysis of the PV/T systems, some of them are discussed in subsequent sections.

Due to the global impact of climate change, it becomes necessary to evaluate the energy systems in terms of carbon dioxide emission mitigation along with economic analysis. Comparison of energy systems in terms of their equivalent carbon dioxide emission and converting the amount of carbon dioxide mitigation achieved during the operation of the device into a monetary value is called Enviro-economic analysis [198].

Raman and Tiwari (2008)[199] have tested PV/T air collector in five different places of India namely Srinagar, Jodhpur, New Delhi, Mumbai and Bangalore with contrasting climatic conditions. It has been reported that climatic condition in Jodhpur is the best for the use of

hybrid photovoltaic thermal (HPV/T) air collector and energy payback time of the HPV/T without balance of system is about 2 years, it can further be reduced for places with higher solar irradiance, long sunshine hours and more number of clear days in a year. With the rate of interest as 2% and subsidy of 25%, the cost of the energy generated from HPV/T air collector is close to Rs 2 /kWh for all the places covered in the study.

Evola and Marletta (2014)[163] have discussed crucially the problems associated with optimal exploitation of PV/T technology and reported a life expectancy of 20 years for a PV/T system when the interest rate is 5%. Evola and Marletta (2014)[163] also reported that the price of electricity ranges from 0.18 to 0.24 €/kWh. Whereas, the per-unit price of the thermal energy produced by the PV/T range from 1 to 10 c€/kWh. Buonomano *et al.* (2016) [200] analyzed the economic performance of roof-integrated PV/T. The use of BIPV/T modules results in a decrease in the primary energy demands from 89% to 67%. Bianchini *et al.* (2017) [201] studied the performance of the PV/T solar plant with and without active cooling and by relating to real environmental conditions. They compared the systems using the Levelized Cost of Energy (LCOE) method to prove PV/T technology as reliable and competitive as that of separate PV and solar thermal collectors. Bianchini *et al.* (2017) [201] reported that the PV/T system could generate about 1,362 kWh/year of electricity when the rated output of the PV panels is 3.2 kWp, while thermal energy yield may vary between 443 and 267 kWh/m^2. Tse *et al.* (2016)[202] demonstrated the advantages of applying a liquid-based PV/T system over separate PV and solar thermal systems in a real office scale building to meet its electricity and hot water demand using computer program simulation. Tse *et al.* (2016) [202] reported that the discounted payback period for PV/T is 14.7 years, which was much shorter than either a PV and solar thermal collector system.

Nayak *et al.* (2012)[203] have calculated Energy Payback Time (EPBT) for hybrid PV/T solar dryer which they found to be 5.6 years, which is much less than the expected life of the dryer and reported an annual gain of 362 INR. Buker *et al.* (2014) [204] carried out a techno-economic analysis of roof-integrated PV/T system having polyethylene based heat exchanger loop beneath the PV modules using the Life Cycle Cost (LCC) method. The roof consists of 84 mono-crystalline modules of 245 W output and dimension (1652 × 994 × 46) mm. They reported that the assessed energy savings of the overall system are 10.3 MWh/year and the cost of power generation is found to be €0.0778 per kWh. It has also been reported that NPV of the system is €19456.14 at the discount rate of 8.75% over a 25-year time. As shown in **Figure 2.10** during the initial years (up to the 3rd year), cash flow is positive. However, from the 6th

year to the 11th year, it becomes negative due to inverter replacement and from 11th year onward cash flow remains positive till the end of the system's life. The payback period of the system is found to be 11 years.

To evaluate the economic feasibility of renewable energy upgrades, a variety of tests are used such as payback period, cost-benefit ratio, and return on investment. All of these tests require an estimate of the capital cost of the upgrade. However, it is not always possible to reliably estimate the capital cost of a potential energy upgrade. To deal with such situations, a new tool called reverse payback analysis or "tolerable capital cost" (TCC) method has been proposed by Nikoofard *et al.*, 2015 [205]. Because this method takes care of uncertainties associated with an investment cost of various retrofits. TCC is the capital cost that consumer can pay for an energy upgrade based on a period (in years) considered acceptable for payback, the annual savings, and the applicable annual rate of interest, and fuel cost escalation rates [205].

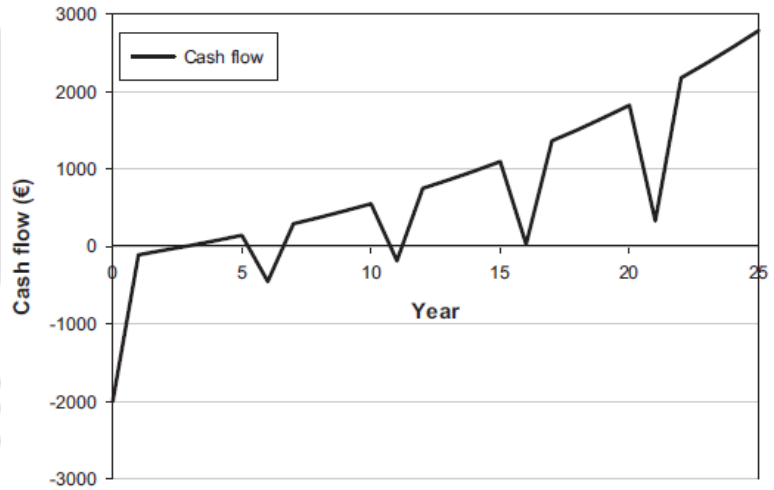

Figure 2.10. Cash-flow diagram[204]

Asaee *et al.* (2017)[206] have used the Canadian Hybrid End-use Energy and Emission Model (CHREM) to evaluate the effect of retrofitting buildings with PV modules and BIPV/T modules. Houses with south, south-east and south-west facing roofs are considered eligible for the retrofit since solar irradiation is maximum on south-facing surfaces in the northern hemisphere. The PV system consists of PV panels installed on the roof while the BIPV/T system adds a heat pump, thermal storage tank, auxiliary heater, domestic hot water heating equipment and hydronic heat delivery system, and replaces the existing heating system in the eligible houses. Finally, the PV and BIPV/T retrofits were evaluated in terms of energy

savings and reduction of GHG emissions in comparison to the "base case" values. It has been reported that the number of houses eligible for BIPV/T retrofitting is less as compared to that of PV retrofitting. However, the energy savings due to BIPV/T system retrofit is much higher compared to PV. The average energy savings per house with the BIPV/T retrofit is reported to be in the range of 90 - 120 GJ/year, whereas for PV system it is 10–15 GJ/year. The economic feasibility results show that the BIPV/T systems are more attractive as compared to PV systems with higher TCC values. The capital costs of BIPV/T systems are higher but with proper energy rebates, incentives and government subsidies, legislations (such as penalising excessive use of fossil fuels) can promote the application BIPV/T systems in larger scale[206].

It is seen from the reviewed literature that PV/T collector is observed to be an economically viable technology. PV/T's can be retrofitted into the existing buildings based on the suitability of the buildings based on criteria such as the direction of the building. PV/T is a future technology that can help combat climate change by reducing GHG emissions and also helpful in cutting down the installation area requirement.

2.7 Summary of the literature review

A range of PV/T systems has been developed by researchers from academia and industry. Numerical works have been carried out extensively on PV/T systems. In general PV/T systems are useful in the locations where high solar insolation is received throughout the year and the ambient temperature remains relatively high. PV/T in those locations can be used for meeting the electricity need together with other applications requiring thermal energy at a lower temperature. Among the available PV/T collectors (water-based, air-based, and heat pipe-based), water-based PV/T collectors are most extensively used throughout the globe due to its ease of construction and for a wide range of applications. The heat pipe integration to PV/T system design complexity, which increases the manufacturing cost. Compared to the air-based PV/Ts, the water-based PV/Ts could achieve the enhanced cooling effectiveness due to higher heat transfer coefficient and therefore both the thermal and electrical efficiencies of the systems would be higher. Tube only PV/T collectors are simple and low–cost to manufacture, because they can be put into use just after installing a PV panel and the tube only thermal absorber together, without any large alterations. To achieve better colling uniformity and enhanced power output PCM can be added with tube only PV/T collectors.

More research and development intervention is required in thermal absorber design and fabrication, coating material development, system optimization, control and reliability. These

issues need to be addressed for future market expansion of PV/T and making it a competitive renewable energy technology with existing renewable energy generation options. Some of the important conclusions that can be drawn from the literature study are as follows;

i. The sheet-and-tube is the most dominating thermal absorber fabrication technique when heat transfer fluid used is a liquid. Fluid flow pattern has a significant impact on the cooling of the PV panel and output temperature of the fluid. The web flow pattern is suitable to be used for better cooling of the PV panel.
ii. PV/T with perforated fins and double pass type PV/T based air heaters having lower channel filled with porous media are most suitable for enhancing both the electrical efficiency of the PV module and thermal efficiency of the PV/T.
iii. Graphite infused PCM along with finned configuration found to enhance the electrical efficiency of PV panel significantly. PCM based PV/T has immense potential to be integrated into building facades and can be an area of research in the future for meeting the heating load of buildings.
iv. SiC-based nanofluids with an optimized weight fraction of nanoparticles can be effectively put into use as heat transfer fluid in PV/T with an additional stirring unit. The use of nanofluid as an optical filter is an area of research that can significantly contribute in the evolution of solar PV modules, which can efficiently work in regions with higher ambient temperature and receives higher solar irradiance.
v. Heat pipe having wick is superior to that of wickless heat pipes for application in PV/T collector. The selection of working fluid is dictated by the value of freezing point, fluids with a lower freezing point are preferred to avoid the problem of freezing when heat pipes are installed in colder regions.
vi. Tolerable Capital Cost (TCC) method used for economic analysis is an appropriate method to study the economic viability of PV/T systems if retrofitted.

2.8 Research gaps

Even though the review of the literature clearly shows the advantages of PV/T collectors, further research is necessary to enhance the efficiency of the PV/T collectors for wider acceptability. Some of the areas which need attention are as follows:

- To obtain a higher fluid temperature of PV/T collector outlet, the absorber can be modified for longer retention time.
- The existing thermal models did not study the effect of thermal contact resistance and Ohmic loss in PV layer on the performance of PV/T collector.

- The uniformity of cooling is an issue identified in PV/T with tube assembly as an absorber. This can be addressed by better absorber design so that hot spots in the PV can be resolved.
- The use of PCM in PV/T is found to be useful for hot climatic areas. The issue of leakage of PCM during the melting process should be addressed. This is because encapsulating the PCM may lead to additional cost and lower heat transfer. Hence, form-stable PCM with appropriate eco-friendly matrix could be a potential candidate for an efficient thermal storage medium in solar applications.

2.9 Objectives of the present work

Based on the importance of the work the following objectives are proposed in the study

- Numerical investigation of the influence of contact resistance and Ohmic heat generation in PV/T collector with sheet and tube absorber.
- Development of PV/T collectors and optimization of absorber configurations for better cooling uniformity and efficiency.
- Process development for preparation of novel form-stable .
- Investigation of cooling uniformity and efficiency of PV/T collector using PCM biocomposite.

2.10 Summary of the chapter

This chapter thoroughly reviewed water-based, air-based, with PCM, with nanofluid as heat transfer fluid, heat pipe-based and available commercial PV/T collectors. Thermodynamic analysis of PV/T collector and enviro-economic analysis methods have been reviewed. Based on the review, a critical summary has been formulated and research gaps have been identified. Based on this objective of the thesis has been proposed. To address the objectives a suitable methodology has been devised. The methodology to address the objectives is presented in the next chapter (Chapter 3).

3

Methodology

3.1 Introduction

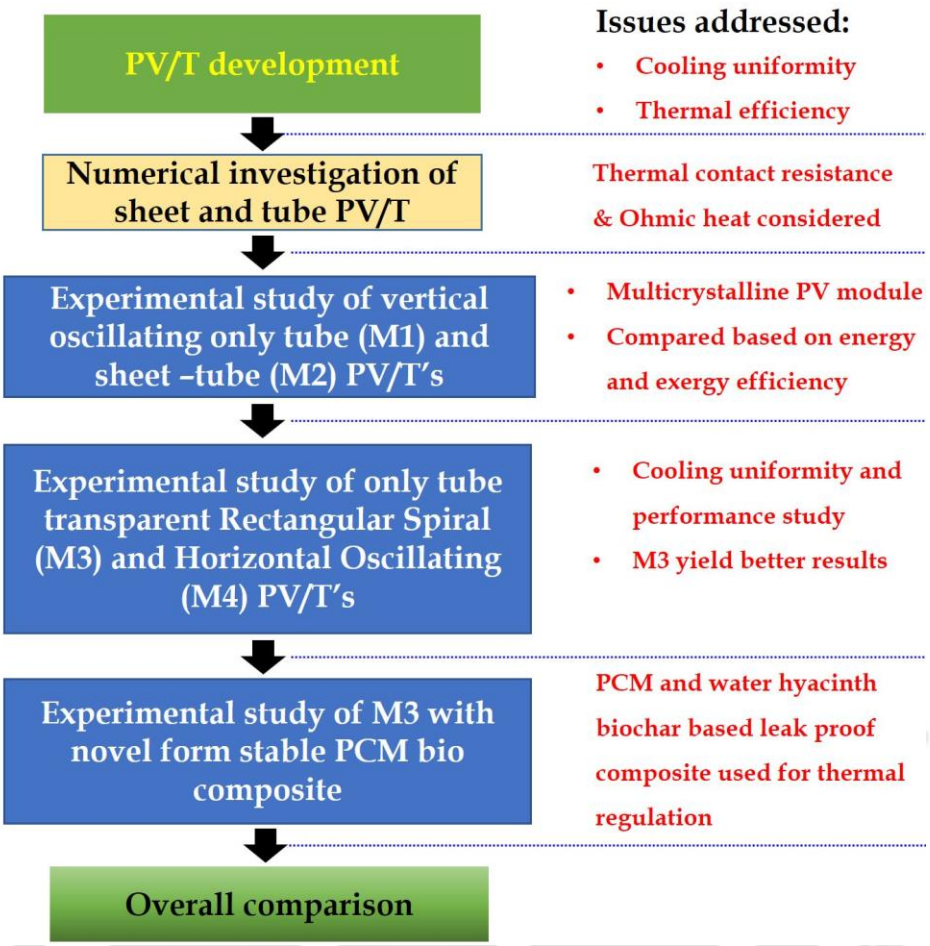

Figure 3.1. Major components of the present work

To accomplish the objectives of the present work, initially, a numerical investigation is carried out through the development of a novel thermal model for a PV/T collector. The model includes the thermal contact resistance between the layers of a PV/T collector, individual resistance of the layers and Ohmic heat generation in the PV layer. The formulation of the novel thermal model, numerical analysis and its validation is dealt with separately in Chapter 4. Based on the results of the numerical study, two PV/T collectors are developed with sheet-tube and only tube absorber configurations using multi-crystalline PV modules. The tubes are arranged in a vertical oscillating configuration in these two PV/T collectors. The oscillating configuration is one in which the tubes makes u-turn alternatively on opposite directions. Oscillating configuration can also be referred to as serpentine configuration. In vertical oscillating, the turns are in vertical direction i.e. top and bottom, while in horizontal oscillating, the turns are in right and left directions. The collectors are extensively studied primarily under outdoor conditions. The indoor test facility has also been developed to

investigate the thermal efficiency of the collectors. Following this study, two transparent PV/T collectors having rectangular spiral and horizontal oscillating absorber has been experimentally evaluated. The PV/T collector with the best results is taken forward for the subsequent study. Finally, a novel form-stable phase change material is developed using water hyacinth biochar as a matrix and integrated to the PV/T collector. The PV/T collector with novel form-stable phase change material has been experimentally investigated. This chapter will discuss the methodologies employed for the experimental expedition. **Figure 3.1** presents the work components involved in the present study.

3.2 Description of developed PV/T collectors

During this study, four PV/T collectors have been fabricated and tested as shown in **Figure 3.2** Different layers of the PV/T collectors are shown in **Figure 3.3**.

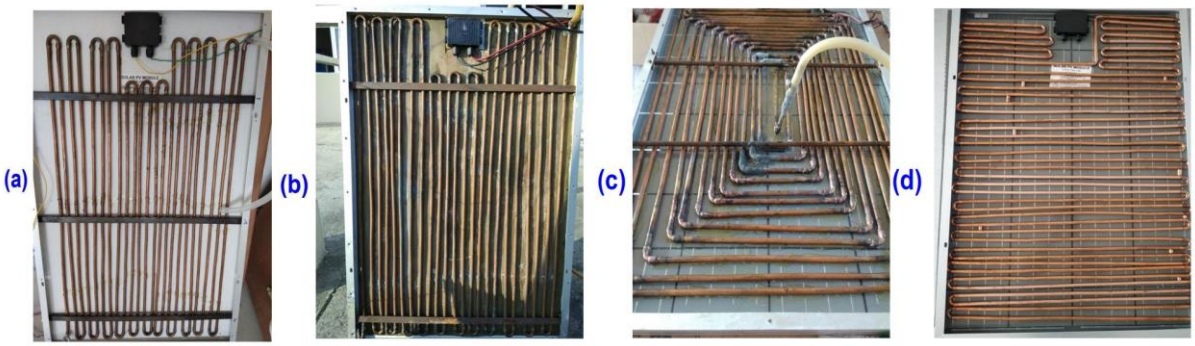

Figure 3.2. Developed PV/Ts, (a) Tube only vertical oscillating (M1); (b) Sheet-tube vertical oscillating (M2); (c) Tube only rectangular spiral transparent PV/T (M3); (d) Tube only horizontal oscillating transparent PV/T (M4)

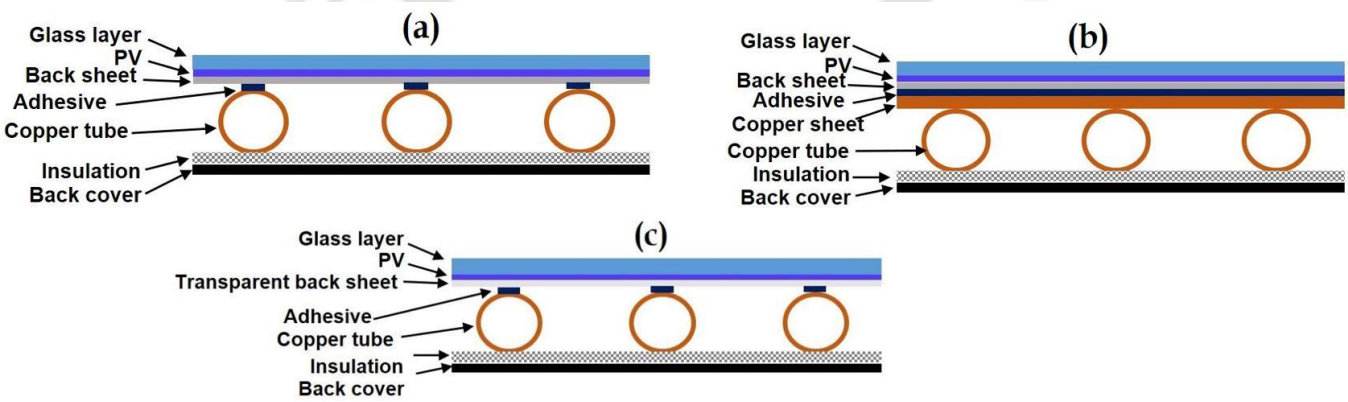

Figure 3.3. Different layers of the PV/T collectors, (a) M1 (b) M2; (c) M3 and M4

M1 and M2 represent tube only vertical oscillating and sheet-tube vertical oscillating PV/T collectors respectively. M1 has a collector with tubes directly glued to the back of the PV using transparent epoxy glue. Whereas M2 has a copper absorber plate (1 mm thick) attached to the PV backside using epoxy glue (Thermal conductivity = 0.14 W/mK) [207] and the copper tubes are brazed over the plate. An insulation layer of polyethylene foam is added to the PV/T's. Traditional multi-crystalline Silicon modules with Tedlar insulation was used in M1 and M2. Since the comparative study of M1 and M2 was carried out to study the effect of absorber sheet on the performance of the system and eliminating the absorber sheet for simplifying the configuration as well as reducing the cost. The absorber configuration of both the PV/Ts is shown in **Figure 3.4**. The tube columns have a gap of 25 mm between, smaller the gap between the tube columns better is the PV cooling and uniformity of the collector temperature field [208]. The compact arrangement of tubes enhances the heat transfer area between PV back and flowing fluid. The compactness also allows a longer flow path for fluid and providing higher retention time. After the first stage of the experimental study, two more PV/T collectors are fabricated for further study. The collectors have copper tubes arranged in a rectangular spiral (M3) and horizontal oscillating (M4) pattern. The PV modules used for M3 and M4 are transparent. The tube assembly dimensions for M3 and M4 are shown in **Figures 3.5 and 3.6,** respectively. Tubes are directly glued to the PV rear surface using an epoxy adhesive.

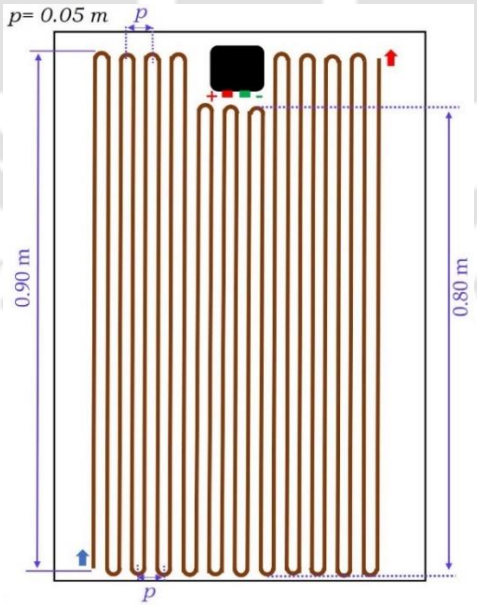

Figure 3.4. Dimensions of tube assembly for vertical oscillating PV/T's, i.e., M1 and M2

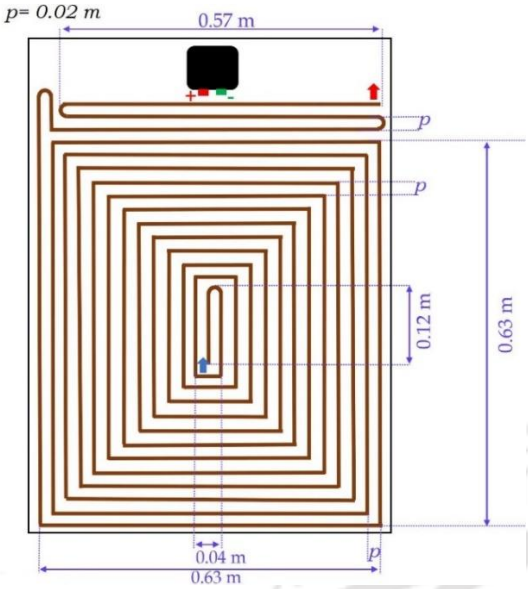

Figure 3.5. Dimensions of rectangular spiral tube assembly (M3)

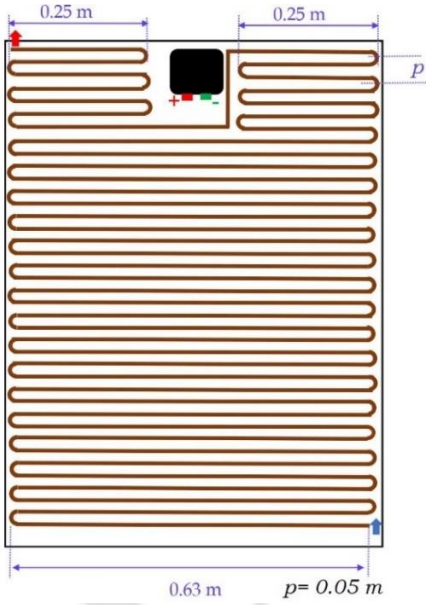

Figure 3.6. Dimensions of horizontal oscillating (M4) tube assembly (M3)

PV component used for fabrication PV/Ts is manufactured at Central Electronics Limited (Sahibabad, India). The electrical characteristics of the PV component used for fabricating the PV/T are presented in **Table 3.1**. The materials used for the fabrication of the absorber sheet is copper in M2. The tube assembly of PV/T's is made of copper tubes of diameter 3/8 inch. The back cover of the PV/T collectors is of the tin sheet.

Table 3.1 The PV module characteristics

Characteristic	Value
Dimension	1020 mm × 660 mm × 35 mm
Power rating	100 W
Number of solar cells	36
Open circuit voltage	21.40 V
Short circuit current	06.31 A
Maximum power current	05.56 A
Maximum power voltage	18.00 V
Glass thickness	3 mm
Tube material	Copper
Tube diameter	7.9 mm
Efficiency	14.5 %

3.3 Experimental methodology

Outdoor and indoor test facilities have been developed with the target of testing the PV/Ts and investigate the collector performance. The following sections discuss the experimental facilities and procedures employed during the experimental expedition.

3.3.1 Outdoor experimental facility

A series of tests were performed under dynamic outdoor conditions. The experiments were performed in Indian Institute of Technology Guwahati (26.18° N, 91.69° E).The author of the present thesis planned, designed and built the testing apparatus from scratch for the testing campaign. Open-loop testing configuration with water as heat transfer fluid has been used in the work. A large water tank (1500 litre) made of High-density polyethylene (HDPE) was used for circulating water into the collectors. This tank was placed in a shaded area, such that the temperature rise in the water is negligible. The setup contains temperature sensors, irradiance measuring device and IV analyser placed at appropriate locations. The ambient temperature, the collector temperature at the inlet and the outlet were measured with calibrated 1.5 mm K-type thermocouples. Flowrate was optimized for thermal efficiency through indoor study and maintained constant throughout the experiment at 0.015 kg/s. The global irradiance on the collector plane was measured with a pyrometer installed near the collector (Apogee Instruments/MP-100) which is installed on the collector structure by maintaining the same slope of the collectors. The weather parameters, such as wind speed and ambient temperature, are also recorded. The measuring sensors are all connected to a data acquisition unit (Keysight /34970A). The thermal image of the collectors is recorded using Testo 885 professional thermal imager. The electrical output of the collectors is measured using IV analyser (Solmetric/PVA-1000S). The list of equipment used in the experiment is presented in **Appendix I.** The developed PV/T's are compared with the PV module in which no cooling is employed. The schematic of the experimental setup is presented in **Figure 3.7**. The actual photographs of the experimental setup are shown in **Appendix IV**.

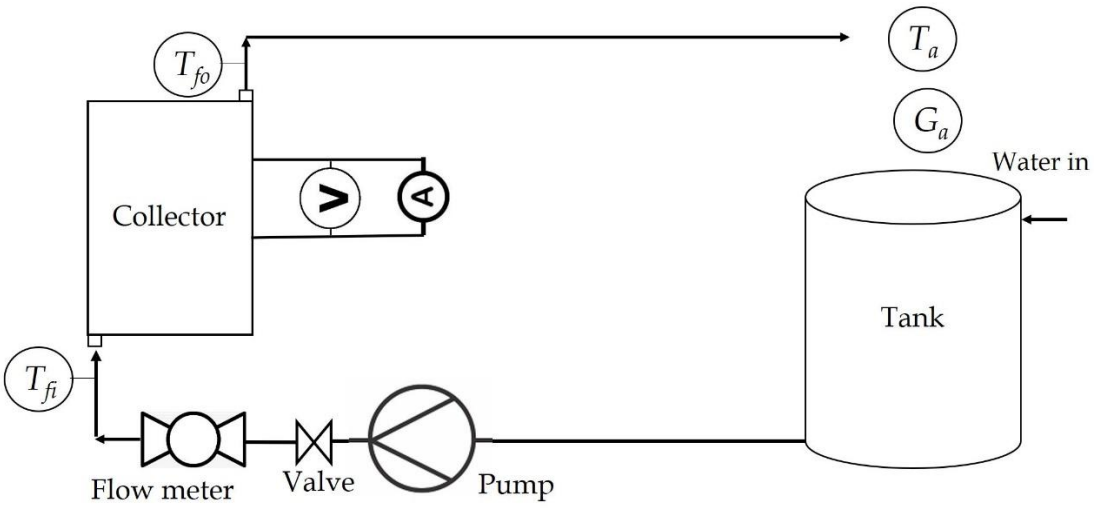

Figure 3.7. Schematic of the outdoor experimental setup

3.3.2 Indoor experimental facility

It is very difficult to evaluate solar energy under daylight due to the unsteady behaviour of solar irradiance. Therefore, most of the solar devices are tested under Standard Test Conditions (STC), which correspond to solar insolation of 1000 W/m², an Air Mass (AM) 1.5 spectrum and temperature of 25 °C at indoor facilities with the help of a solar simulator [209]**.** Solar simulators are preferred for reasons such as reliability, simplicity, and reproducibility [210,211]. A solar simulator mainly has the light field, power supply, optical filter, control elements and adjustable platform to hold the solar collector. Depending on the application, a few of the elements can be added or removed. For example, to test solar thermal devices, the optical filters are not necessary, whereas to test PV modules, filters can be mounted. Irwan *et al.* (2015) [212] successfully designed a solar simulator with halogen lamp bulbs for studying the effect of water cooling on PV module efficiency and reported that an irradiance range of 413-1016 W/m² can be achieved when 20 units of halogen lamps (Philips, 500 W;230 V) are arranged in an array of 4×5 with a gap of 0.32 m between two lamps. Meng *et al.* (2011) [213] developed a large-scale multiple-lamp solar simulator which conforms to Class B of the ASTM (American Society for Testing and Materials). The light field of the simulator consists of 188 lamps mounted on a steel frame (4.5×3.88 m), costing around 13000 USD. The irradiance on the test plane is adjusted by moving the collector test frame vertically. Solanki *et al.* (2009) [214] developed an indoor test procedure for air based PV/T collectors with sixteen tungsten halogen lamps (500 W) as light field. In this work a low cost and efficient indoor solar testing facility has been developed. The facility has all the important considerations required for a standard solar simulator. A combination of metal halide and

white LED lamps has been used to get desired irradiance level to successfully test a developed PV/T collector.

3.3.2.1 Description of indoor collector test facility

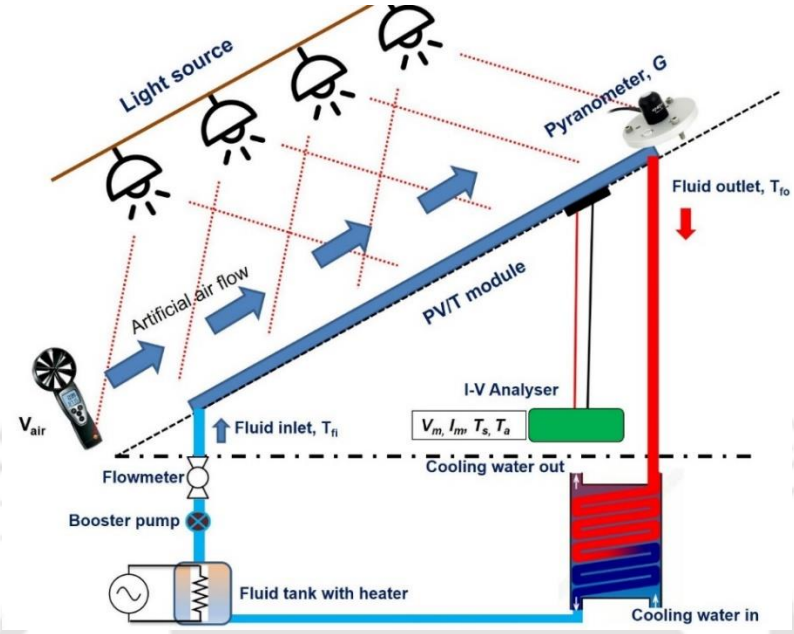

Figure 3.8. Indoor collector test setup

The test specimen is mounted on the top of the test platform, which can be adjusted for various tilt angles and distances from the light source. All the sensors are installed at various positions of the test platform during the time of the experiment. The test platform is made up of steel with an area of 2 m × 2 m. The first step involved in designing the solar simulator is to select the best light source based on the three major criteria mentioned in earlier sections. In this work, LED and metal halide lamps have been used as light sources. The irradiance value at three different positions (30 cm, 40 cm and 50 cm) from the light source has been measured. The light field has been fixed by steel structure with a tilt of 26°. **Figure 3.8** shows the schematic of the indoor solar testing facility. The indoor test is carried out in a closed loop. Arrangement of reconditioning of inlet fluid arrangements are provided in the setup and standard test protocol has been followed throughout the experiment.

In this study IEC 60904-9 has employed to study the PV characteristics and thermal efficiency under the indoor test facility. The steady-state efficiency is obtained by testing the collector over a range of inlet temperatures at global irradiance ≥ 800 W/m^2. From a practical perspective, repeatability of results from the experimental method was difficult to achieve in

an outdoor setting and the results were sensitive to environmental conditions. Therefore, the steady-state thermal efficiency test was carried out under the indoor test facility. In order to compare the thermal efficiency of the different collectors, the flow rate was kept at the same value of 0.015 kg/s during all tests. The initial temperature of inlet water was steadied, then the inlet temperature was adjusted in a range of 25–45 °C with the aid of a 1.5 kW electric heater. The range of inlet temperature was chosen such that the temperature of the fluid well within the safe limit of the pump. The ambient temperature during the test period was 26-31 °C. The steady-state collector efficiency is obtained as follows [215]:

$$\eta_{th} = \frac{\dot{m} c_p (T_{fo} - T_{fi})}{G A_c} = \eta_o - a\, T^* \tag{3.1}$$

η_o is the optical efficiency (or efficiency at zero reduced temperature, that is the efficiency achieved when the convective heat losses from the top collector temperature are zero and the radiative heat losses are negligible for low-emissivity coated collectors), and a is temperature dependent heat loss coefficient. To determine the coefficients η_o and a the thermal efficiency measured in steady-state over a range of inlet temperatures is plotted against the reduced mean temperature $T^* = \frac{(\bar{T}_f - T_a)}{G}$, where $\bar{T}_f$ is the arithmetic average of the measured inlet and outlet temperatures.

3.3.2.2 Solar simulator characteristics

Light sources and spectral distribution of solar simulator performance

Light source selection is the first and the most important part of solar simulator design, its wavelength range should be closer to that of solar irradiance spectra and should have an acceptable uniformity of irradiance on the test platform and having stable irradiance over the time of testing [216]. The reference spectra that are used across various global testing laboratories, organizations, are the "global" and "direct normal" AM 1.5 spectra. Air mass (AM) refers to the relative path length of the direct solar beam through the atmosphere.

Testing of solar devices under solar simulator dates to the 1960s, scientists and researchers tried with different light sources [217]. Carbon arc lamps, quartz-tungsten halogen lamps, sodium vapour lamps, argon arc lamps, mercury xenon lamps, xenon flash lamps,

xenon arc, metal halide lamps, LED and supercontinuum laser light sources were used in the past [218]. Fast advances in high-intensity light-emitting diodes (LEDs) have given adequate apparatuses to LED-based indoor solar test systems to precisely imitate the sun. LEDs offer numerous advantages over lamp-based technology currently used. However, these advantages have not been harnessed because of limitations in creating a solar simulator with the highest rating (AAA) for spectral match, temporal stability, and light uniformity. An LED is a solid-state light source that emits light via electroluminescence over a narrow range of the electromagnetic spectrum (30-50 nm). The parallel combination of unique LEDs can be used to match the AM1.5G spectrum in addition to allowing output control of the light source with a 30-50 nm resolution [219–222]. LED-based simulator produced a more stable, flexible, and accurate match to AM1.5G than the xenon lamp with similar marks in the quality of the PV cell response [223]. **Figure 3.9** shows an approximate comparison of various lamp spectrum with sunlight spectrum.

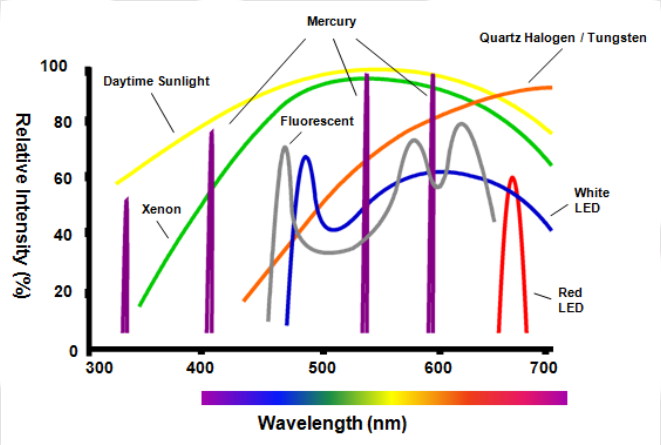

Figure 3.9. Comparison of spectrum of different light sources with sunlight spectrum [224]

To give a replacement to daylight, Metal-halide lamps and white LED lamps are used for the construction of the solar simulator light field. The solar simulator consists of 3 Metal-halide lamps and 6 white LED lamps and arranged, as shown in **Figure 3.10.** This facility uses metal halide lamps and white LED lamps to generate a spectrum equivalent to daylight. The Metal-halide lamps have a power rating of 400 W while that of white LED lamps is 200 W. The amount of irradiance in the irradiated surface is controlled by changing the distance between the lamp field and test stand. An approximate comparison between the spectrum of the indoor test facility and the solar spectrum is shown in **Figure 3.11.**

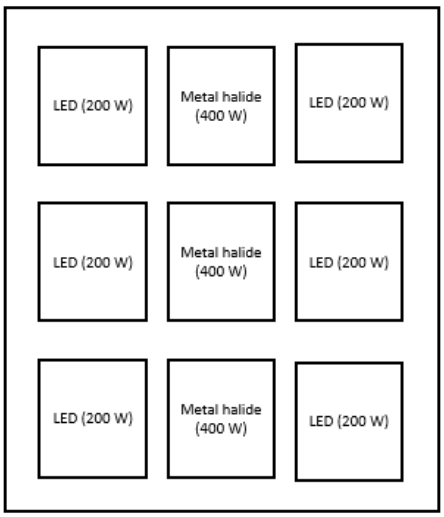

Figure 3.10. Light field arrangement

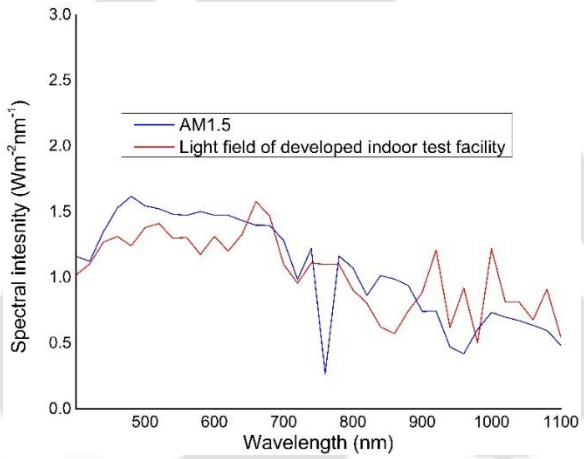

Figure 3.11. Spectral intensity comparison

Of the total solar irradiance that reaches the earth's surface, infrared radiation makes up 49.4% while visible light makes 42.3%. Ultraviolet radiation makes up just over 8% of the total solar radiation [225]. For the accurate design of the solar simulator, the wavelength of radiation below 300 nm and above 2500 nm is not required. The spectral match with daylight is extremely important for accurate testing of collectors under indoor condition. The spectral distribution was evaluated to see how well the spectral distribution matches a reference distribution between 400 nm and 1100 nm when partitioned into six intervals. The deviation of the spectrum generated by the light field of the indoor test facility against the AM1.5G spectrum integrated along each one of the wavelengths intervals specified in the standard: 400–500 nm, 500–600 nm, 600–700 nm, 700–800 nm, 800–900 nm, and 900–1100 nm [226]. The

spectral match is defined as the ratio of the required irradiation percentage to the real percentage of light falling along the respective wavelength interval [227]. Spectral match comparison for indoor solar collector testing facility is presented in **Table 3.2**.

Table 3.2 Spectral match comparison for indoor solar collector testing facility

Wavelength range (nm)	Percentage of total irradiance AM1.5G (%)	Indoor facility (%)	Spectral match
400-500	18.4	12.4	0.68
500-600	19.9	13.6	0.68
600-700	18.4	16.5	0.90
700-800	14.9	14.7	0.99
800-900	12.5	11.7	0.94
900-1100	15.9	31.0	1.95

From the above table, it can be seen that spectral match varies in each range of wavelength. The spectral match found to be in the range of 0.68-1.95, this range corresponds to Class C solar simulator category under all prescribed International standards.

Spatial difference or non-uniformity

For defining non-uniformity of irradiance a wooden board with a white top is shaped rectangular to act as the test area of the dimension 1.2 m × 0.9 m. It consists of 48 squares of dimension 15 cm × 15 cm, i.e., 11 rows, 6 columns and 63 experimental points. This is presented in **Figure 3.12**.

Spatial non-uniformity (SNU) is the hardest property that minimizes hot spots due to concentration of light in certain points, especially in simulators with large surface areas. This may result in localised heating of the cells, thus non-uniformity should be minimized. It can be calculated as follows [213]

$$\text{Non-uniformity}\ (\%) = \frac{E_{\max} - E_{\min}}{E_{\max} + E_{\min}} \times 100\% \tag{3.2}$$

where $E_{\max}$ is the maximum irradiance measured by the pyranometer over the target test area in W/m^2 , and, $E_{\min}$ is the minimum irradiance measured by a detector(s) over the target test area in W/m^2.

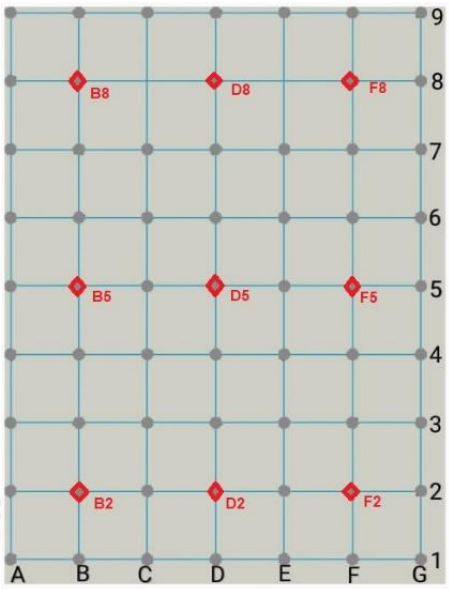

Figure 3.12. Construction of grid for characterization of the solar simulator

Average irradiance and the long term average temporal stability are important for solar thermal applications. **Figure 3.13 – 3.15** shows the irradiance distribution on the test plane at a distance of 30 cm, 40 cm and 50 cm, respectively. It has been observed that the non-uniformity increases as the gap are reduced between the lamps and the test plane. The non-uniformity is found to be 11.7 %, 5.71 % and 4.16 % at distances of 30 cm, 40 cm and 50 cm, respectively.

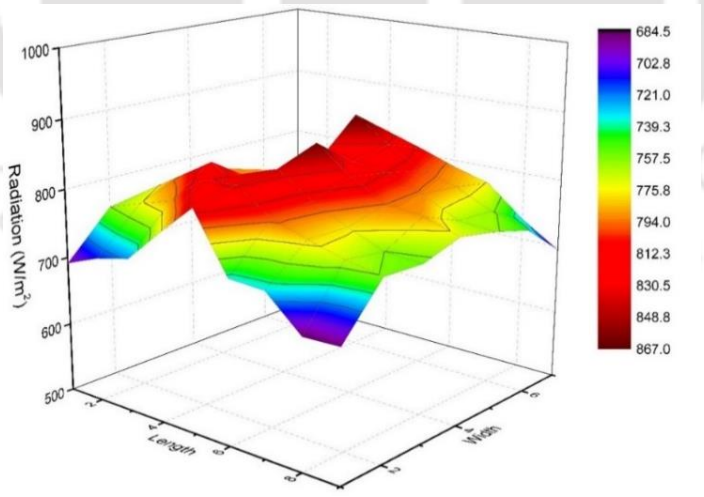

Figure 3.13. Irradiance distribution on the test plane at a distance of 30 cm from light field

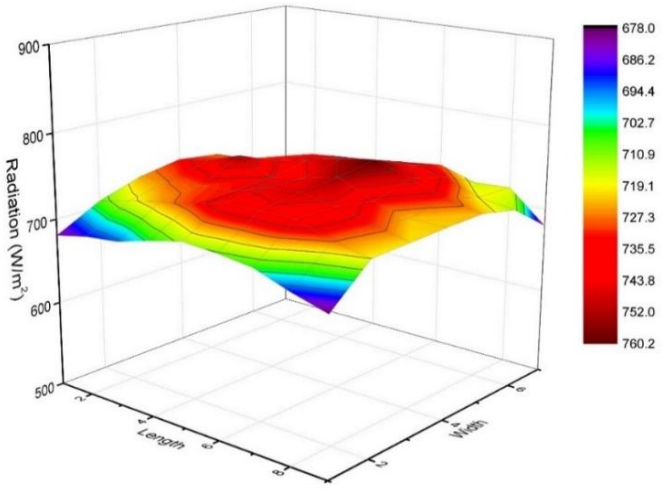

Figure 3.14. Irradiance distribution on the test plane at a distance of 40 cm from light field

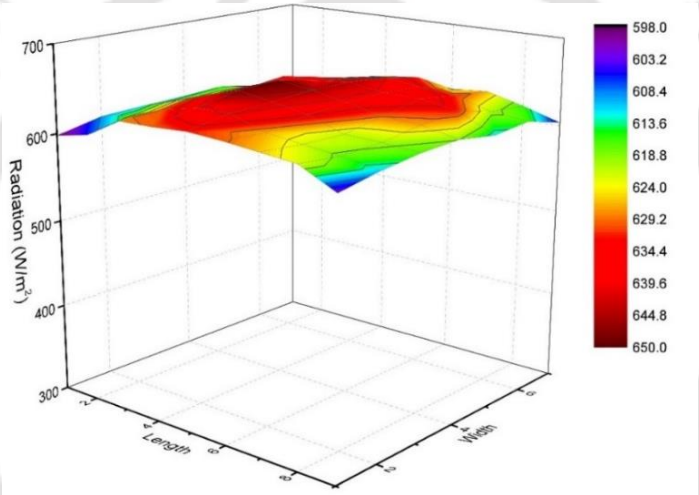

Figure 3.15. Irradiance distribution on the test plane at a distance of 50 cm from light field

Temporal constancy or instability

Ten points are considered here for temporal stability test. These points are chosen in a special manner considering the position of the lamps to get the overall perspective of this characterization. The selected points are shown as red dots in **Figure 3.11.** At an interval of 1 minute, data has been logged using a pyranometer over a duration of 2 hr for individual point. The temporal instability is the maximum relative error at the selected particular point on the target area over the nominated time of data acquisition, which is expressed using the following equation [213]

$$\text{Temporal instability } (\%) = \frac{E'_{max} - E'_{min}}{E'_{max} + E'_{min}} \times 100\ \% \tag{3.3}$$

where E'_{max} is the maximum irradiance at the selected point on the target area during the nominated time, and E'_{min} is the minimum irradiance at the selected point on the target area during the nominated time, both measured in W/m^2.

It has been observed from **Figure 3.16**, that the irradiance on the points along the central section is higher as compared to the points on the edges. However, the variation of irradiance in all the representative points considered for temporal instability is not significant. The temporal instability of irradiation at the points along the centre line, i.e., B5 (Left of centre), D5 (Centre point) and F5 (Right of the centre) are 1.46 %, 1.46 % and 1.16 % respectively.

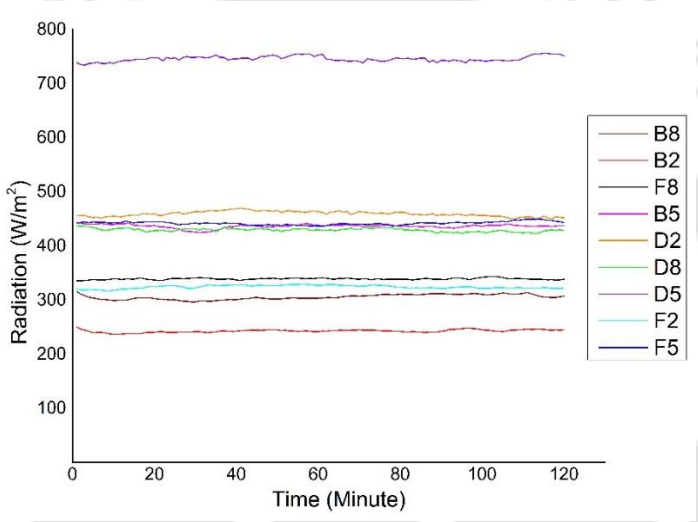

Figure 3.16. Temporal instability at selected points on the test plane

3.3.2.3 Standards of solar simulators

Around the world, there are several standard test procedures available for PV testing, which are mentioned in **Table 3.3.** According to ASTM E927 and IEC 60904-9, solar simulators are defined under three classes; Class A, Class B and Class C; this is given in **Table 3.4**. Based on the characteristics discussed, the developed indoor test facility comes within category C based on spectral match and category B based on irradiance spatial non-uniformity at distance 40 cm and 50 cm of the test plane from the light field. The developed indoor test facility comes under category C at 30 cm distance between the test plane and light field. Thermal instability in all cases conforms to category A. When evaluating the test facility based on all three characteristics it comes under Category C of all the standards mentioned in **Table 3.4**.

Table 3.3 International standard references for solar simulator

Organization	*Standard*	*Description of the standard*
International Engineering Consortium (IEC)	*IEC 60904-9*	*Requirements for solar simulators used for indoor testing of terrestrial flat plate (non-concentrating) photovoltaic devices in conjunction with a spectrally matched reference device.* [228]
American Society for Testing and Materials (ASTM)	*ASTM G173-03*	*Air Mass 1.5 reference solar spectral irradiance* [229]
	ASTM E927-05	*Specification for Terrestrial PV Testing with solar simulator* [230].
	ASTM E927-10	*Standard specification for Solar Simulation for Photovoltaic Testing* [231].
	ASTM E948-16	*Standard Test Method for Electrical Performance of Photovoltaic Cells Using Reference Cells Under Simulated Sunlight* [232]
	ASTM E973-16	*Standard Test Method for Determination of the Spectral Mismatch Parameter between a Photovoltaic Device and a Photovoltaic Reference Cell* [233]
Japanese Industrial Standards	*JIS C 8912*	*Solar simulators for crystalline solar cells and modules* [234]

Table 3.4 Categories of Solar simulators

Category	*Spectral Match*			*Irradiance spatial non-uniformity*			*Temporal instability*		
	ASTM	**IEC**	**JIS**	**ASTM**	**IEC**	**JIS**	**ASTM**	**IEC**	**JIS**
Class A	0.75-1.25	0.75-1.25	0.75-1.25	≤2%	≤2%	≤2%	≤2%	≤2%	≤1%
Class B	0.6-1.4	0.6-1.4	0.6-1.4	≤5%	≤5%	≤3%	≤5%	≤5%	≤3%
Class C	0.4-2.0	0.4-2.0	0.4-2.0	≤10%	≤10%	≤10%	≤10%	≤10%	≤10%

3.4 Development of novel form-stable PCM-biocomposite and its integration to rectangular spiral PV/T (M3) collector

The uniformity of cooling and temperature of the outlet fluid are the two major parameters that should be taken care of while selecting the absorber configuration. Cooling uniformity of PV/T is always a concern for the researcher working in the field of PV/T. Achieving full surface uniformity of cooling is difficult when water is used as a working fluid which flows through the tubes. Water-based PV/T collectors can be broadly classified into sheet-tube, tube only and channel flow types. Channel flow type PV/T has the risk of cell damage if fluid comes in direct contact. Sheet-tube configuration has higher thermal resistance as compared to tube only PV/T [12]. Whereas, the tube only PV/T collectors have the limitation of not covering the entire PV surface with tubes due to material constraints. One of the promising solutions to the cooling uniformity challenge is the application of PCM in PV modules. PCMs are proposed for use in PV modules to limit the cell temperature by absorbing heat during melting. The most important criteria followed for selecting PCM is its melting point. PCM with an adjustable melting point is necessary for solar applications. The melting point of PCM lies above 15 °C and below 90 °C, which is suitable for solar heating as well as for heat load-levelling applications. The direct employment of PCMs has a long-standing bottleneck for large energy harvesting capacity due to leakage above the normal melting temperature and low heat transfer performance. Consequently, it hinders the heat transfer within PCMs and sluggish the movement of phase-transition interfaces and energy absorb/release rate thereby restraining on-time energy charging. To resolve the above problems, the shape-stabilized PCMs composites were prepared. In the form-stable PCM composites, the PCMs could be encapsulated by some materials, which have a porous structure, large surface area and great thermal stability, such as mesoporous silica, activated carbon, diatomite and so on [235–239]. The development of sustainable, and "green" composites for PCMs is an essential route for their large-scale production. In response to the call for fabricating highly value-added supporting materials and preventing seepage of PCMs, biochars have been introduced for the adsorption of organic PCMs [240].

Organic PCM exhibits many favourable characteristics, such as it is chemically inert, non-corrosive, durable, abundantly available, ecologically harmless and nontoxic[241]. The PCM selected in this study for making composite is OM35 having a nominal melting temperature of 35 °C [242]. It is an organic PCM and qualifies above mentioned criteria's. The optimum temperature range of PCM for use in PV/T is 30-45 °C [243]. The thermal properties

degrade after a certain number of melting/solidification cycles (referred to as thermal cycle), in case of OM35 thermal properties remains stable up to 2000 cycles [244]. If the PCM has a melting temperature below the average ambient temperature, the frequency of thermal cycle will be higher and replacement of PCM should be carried out at a shorter interval over the life of the PV/T. Since the cooling requirement is not necessary during the winters when the PV module temperature remains lower. The PCM is selected such that its melting temperature is close to the ambient temperature during the summer days when cooling of the module is actually essential. PCMs which have all the mentioned characteristics, they still need to be low-cost, while the truth is that currently commercial PCMs with high performance are very expensive [241]. The OM35 is easily available in the Indian market at a lower cost, which makes its application in PV/T economically viable.

Biochar produced from water hyacinth through pyrolysis process has been used as encapsulant material in the composite. Biochar is a solid residue with high carbon content obtained during the pyrolysis of biomass, could be one of the most adaptable materials applied in the field of current energy storage because of its flexible surface properties, porosity, abundancy and carbon-neutral nature [245]. This study discusses the characteristics and applicability of eco-friendly and cost-effective biochar having high porosity prepared from water hyacinth (Scientific name: *Eichornia crassipes*; Local name: *Meteka*). Water hyacinth is an invasive aquatic plant which forms a dense mat on the water surface, this increases more nutrient absorption from the water thus reducing light penetration and limiting the productivity of phytoplankton [246,247]. The water hyacinth also reduces the level of dissolved oxygen concentration by preventing oxygen transfer from the air and the reduced effects of mixing [248]. The use of water hyacinth biochar as the matrix for the PCM-biocomposite is a sustainable way to tackle this invasive weed and lower its harmful effects on the aquatic ecosystem. The porous nature of the biochar produced from water hyacinth makes it an excellent candidate for the matrix in the PCM-biocomposite. The form-stable PCM-biocomposite has been produced by direct impregnation method and characterised. **Figure 3.17** shows the schematic illustration of PCM- biocomposite. The thermal and physical properties of the PCM- biocomposite will be discussed thoroughly in *Chapter 5*.

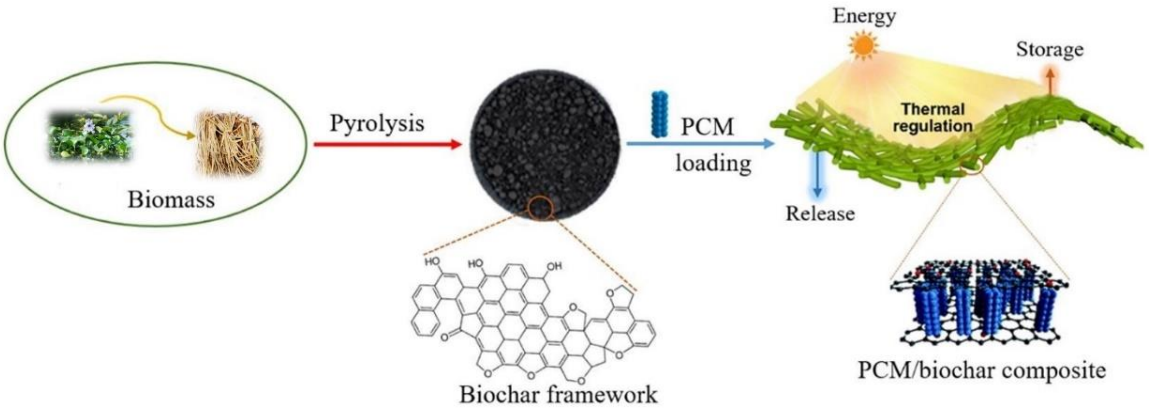

Figure 3.17. Schematic illustration of PCM-biocomposite synthesis from biochars [240]

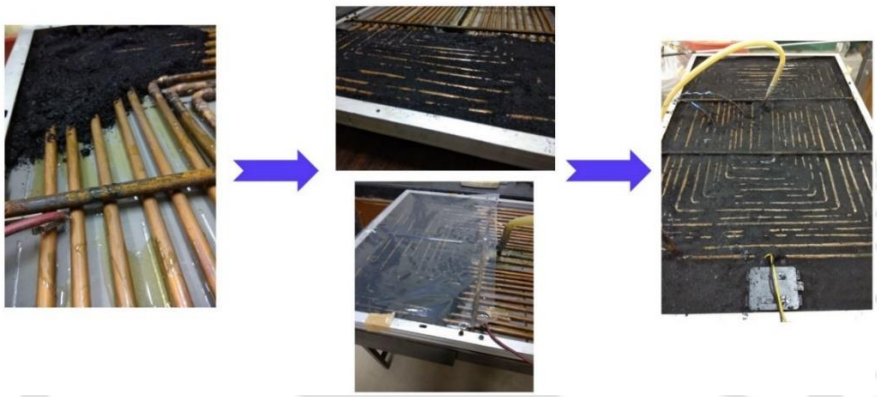

Figure 3.18. Steps of incorporating PCM-biocomposite

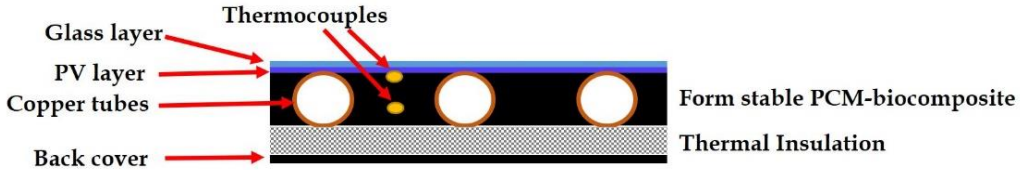

Figure 3.19. Cross-sectional view of developed PV/T collector

The composite presented in this study has the potential to solve the major limitations viz. leakage and lower thermal conductivity associated with pure PCM. The issue of thermal conductivity is addressed using Aluminium powder (5% by weight) to the composite. Maintaining the temperature of the module at an optimum level is the aim of this study. The PV/T with a layer of form-stable PCM-biocomposite is tested under outdoor conditions. In this stage of the study PV/T collector with rectangular spiral absorber configuration (M3) having novel PCM-water hyacinth biochar composite (*referred to as PCM-biocomposite*) embedded to it has been fabricated and studied. The collector M3 is selected based on the

results of the previous study. The PV/T collector is compared with PV of similar specifications as that used in PV/T. A preliminary experimental investigation is also carried out without employing the novel PCM- biocomposite material into the PV/T. After fixing the tube assembly onto the PV surface, a 10 mm thick layer of PCM- biocomposite is inserted, as shown in **Figure 3.18.** The PCM-biocomposite is inserted from a corner and diagonally filled up. It is recommended to immediately cover the PCM-biocomposite after putting into the PV/T to avoid absorption of moisture from the air. Once the PCM- biocomposite is applied, an insulation layer of Polyethylene foam sheet is added to the system. Finally, a plexiglass back cover is integrated to protect the collector from climatic parameters such as moisture, duct and wind. Two T-type thermocouples are placed in the heat storage material layer, one at 4 mm and other at 9 mm from the rear surface of the PV/T as seen from the cross-sectional view in **Figure 3.19**.

3.4.1 Preparation of form-stable PCM-biocomposite

The water hyacinth plant is collected from the waterbodies in the locality of Guwahati. The biomass is dried for 24 hours in a hot air oven at 105 °C. The dried biomass is then ground to a powder with particle size 2 mm and pyrolyze in a fixed batch bed reactor. The pyrolysis is done at a temperature of 550 °C at a heating rate of 10°C min^{-1} for the residence time of 1 hour with the supply of Argon gas to provide an inert atmosphere. The biochar produced is abbreviated as (WH 550) and is used for making the biocomposite. The organic PCM (savE® OM 35) is purchased from Pluss Advanced Technologies, which has a melting temperature range of 35-39 ˚C [249]. The PCM-biochar composite material is manufactured via direct impregnation method. Six different mass ratios of PCM and biochar are selected to optimize, which would give better results in terms of stability, leakage test and conductivity. The PCM-biochar (PCM: WH 550) mixture ratio is taken as 4:6, 5:5, 6:4, 7:3, 8:2 and 9:1 (w/w%) respectively. The PCM and biochar are put in a glass beaker with mouth covered in aluminium foil and put inside a hot air oven for 16 hours at a set temperature of 50 ˚C. The mixture is stirred at an interval of 4 hrs to achieve the desired homogeneity. After 16 hours, the samples are taken out from the oven and cool to room temperature by natural air cooling. The entire process starting from biochar to bio-composite preparation is shown in **Figure 3.20**.

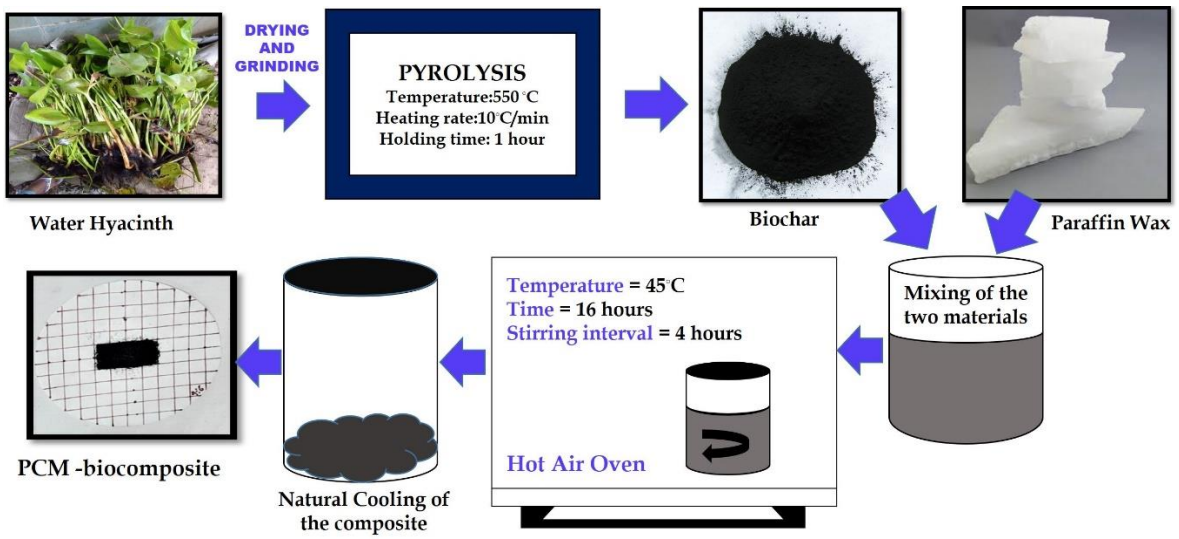

Figure 3.20. Steps of PCM-biocomposite preparation

3.4.2 Characterization of the novel PCM-biocomposite material

3.4.2.1 Leakage test

The leakage test for all the samples was carried out by putting the samples on filter paper with gridlines. The gridlines were drawn on the filter paper, which divided the circular filter paper (12.5 cm in diameter) into squares of known dimensions (1 cm^2). The samples were kept in a hot air oven for 30 minutes at 40°C and then place on the filter paper. The total area of each filter paper was 122.72 cm^2. The PCM-biochar samples were placed within an initial area of 8 cm^2 at the centre of the filter paper and observed for any leakage of the PCM material from the initial stage. The most form-stable sample is chosen for further characterization. Aluminium metal powder (5% by weight) has been added additionally to the most form-stable sample to enhance the thermal conductivity.

3.4.2.2 Characterization techniques

The surface morphologies of the materials were analysed using Field Emission Scanning Electron Microscope (FESEM) (Make: Zeiss, Model: Sigma). Crystallinity and phase change identification was analysed using X-ray powder diffraction(XRD) (Model No: D8 Advance, Make: Bruker, Netherlands). The XRD measurements were done using Cu Kα (λ = 0.05°/s, 1.54,056 nm) radiation a step size of 0.05° in the 2 theta degree range of 10° to 70° is employed while scanning the samples. Functional groups were identified by a Fourier transform infrared spectrometry (FTIR, Nicolet iS10, Thermo Scientific, USA) the scanning scan range was from 4000 cm^{-1} to 500 cm^{-1}. Thermal conductivity meter used in this work was a KD2 Pro. The KD2 Pro thermal conductivity meter has a needle of length 10 cm long and 2.4

mm diameter with a measurement range of 0.02 to 2.00 W/mK. Thermal stability was determined using high-temperature Thermo Gravimetric (TG) System (Make: Netzsch, Model: STA449F3A00) at a heating rate of 10 °C/min from 20° to 500 °C using Nitrogen. The Differential scanning calorimetry (DSC) experiments were performed using the same equipment under similar conditions. The characteristic temperatures and heat of fusion were determined from the DSC peaks using a standard tangent method. Charging and discharging time estimation has also been carried out for the PCM and PCM-biocomposite. A fixed amount of pure PCM and PCM-biocomposite is put in a cylinder and heated inside a hot air oven at 40 °C. The temperature of the samples was noted at various intervals by placing a thermocouple into the sample. Once the sample reached the melting temperature and temperature of the sample steadied, it was removed from the oven and kept in the room temperature and measured the temperature of the sample. The two samples were compared based on the time it took to reach the melting temperature from the room temperature and to reached back the room temperature from the melting temperature. Airflow was restricted in the room during the experiment to avoid errors in the measurement.

3.5 Energetic and exergetic analysis

The PV/T collectors have been evaluated by energetic and exergetic analysis. The basic formulations used are presented in this section.

3.5.1 Energy analysis

Energy analysis includes calculation of electrical efficiency of the PV module, thermal efficiency of the thermal absorber and overall efficiency of the PV/T.

Electrical efficiency is defined as the ratio of the maximum electrical power output of the photovoltaic module to the effective solar irradiance energy reaching the photovoltaic module surface. Electrical efficiency can be calculated using the following expression [159,250];

$$\eta_{el} = \frac{P_m}{A_C G} = \frac{V_m \times I_m}{A_C G} \tag{3.4}$$

where A_C and G are collector area (m^2) and solar irradiance (W/m^2) respectively.

The thermal efficiency is defined as the ratio of useful thermal energy absorbed by the collector and the amount of solar energy incident on the collector surface; it is expressed as [192] ;

$$\eta_{th} = \frac{\dot{m} c_p \left(T_{fo} - T_{fi}\right)}{A_C G} \tag{3.5}$$

Thus the overall energetic efficiency is expressed as follows,

$$\eta_{en} = \eta_{th} + \eta_{el} \tag{3.6}$$

3.5.2 Exergy analysis

In PV/T collector part of incoming solar energy is converted to electricity with high exergy content, and the remaining into heat [251]. This analysis gives the maximum amount of work that can be extracted from a given collector at some given condition with respect to the surrounding. For a system, the exergy balance equation is given by [252];

$$\dot{E}x_{in} = \dot{E}x_{out} + \dot{E}x_{loss} \tag{3.7}$$

Total exergy input is given by the following equation [253–255];

$$\dot{E}x_{in} = A_c G \left[1 - \frac{4}{3}\left(\frac{T_a}{T_{sun}}\right) + \frac{1}{3}\left(\frac{T_a}{T_{sun}}\right)^4\right] \tag{3.8}$$

The total exergy output is the amount of exergy extracted from the solar radiation falling on the system. It is the combination of electrical exergy generated by PV and thermal exergy which is recovered by the absorber plate; mathematically it can be expressed as;

$$\dot{E}x_{out} = \dot{E}x_{el} + \dot{E}x_{th} \tag{3.9}$$

The thermal exergy of a collector depends upon the useful heat recovered from the output heated water [256], and it is given by;

$$\dot{E}x_{th} = \dot{Q}_u \left[1 - \frac{T_a + 273}{T_{fo} + 273}\right] \tag{3.10}$$

The electrical exergy is the maximum power extracted from the solar radiation by the PV module and is given by;

$$\dot{E}x_{el} = V_m \times I_m \tag{3.11}$$

The overall exergetic efficiency of a PV/T is given as;

$$\eta_{ex} = \frac{\dot{E}x_{out}}{\dot{E}x_{in}} \tag{3.12}$$

3.6 Economic assessment and environmental analysis

The high initial cost is a bottleneck to widespread commercial use of solar PV/Ts. It is therefore required to do an economic analysis, which is usually specific to the technology of the solar modules, solar irradiance and climate at the installation site, load pattern profile, bank interest rates and the cost of conventional sources of energy. The total cost of a solar PV/T collector involves material costs and installation costs, the break-up cost of individual components is presented in **Table 3.5** and **Figure 3.22**. The benefits of the system are the electricity and thermal energy generated using the PV/T system. To systematically carry out an economic evaluation of PV/T collector, there is a need to obtain the average conversion efficiency, other relative cost factors to it, throughout its estimated life cycle or duration of its fine working period (days). In the present work average electrical and thermal efficiencies has been used to compute the useful energy generated from the collectors. An efficiency reduction of 0.3%/year has been considered for both electrical and thermal efficiency. The climatic data of the year 2018 for Guwahati, Assam, India (**Figure 3.21**) has been considered for economic analysis. The initial investment on PV/Ts has been found out by summing up the cost of the PV component, copper tubing, adhesives, insulations, battery, charge controller and other components. The economic parameters *viz.* Net Present Value (NPV), Internal Rate of Return (IRR), Levelised Production Costs (LPC) and Environmental cost, are calculated for each case. NPV has been calculated using the average inflation rate from the last twenty years data as shown in **Figure 3.23**. NPV is calculated at varying discount rate by keeping the inflation rate constant. LPC for the collectors has been computed at three inflation rates by maintaining the discount rate constant at the current.

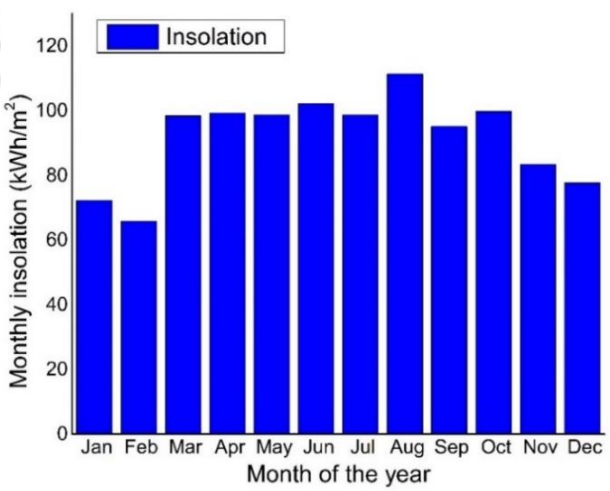

Figure 3.21. Monthly solar irradiance data for the year 2018 at Guwahati, Assam, India

Table 3.5 The breakdown cost of PV/T collectors and other components (all cost in INR)

	PV	Tubing	Absorber sheet	Epoxy glue	Insulation	Back cover	Piping	Valves	Flowmeter	PCM bio-composite	Cable cost	Battery	Charge controller	Installation cost	Total
M1	5400	4226	0	500	420	180	640	350	1200	0	680	8300	1050	1500	**24446**
M2	5400	4226	5250	1000	420	180	640	350	1200	0	680	8300	1050	1500	**30196**
M3	6200	4301	0	500	420	180	640	350	1200	0	680	8300	1050	1500	**25321**
M4	6200	4955	0	500	420	180	640	350	1200	0	680	8300	1050	1500	**25975**
M3+PCM bio-composite	6200	4301	0	500	420	180	640	350	1200	1772	680	8300	1050	1500	**27093**

** The following table is obtained from a survey performed in the Indian market.*

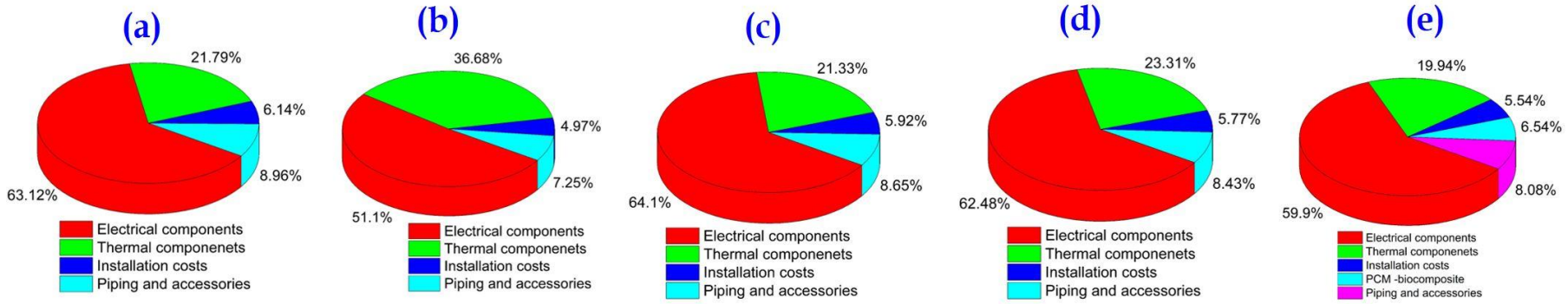

Figure.3.22. Cost break-down of the PV/Ts, (a) M1; (b) M2; (c) M3; (d) M4; (e) M3 with PCM-biocomposite

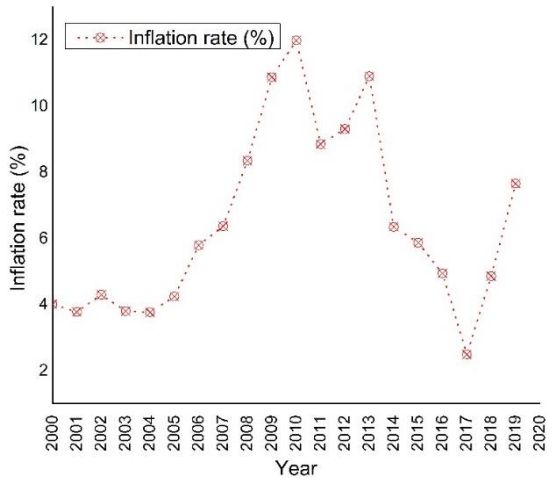

Figure.3.23. Inflation rate of India in last 20 years[257]

3.6.1 Net Present Value (NPV)

The NPV consider the time value of benefits. The net present value method achieves this by quantifying the impact of time on any particular future cash flow. The present value (PV) is determined by using an assumed interest rate, usually referred to as a discount rate. The NPV method calculates the present value of all the yearly cash flows (i.e. capital costs and net savings) incurred or accrued throughout the life of a project and summates them. Costs are represented as a negative value and savings as a positive value. The sum of all the present values is known as the net present value (NPV). The higher the net present value, the more attractive the proposed project. The net present value (NPV) represents the cumulative cost of the system over its lifetime and is calculated as the sum of the capital cost C_o and the present worth value of the annualised costs for each year of operation S accounting for the energy savings;

$$NPV_n = C_o + \sum_{n=1}^{n}\left(\frac{S(1+i)^{n-1}}{(1+d)^n}\right) \tag{3.13}$$

where d is the discount rate and i is the inflation rate. The inflation rate has been taken as an averaged value of the yearly inflation rate from 2000 to 2019. The economic assessment is also carried out considering the highest, lowest and base inflation rate scenario.

3.6.2 Internal Rate of Return

It is the discount rate which must be applied, to achieve a net present value of zero. This can be obtained from the plot of NPV versus the discount rate.

3.6.3 Levelised production costs

The system costs are divided into capital costs and annual incurred running costs. Levelised production cost can be computed by dividing the summation of the present worth of all annual non-revenue cash flows ($NPV_{n,NR}$) by the annualized production rate with an adjustment. The annual non-revenue cash flow is comprised of the operations and maintenance (OM) costs and replacement costs. The systems will be compared in terms of their levelised production costs of combined heat and power, over an assumed 20-year system lifetime. Levelised production costs can be calculated as,

$$LPC = \frac{NPV_{n,NR}}{\sum_{n=1}^{n}\left(\frac{Q}{(1+d)^n}\right)} \tag{3.14}$$

where Q is the sum of the annual production of electrical and thermal energy. The levelised cost and payback time of the system is highly dependent on the choice of discount rate for the analysis.

3.6.4 Enviroeconomic analysis

In this study, enviroeconomic analysis is carried out to see how much energy produced by solar energy in the system prevented CO_2 emissions. Determination of a carbon price is an important tool in the mitigation of the national emission of greenhouse gases. CO_2 mitigation per annum from PV/T can be calculated using equation [198];

$$\phi_{CO_2} = \frac{\psi_{CO_2} \times Q_{overall}}{10^3} \tag{3.15}$$

where ϕ_{CO_2} is tons of CO_2 mitigated by PV/T system per annum, ψ_{CO_2} is the average CO_2 which is released into the atmosphere for electricity generation from coal-based power plants and $Q_{overall}$ is the annual energy produced (kWh) from the PV/T system. The amount of carbon dioxide released per unit of electricity generation in India ranges from 0.61 kg/kWh to 1.0 kg/kWh [258]. Thus, the environmental cost is calculated by using the following relationship [198];

$$Z_{CO_2} = z_{CO_2} \times \phi_{CO_2} \tag{3.16}$$

where Z_{CO_2} is the environmental cost CO_2 mitigation price, z_{CO_2} is the price per ton of CO_2. The carbon price in this study considered to be 14.5$/t$CO_2$ (1072 INR/tCO_2, considering USD to INR conversion rate on 11th November 2020)[259].

3.7 Summary of the chapter

The chapter presents the experimental methodology and procedures (outdoor and indoor) to address the objectives of the thesis. The development of different configurations of PV/T collectors has also been presented. The process for the development of novel phase change material to be used in the PV/T system and characterization techniques adopted are discussed in detail. A brief discussion is also included for the economic analysis of the PV/T collector. The results obtained from the mentioned experimental studies are discussed in Chapter 5. In the next Chapter (Chapter 4), study related to the development and validation of the novel thermal model is presented.

4

Novel thermal model and its validation

4.1 Introduction

A critical review of the literature was performed in Chapter 2 to understand the on-going research on PV/T systems including their numerical modelling and thermodynamic analysis. In the past few decades, researchers have attempted to develop thermodynamic models to compute temperature, electrical conversion efficiency and overall energetic efficiency of a PV cell as well as the overall exergetic efficiency of PV/T systems. Although the literature can provide important tools for simulations of PV/T collectors, the deviations observed between experimental and numerical values are significant under outdoor conditions. It becomes essential to develop an accurate and comprehensive mathematical model to predict the performance of a PV/T system for effective use of electrical and thermal energies. As evident from the literature studied, extensive numerical and experimental studies were carried out on PV/T systems. However, some issues, such as the effect of thermal contact resistance and Ohmic loss at PV layer on the performance of a PV/T system, are still unresolved. The purpose of the present study is to develop and validate a comprehensive thermal model for a hybrid sheet-and-tube PV/T collector with improved prediction capability compared to the existing models. All the above-mentioned studies did not consider the role of the thermal contact resistance that exists between different layers of a PV/T collector while establishing numerical models for PV/T systems. Based on the findings of the reported studies, an attempt is made in the present study to put forward a thermal model for a PV/T system in which both thermal contact resistance between the layers of PV/T system and individual resistance of different layers are considered. The heat generation due to the internal resistance of PV cells is also taken into account in the present study, which is aimed at providing a precise prediction of the temperature variation of different layers of a PV/T collector. The developed thermal model can be used as a tool for predicting the fluid output temperature under a given set of climatic conditions by knowing the ambient conditions. This model is also expected to provide a clear understanding of how the properties of individual layers of a PV/T collector influence the overall performance. The developed model has been compared with the one developed by Huide *et al.* (2017) [192]. The present model is further validated using the data generated from the present experiments. This model will help to understand the behaviour of a PV/T collector under varied climatic conditions on the component scale because this model incorporates most of the details related to heat transfer in the PV/T collector and material properties of various components. The development of the present model is based on the well-established energy balance equations and procedure.

4.2 Methodology

The objective of this study is to develop a thermal model considering the thermal contact resistances between different layers of a PV/T collector along with solid contact resistances. The development of the model follows an established methodology [192,193] and the same has been presented as an integral part of the present work to provide a deeper understanding. In the developed model the ambient temperature and solar irradiation data are taken as inputs. The wind speed is considered to be constant at a value of 1.5 m/s. After analysing and deriving the governing equations for various PV/T components, a MATLAB(R) code for the system of equations was formulated and the numerical solution was obtained. The simulation results of the developed model are compared with a reference thermal model of Huide *et al.* (2017) [192], which was developed without considering the thermal contact resistance and Ohmic heat generation. The reference model was also numerically solved using MATLAB by providing the same input parameters as the present developed model. Finally, the results of the simulation compared using data generated from the experimental study on M2. The results of the experiments are compared with both the developed and reference models.

4.2.1 Formulation of mathematical model

In an ordinary PV collector, the majority of the incident solar heat flux is conducted through the PV layers from the front (mostly glazing or glass cover) to the back (Tedlar sheet). There are thermal resistances of the individual layers and thermal contact resistance at the interface of different layers. Thermal resistances of the individual layers depend on the thickness of layers and thermal conductivity of the constituent material. The thermal contact resistance depends on various factors, such as the surface asperity, average surface roughness, mean surface separation, nature of filler, the hardness of the surface material in contact and pressure imposed on the layers to hold them in proper places [260]. The task of finding thermal contact resistance between surfaces in contact involves several details. Apart from the conduction, there are heat losses from the front and back surfaces by radiation and convection to the ambient. Minor heat loss from the metal casing surrounding the module is accounted for. Since the area of the casing is usually small, the heat loss from the casing can be neglected in the thermal resistance network. The heat transfer from the PV/T collector surfaces includes free convection and radiation heat transfers. Forced convection heat transfer is influenced significantly by flow velocity, viscosity, thermal diffusivity and temperature of the fluid. An analytical evaluation of the heat transfer coefficient associated with convection is difficult due

to the involvement of a host of thermo-physical parameters. Therefore, an empirical relation is used to obtain Nusselt number depending on the nature of flow defined by Reynolds number and Prandtl number. In the case of natural convection, the Rayleigh number is linked to the convective heat transfer coefficient.

In the energy balance for a PV/T collector, the solar radiation is considered as the input energy. The front glazing allows the solar radiation to penetrate it and reach the PV cell with minimum absorption in the glazing. A PV cell converts some portion of the solar radiation in the visible spectrum into electrical energy and the rest is converted into thermal energy. Due to the internal resistance of a PV cell, there is a considerable Ohmic loss [187]. By accounting for this fact, it can be assumed that a PV layer experiences a uniform volumetric heat generation. The energy transfer in a typical PV/T collector is shown in **Figure 4.1**. Heat generated in a PV module is carried away by the fluid that flows continuously through the tubes.

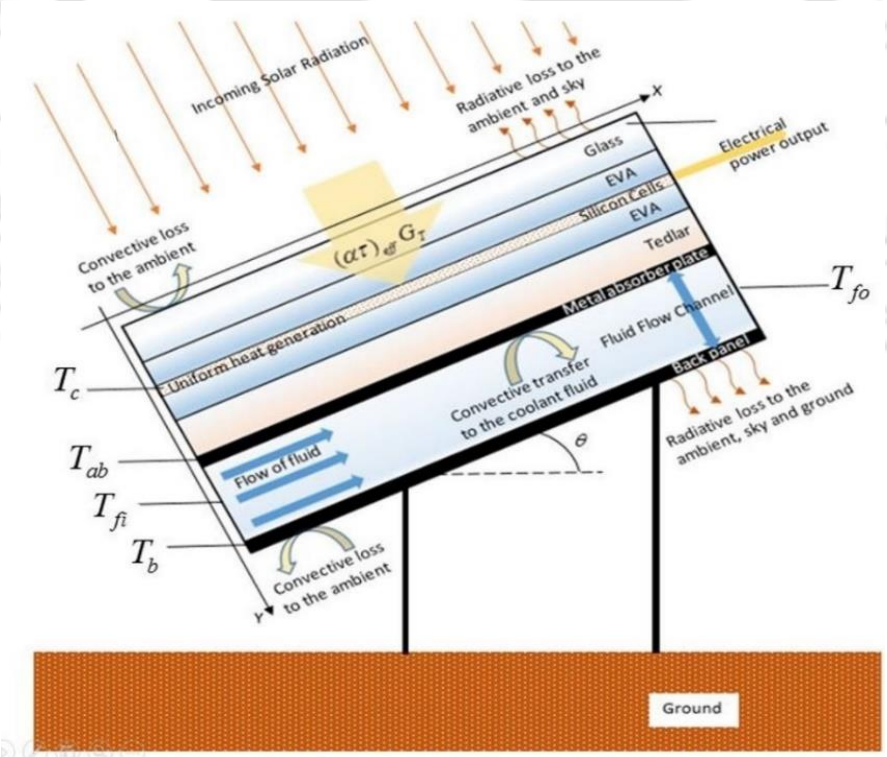

Figure 4.1. Energy flow in a typical PV/T collector

Due to the presence of solid layers in the construction of a PV/T collector, a major portion of heat transfer takes place by conduction. The layers of a PV module are thin

compared to its surface area. Therefore, the usual practice is to consider the mean temperature of the entire layer. The mean temperature is also considered invariant through the width of layers for simplification. During transient state, some amount of heat is generated in PV layers thus increasing its temperature. As the solar radiation varies throughout the day, a PV/T collector mostly stays in a transient state during the day time. Due to the conduction along the *y* direction and flow of fluid along the *x* direction temperature varies in both *x* and *y* directions. **Figure 4.1** shows different losses associated with a PV/T system. The details of the various losses and correlations used for calculation of the losses are presented in **Table 4.1**.

Thermal resistance

Heat transfer through the cross-section of a PV/T collector is hindered by the thermal resistance of solid layers as well as the resistance at interfaces of different layers. Different thermal resistances involved in the heat transfer mechanism of PV/T collector are shown in **Figure 4.2**. In the present study, the emphasis has been given to the effect of contact resistance on the mechanism of heat transfer within a PV/T collector.

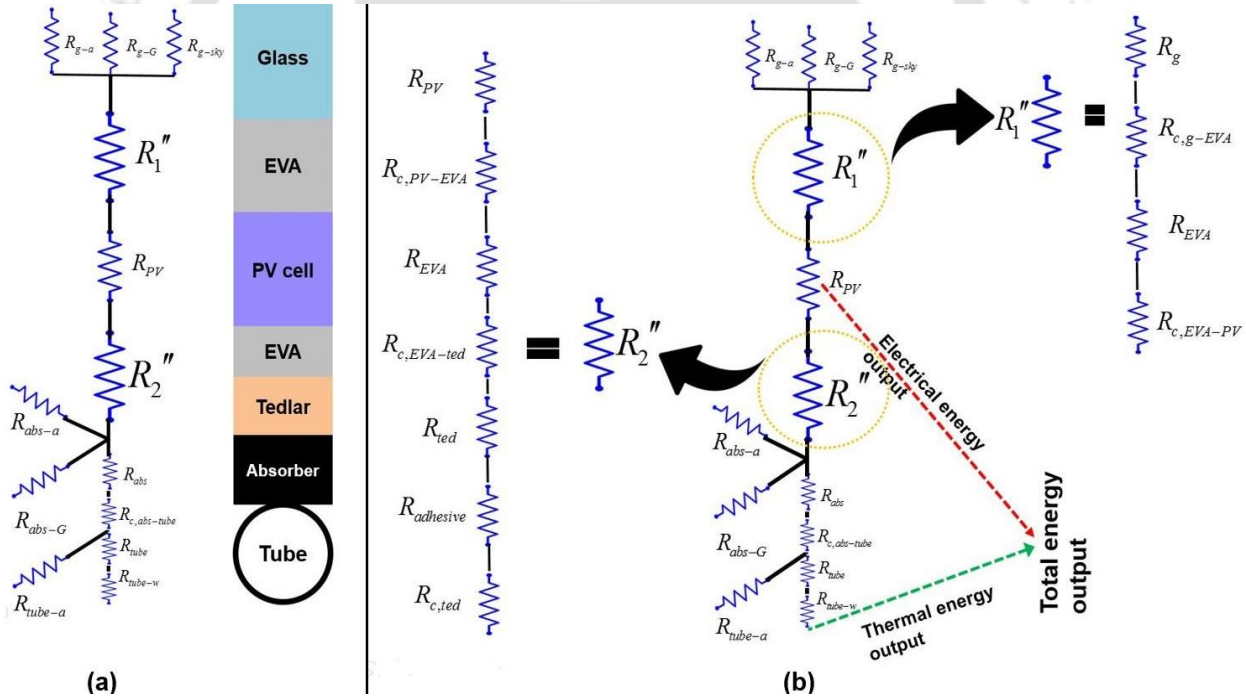

Figure 4.2. (a) Thermal resistances associated with different PV/T components, and (b) detailed thermal resistance network diagram

Table 4.1 Thermal losses in a PV/T collector

Mode of heat loss	Location of heat loss	Correlations
Convective Losses	• Forced and free convection takes place at the front glass covering as well as at the insulated metal back module. • Forced convective heat transfer occurs in the fluid flow channel.	• $h_w = 2.2v_w + 8.3$ [261] • $h = 1.78\,(T_s - T_a)^{1/3}$ [262] • $h_{w,t} = Nu_D \frac{k_w}{d_{t,in}}$ • Fully developed laminar flow: $Nu_D = 4.364$ • Fully developed turbulent flow: $Nu_D = 0.023\mathrm{Re}_D^{0.8}\,\mathrm{Pr}^{0.4}$
Radiative Losses	• Radiative heat losses take place at the front glass and back module. At both the surfaces radiative heat loss takes place to the ground, sky and ambient. • The effect of tilt angle (θ) is compensated by appropriate view factors.	View factor [263]: $F_{ij} = \frac{1}{A_i}\int_{A_i}\int_{A_j}\frac{\cos\theta_i Cos\theta_j}{\pi R^2}dA_i dA_j$ $F_{fs} = \frac{1}{2}(1+\cos\theta)$ $F_{bs} = \frac{1}{2}[1+\cos(\pi-\theta)]$ $F_{fg} = \frac{1}{2}(1-\cos\theta)$ $F_{bg} = \frac{1}{2}[1-\cos(\pi-\theta)]$
Ohmic Loss	• PV cells	• $Q''_{ohmic} = i^2 R_{\text{internal}}$ • The internal resistance of a series of 54 cells PV module was 0.33Ω [187]. • For a 36 cells module the value of internal resistance was 0.22 Ω.

Thermal resistance of solid layers

For the solid layers the thermal resistances are obtained by the formula [264];

$$R = \frac{\delta}{k} \tag{4.1}$$

where δ and k represent the thickness of the layer and the thermal conductivity of the material, respectively. Thermal properties of the individual layers of PV/T are presented in **Table 4.2**.

Thermal contact resistance at the interfaces

It has been reported that whenever two different surfaces are physically connected, there is a variation from the usual trend in the temperature gradient at the interface compared to the bulk material. Even without defects on contact surfaces, there exists an impedance to thermal transport at interfaces [265]. In the case of a PV/T collector, the PV cells are laminated within two thin layers of Ethylene Vinyl Acetate (EVA). The top surface of a PV module is covered by a low iron tempered glass (glazing material). The back surface is covered by a Tedlar sheet followed by the metal absorber plate. Thus there are six such interfaces. EVA and Tedlar are both polymers and therefore joining of these two materials by applying pressure and heat will result in an elastoplastic deformation [266]. Thus, no contact resistance in the layer is considered and the thickness and thermal conductivity of the layers are considered for calculations of solid resistance.

Table 4.2 Properties of different layers of a PV module [267–269].

Material	**Thickness** (m)	**Thermal conductivity** (W/mK)	**Density** (kg/m^3)	**Specific heat** (J/kgK)	**Absorptivity** (α)	**Transmissivity** (τ)	**Emissivity** (ε)
Glass	0.003	1.8	3000	500	0.01	0.95	0.95
EVA	0.0005	0.35	960	2090	-	0.85	---
Silicon cells (PV layer)	0.0003	148	2330	677	0.93	---	---
Tedlar	0.0005	0.2	1200	1250	---	---	---
Copper absorber plate	0.001	310	2702	377	---	---	0.10
Copper tubes	0.0005	310	2702	377	---	---	0.03

EVA is used to encapsulate a PV cell as well as to bind the layers together. EVA is a thermoplastic resin copolymer. The process of lamination suggests that the entire process is carried out in a vacuum. The top glass used in a PV module is significantly rough to stick to other layers [270]. During the lamination process, the rough surface is covered by EVA. When two real surfaces are in contact, there are discrete point of contacts at the interface [271].

Heat flux passes through real contacts and vacuum at the interface. At any interface, net interface conductance can be expressed as [272];

$$h_{\text{interface}} = h_c + h_r \tag{4.2}$$

where, h_c represents the material contact conductance and h_r the radiation heat transfer coefficient between the surfaces. According to Savija and Culham (2003) [273] for temperatures less than approximately 600 °C the radiation heat transfer is negligible for vacuum condition, *i.e.*, $h_r = 0$ and therefore $h_{\text{interface}} = h_c$.

The thermal contact resistance is influenced by several parameters, namely, surface roughness and waviness, surface hardness and effective modulus of elasticity, thermal conductivity and apparent pressure at the interface [274]. The thermal contact conductance can be given by the expression [271];

$$h_c = \frac{\varphi_2 k_s}{2\pi\psi} \cdot \frac{m_{rms}}{Ra_{rms}} \cdot \exp\left[-erfc^{-1}\left\{ \frac{2P_{apparent}}{\varphi_1 (P+H)} \right\}^2 \right] \tag{4.3}$$

where m_{rms} represents the root mean square value of the average asperity slope of the two surfaces in contact, Ra_{rms} the root mean square value of the average surface roughness of two surfaces in contact and k_s the harmonic mean of the thermal conductivity (W/mK) of the materials in contact. Mikic (1974) [275] proposed a simplified expression for calculation of the thermal contact resistance conforming rough joints assuming elastic deformation, this is as follows

$$h_c = 1.55 k_s \left(\frac{m_{rms}}{Ra_{rms}} \right) \left(\frac{P_{apparent}}{H} \right)^{0.94} \tag{4.4}$$

$$\varphi = \frac{H}{m_{rms} E} \tag{4.5}$$

where H represents the hardness (MPa) of the softer material in contact.

$E = \left[\frac{1-\upsilon_1^2}{E_1} + \frac{1-\upsilon_2^2}{E} \right]^{-1}$, here υ and E represent the Poisson ratio and elastic moduli of a material.

$$\phi_1 = \frac{1}{(1+2.5\phi^{1.2})}$$
$$\phi_2 = \frac{1}{(1+1.05\phi)} \quad (4.6)$$

$$\psi = \left(1-\sqrt{\frac{A_r}{A_a}}\right)^{1.5}; \quad (4.7)$$

$$\text{where } \frac{A_r}{A_a} = \frac{P_{apparent}}{\left(P_{apparent}+H\right)}$$

The numerical value of ϕ is vital to the determination of the type of contact. In the case of layers of a PV module, materials at the interfaces undergo elastoplastic deformation [271]. The average surface roughness (Ra) can be approximated as $0.72\,\mu m$ for industrial pre-cursor surfaces [276]. The mean absolute surface asperity slope (m) of the interface can be approximated to be 0.125 for the condition $0.216\mu m < Ra < 9.6\mu m$ and the following expressions are applicable [277];

$$Ra_{rms} \approx 1.25Ra \quad (4.8)$$

$$m_{rms} \approx 1.25m \quad (4.9)$$

Apparent pressure developed at interfaces

Unlike other usual adhesives, EVA is a thermo-setting copolymer, which exhibits thermo-elastic behaviour. As a result, a compressive force is built up in EVA during cooling from a higher temperature (softening point $\approx 108°C$) to a lower temperature (ambient temperature) [278]. This strain causes stress in the EVA layer, which imparts pressure at the interface. An inherent assumption is based on the fact that the adhesive strength is much higher than the stress developed due to this thermal treatment. Such force can be estimated as

$$Y = \frac{FL}{A\Delta L} \quad (4.10)$$

The interconverted Young's modulus varies significantly for such range of temperature variation (108 °C to the ambient temperature). Eitner *et al.* (2011)[279] developed a model for the viscoelastic behaviour of EVA based on the generalized Maxwell model. The model provides a plot for the interconverted Young's modulus with temperature.

Considering the effect of temperature on parameters the expression for the small apparent pressure (dP), which is equal to the magnitude of the compressive stress, developed for a small temperature drop (dT) becomes

$$\frac{dF}{A} = -\{Y(T)\alpha\}dT \tag{4.11}$$

$$dP = \left|-\{Y(T)\alpha\}dT\right| \tag{4.12}$$

For the entire range of temperature variation (381 K to the ambient temperature), the total apparent pressure developed ($P_{apparent}$) becomes the pressure developed due to cooling and the atmospheric pressure imparted on a PV module

$$P_{apparent} = P_{atm} + \int_0^P dP = P_{atm} + \left|-\int_{381K}^{T_{ambient}} \{Y(T)\alpha\}dT\right| \tag{4.13}$$

The negative sign in the expression for dP is due to a decrement in temperature during the process. Apparent pressure developed is calculated using numerical integration.

4.2.2 Development of thermal model

To develop a thermal model considering contact resistances and Ohmic losses, the following assumptions are made:

- The physical properties of the PV/T collector components are constant.
- There is a negligible variation in temperature in a layer.
- There are negligible losses through the metallic casing of PV module.
- Ground temperature is 2 degrees more than the ambient temperature.

For one-dimensional heat conduction with uniform heat generation per unit area and incident radiation falling on the substance, the energy balance becomes

$$\delta_{layer}\rho C_p \frac{\partial T}{\partial t} = -k\frac{\partial T}{\partial y} + Q''_{generation} + h_{equivalent}(T_s - T_a) + G_T \tag{4.14}$$

Equation (16) can be simplified as

$$\delta_{layer}\rho C_p \frac{dT}{dt} = \frac{\Delta T}{R''} + Q''_{generation} + h_{equivalent}(T - T_a) + G_T \tag{4.15}$$

For PV cell layer

A portion of the actual solar irradiance incident on the front glass is transmitted to PV layers. A portion of that transmitted radiation is then absorbed by the PV cell. Here the expression $f\alpha_c\tau_g G_T$ denotes the amount of solar radiation absorbed by PV cell layers. The variable $\frac{T_c - T_g}{R_1''}$ provides the conduction heat flux from the cells to the front glass and $\frac{T_c - T_{ab}}{R_2''}$ provides the conduction heat flux from the cells to the back absorbing plate. The variable $\frac{i^2 R_{internal}}{A}$ represents the area-averaged Ohmic loss and the expression $\eta_c f\alpha_c\tau_g G_T$ represents the electrical output per unit area of the PV/T collector. By applying Eq. (4.15) to the PV layer the following expression can be obtained

$$\frac{dT_c}{dt} = \frac{1}{\delta_c\left(\rho C_p\right)_{av}}\left[-\left(\frac{T_c - T_g}{AR_1''}\right) - \left(\frac{T_c - T_{ab}}{AR_2''}\right) + \frac{i^2 R_{internal}}{A} + f\alpha_c\tau_g\tau_{EVA}G_T(t) - \eta_c f\alpha_c\tau_g\tau_{EVA}G_T(t)\right] \tag{4.16}$$

For the PV cell layer, the average specific heat capacity becomes

$$\left(\rho C_p\right)_{av} = f\cdot(\rho C_p)_{PV} + (1-f)\cdot(\rho C_p)_{EVA} \tag{4.17}$$

Front glass layer

The net incoming heat flux is given by the expression $\left(\frac{T_c - T_g}{AR_1''}\right) + \alpha_g G_T$ where the first term represents the incoming conduction heat flux and the second term represents the solar radiation flux absorbed. The variable $\sigma\varepsilon_g\left[F_{fs}(T_g{}^4 - T_{sky}{}^4) + F_{fg}(T_g{}^4 - T_{gr}{}^4) + F_{fa}(T_g{}^4 - T_a{}^4)\right]$ represents the net radiation heat loss to the sky, ground and atmosphere and the expression $h_w(T_g - T_a)$ represents the convection heat flux. F_{fs}, F_{fg} and F_{fa} represents the view factor between front glass to the sky, between front glass to ground and between front glass to the ambient respectively.

$$\delta_g(\rho C_p)_g\frac{dT_g}{dt} = \left[\frac{T_c - T_g}{AR_1''}\right] + \tag{4.18}$$
$$\alpha_g G_T(t) - \sigma\varepsilon_g\left\{F_{fs}(T_g{}^4 - T_{sky}{}^4) + F_{fg}(T_g{}^4 - T_{gr}{}^4) + (T_g{}^4 - T_a{}^4)\right\} - h_w(T_g - T_a)$$

where, sky temperature [280] can be determined from the following empirical relation

$$T_{sky} = 0.037536\ T_a^{1.5} + 0.32\ T_a \tag{4.19}$$

Absorber Plate

The net incoming heat flux is given by the expression $\left[\frac{T_c - T_{ab}}{AR_2''}\right] + (1-f)\tau_g \tau_{EVA} \alpha_{tedlar} G_T$. The first term corresponds to the conduction heat flux and the second term represents the absorbed radiation flux.

$$\delta_{ab}(\rho C_p)_{ab}\frac{dT_{ab}}{dt} = \left[\frac{T_c - T_{ab}}{AR_2''}\right] + (1-f)\tau_g \tau_{EVA_1} \tau_{EVA_2} \tau_{ted} \alpha_{ab} G_T(t) - \sigma\varepsilon_{ab}\left\{F_{fg}(T_{ab}^{\ 4} - (T_a + 2)^4) + (T_{ab}^{\ 4} - T_a^{\ 4})\right\} - h_w(T_{ab} - T_a) - \frac{(T_{ab} - T_{tube})}{A_{ab-t}R_{ab,t}} \quad (4.20)$$

For the tube

In the proposed model the fluid is considered to flow through copper tubes arranged in a serpentine configuration.

$$\delta_t A_t \rho_t c_t \frac{dT_t}{dt} = \pi d_{t,in} L h_{w,t}(T_{fi} - T_{tube}) + \frac{(T_{ab} - T_{tube})}{A_{ab-t}R_{ab,t}} - \sigma\varepsilon_t(T_{tube}^{\ 4} - T_a^{\ 4}) - h_w A_t(T_{tube} - T_a) \quad (4.21)$$

where $A_t = \frac{\pi}{4}(D^2_{t,out} - d^2_{t,in})$ and convection heat transfer between the tube wall and fluid is expressed as

$$h_{w,t} = Nu_D \frac{k_w}{d_{t,in}} \quad (4.22)$$

For the fully developed laminar flow: $Nu_D = 4.364$ (4.23)

For the fully developed turbulent flow: $Nu_D = 0.023 \mathrm{Re}_D^{\ 0.8} \mathrm{Pr}^{0.4}$ (4.24)

For fluid in tube

The heat that is transferred from the absorber plate to the tube surface is collected by the flowing fluid, which then gets heated up and is used for some low-temperature applications.

$$A_{t,in}\rho_f c_f \frac{dT_f}{dt} = \pi d_{t,in} L h_{w,t}(T_{tube} - T_{fi}) - \dot{m}_f c_{pf}(T_{fo} - T_{fi}) \quad (4.25)$$

4.2.3 Numerical methodology

Equations (4.16), (4.18) and (4.20) form a system of nonlinear ordinary differential equations. These equations were numerically solved using six stages, fifth-order Runge-Kutta method by employing in-built MATLAB® function "ode45". It uses an adjustable time step and evaluates six functions at each time step to calculate a fifth-order accurate solution at the next time step. Equations (4.21) and (4.25) form a separate set of linear ordinary differential equations, where T_{ab} acts as a known variable. These equations were solved using the finite-difference method. At each time step equations were discretized implicitly and the resulting system of algebraic equations was put in the matrix form [A] [T] = [B] and solved. Here [A] is a 2x2 matrix while [T] and [B] are 2x1 matrices.

Root-mean square error (RMSE)

It is a frequently used measure of the difference between values of a parameter predicted by a model and values obtained from experiments. RMSE can be calculated from the expression

$$RMSE = \sqrt{\frac{\sum_{j=1}^{n}\left(\text{Actual value} - \text{Predicted value}\right)^2}{n}} \tag{4.26}$$

here n denotes the number of observations.

4.3 Validation of the novel thermal model

4.3.1 Temperature variations

In this section, the results obtained from the experimental study of the developed tube and sheet type PV/T collector are discussed. The parameters measured during the experiment are the glass temperature, cell temperature, absorber plate temperature, fluid outlet temperature, fluid inlet temperature, ambient temperature, the electrical output of the modules, solar irradiance, relative humidity and wind speed. Variations of solar irradiance, ambient temperature, relative humidity and wind speed are presented in **Figure 4.3**, while **Figure 4.4** shows variations of fluid outlet temperature, fluid inlet temperature, glass surface temperature, cell temperature and absorber temperature. It can be observed that the temperature of the PV cell layer is the highest (315 – 331.6 K) followed by glass (312 - 328.5 K) and absorber temperature (310.7 - 324 K). A higher value of the cell temperature might be due to Ohmic heat generation and high absorptivity of silicon. The glass temperature was relatively lower than the PV cell temperature because of continuous convective heat loss due

to wind. The copper absorber plate in the PV/T collector was attached to the tubes which carried the water, thus extracting heat from the absorber plate leading to lowering the temperature of the absorber plate surface. The difference between the outlet and inlet fluid temperatures is in the range 1-6.3 K. The highest temperature rise in the fluid was observed at noon and thereafter the fluid temperature decreased with time.

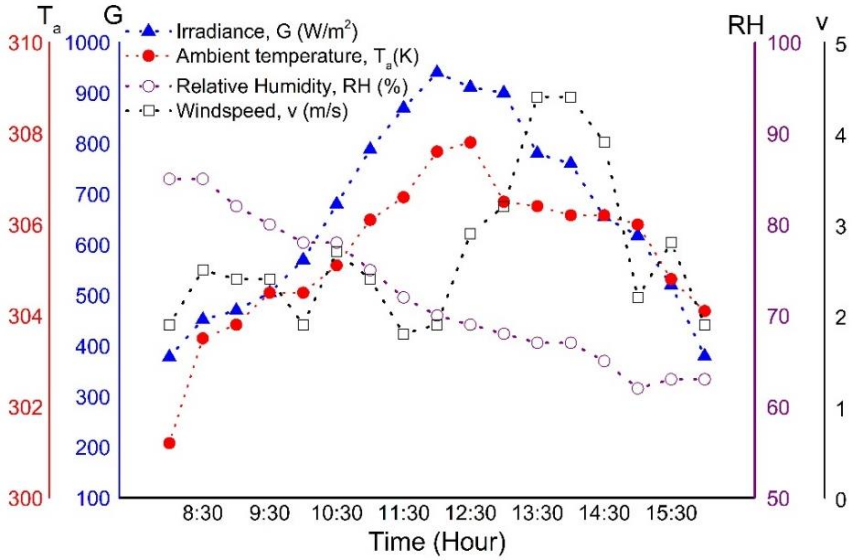

Figure 4.3. Variations of irradiance, ambient temperature, relative humidity and wind speed

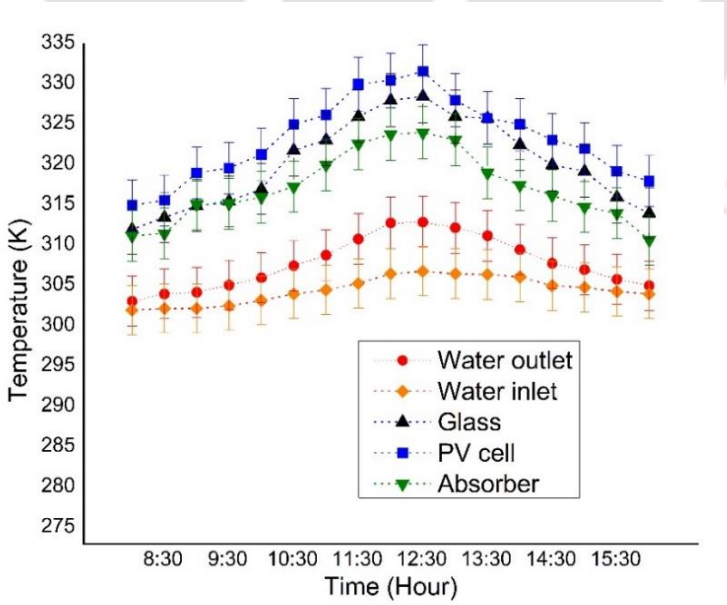

Figure 4.4. Variations of different temperatures observed in experiment

4.3.2 Performance evaluation

It is always important to assess the performance of a solar collector to justify its applicability and acceptability. In the present study energy and exergy analysis was carried out for obtaining values of various performance parameters, such as electrical, thermal, overall energetic and exergetic efficiencies of the developed PV/T system. **Figure 4.5** shows variations in these four efficiencies of the present PV/T system with the time of the day. It can be observed that the electrical efficiency varies from 11.78 - 13.02% and the thermal efficiency varies from 29.97 – 76.37%. The highest value of both the electrical and thermal efficiencies was observed at 12:00 p.m., at solar insolation of 940 W/m^2. The overall energetic efficiency of the system, which combines electrical and thermal efficiencies was found to be in the range of 33.9 – 80.7 %. The efficiency of a PV/T collector is directly influenced by the solar insolation and therefore the efficiency variation is dictated by variation in the solar irradiance. The overall exergetic efficiency is however having lower values as compared to the energy efficiency, it varies in the range 12.7 - 14.97%. The lower value of overall exergetic efficiency is due to the low-temperature fluid output from the system.

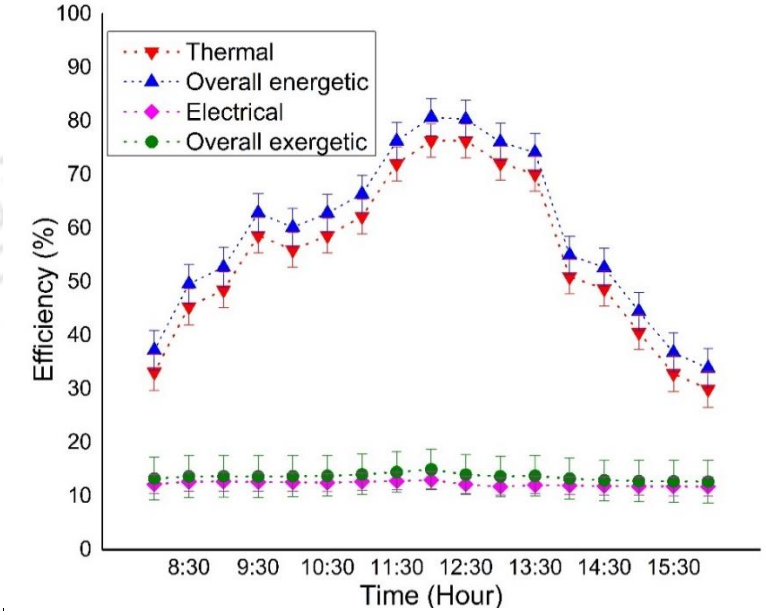

Figure 4.5. Experiemental values of electrical, thermal and overall efficiencies

4.3.3 Comparison of simulation and experimental results

For assessing the model developed in the present study, its results were compared with the ones obtained using the set of equations proposed by Huide *et al.* [192]. The experimental data for solar irradiance and ambient temperature were used as the inputs to

both the models. The values of different temperatures obtained were compared with the present experimental data. Variations in the temperature of various components of the PV/T collector obtained from the present simulations are presented in **Figure 4.6**. All the temperatures increase from **the** morning and attain the maximum values at approximately 12:15 noon and thereafter these start decreasing . The maximum temperature of the glass, PV cell, water outlet and absorber are found to be 329.3 K, 330.8 K, 320.5 K and 316 K, respectively. The observed trends in temperature variations are due to variation in solar irradiance during the day, which increases from the morning, reaches the maximum at noon and then starts decreasing towards evening.

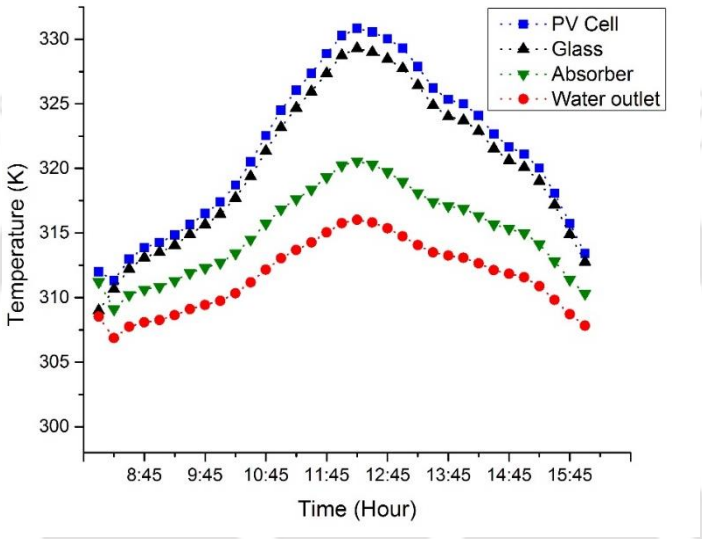

Figure 4.6. Variations of temperature of different layers obtained from the present model

Figures 4.7 - 4.9 provide a comparison of glass, cell and water outlet temperatures obtained from the models and experiment. It can be observed that the simulation results of temperature obtained from the present model are in better agreement with the experimental data than those by the reference model [192]. A close agreement in the glass temperature observed might be due to the fact that the present model accounts for the radiative heat loss to the sky as well as to the ground along with the convective heat loss due to wind. The root mean square error for the glass temperature for the developed model with respect to the experimental data is calculated to be 1.36 K whereas for the reference model it is 2.27 K.

The PV cell temperature is an important parameter for performance evaluation of PV systems since its variation has a direct impact on the electrical efficiency of PV systems. With a rise in the temperature of a PV cell its efficiency decreases [281,282]. Therefore, it is always important to have a precise prediction of a PV cell temperature. The experimental results for cell temperature were found to vary from 315 K to 331.6 K between 8:00 a.m. to 16:00 p.m. PV

cell temperature was found to be 310.56 - 330.86 K and 308.96 – 327.12 K for the present and reference models, respectively. The RMSE value of the PV cell temperature for the developed model was calculated to be 2.71 K whereas for the reference model it was 11.02 K. A lower RMSE value of the cell temperature in the case of the developed model is due to the consideration of the Ohmic heat dissipation due to the internal resistance of the cells while formulating the present set of equations.

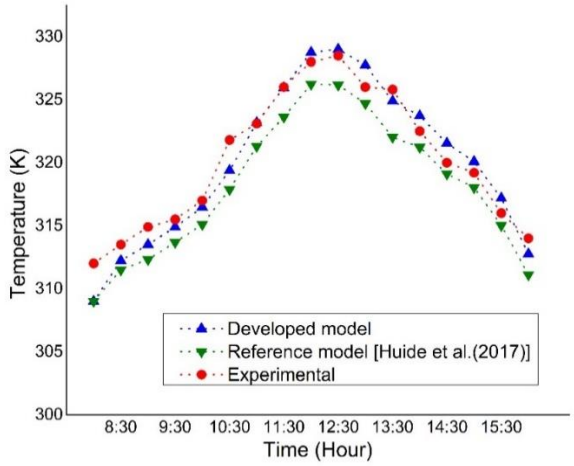

Figure 4.7. Comparison of experimental and simulated values of glass temperature

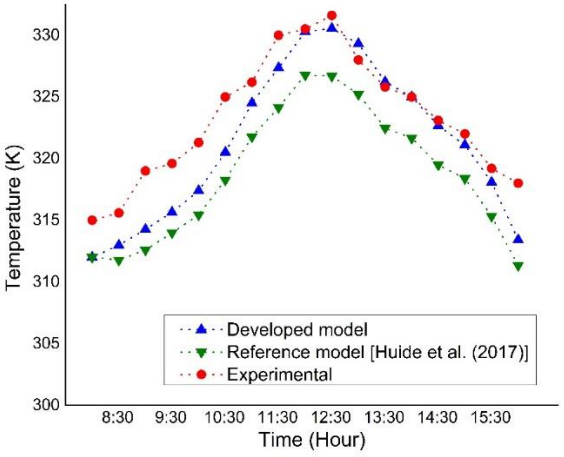

Figure 4.8. Comparison of experimental and simulated values of PV cell temperature

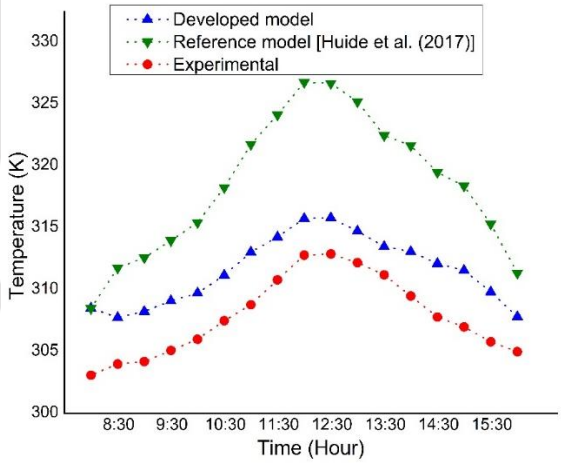

Figure 4.9. Comparison of experimental and simulated values of water outlet temperature

The experimental value of the water outlet temperature of the PV/T collector was observed to be less than the values predicted by the two models. However, the experimental

values were found to be closer to the simulation results for the water outlet temperature obtained from the present model compared to that using the reference model (**Figure 4.9**). The RMSE value of water temperature for the developed model and the reference model were 3.75 K and 11.89 K, respectively. The difference between the results obtained from the two models is significant. The water temperature obtained from the developed model increased from 306 K at 8:00 a.m. to the maximum value of 316 K at 12:20 p.m. Thereafter it started to decrease and reached a value of 307.8 K at 4:00 p.m. The variation in the water outlet temperature obtained using the reference model was 309 K to 327.12 K. The water outlet temperature obtained from the reference model was higher than the results obtained from the present model as well as the experimental data. A higher deviation of the water outlet temperature obtained from the reference model [25] and a closeness of the results using the present model is due to the fact that the developed model accounts for the contact resistances that the thermal energy faces in its flow direction from PV cells to absorber plate and finally makes its way to the incoming fluid through the tube walls. The combined thermal resistance represented by R_1'' and R_2'' (shown in **Figure 4.2 (b)**) are calculated to be $3.263\times10^{-3}\ m^2K/W$ and $1.10\,m^2K/W$ respectively. The thermal contact resistance between the Tedlar back sheet and the absorber plate ($R_{c,ted}=1.098\ m^2K/W$) is found to be significant among all the thermal contact resistances that exist in a PV/T collector. The thermal model developed by Hulide *et al.* did not consider the thermal contact resistance parameter in their formulation and thus deviation in the results of the reference model is large compared to that by the present model.

4.4 Summary of the chapter

The chapter includes step by step derivation of the novel thermal model and its validation method. The chapter discussed the results of the simulation study for the novel thermal model developed. The comparison of the simulation and experimental study has also been addressed. The numerical model in the study is found to be precise as compared to one of the standard model developed earlier. In the next chapter characterization of the developed PCM-biocomposite and experimental results of the developed PV/T collectors with and without PCM-biocomposite are discussed.

5

Results and discussion

5.1 Introduction

The results of the experiments performed based on the methodology described in Chapter 3 are presented systematically in this chapter. Extensive discussion on experimental investigations on four different PV/T collector configurations viz. PV/T without absorber-vertical oscillating (M1), PV/T with absorber–vertical oscillating (M2), PV/T without absorber-rectangular spiral (M3) and PV/T without absorber- horizontal oscillating absorbers (M4) have been carried out. A novel form-stable PCM-biocomposite has been prepared, characterized and applied in the best performed collector (M3) to provide uniform optimum cooling of PV for better performance.

5.2 Variation of climatic parameters

It has been observed that the climatic parameters influence the performance of PV/T systems. **Figures 5.1 and 5.2** show the diurnal variation of climatic parameters such as solar irradiance, wind speed, relative humidity and ambient temperature. In the present investigation, experiments are performed on clear days. During clear sunny days, the incoming solar irradiance and ambient temperature uniformly increase with time and reached a peak at the noon thereafter decreases. The relative humidity observed to be decreased from the morning till the solar noon, thereafter, slowly increases. This is due to the increase in water holding capacity with an increase in air temperature. Stochastic nature of wind speed variation has been observed.

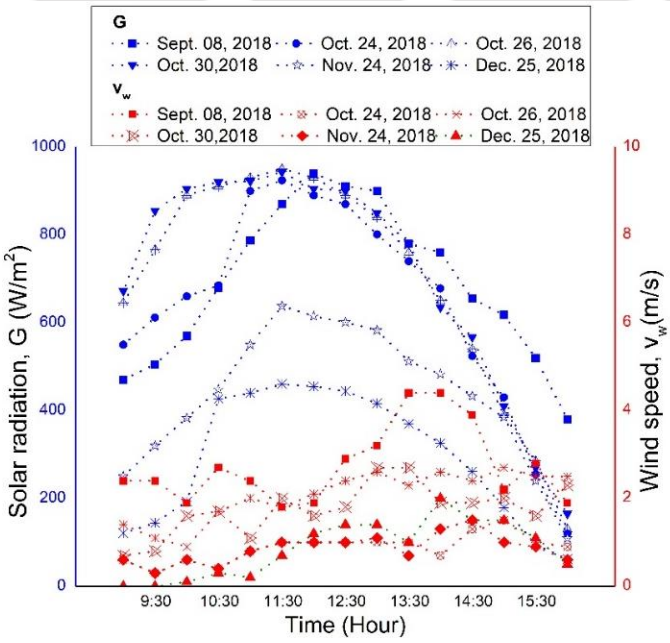

Figure 5.1. Variation of solar irradiance and wind speed with time

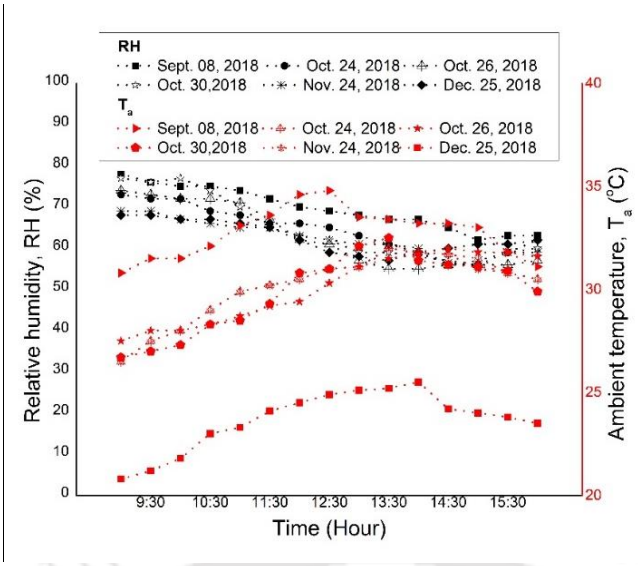

Figure 5.2. Variation of relative humidity and ambient temperature with time

5.3 Experimental study on tube only vertical oscillating (M1) and sheet-tube vertical oscillating (M2) PV/T collectors

The performance of the developed PV/T collectors (M1 and M2) have been experimentally analyzed under outdoor and indoor conditions. The results of the experimental analysis are presented in the following subsections.

5.3.1 Performance evaluation

Figure 5.3 show the variation of electrical efficiency on a clear sunny summer day in the Indian Institute of Technology Guwahati (26.18° N, 91.69° E). The electrical conversion efficiency for M1 on a typical summer day (on 8th Sept 2018) is found to vary from 11.65% to a maximum of 12.30% at 12:00 hr at a corresponding solar irradiance of 940 W/m^2. Whereas for M2 electrical efficiency found to vary from 12.38% to 13.6% at the same solar irradiance value. Under the same ambient condition, the PV conversion efficiency is observed to be in the range of 9.6% to 11.7%. The higher value of electrical conversion efficiency for M2 is due to the emission of radiation by the copper absorber sheet and the radiation incident on the PV surface. The average electrical efficiency for PV, M1 and M2 collectors are 10.5%, 11.6% and 12.26% respectively on 8th Sept 2018. The results show that there is an improvement in the PV electrical efficiency when cooling tubes are installed. It has been observed from the experimental results that cooling improves the electrical conversion efficiency of M1 and M2 by 10.5% and 16.7%, respectively, as compared to a PV module without cooling on a typical summer day. The electrical efficiency improvement in M1 and M2 are found to be 10.2% and

13.8% as compared to PV module without cooling on a typical winter day. Influence of heat transfer fluid circulation for cooling on electrical efficiency is not so significant in winter. The electrical efficiency is primarily dependent on the intensity of solar insolation, as compared to the other climatic parameters when cooling is employed. The performance of the collectors was also investigated during a winter day (on 25th Dec 2018). The electrical efficiency of M1 and M2 collectors was found to be varying from 10.8 - 13.14% and 11.5 - 13.6% respectively whereas, for PV module without cooling it ranges from 10.6% to 12.0%. **Figure 5.5** presents the variation of electrical efficiency of M1 and M2 collectors from 9:00 to 16:00 hrs. The average electrical conversion efficiency is found to be higher in winter months as compared to summer months. This is due to lower ambient and lower PV operating temperatures during the winter months.

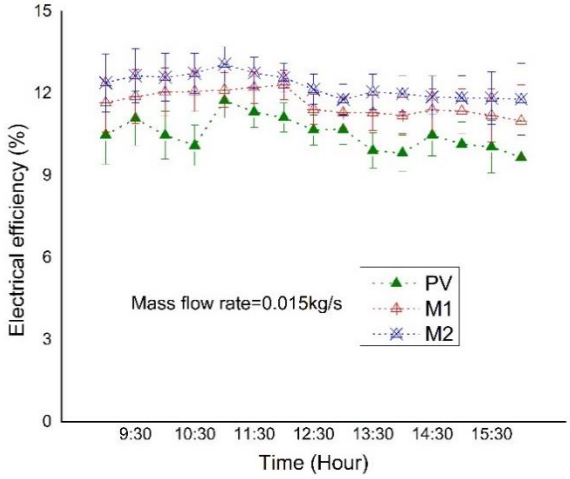

Figure 5.3. Electrical efficiency on a typical summer day

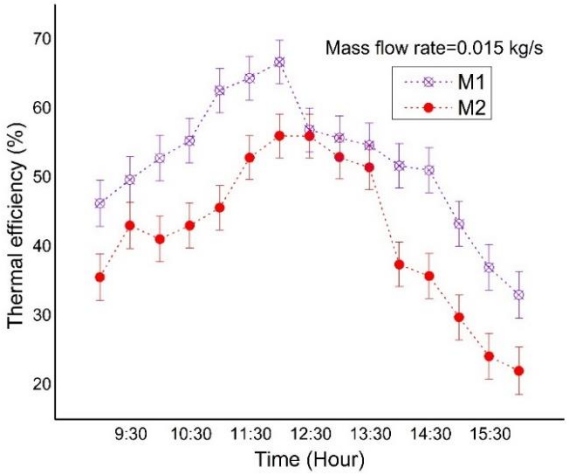

Figure 5.4. Thermal efficiency on a typical summer day

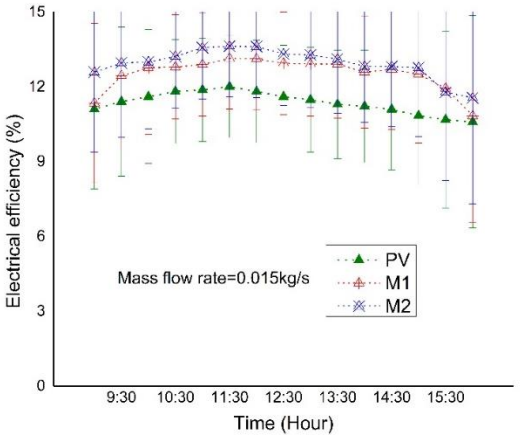

Figure 5.5. Electrical efficiency on a typical winter day

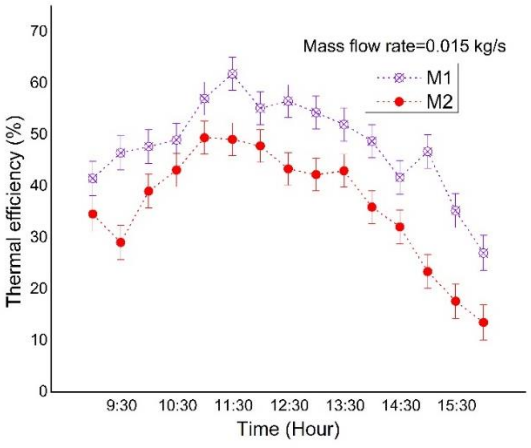

Figure 5.6. Thermal efficiency on a typical winter day

The thermal efficiency, on the other hand, is observed to be higher for M1 as compared to M2 collector. The thermal performance is influenced by the difference between inlet and outlet temperature as well as the solar irradiance pattern. On a clear sky, as the solar irradiance increases from the dawn reached a maximum at the noon, the temperature of the PV layer and absorber keep on increasing and the heat transfer to the fluid flowing through the tube increases, subsequently the outlet temperature of the fluid increases. The thermal efficiency for M1 gradually increases from 46.24% at 9:00 hr to a maximum value of 66.7% at 12:00 hr and then it starts decreasing and reaches a value of 33% at 16:00 hr, this can be seen from **Figure 5.4**. For M2, thermal efficiency is found to be in the range of 22-56%. The average value of thermal efficiency is observed to be 52% and 41.7% for M1 and M2, respectively. The higher thermal efficiency of the M1 is due to the higher heat transfer rate (less thermal resistance) from the top surface of the PV/T to the fluid flowing through the tubes as compared to M2 [12]. Thermal efficiency during a sunny winter day is lower as compared to that of a typical clear summer day. The average thermal efficiency on 25th Dec 2018 for M1 and M2 is 48% and 36%, respectively (**Figure 5.6**).

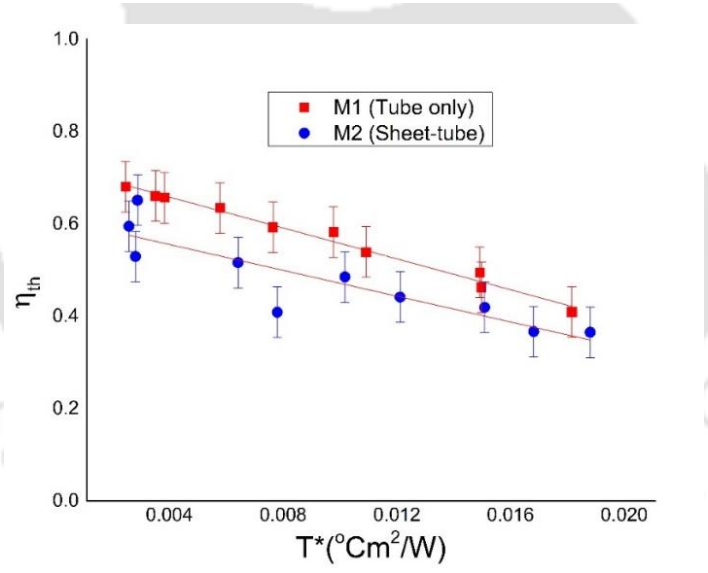

Figure 5.7. Thermal efficiency curves for M1 and M2 collectors

The collector efficiency curves over a range of T^* values for M1 and M2 are shown in **Figure 5.7**. From the results, it is evident that the absence of absorber sheet (in M1) results in an improvement in the thermal efficiency. From the trend lines in **Figure 5.7,** the intercepts are 0.72 and 0.61, indicating the thermal efficiency at zero reduced temperature for M1 and M2 respectively. Also, the slopes are 16.72 $Wm^{-2}/°C$ and 13.98 $Wm^{-2}/°C$ for M1 and M2

respectively. It can be observed that the thermal efficiency of M2 experiences more deterioration at increased fluid temperatures as compared to M1.

The overall energetic efficiency of M1 varies from a value of 57.9% at 9:00 hr to a maximum of 79% at noon and then reduces to 43.99% on a summer day (8th Sept 2018) as shown in **Figure 5.8.** The overall energetic efficiency for M2 on the other side varies from 46.05% to 67.14% and then decreases towards the afternoon. It has been observed from the experimental results that overall energetic efficiency during a winter day fairly remains similar to that of a summer day for M1, but it reduces in the case of M2 during the winter as compared to a summer day. During winter, the temperature of the absorber sheet in M2 remains low as compared to summer. The overall energetic for M1 varies from 52.8% in the morning to 74.93% in the noon and then decreases to 37.8% at 16:00 hr (**Figure 5.10**). But for M2, overall energetic efficiency increases from 45.64% reaches a maximum of 61.2% and then falls to 24.07% in the latter half of the day.

Overall exergetic efficiency follows the same trend as that of electrical efficiency. As overall exergetic efficiency is a strong function of electrical efficiency. Thus, the effect of low-temperature thermal energy in overall exergy output of the PV/T is not significant. Overall exergetic efficiency increases from the morning as the solar irradiance value increases to a maximum at noon and then decreases. The overall exergetic efficiency varies from 11.14 - 13.6% and 12.7-14.49% for M1 and M2 respectively, on a summer day (8th Sept 2018). The average overall exergetic efficiency over the day for M1 and M2 is 12.26% and 13.6%, respectively. It can be observed from the **Figures 5.9 and 5.11**, that the average overall exergetic efficiency for the PV/T collectors (12.59% for M1 and 13.6% for M2) are higher as compared to summer (12.25% for M1 and 13.87% for M2). The improvement in the average overall exergetic efficiency is due to the low operating temperature of the PV.

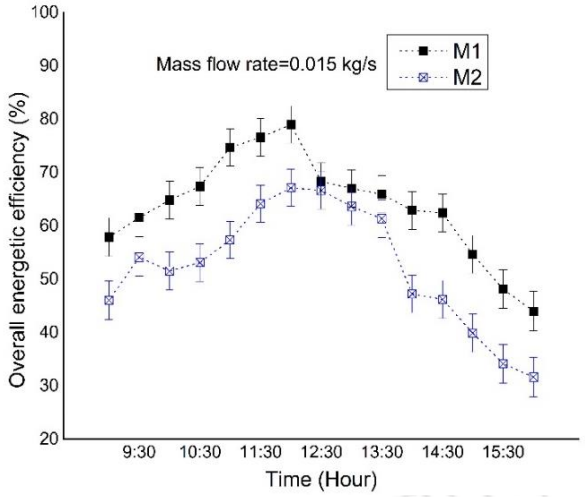

Figure 5.8. Variation of overall energetic efficiency on a typical summer day

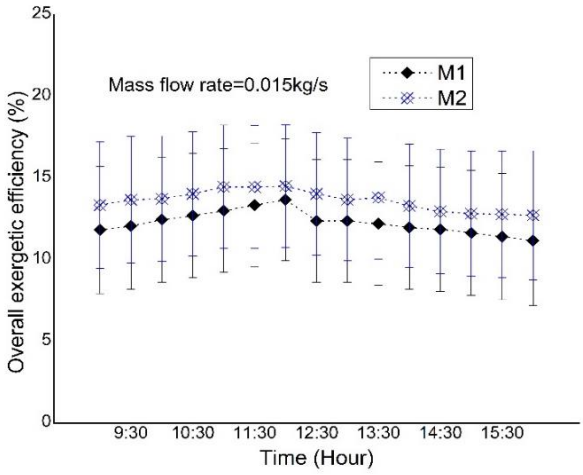

Figure 5.9. Variation of overall exergetic efficiency on a typical summer day

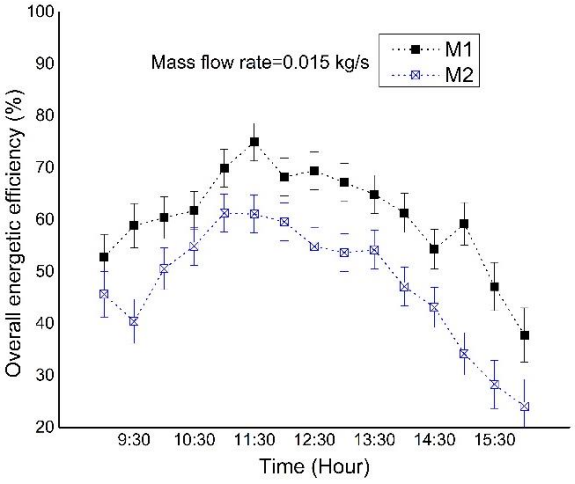

Figure 5.10. Variation of overall energetic efficiency on a typical winter day

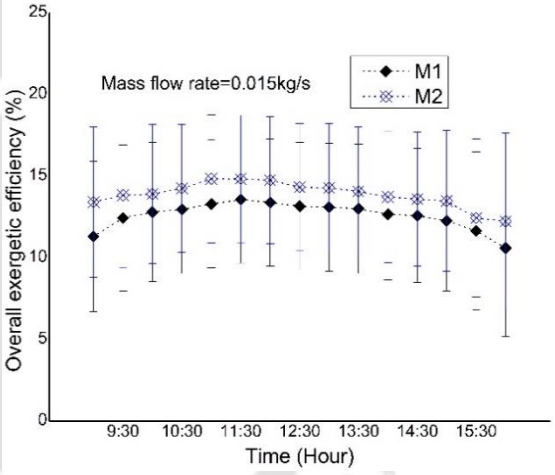

Figure 5.11. Variation of overall exergetic efficiency on a typical winter day

5.3.2 Collector temperature rise

The time necessary to achieve the desired hot water temperature from the inlet water condition in the collector is an important parameter to define the applicability of a newly designed solar hot water generation system. Generally, water is allowed to get heated inside the collector under a steady-state for some duration of time; then, the heated water is taken out for end users. Therefore, it is necessary to know the temperature rise of the fluid at various time intervals so that the user can have more flexibility to decide on the end-use of generated hot water. The rate of temperature rise of fluid under the stagnant condition for PV/T collectors was performed. The weather parameters on 31st October 2018 is shown in **Figure**

5.12. The outlet temperature for the PV/T collectors and inlet temperature at each interval were measured. The variation of temperature for the collectors is shown in **Figure 5.13.** Fluid outlet temperature increases with an increase in the retention time of the fluid in the collector. Temperature rise in M1 is higher than M2, the temperature rises of 9.39 °C and 7.59 °C are reported for M1 and M2 respectively at a heating time of 1 min. At 60 min heating time, the temperature rise of 34.5 °C and 30.5 °C for M1 and M2 have been observed. As seen from **Figure 5.13**, the heating rate for M1 decreases from 9.39 °C min^{-1} to 0.57 °C min^{-1} when heating time is increased from 1 min to 60 min. For M2, the heating rate decreases from 7.59 °C min^{-1} (1 min) to 0.50 °C min^{-1} (60 min). The water reaches a saturation limit for thermal energy absorption after a particular time, so the temperature rise reduces.

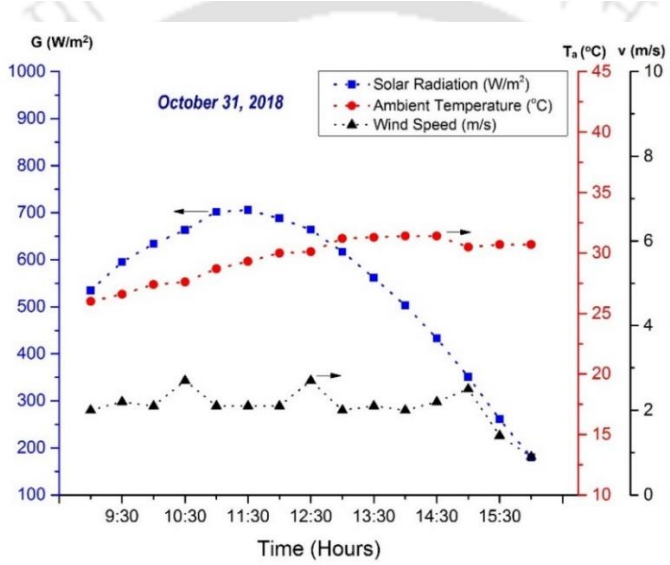

Figure 5.12. Weather data on October 31, 2018

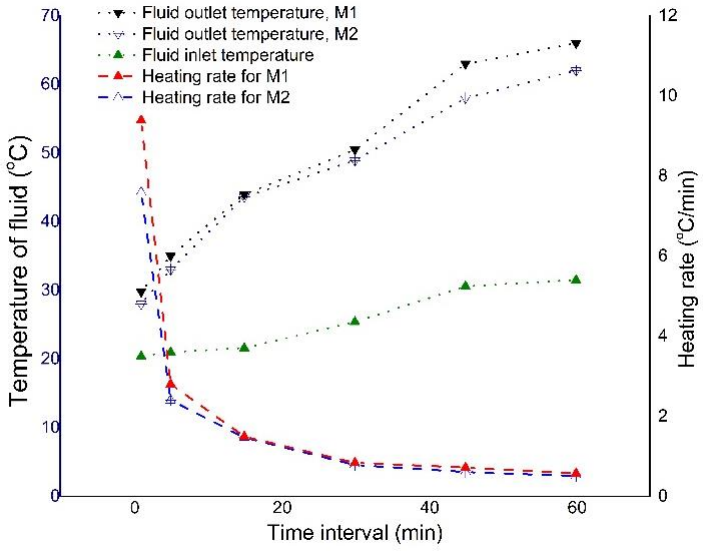

Figure 5.13. Collector temperature rise in PV/Ts

5.3.3 Cooling uniformity

Cooling uniformity of PV module is very important to avoid hotspot generated during sunny days, hotspots results in reduction of current output and life of the PV cells. **Figure 5.14** shows the temperature map of PV/T surfaces. The temperature of the M1 collector surface is found to be relatively lower than M2. The temperature at the central region in M2 found to be higher as compared to the sides. It is because of the reason that when the insulation layer is used at the bottom, heat loss is restricted, only sides of the PV/T acts as the heat transfer surface. It is important to note that both the PV/T collectors have a surface temperature below 50 °C because of absorber with higher tube density and especially M1 where tubes are directly glued to the PV backside has shown better cooling than M2.

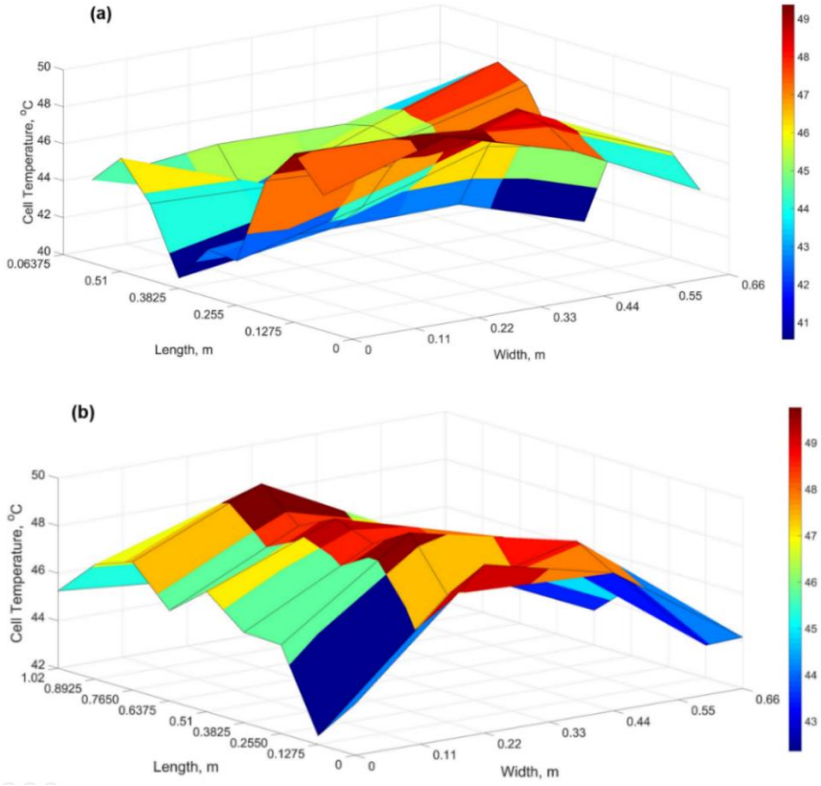

Figure 5.14. Temperature distribution on PV surfaces: (a) M1; (b)M2

5.3.4 Comparison of developed PV/T collectors with existing sheet and tube PV/Ts

The developed PV/T collectors have been compared with some of the PV/Ts developed by researchers across the globe in **Table 5.1.** From the table, it can be concluded that the performance of the developed PV/T is comparable with existing PV/Ts. The spiral flow absorber developed by Fudholi *et al.* (2014) [67] found to be more efficient among the PV/Ts considered for comparison. This is attributed to constant higher and constant

irradiance the experimental study by by Fudholi *et al.* (2014) [67], whereas in the present case the irradiance variation is wide and average value is lower than those reported by Fudholi *et al.* (2014) [67]. The performance of the developed PV/T collectors mentioned in the study is also compared with other PV/T collectors developed in India. It has been found that the developed PV/T in the present study provides better electrical and exergy efficiency as compared to available PV/T collectors. The detailed experimental results and performance parameters are given in **Appendix I.**

Table 5.1 Comparison of developed PV/T with existing water based PV/Ts

Reference	Country	Absorber configuration	η_{el} ,%	η_{th} , %	η_{exergy} ,%	Experimental conditions
[67]	Malaysia	Spiral flow absorber	13.8	54.6	-	$G = 800$ W/m², $\dot{m} = 0.041$ kg/s.
[63]	Iran	--	--	--	13.95%	$\dot{m} = 0.002$ kg/s.
[283]	Kerala, India	Serpentine tube arrangement	11.0	46.2	--	Average electrical efficiency is found to be highest at $G = 668$ W/m² and thermal efficiency at $G = 727.41$ W/m²
[284]	Chennai, India	0.2 mm thickness copper sheet is bonded to the PV cells	7.72	15	---	$\dot{m} = 0.01$ kg/s $G \geq 800$ W/m²
[285]	Rajasthan, India	Enclosure made of Galvanized iron (GI) sheets mounted on the backside of PV module	8.4 – 8.7	46.55 - 57.01	8.16 - 8.54	G varies from 494 to 953 W/m² and T_a in the range 31.2–37.7 ˚C.
[286]	Patras, Greece	Micro PV/T having copper absorber with insulation	9.8 (annual)	20.3 (annual)	--	Global monthly horizontal irradiation varies in the range 80-131 kWh/m²
[57]	Kuala Lumpur, Malaysia	Parallel serpentine pipe flow based PV/T with thermal conductive paste to bond tube to PV back	10.46	74.62	12.98	Collector area=1.61 m², $\dot{m} = 0.017$ kg/s
M1	Assam, India	Only tube assembly, absorber sheet is absent	13.1	66.7	13.66	Collector area=0.67 m², $\dot{m} = 0.015$ kg/s.
M2		Sheet and tube absorber made of copper integrated to the PV backside	13.6	56	14.8	

5.4 Experimental study on tube only rectangular spiral (M3) and horizontal oscillating (M4) transparent PV/T collectors

During the experiment period, a few selected days meet steady-state weather conditions in accordance with thermal performance test standards. The performance parameters are derived from the data obtained on these days to avoid unwanted data points.

5.4.1 Temperature profile

Figure 5.15 shows the temperature map of PV and PV/T collectors. The temperature mapping clearly shows that the surface temperature of PV/Ts is lower as compared to that of PV. M3 has better cooling uniformity than that of M4. It is also important to note that there are local hotspots present on M4. The PV temperature reaches a maximum temperature of 46.4 ˚C, while the M3 and M4 reach 38.3 °C and 43.2 °C, respectively. The average surface temperature of M3 is lowest among all of the three collectors. This is due to better cooling of the module owing to the positioning of the fluid inlet port. M3 has an inlet at the centre thus make the central region of the module get cooled efficiently and the edges are naturally cooled by the air.

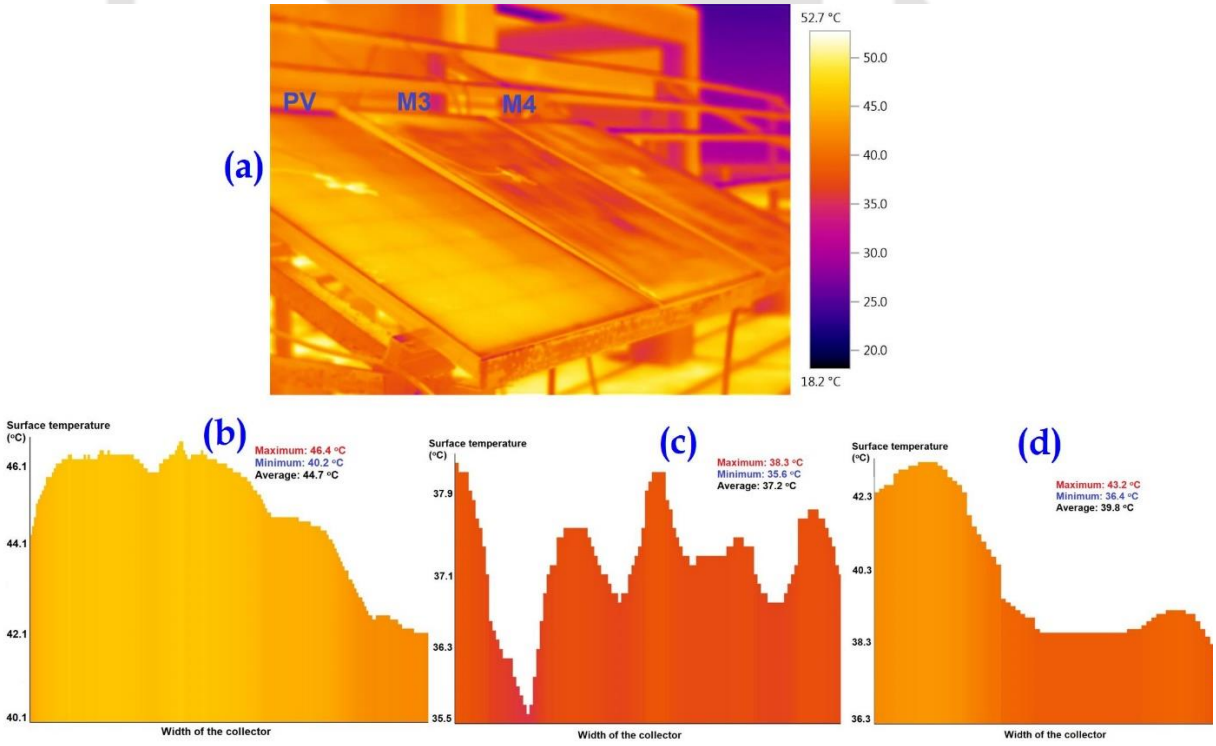

Figure 5.15. (a) Thermal images of the collectors; (b) Temperature profile of PV; (c) Temperature profile of M3, and (d) Temperature profile of M4

5.4.2 Electrical output variation

The most important parameter to study in PV/T system is the electrical output since this is high-grade energy as compared to low-grade thermal energy that is collected from the collectors. **Figure 5.16** shows the variation of electrical power output throughout the day. Electrical output follows a similar trend that of solar irradiance. It initially keeps on increasing till the solar noon and then start descending. The electrical output is found to be maximum for M3 followed by M4 and PV. It has been observed that the difference in electrical output of the three collectors reduces towards the latter half of the day. The reason for this is the reduction in PV temperature in the afternoon as the solar irradiance and ambient temperature reduces. The cause of the deterioration of the output power at the elevated temperature condition can be attributed to the reduction of the p–n junction built-in voltage and junction ability to separate electrons from holes in the photo-generated pairs [16]. The electrical output found to be varying from 61.1 W at 9:00 hr and reaches a maximum of 75.32 W at 11:30 hr for M3. The maximum electrical output reported for M4 and PV is 72.6 W and 66 W respectively. **Figure 5.17** shows the I-V and P-V characteristics of M3 and M4 at solar noon. Due to higher temperature in M4 the open-circuit voltage reduced with a slight increase in short circuit current and finally decreasing the overall electrical power output from the module.

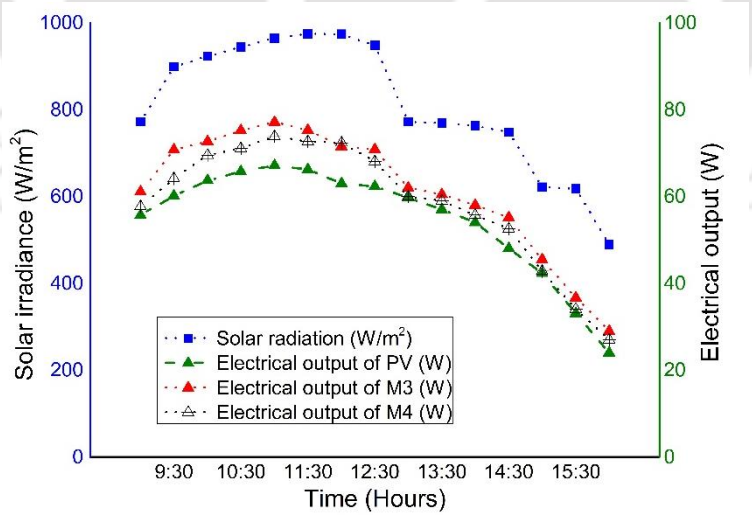

Figure 5.16. Variation of electrical output over the day

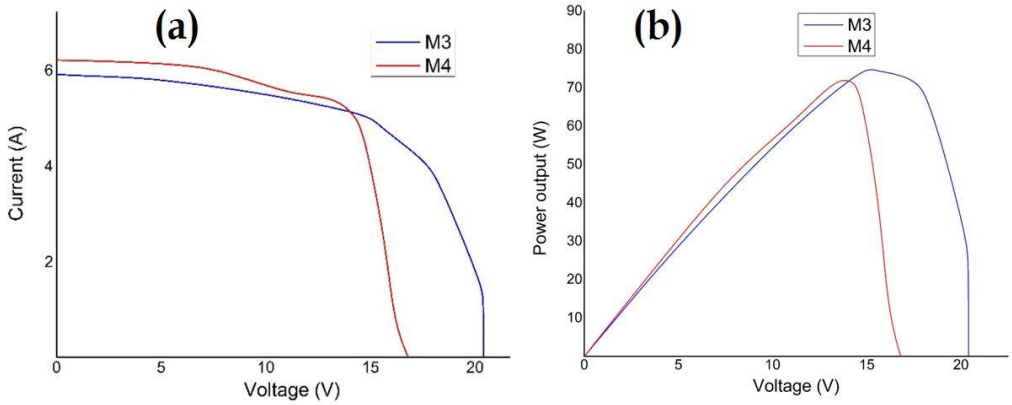

Figure 5.17. Measured: a) I−V and (b) P-V characteristics of the collectors

The electrical efficiency decreases during the middle hours (11:00 to 13:00 hr) of the day as shown in **Figure 5.18** when the irradiance is higher; this is due to higher module operating temperature, which negatively affects electrical conversion efficiency. The electrical efficiency is higher for M3 than M4. The higher electrical efficiency of M3 is owing to the better cooling uniformity of the module; this is evident from the temperature profile of the collectors as shown in **Figure 5.15.** The electrical efficiency for M3 is 11.8% at 9:30 hr, which increases to 11.92%, then it experiences a dip at 12:00 hr and finally shows an increasing trend past noon reaching a value of 11.97%. Finally, the electrical efficiency keeps on decreasing towards the end hours of the experiment. The electrical efficiency for the PV module without cooling varies in the range 7.3 - 11.5%. The average electrical efficiency throughout the experiment is found to be 10.17 ± 0.96%, 11 ± 0.96% and 12.15 ± 0.96% for PV, M4 and M3 collector, respectively.

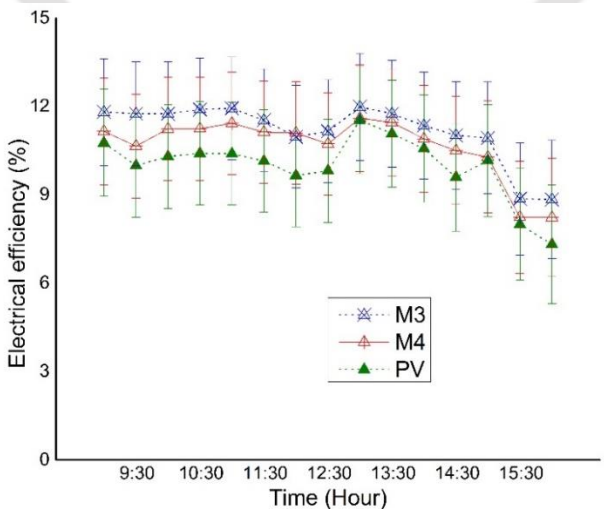

Figure 5.18. Variation of electrical efficiency over the day

5.4.3 Thermal characteristics of PV/T collectors

The temperature rise of the fluid in the PV/T's can be seen from **Figure 5.19**. The temperature rise depends on the irradiance. The difference between outlet and inlet fluid increases from morning to noon, and then it decreases in a similar fashion. The difference is found to be more in case of M4 with oscillating horizontal tubes as compared to M3. This is due to the fact that residence time is higher in the collector because of the longer tube length in the absorber. The temperature difference in the M4 ranges from 4.4 °C at 9:00 hr to 11.6 °C at 12:00 hr. In the case of M3 the difference is found to increase from 3.4 °C to 11.3 °C at 12:00 hr. An average temperature rise of 7.74 °C and 6.9 °C is calculated for M4 and M3 respectively on a clear sky day.

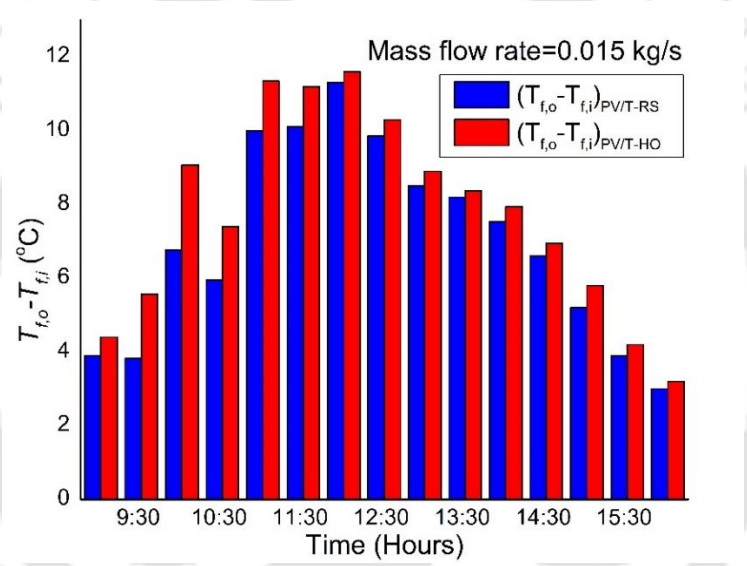

Figure 5.19. Temperature rise in collectors

Figure 5.20 shows the variation of thermal efficiency. The thermal efficiency has been observed to follow a similar trend as the temperature rise. The thermal efficiency for M4 is higher than that of M3. For M4, it varies from 35.5% at 9:00 hr and reaches a maximum of 74.3% at 12:00 hr when the solar irradiance is at the peak value of 974 W/m^2. In the case of M3, thermal efficiency found to be in the range of 26.5 - 72%. The trend shows some fluctuations due to variation of wind speed, which removes heat from the top surface and reduces the fraction of thermal energy that is available for transfer to the fluid stream. **Figure 5.21** shows the thermal efficiency curve for the M3 and M4 collectors. The intercepts obtained from the trend lines for M3 and M4 are 0.77 and 0.86 respectively. The intercepts correspond to the thermal efficiency at zero reduced temperature. It can be observed that the thermal efficiency of M4 deteriorates more at increased fluid temperatures than that of M3 collector.

The average thermal efficiency calculated from the experimental results of the outdoor experiments are 50.7 ± 2.94%and 56.9 ± 2.94%, for M3 and M4 collector, respectively.

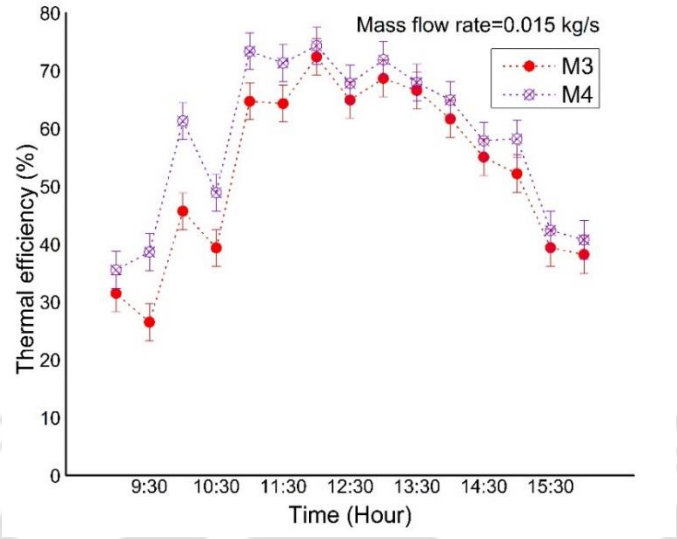

Figure 5.20. Variation of thermal efficiency over the day

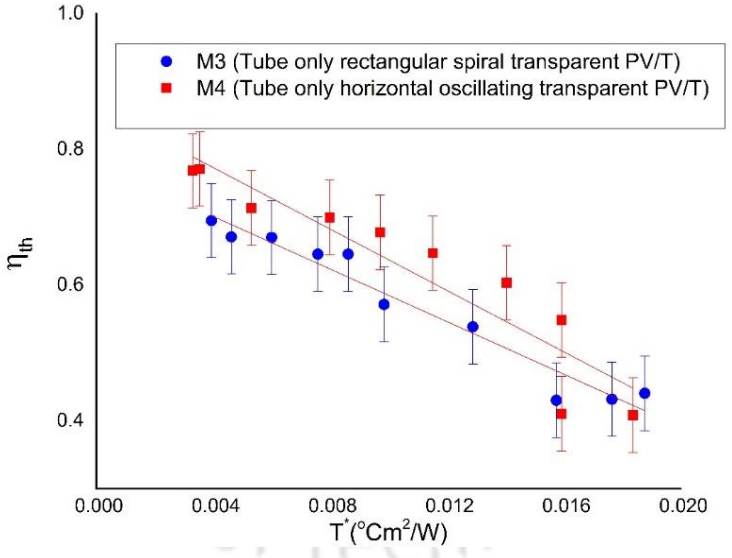

Figure 5.21. Thermal efficiency curves for M3 and M4

The output fluid temperature has also been measured during a cloudy day. **Figure 5.22** shows the variation of solar irradiance, the fluid outlet temperature of the PV/T's and fluid inlet temperature on a cloudy day. The average outlet temperature calculated for M3 and M4 is found to be 36.2 ˚C and 36.64 ˚C. The established safe bathing temperature range is 38 - 43 ˚C [287] and the temperature of water obtained from PV/T collectors closer to this

value. The outlet temperature variation of PV/Ts is not highly sensitive to short term fluctuations because the material of the PV/T stores thermal energy owing to heat capacities of the air in the gap between the tubes also acts as a source of heat to the fluid stream.

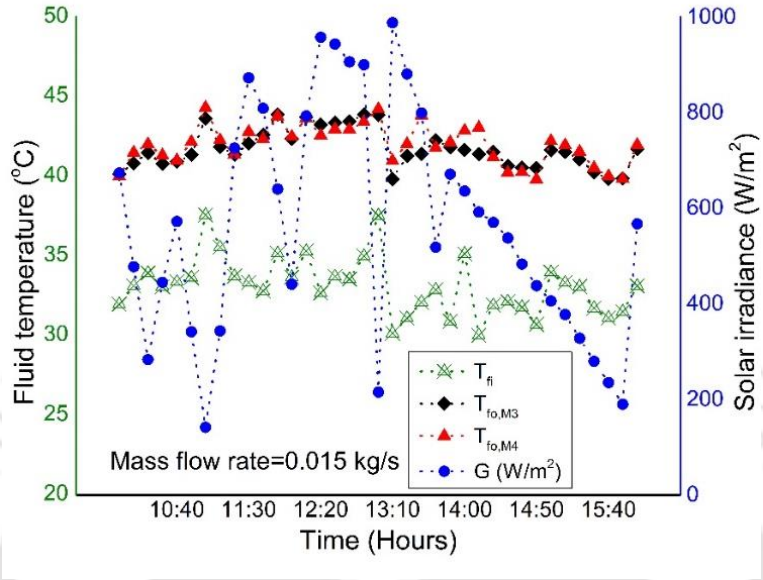

Figure 5.22. Variation of fluid outlet temperature

Figure 5.23 shows a comparison between various PV/Ts earlier developed with the PV/Ts developed in the present work. It has been observed that Hossain *et al.* (2019) [57] has found the maximum thermal efficiency of 74.2% among the compared works. This result is higher than the PV/T's mentioned in the present investigation; this is due to the use of the thermal conductive paste, whereas, in the present work, epoxy glue has been employed. However, in terms of electrical efficiency, the PV/Ts developed is comparable with the mentioned works.

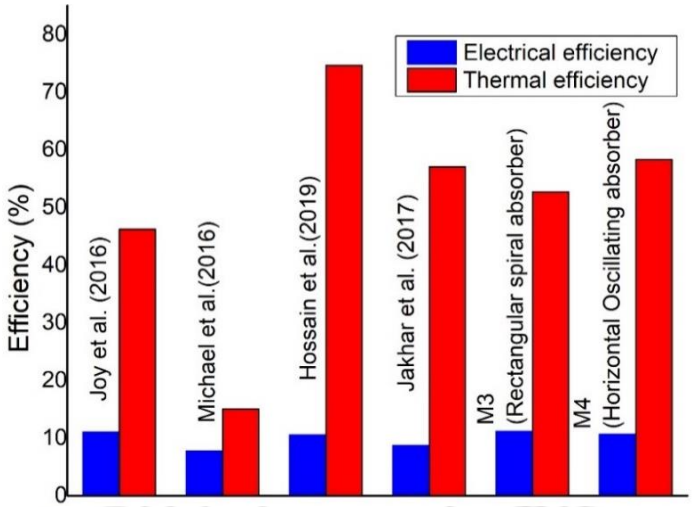

Figure 5.23. Comparison with some existing PV/Ts [57,283–285]

5.5 Experimental study on tube only rectangular spiral (M3) transparent PV/T collector with form stable PCM-biocomposite

5.5.1 Characterization of form stable PCM-biocomposite

5.5.1.1 Leakage test results

The leakage of the composite material during melting is observed through visual inspection followed by calculation of area covered by the melting PCM on the filter paper. The percentage of the area covered after the melting is given in **Table 5.2**. **Figure 5.24** shows photographs of the leakage test. Two samples (4:6 and 5:5) show no leakage of PCM on the filter paper. The 4:6 and 5:5 samples are observed to be mostly in powder form, which indicates that the composite formation is not proper. Sample 6:4 shows a little leakage because the porous biochar protected the melting of PCM through capillary action and surface tension force. The other three samples (7:3, 8:2 and 9:1) show a noticeable amount of leakage. This is because the amount of paraffin wax is excessive compared to biochar and so the adsorption of PCM on biochar pores fails. The mixture 6:4 shows the best formation stability on filter paper. Hence, it is selected for further characterization. PCM gets entrapped in the biochar matrix because of mechanical interaction providing form stability to the composite. Form stable PCM has an advantage over regular PCMs with respect to leakage and can be easily used with or without any encapsulation.

Table 5.2 Extent of leakage of the samples

Sample (PCM:Biochar)	Area covered after melting (cm^2)	% of filter paper area covered
4:6	No leaks were detected.	0
5:5	No leaks were detected	0
6:4	15	12.8
7:3	29.5	25.27
8:2	73	62.55
9:1	83	71.12

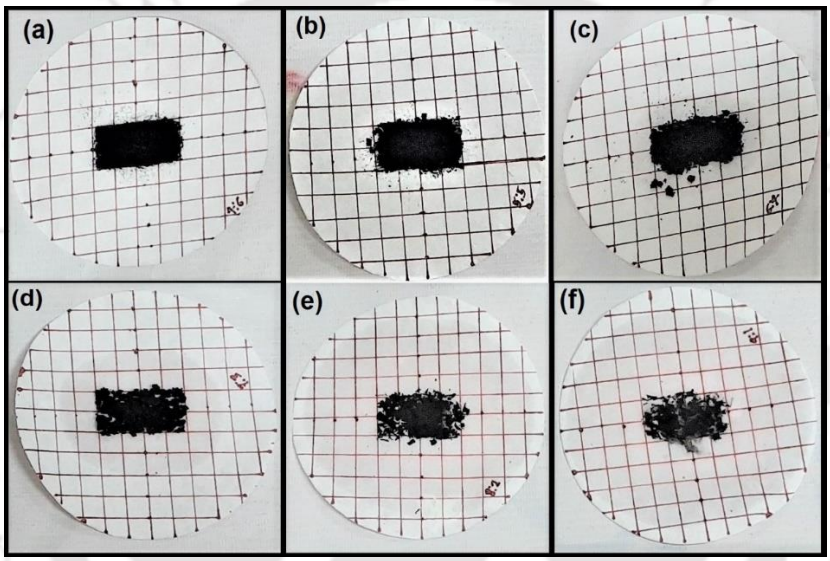

Figure 5.24. Leakage test of samples (a) 4:6, (b) 5:5, (c) 6:4, (d) 7:3, (e) 8:2, (f) 9:1.

5.5.1.2 Morphological analysis of the PCM-biocomposite

The morphological structure of both water hyacinth biochar produced at 550 °C (WH-550) and the PCM-biocomposite is presented in **Figure 5.25 (a) and (b).** The average pore size and pore volume of WH 550 obtained as 11.92 nm and 0.0417 cm^3/g, respectively from Brunauer, Emmett and Teller (BET) analysis, which confirms that WH 550 has a mesoporous (2-50 nm) surface structure. The abundance of wide pore size distribution is suitable for the absorption of melting paraffin wax during phase transition. **Figure 5.25 (b)** shows that the PCM is dispersed in the network of biochar. After solidification of the biocomposite, the shape remains stable without any seepage of melted Paraffin because the dispersion provides mechanical strength to the whole biocomposite.

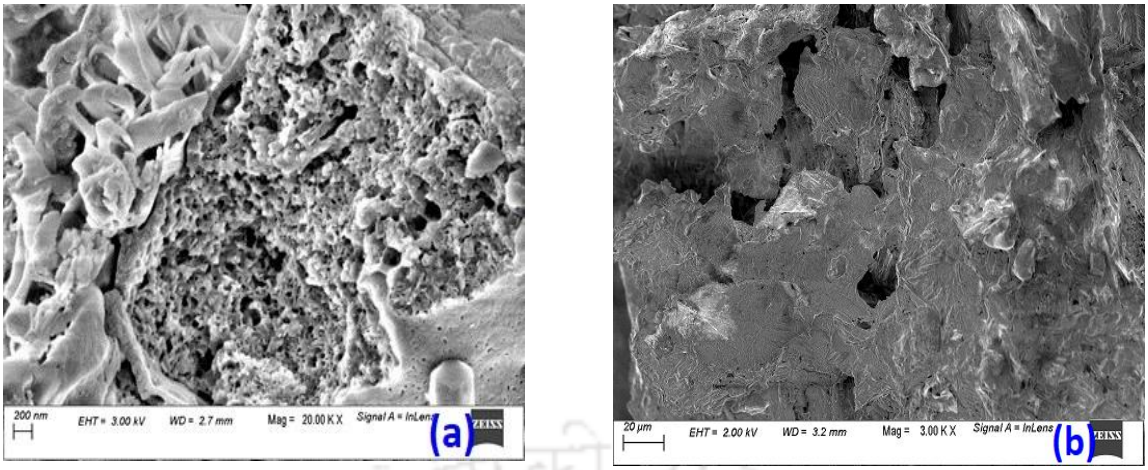

Figure 5.25. SEM images , (a) WH 550; (b) PCM-biocomposite

5.5.1.3 Fourier-transform infrared spectroscopy (FTIR)analysis

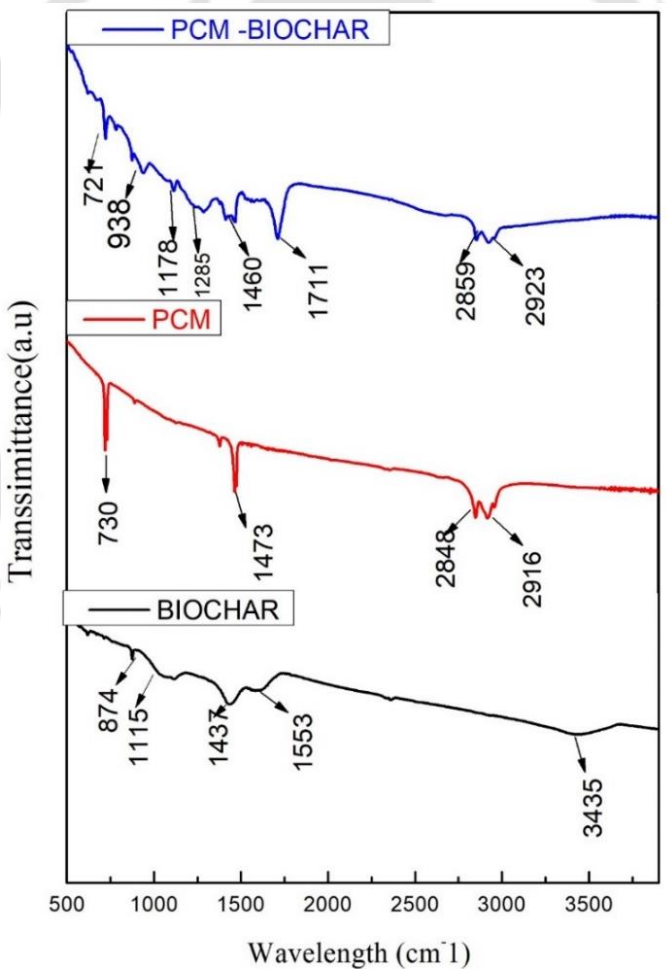

Figure 5.26. FTIR comparison curve for biochar, PCM and PCM-biocomposite

Figure 5.26 shows the FTIR spectral analysis of the three materials investigated in this study. The FTIR spectra of the composite material comprise all characteristic transmittance

bands of its pure constituents, which lie within the same range. Some little shift in the wavenumbers of the spectra is detected for the biocomposite material compared to pure PCM. For example, asymmetric stretching vibration of bending vibration bands detected at 2848 cm^{-1} shifted to 2859 cm^{-1}. These shifts might be attributed to the weak physical attractions caused by surface tension and capillary forces present in the material. Furthermore, no new band is identified in the spectral of the composite material. This shows that no chemical interactions happened amongst the constituents during preparation and after the formation of the composite. From the FTIR results, it can be inferred that there is a good physicochemical affinity among the raw materials used for the preparation of the composite.

5.5.1.4 X-ray diffraction (XRD) analysis

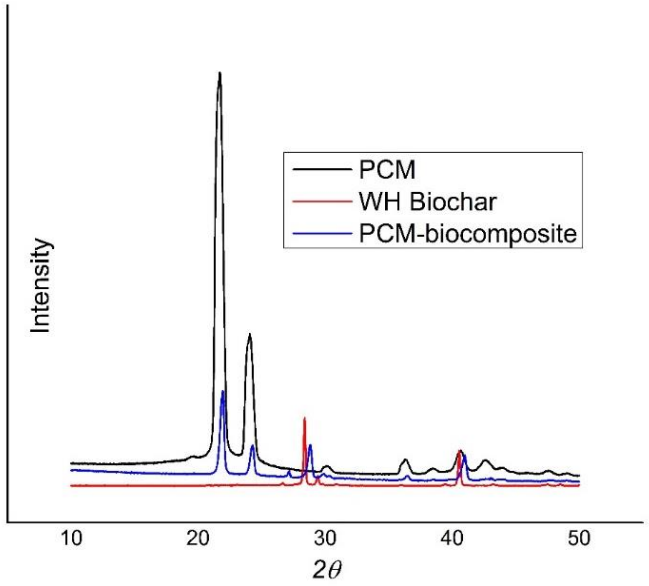

Figure 5.27. XRD comparison curve for biochar, PCM and PCM-biocomposite

The sharp peaks in between 20-25° in **Figure 5.27** for PCM indicates that PCM has good crystallization. The only visible difference is that the intensities of the composite material at the peak points are lower than that of the PCM. The justification for this result can be stated as the influence of biochar pores, which limits some crystal formation in the composite. A similar trend in the XRD pattern of PCM biocomposite confirms that the PCM can be held by the biochar matrix with no chemical reaction.

5.5.1.5 Thermal stability of the PCM-biocomposite

The thermal stability of phase change materials is one of the important criteria to determine its applications in thermal energy storage. **Figure 5.28** shows the

Thermogravimetric analysis (TGA) and Derivative Thermogravimetry (DTG) curves of the PCM. It can be observed that PCM has a single step degradation that starts approximately at 128 °C and full degradation of the sample takes place at 252 °C. The maximum degradation temperature required for the PCM is 240 °C, which is depicted by the sharp peak on the DTG curve. The TGA curve shows that the mass of the prepared PCM-biocomposite does not decrease until the temperature exceeded 128 °C, this shows that the composite has good thermal stability. Thus, the PCM-biocomposite can withstand higher temperatures than the PCM alone. Additionally, PCM has an approximate 99.1% of the weight of loss, whereas the composite has 63.84%. The values obtained in PCM-biocomposite are lower than in the PCM because of the existence of surface tension and capillary and forces in the materials used to prepare the composite. The presence of these forces not only assists in the shaping of the composite also increases the thermal stability of the material.

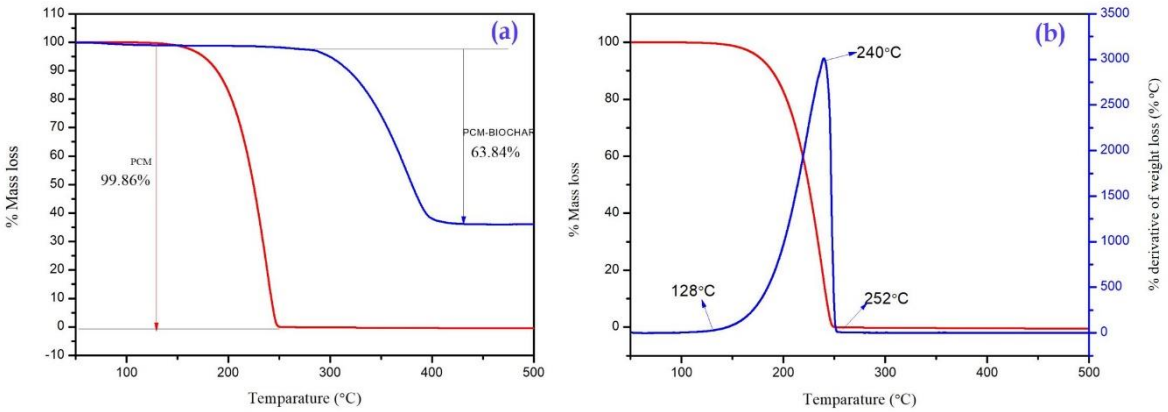

Figure 5.28. (a) TGA; (b) DTG curves for the PCM-biocomposite

5.5.1.6 Thermal properties

Melting point and heat of fusion

The Differential Scanning Calorimetry (DSC) results of the PCM-biocomposite is shown in **Figure 5.29**. The melting temperature of the biocomposite is found to be 31.49 °C which is slightly lower than that of pure PCM. This is due to the reduction in the crystal nucleus with the addition of biochar. The heat of fusion calculated from the figure is 78.12 J/g. This is lower than that of pure PCM. As the specific heat of PCM and biochar is high, so the overall thermal absorbance of the PCM-biocomposite decreases. The other reason attributed to the lower heat of fusion is the homogeneity of the distribution of biochar in the composite.

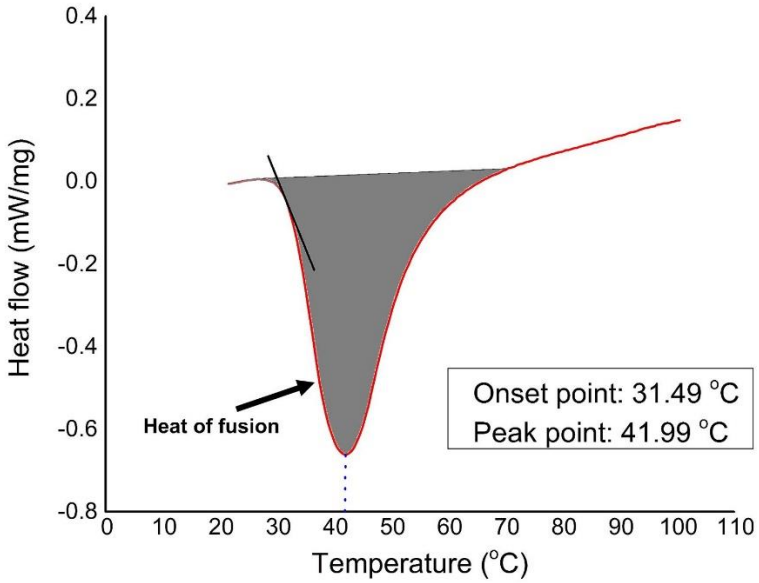

Figure 5.29. DSC curve for the PCM-biocomposite

Thermal conductivity

Table 5.3 Thermal conductivity result of PCM and PCM-biocomposite material

Material	**Solid Thermal Conductivity(W/mK) at 24 °C**	**Liquid Thermal Conductivity(W/mK) at 48 °C**
Pure PCM (Paraffin Wax)	0.18 ±0.0109	0.14 ±0.009
PCM-biocomposite	0.271 ±0.009	0.224 ±0.009
PCM-biocomposite with metal powder	0.302 ±0.009	0.238 ±0.009

Table 5.3 shows the thermal conductivity of three samples of thermal storage material at solid and liquid phase. The thermal conductivity of the PCM is enhanced up to 1.5 times with the addition of WH550 as a supporting matrix. The reason behind this enhancement is because of the filling of PCM material into the pores of WH550. Thus the resistance offered by air pores has been reduced and the thermal conductivity increases. Also, the addition of WH550 increases the amount of carbon in the composite material. The carbon content in WH550 biochar is 40.32%[288]. The addition of Aluminum metal powder further increases the thermal conductivity by 1.66 times higher than that of PCM alone. This is because of the high thermal conductivity range of metal powder. The metal powder acts as the bridge for thermal flow between adjacent biochar particles. Thermal effusivity is a property of PCM material to

exchange heat with its surroundings. Higher the thermal effusivity of PCM more is the rate of absorbance and release of thermal energy. The reason is that as the thermal effusivity increases the material can store more thermal load during a dynamic thermal process [289]. **Table 5.4** presents a summary of various key properties of the materials used for preparing the PCM-biocomposite.

Table 5.4 Properties of the PCM-biocomposite and its constituents

	Thermal conductivity (W/mK)	**Specific heat** (kJ/kgK)	**Heat of fusion** (kJ/kg)	**Melting point** ($^{\circ}C$)
Aluminium powder [290]	237	0.89	10.67	660
PCM (OM35)	0.14 (liquid) 0.18 (solid)	1.65	197	35
Water hyacinth biochar	0.12	1.03	7.18	228
PCM-biocomposite	0.224 (liquid) 0.271 (solid)	0.42	78.12	31.49

Charging-discharging time

Figure 5.30 shows the temperature history of the PCM and PCM-biocomposite under natural cooling at ambient temperature. The time taken by the pure PCM to reach the melting temperature (35 °C) from 25 °C is 28 minutes whereas, for the PCM-biocomposite, it is 34 minutes. The trend is reversed in case of the discharging process; the PCM-biocomposite is found to have longer thermal energy retention as compared to the pure PCM. The PCM-biocomposite and pure PCM takes 40 minutes and 36 minutes, respectively, to reach a temperature of 25 °C.

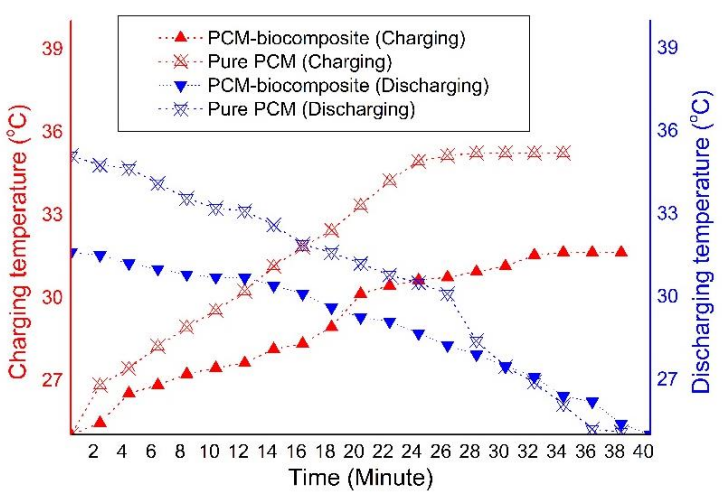

Figure 5.30. Temperature variation during charging and discharging

5.5.2 Outdoor experimental investigation

The tube only PV/T collectors have the limitation of not covering the entire PV surface with tubes due to material constraints. Therefore, PCM can be used as an effective solution with tube only absorber to arrive at an efficient PV/T system. But, before using PCM, the inherent drawback of leakage and lower thermal conductivity need to be addressed. The issue of leakage has been addressed by creating a form-stable PCM-biocomposite material using porous water hyacinth biochar. Water hyacinth biochar acts as shape stabilizers and did not allow the PCM to flow from its matrix, thus providing form stability to the PCM-biocomposite. The second issue of thermal conductivity is addressed using Aluminium powder (5% by weight) to the PCM-biocomposite. The M3 collector with a layer of form-stable PCM-biocomposite is tested under outdoor and indoor conditions. The experimental findings show that among the developed collectors, the collector with rectangular spiral configuration (M3) exhibited satisfactory performance.

In an experimental study of solar collectors, it is essential to know the pattern of climatic parameters to understand the dynamics of the system. **Figure 5.31** shows the variation of solar radiation, ambient temperature and wind speed on a clear sunny day. The ambient temperature observed to increase from the morning and remain higher from 11:30 hr to 14:00 hr and decreases towards the evening. The wind speed variation cannot be attributed to any specific pattern.

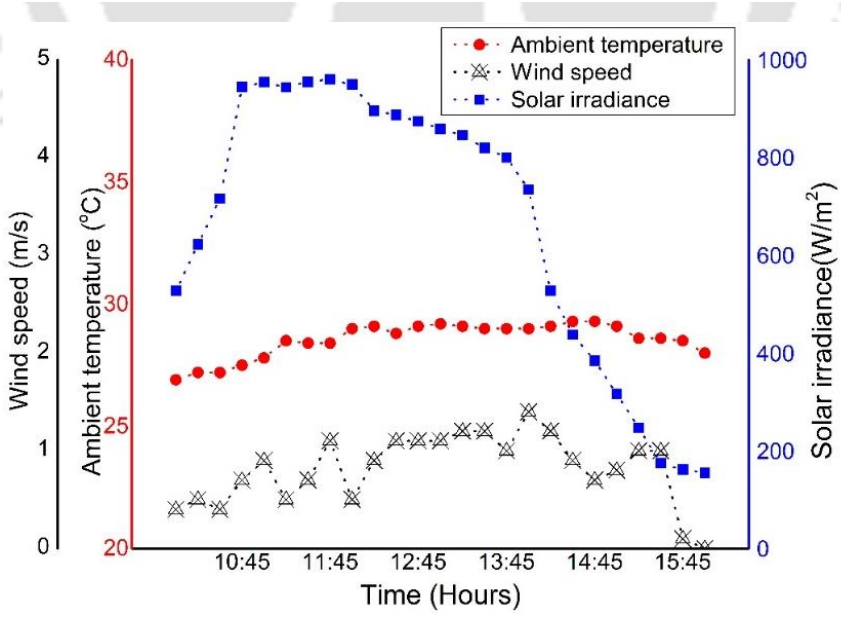

Figure 5.31. Climatic parameters variation

5.5.2.1 Surface temperature profile

Figures 5.32 - 5.34 show the temperature profile of the M3 with PCM- biocomposite and PV system at 12:00 hr, 12:30 hr and 13:00 hr, respectively. It can be seen from the figures that the surface temperature of M3 with PCM- biocomposite is reasonably lower than that of PV at all three instances. The average surface temperature of the PV is found to be 43.1 °C at 12:00 hr, whereas, in case of the M3 with PCM- biocomposite the temperature is reduced by 12.5 C under the same conditions. The reduction in the surface temperature at 12:30 hr and 13:00 hr is calculated to be 12.2 °C and 8 °C, respectively. A maximum of 29% reduction in the surface temperature of the M3 as compared to PV has been observed using the form the stable PCM-biocomposite. This reduction results in 18.4% improvement in electrical output. The average temperature of the modules found to decrease with the decrease of the solar irradiance. One of the important heat sources in the PV is the Ohmic heat generation [291], the intensity of this source is directly dependent on the solar radiation. Thus the intensity of the solar radiation is the key parameter that influences the PV temperature. An interesting observation that can be drawn from all the figures is that the use of PCM-biocomposite successfully maintained the surface temperature of M3 below its melting point. The insertion of the PCM-biocomposite to the M3 is useful to check the maximum working temperatures within a safe limit, thus acting as a protection for the PV module from overheating and helps to enhance the lifespan of the system.

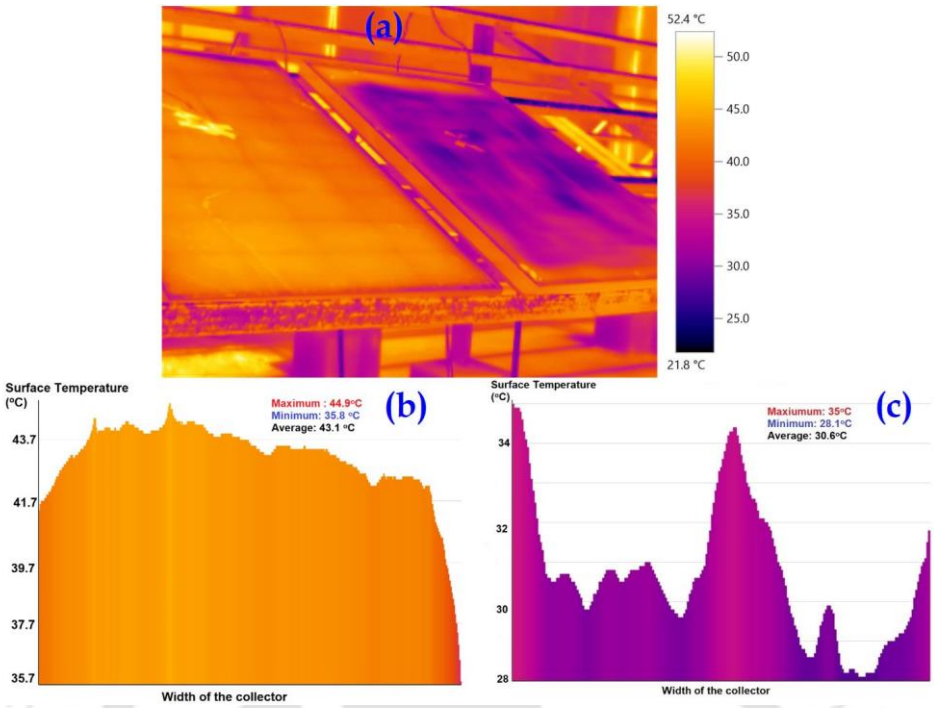

Figure 5.32. At 12:00 hr: (a)Temperature profile of the collectors ;(b) Temperature variation across width of the PV; (c) M3 with PCM-biocomposite

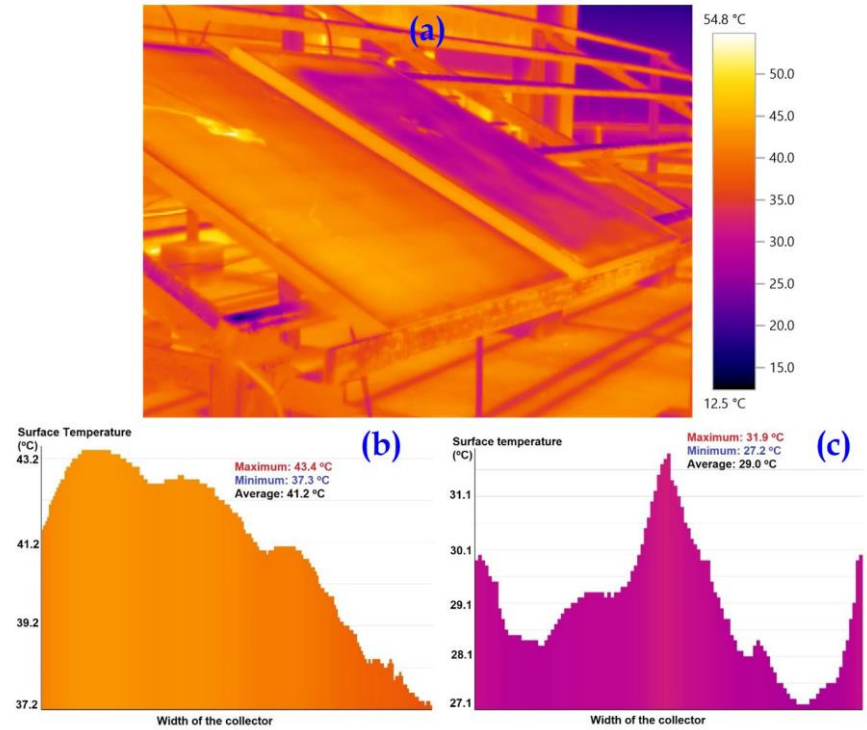

Figure 5.33. At 12:30 hr: (a)Temperature profile of the collectors ;(b) Temperature variation across width of the PV; (c) M3 with PCM-biocomposite

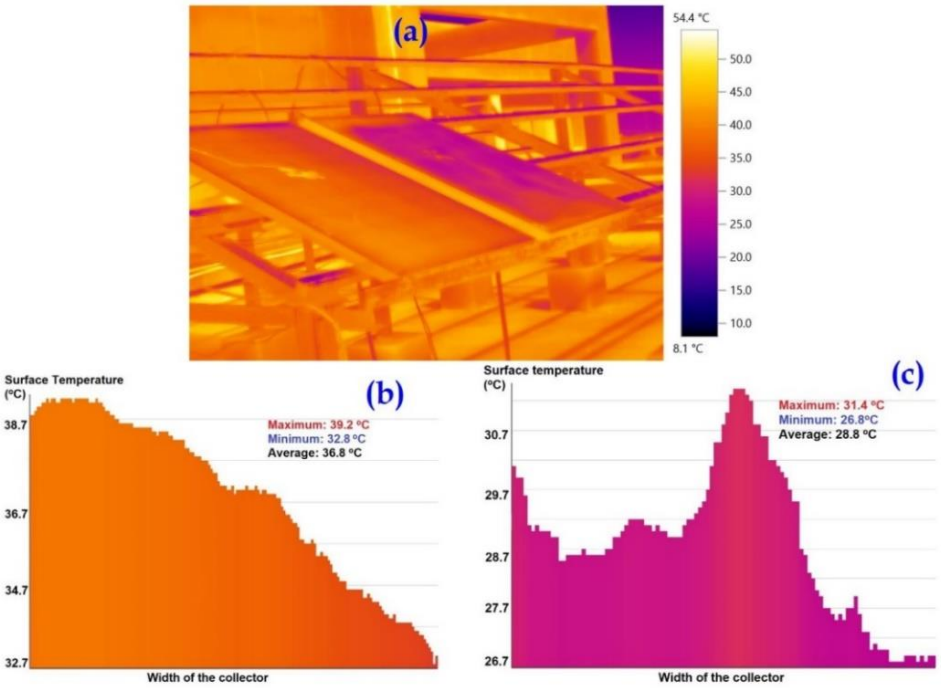

Figure 5.34. At 13:00 hr: (a)Temperature profile of the collectors ;(b) Temperature variation across width of the PV; (c) M3 with PCM-biocomposite

The temperature is found to be dependent on solar irradiance. The fluid outlet temperature increases as the solar irradiance increases. The difference between the outlet and inlet fluid is higher during noon but the gap narrows down toward the end hours of the experiment; this can be observed from **Figure 5.35**. Temperature of the PCM-biocomposite layer was recorded at two different locations (shown in **Figure 3.19**) i.e. at the PCM-biocomposite surface closer to the PV rear surface and at a depth of 8 mm from the PV rear surface. The PV module temperature measure on its back surface varies from 44.39 °C to a maximum of 54.80 °C at 12:15 hr and then decreases to a value of 37.37 °C. The temperature of PV/T back surface is found to be in the range of 33.42 - 44.40 °C. The cooling provision and PCM-biochar composite help to keep the PV/T surface cool.

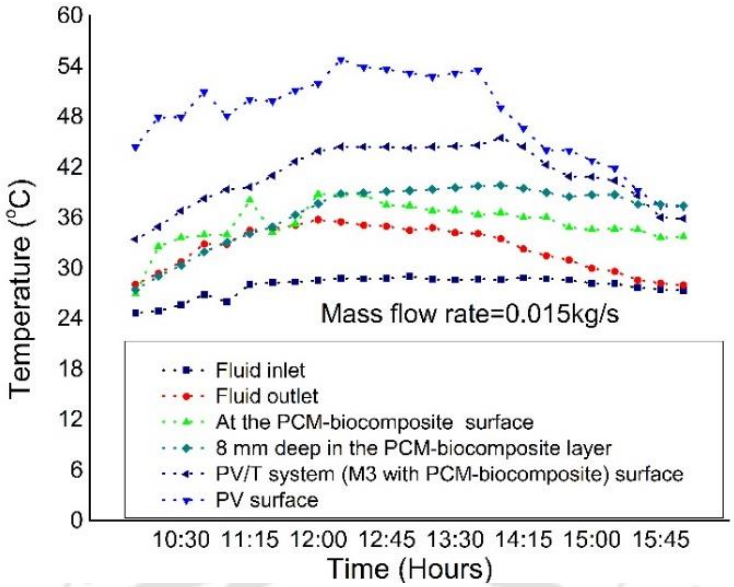

Figure 5.35. Temperature of various components of M3 with PCM- biocomposite

5.5.2.2 Performance evaluation

Figure 5.36 shows the variation of electrical power output throughout the day. Electrical output follows a similar trend that of solar irradiance. It initially keeps on increasing till the solar noon and then start descending. The electrical output is found to be higher for the PV/T system as compared to the PV. It has been observed that the difference in electrical output between PV/T and PV is more during the peak hours of the day. This difference is found to be a maximum of 18 W at 13:00 hr. The difference in the electrical output between the two collectors decreases as the irradiance reduces. The reason is the reduction in the intensity of solar radiation towards the latter half of the day, the temperature difference between the surface of the PV in the two collectors keeps on decreasing. The electrical output varies from 46.6 W at 10:00 hr and reaches the maximum of 86.2 W at 11:30 hr when the corresponding solar irradiance is 954.9 W/m^2.

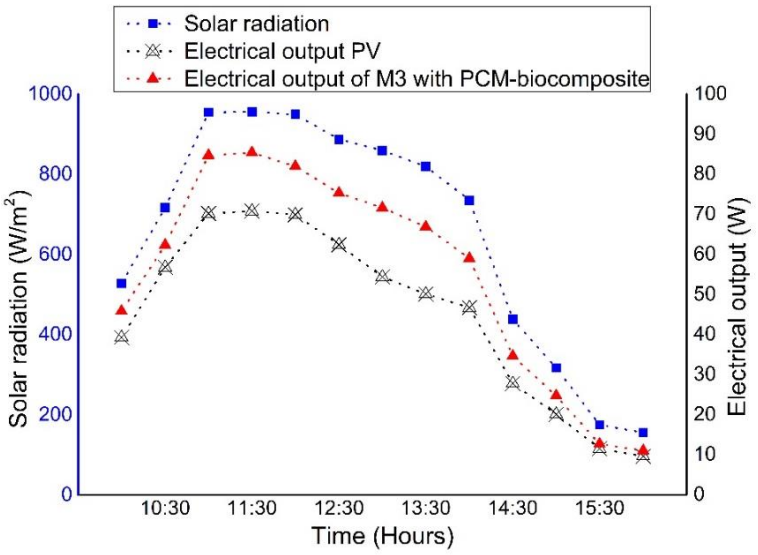

Figure 5.36. Variation of electrical output for M3 with PCM-biocomposite and PV

Figure 5.37 shows the variation of electrical efficiency for PV and M3 with PCM-biocomposite. The electrical efficiency is observed to be mainly dependent on solar irradiance and operating temperature. A dip in the electrical efficiency of the PV module without cooling is observed between 11:30 hr to 13:30 hr. During this period the irradiance is higher in the day and the PV surface temperature remains above 50 °C. The temperature has been reported to affect the electrical conversion efficiency negatively. The electrical efficiency for the M3 with thermal regulation through the use of PCM-biocomposite observed to be unaffected during peak sunshine hours. Even during the peak hours of the day temperature of the PV surface in the M3 with PCM-biocomposite remains between 42.6 and 45.4 °C. The electrical efficiency for M3 with PCM-biocomposite at 10:00 is 13.1%, which increases to 13.47% at 11:30 hr and slowly decreases and reaches a minimum value of 11.3% at 16:00 hr. The average electrical efficiency of the collector M3 with PCM-biocomposite is found to be 12.54 ± 1.31%, whereas for the bare PV 10.2 ± 1.31%.

The application of the form stable PCM-biocomposite has successfully regulated the thermal output of the M3. The thermal efficiency even after the solar radiation drops remains closer to 50 %, whereas, without PCM-biocomposite, it drops to 38%. This is due to the release of stored energy in the PCM-biocomposite layer once the thermal energy supplies reduced, i.e., after removing sun exposure. The thermal efficiency for the M3 with PCM-biocomposite found varying from 60.3% to a maximum of 71.2%, as shown in **Figure 5.38**. Though the addition of PCM-biocomposite did not affect the thermal efficiency significantly in the peak hours but it caused improvements in a better distribution of the heat produced during the day

thus increasing the average thermal efficiency over the day. The average thermal efficiency for the PV/T system found to be 61 ± 3.08%. The PV/T system with energy storage material has the potential to shift the time of availability of thermal energy. The thermal energy during peak sunlight hours can be stored and discharged to the water at a later time.

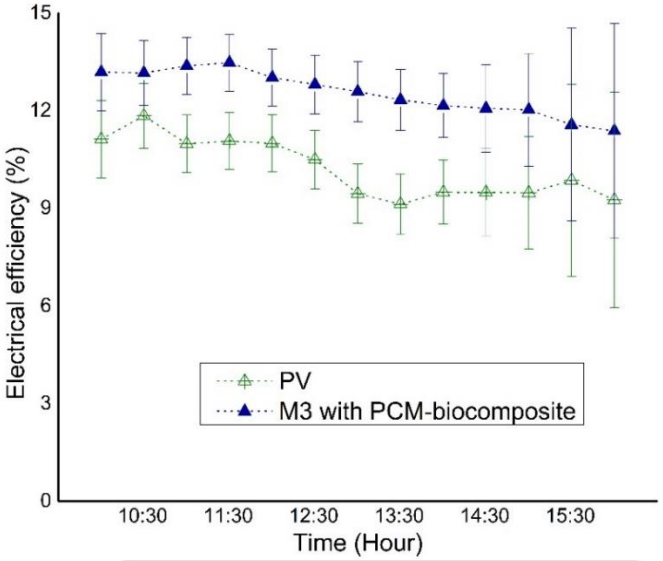

Figure 5.37. Variation of electrical efficiency

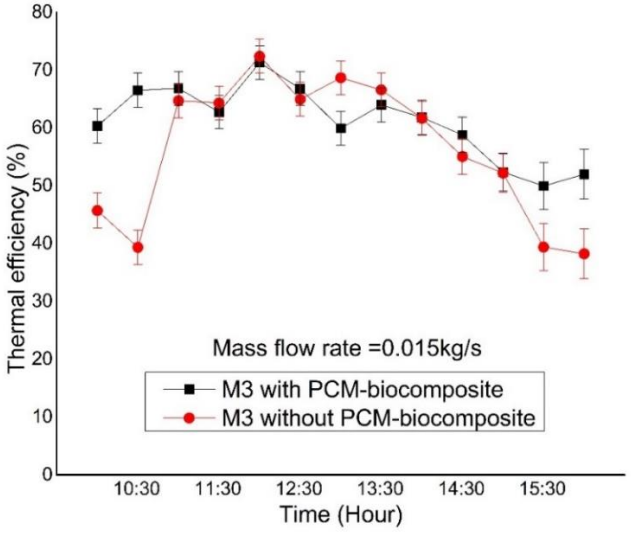

Figure 5.38. Variation of thermal efficiency of M3 with and without PCM-biocomposite

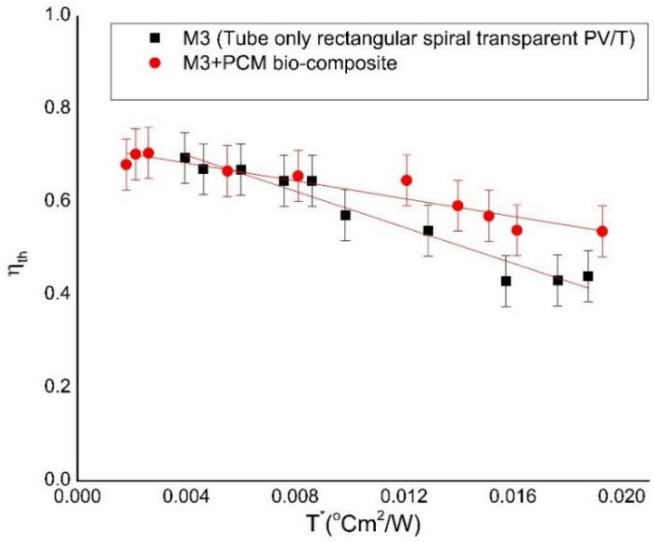

Figure 5.39. Thermal efficiency curves for M3 and M3 with PCM-biocomposite

The thermal efficiency curves for M3 and M3 with PCM-biocomposite are shown in **Figure 5.39**. The application of PCM-biocomposite help in checking the sudden drop in the thermal efficiency even at the higher inlet temperatures. The thermal efficiency at zero reduced temperature for M3 without PCM-biocomposite and M3 with PCM bio-composite as represented by the intercepts of the trend lines shown in the figure are 0.77 and 0.72 respectively. The slopes for M3 without PCM-biocomposite and M3 with PCM bio-composite are 19.37 $Wm^{-2}/°C$ and 9.56 $Wm^{-2}/°C$ respectively. The heat loss in case of the PV/T collector with PCM-biocomposite is lower as that of the collector M3. This is due to the heat which otherwise would have been lost from PV back surface to the ambient is absorbed by the PCM-biocomposite and transfer into the fluid flowing through the tubes.

The overall exergetic efficiency for the developed collectors has been shown in **Figure 5.40**. It has been observed that overall exergetic efficiency follows a similar trend as that of electrical efficiency. Since electrical energy is a high grade of energy as compared to the low-temperature thermal energy generated from the PV/T collector. Thus, the effect of electrical efficiency in the calculation of overall exergetic efficiency is significant. The overall exergetic efficiency for M3 with PCM-biocomposite found to be higher than other PV/Ts. It varies in the range of 12.21 to 15.8%. The average overall exergetic efficiency for M1, M2, M3, M4 and M3 with PCM-biocomposite are 12.3%, 13.6%, 13.9%, 13.2% and 14.3%, respectively. The improvement in the overall exergetic efficiency of the M3 collector with the integration of

PCM-biocomposite is attributed to the efficient cooling and better distribution of thermal output over the day.

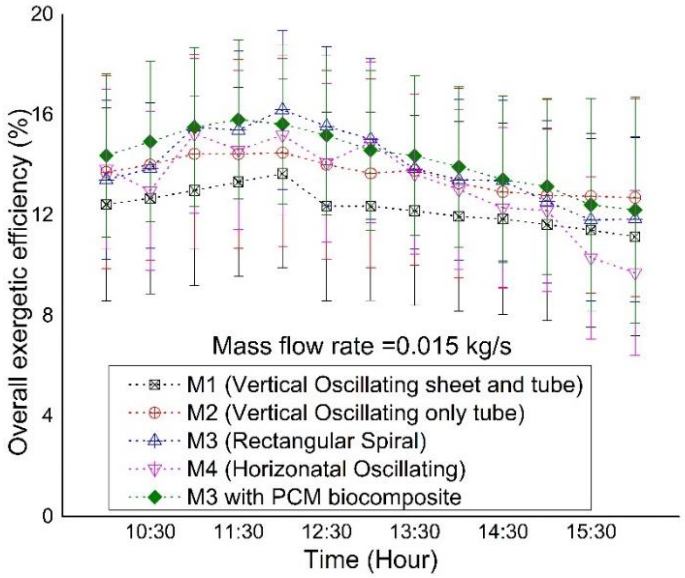

Figure 5.40. Variation of overall exergetic efficiency of the PV/Ts

5.6 Economic assessment and environmental analysis

The Net Present Value (NPV) has been calculated at various discount rates (2-30%) by keeping the inflation rate fixed. It has been observed from **Figure 5.41** that NPV decreases as the discount rate increases. NPV is found to be highest for M3 with PCM-biocomposite followed by M4 collector. The Internal Rate of Return (IRR) can be calculated from **Figure 5.41**. IRR for M1, M2, M3, M4 and M3 with PCM-biocomposite are 22%, 12%, 22%, 24% and 28%, respectively. The higher an IRR, the more desirable an investment is to undertake. Thus, it can be concluded that M3 with PCM-biocomposite provide a satisfactory investment option for consumers based on NPV and IRR.

Levelised production cost (LPC) is focussed on cost and provide a convenient method of evaluating the contribution of individual cost components toward the system levelised cost. LPC has been calculated at three different inflation rates (low, average and high) considering last 20-year data. LPC for M3 with PCM-biocomposite is found to be lowest, while highest for M2 at all the inflation rates (**Figure 5.42**). The LPC for M3 with PCM-biocomposite is found to be 4.0 INR/kWh while for M3 without the PCM-biocomposite, the LPC is 4.3 INR/kWh. The decrease in the LPC for M3 with PCM-biocomposite is due to improved electrical and thermal output. **Figure 5.43** shows the influence of capital cost on LPC. In the present study, the reduction in capital cost is considered by keeping in mind the decreasing price trend for PV

modules, electrical components and batteries with technological advancements. With the reduction of capital expenditure on the collectors, the LPC goes down. For collector M1, M2, M3, M4 and M3 with PCM-biocomposite the LPC decrease by 20.3%, 21.4%, 20.6%, 20.7% and 19.9% respectively, with 30% reduction in the capital cost of the PV/T systems. LPC value of M3 with PCM-biocomposite and M4 are close, due to the additional cost of PCM-biocomposite at a specific interval of time through the lifespan of the collector M3 with PCM-biocomposite.

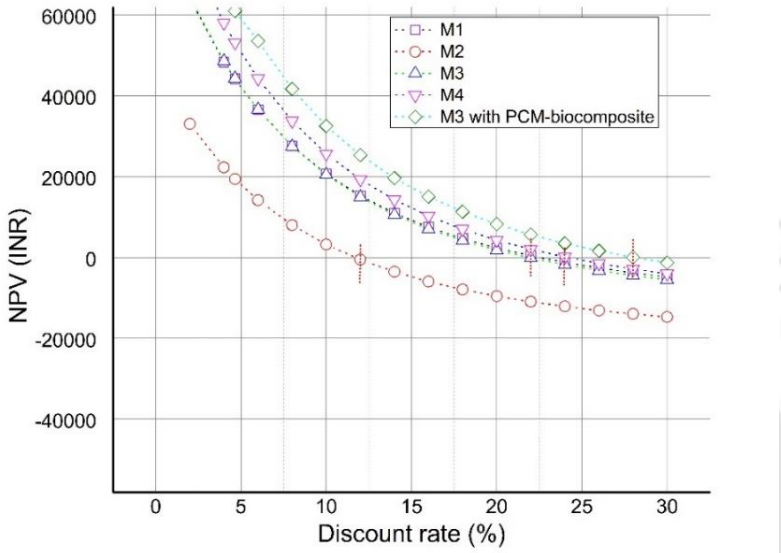

Figure 5.41. Effect of discount rate on NPV

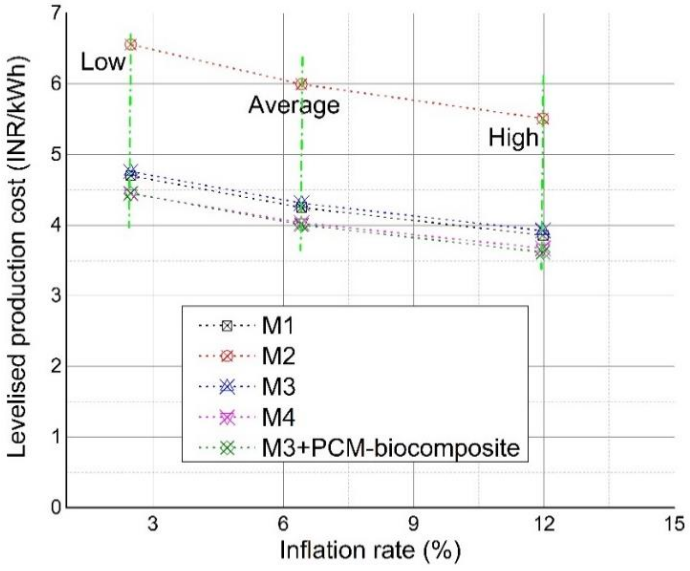

Figure 5.42. Effect of inflation rate on LPC

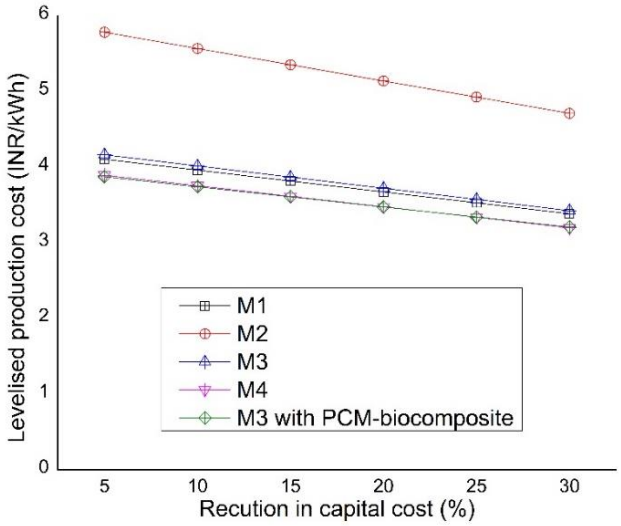

Figure 5.43. Effect of reduction in capital cost on LPC

The carbon dioxide mitigation achieved during the lifetime of the collectors and environmental cost is shown in **Figure 5.44.** It is possible to mitigate 12.5 tCO_2, 10.4 tCO_2, 12.7 tCO_2, 13.9 tCO_2, and 15.2 tCO_2 by collector M1, M2, M3, M4 and M3 with PCM-biocomposite, respectively, over the lifespan of the collectors. These results show that M3 with PCM-biocomposite has a higher possibility of CO_2 emission reduction and higher environmental cost reduction compared to other collectors mentioned in this work. This is because the M3 with PCM-biocomposite exhibited higher energy production. It can be resumed from the above results that M3 with PCM-biocomposite offers higher benefits in terms of environmental cost and is a better choice based on this enviro-economic analysis as compared to other collectors investigated in the present work.

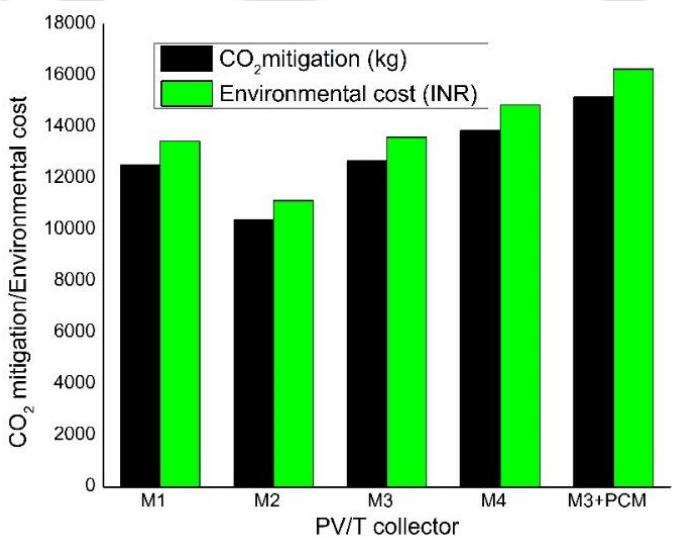

Figure 5.44. CO_2 emission reduction and environmental cost of the PV/Ts

5.7 Summary of the chapter

The results of the experimental investigation study on M1 (tube only vertical oscillating), M2 (tube and sheet vertical oscillating), M3 (tube only rectangular spiral), M4 (tube only horizontal oscillating) and M3 with PCM-biocomposite, and enviro-economic analysis have been presented in this chapter. The thermal efficiency of M1 is higher as compared to M2. While the average electrical efficiency of collector M2 found to be only 0.6% more as compared to M1. However, from economics perspective, M1 is found to be way better than M2. Both, NPV and IRR for M1 is higher as that of M2. Therefore, M3 and M4 collectors were developed without an absorber sheet and experimentally investigated. The electrical and overall exergetic efficiency for M3 has been observed to be higher than M4. The average electrical efficiency is found to be 10.17%, 11% and 12.15% for PV, M4 and M3 collector, respectively. M3 is considered for application of novel PCM-biocomposite material and its performance investigation. Detailed characterization of the PCM-biocomposite material was discussed and the PV/T system performance with its application has been investigated. The novel PCM-biocomposite material developed using simple impregnation method was found to have better form stability and thermal properties appropriate for application in thermal and electrical output regulation of PV/T system. The thermal efficiency even after the solar radiation drops remains closer to 50%, whereas, without PCM-biocomposite, it drops to 38%. The average overall exergetic efficiency for M1, M2, M3, M4 and M3 with PCM-biocomposite are 12.3%, 13.6%, 13.9%, 13.2% and 14.3%, respectively. NPV is found to be highest for M3 with PCM-biocomposite followed by M4 collector. IRR for M1, M2, M3, M4 and M3 with PCM-biocomposite are 22%, 12%, 22%, 24% and 28%, respectively. M3 collector with PCM-biocomposite also has a higher possibility of CO_2 emission reduction and higher environmental cost reduction. M3 with PCM-biocomposite is found to be suitable in terms of economic and environmental analysis as compared to other collectors investigated in the present work. The summary of the research findings of the present investigation is presented in the next chapter (Chapter 6).

6

Conclusions and scope for future work

6.1 Brief summary of the investigation

The present investigation is attempted to enhance the performance of PV/T collectors by addressing the current challenges associated. The investigation includes thorough thermal modelling of conventional sheet and tube type PV/T collector (M2) to understand the effect of various component on the overall efficiency of the system. The model also considers the thermal contact resistance between the layers of PV/T system, individual resistance of the layers and Ohmic heat generation in the PV layer. The simulation results of the novel thermal model showed that the use of the absorber sheet augments the thermal resistance and inhibits the heat flow from the PV layer to the fluid stream in the tubes. To address this fact a detailed and long term comparative experimental study has been carried out in which tube type (M1) and sheet and tube type PV/T (M2) collectors are used. The study showed that collector M1 was better compared to M2, both in terms of thermal efficiency and economic feasibility. Furthermore, to address the challenges of enhancing thermal efficiency and cooling uniformly of PV, two more new designs of absorber system namely rectangular spiral (M3) and horizontal oscillating (M4) have been developed and tested. Based on the experimental observation, the rectangular spiral absorber collector (M3) has been found to give better thermal efficiency and cooling uniformity as compared to M4 collector and hence M3 collector is taken forward for the subsequent study. The final component of the study was the development of a novel form-stable phase change biocomposite material using water hyacinth biochar as a matrix and its integration with the PV/T collector. The novel material developed showed satisfactory thermal properties desired for application as a thermal energy storage medium. The integration of the PCM-biocomposite material in M3 collector showed enhanced thermal performance and cooling uniformity, which results in improvement of electrical output. The economic analysis also showed the feasibility of such an integrated system. The important findings of various components of the present study are presented in the subsequent subsections.

6.1.1 Summary of numerical investigation

A novel thermal model has been developed to investigate the influence of thermal contact resistance between different layers of a sheet and tube PV/T system, individual resistance of the layers and Ohmic heat generation. This has been explained in Chapter 4. The performance of the developed thermal model has been compared with the model developed by Huide *et al.* (2017) [192] where thermal contact resistance and heat generation in PV cells

were not considered. Finally, the model results have been compared with experimental findings. It is observed that both the experimental and simulation results of the developed model are in good agreement. The Root Mean Square Errors (RMSE) of 3.75 K, 1.36 K and 2.71 K were found for the water outlet temperature, glass surface temperature and cell temperature, respectively. The inclusion of the contribution of thermal contact resistance and Ohmic loss in the PV/T system improves the model performance significantly.

6.1.2 Summary of experimental study on tube only vertical oscillating (M1) and sheet-tube vertical oscillating (M2) PV/T collectors

Two different PV/T collectors viz. tube only vertical oscillating collector (M1) and sheet-tube vertical oscillating collector (M2) were designed and fabricated to validate the model results. The methodology of the experimental study on M1 and M2 and experimental results are presented in Chapter 3 (section 3.3) and 5 (section 5.3) respectively. The electrical conversion efficiency of M1 collector found to be varied from 11.65 % to a maximum of 12.30 % at 12:00 hr at a corresponding solar irradiance of 940 W/m^2. Whereas, for M2 collector electrical efficiency found to vary from 12.38 % to 13.6 % at the same solar irradiance. The thermal efficiency of M1 collector is observed to be higher than M2. The higher thermal efficiency of M1 is due to higher teat transfer rate (less resistance) from the top surface of the PV/T to the fluid flowing through the tubes as compared to M2. The thermal efficiency of M1 was higher as compared to M2. While the average electrical efficiency of collector M2 found to be approximately 0.6% more as compared to M1. The average electrical efficiency of M1, M2 and PV collector were calculated to be 11.67%, 12.27% and 10.30% respectively. The thermal efficiency of M2 collector found to be in the range of 33 - 66.7%. However, from economics perspective, M1 is found to be better than M2. Both, NPV and IRR for M1 is higher as that of M2. Therefore, M3 and M4 are fabricated without an absorber sheet.

6.1.3 Summary of experimental study on tube only rectangular spiral (M3) and horizontal oscillating (M4) transparent PV/T collectors

A comparative experimental study on two water type PV/T collectors viz. rectangular spiral (M3) and horizontal oscillating (M4) have been carried out which were presented in Chapter 5 (section 5.4). The test results demonstrate that the thermal efficiency of M4 collector was higher, whereas electrical efficiency of M3 collector was higher. The calculated average thermal efficiency of M4 collector (58.3%) is found to be 10.6% higher than that of M3 collector.

The average surface temperature of M3 collector is lower than M4. An improvement of electrical efficiency by 14% in the case of M3 collector as compared to PV has been observed. The outlet fluid temperature of the PV/T collectors is found to be in the range of 36 -38 °C. This is a suitable temperature for an application like taking shower. This confirms that use of PV/T's to electricity along with heat energy for meeting hot water demand. Further, this technology could reduce the dependence on electrical geyser for the generation of hot water. Based on the experimental investigation, M3 collector is found to be best, because the M3 collector outweighs the other PV/Ts in terms of electrical efficiency and economics. Hence PCM based bio-composite is applied in M3 for further investigation of cooling uniformity.

6.1.4 Summary of experimental study on tube only rectangular spiral (M3) transparent PV/T with form stable PCM-biocomposite

A novel form stable PCM-biocomposite has been developed using biochar derived from water hyacinth is embedded on the enclosure formed by the PV and back cover to improve cooling uniformity and better absorption of incoming radiation. The process development for preparation of PCM-biocomposite and results are explained in Chapter 3 (section 3.4) and 5 (section 5.5) respectively. The PCM-biocomposite contains a small fraction of metal powder (5% wt.) to improve the thermal conductivity. A simple Impregnation method is employed to produce form stable composite material. The form-stable PCM-biocomposite material has the characteristics of good thermal and structural stability. The best mixing ratio (PCM:biochar) is found to be 6:4 (wt/wt%) with minimum leakage of PCM from the biocomposite. The chemical properties of the composite remain the same as the pure PCM, this confirms no chemical interaction between the PCM and biochar. The heat of fusion is calculated to be 78 J/g. The thermal conductivity of the PCM is enhanced up to 1.5 times with the addition of Water Hyacinth biochar as a supporting matrix. The addition of Aluminum metal powder further enhances the thermal conductivity by 1.66 times higher than that of PCM alone. The charging and discharging time is also evaluated experimentally and results are found to be satisfactory. A comparative study with conventional PV module is also carried out as part of the study. The average surface temperature of the PV collector was found to be 43.1 °C at 12:00 hr whereas, the surface temperature of PV/T collector was found to be 30.6 °C at 12:00 hr under similar climatic condition. This is about 29% reduction in the surface temperature when PV/T collector with form stable PCM-biocomposite is applied. Further, this reduction results in 18.4% improvement in electrical output. The insertion of the PCM-

biochar composite to the PV/T collector is found to be useful to check the working temperatures within a safe limit, thus acting as a protection for the PV module from overheating and helps to enhance the lifespan of the system. A maximum difference of electrical output between PV/T collector and PV is found to be 18 W at peak sunshine hours. The difference in the electrical output between the two collector's decreases as the irradiance reduces. The thermal efficiency of the PV/T collector is found to be varying from 60.3% to 71.2%. The use of the PCM-biocomposite results in better distribution of the heat production, and maintains thermal efficiency at a higher range in off sun hours. The average electrical and thermal efficiency of the PV/T collector is found to be 12.54 % and 61 % respectively. This study is expected to serve as a foundation for the synthesis of "green PCM-biocomposite" in the thermal energy storage domain. The refinement of this technology and commercialization will give a new dimension to the solar industry for effective generation of electricity and heat.

6.2 Scope for future work

A detailed experimental study has been carried out in the study to arrive at an efficient PV/T collector design based on the performance parameters. Development of PV/T collectors and optimization of absorber configurations for better cooling uniformity and thermal efficiency has been carried out as well as novel form-stable bio-composite also been employed for better results. Further, this research may be extended to the following outlined areas

- In the current investigation, PV/T collectors are tested under hot and humid condition. Recycling of the heat transfer fluid when the system is operating in a hot climate the fluid temperature will increase with time and thus its cooling capacity will be reduced. Therefore, there is a need of an efficient cooling mechanism for such conditions, keeping the energy consumption at a minimum level and higher exergy output of the system.
- Application of PCM is an effective solution for thermal management of PV/T collectors but the use of a single PCM with a fixed melting point is not sufficient to cool the PV throughout the year as the ambient temperature is varying. Therefore, mixing of multiple PCM with different melting point can be studied for better performance.
- Optimization of solar cell geometry, the gap between successive cells and the transparency of the back sheet are some of the important areas of study to improve the performance of the PV/T hybrid systems.

- The consideration of wind speed and relative humidity are two important meteorological parameters, which may have some effect on the output of the PV/T collector. Including these two parameters in the developed thermal model may provide more accuracy.
- A better method such as vacuum impregnation may be employed for the preparation of efficient form stable PCM bio-composite.
- Incorporation of all the chemical and thermal properties of PCM and other material in the model for numerical investigation of PV/T collectors.

References

[1] Razdan A. August 2016, Power for All 2016;Aug:7–14.

[2] Breitschopf B, Held A, Resch G. A concept to assess the costs and benefits of renewable energy use and distributional effects among actors: The example of Germany. Energy Environ 2016;27:55–81. doi:10.1177/0958305X16638572.

[3] WEF. Energy Vision 2013 Energy transitions: Past and Future. World Econ Forum 2013:22.

[4] Chen N. Energy in the 21st century. China Pet Proc Petrochem Technol Q 2000;1:14–21.

[5] Impacts CC. Not Just a Number : n.d.

[6] CO2.earth n.d. https://co2.earth/.

[7] 350.org n.d. http://400.350.org/.

[8] Al-Maamary HMS, Kazem HA, Chaichan MT. The impact of oil price fluctuations on common renewable energies in GCC countries. Renew Sustain Energy Rev 2017;75:989–1007. doi:10.1016/j.rser.2016.11.079.

[9] Scripps Institution of Oceanography. The Keeling curve n.d. https://scripps.ucsd.edu/programs/keelingcurve/.

[10] Husain AAF, Hasan WZW, Shafie S, Hamidon MN, Pandey SS. A review of transparent solar photovoltaic technologies. Renew Sustain Energy Rev 2018;94:779–91. doi:10.1016/j.rser.2018.06.031.

[11] Kim I-S. Robust maximum power point tracker using sliding mode controller for the three-phase grid-connected photovoltaic system. Sol Energy 2007;81:405–14. doi:10.1016/j.solener.2006.04.005.

[12] Das D, Kalita P, Dewan A, Tanweer S. Development of a novel thermal model for a PV/T collector and its experimental analysis. Sol Energy 2019;188:631–43. doi:10.1016/j.solener.2019.06.005.

[13] Neises TW, Klein SA, Reindl DT. Development of a Thermal Model for Photovoltaic Modules and Analysis of NOCT Guidelines. J Sol Energy Eng 2011;134:011009. doi:10.1115/1.4005340.

[14] Migan G-A. Project Report 2013 MVK160 Heat and Mass Transfer Study of the operating temperature of a PV module 2013.

[15] Alfred. Effect of Temperature on Solar Panels 2010. http://www.reuk.co.uk/wordpress/solar/effect-of-temperature-on-solar-panels/

(toegang verkry 03 Maart 2020).

[16] Radziemska E. The effect of temperature on the power drop in crystalline silicon solar cells. Renew Energy 2003;28:1–12. doi:10.1016/S0960-1481(02)00015-0.

[17] Evans DL, Florschuetz LW. Cost studies on terrestrial photovoltaic power systems with sunlight concentration. Sol Energy 1977;19:255–62. doi:10.1016/0038-092X(77)90068-8.

[18] Mohring HD., Stellbogen D, Schaffler R, Oelting S, Gegenwart R, Konttinen P, Carlsson T, Cendagorta M HW. No Title. Proc 19th EC Photovolt Sol Energy Conf 2004.

[19] Notton G, Cristofari C, Mattei M, Poggi P. Modelling of a double-glass photovoltaic module using finite differences. Appl Therm Eng 2005;25:2854–77. doi:10.1016/j.applthermaleng.2005.02.008.

[20] Taylor RA, Phelan PE, Otanicar TP, Walker CA, Nguyen M, Trimble S, et al. Applicability of nanofluids in high flux solar collectors. J Renew Sustain Energy 2011;3. doi:10.1063/1.3571565.

[21] AK S. Handbook for Solar Photovoltaic (PV) Systems. 2010.

[22] Staebler DL, Wronski CR. Reversible conductivity changes in discharge-produced amorphous Si. Appl Phys Lett 1977;31:292–4. doi:10.1063/1.89674.

[23] Singh P, Singh SN, Lal M, Husain M. Temperature dependence of I–V characteristics and performance parameters of silicon solar cell. Sol Energy Mater Sol Cells 2008;92:1611–6. doi:https://doi.org/10.1016/j.solmat.2008.07.010.

[24] Landis G a, Merritt D, Raffaelle RP, Scheiman D. High-temperature Solar Cell Development. Nasa/Cp—2005-213431 2005;CP-2005-21:241–7.

[25] Barnett AM. The Spectral p-n Junction Model for Tandem Solar-Cell Design. IEEE Trans Electron Devices 1987;34:257–66. doi:10.1109/T-ED.1987.22916.

[26] Rawat R, Lamba R, Kaushik SC. Thermodynamic study of solar photovoltaic energy conversion: An overview. Renew Sustain Energy Rev 2017;71:630–8. doi:10.1016/j.rser.2016.12.089.

[27] International Energy Agency I. Renewable capacity growth worldwide stalled in 2018 after two decades of strong expansion 2019. https://www.iea.org/newsroom/news/2019/may/renewable-capacity-growth-worldwide-stalled-in-2018-after-two-decades-of-strong-e.html#targetText=New net capacity from solar,International Energy Agency's latest data. (toegang verkry 10 Oktober 2019).

[28] Gielen D, Boshell F, Saygin D, Bazilian MD, Wagner N, Gorini R. The role of renewable energy in the global energy transformation. Energy Strateg Rev 2019;24:38–50. doi:10.1016/j.esr.2019.01.006.

[29] IEA-PVPS. Trends in photovoltaic applications: Survey report of selected IEA countries between 1992 and 2006 2007:1–36. doi:10.1021/ac50054a041.

[30] Race for Water Foundation. Solar Energy's Rapid Growth to Save the Oceans 2017. https://voices.nationalgeographic.org/2017/06/22/solar-energy-to-save-the-oceans/ (toegang verkry 22 Junie 2017).

[31] Bloomberg. Earth Policy Institute. 2015.

[32] Marsh G. Solar PV and thermal – a marriage made in heaven? 2010. http://www.renewableenergyfocus.com/view/10922/solar-pv-and-thermal-a-marriage-made-in-heaven/ (toegang verkry 15 Julie 2017).

[33] Matthew W. Waste Not, Want Not: A New Approach to Solar n.d.

[34] Mellor A, Alonso Alvarez D, Guarracino I, Ramos A, Riverola Lacasta A, Ferre Llin L, et al. Roadmap for the next-generation of hybrid photovoltaic-thermal solar energy collectors. Sol Energy 2018;174:386–98. doi:10.1016/j.solener.2018.09.004.

[35] Department of Economic and Social Affairs U. 68% of the world population projected to live in urban areas by 2050, says UN 2018. https://www.un.org/development/desa/en/news/population/2018-revision-of-world-urbanization-prospects.html#targetText=Today%2C 55%25 of the world's,increase to 68%25 by 2050. (toegang verkry 10 Oktober 2019).

[36] Hazi A, Hazi G, Grigore R, Vernica S. Opportunity to use PVT systems for water heating in industry. Appl Therm Eng 2014;63:151–7. doi:10.1016/j.applthermaleng.2013.11.010.

[37] Mellor A, Alonso Alvarez D, Guarracino I, Ramos A, Riverola Lacasta A, Ferre Llin L, et al. Roadmap for the next-generation of hybrid photovoltaic-thermal solar energy collectors. Sol Energy 2018;174:386–98. doi:10.1016/j.solener.2018.09.004.

[38] Zondag HA. Flat-plate PV-Thermal collectors and systems: A review. Renew Sustain Energy Rev 2008;12:891–959. doi:10.1016/j.rser.2005.12.012.

[39] Sandnes B, Rekstad J. A photovoltaic/thermal (PV/T) collector with a polymer absorber plate. Experimental study and analytical model. Sol Energy 2002;72:63–73. doi:10.1016/S0038-092X(01)00091-3.

[40] El Amrani A, Mahrane A, Moussa FY, Boukennous Y. Solar module fabrication. Int J Photoenergy 2007;2007. doi:10.1155/2007/27610.

[41] Aste N, del Pero C, Leonforte F. Water flat plate PV-thermal collectors: A review. Sol Energy 2014;102:98–115. doi:10.1016/j.solener.2014.01.025.

[42] Assoa YB, Sauzedde F, Boillot B, Boddaert S. Development of a building integrated solar photovoltaic/thermal hybrid drying system. Energy 2017;128:755–67. doi:10.1016/j.energy.2017.04.062.

[43] Stropnik R, Stritih U. Increasing the efficiency of PV panel with the use of PCM. Renew Energy 2016;97:671–9. doi:10.1016/j.renene.2016.06.011.

[44] Al-Waeli AHA, Sopian K, Chaichan MT, Kazem HA, Ibrahim A, Mat S, et al. Evaluation of the nanofluid and nano-PCM based photovoltaic thermal (PVT) system: An experimental study. Energy Convers Manag 2017;151:693–708. doi:10.1016/j.enconman.2017.09.032.

[45] Hu M, Zheng R, Pei G, Wang Y, Li J, Ji J. Experimental study of the effect of inclination angle on the thermal performance of heat pipe photovoltaic/thermal (PV/T) systems with wickless heat pipe and wire-meshed heat pipe. Appl Therm Eng 2016;106:651–60. doi:10.1016/j.applthermaleng.2016.06.003.

[46] Millennium Electric T.O.U. Ltd. Above & Beyond Photovoltaics n.d. http://www.millenniumsolar.com/ (toegang verkry 01 Januarie 2017).

[47] Herrando M, Markides CN, Hellgardt K. A UK-based assessment of hybrid PV and solar-thermal systems for domestic heating and power: System performance. Appl Energy 2014;122:288–309. doi:10.1016/j.apenergy.2014.01.061.

[48] Chow TT, Pei G, Fong KF, Lin Z, Chan ALS, Ji J. Energy and exergy analysis of photovoltaic-thermal collector with and without glass cover. Appl Energy 2009;86:310–6. doi:10.1016/j.apenergy.2008.04.016.

[49] Weitbrecht V, Lehmann D, Richter A. Flow distribution in solar collectors with laminar flow conditions. Sol Energy 2002;73:433–41. doi:10.1016/S0038-092X(03)00006-9.

[50] Aste N, Leonforte F, Del Pero C. Design, modeling and performance monitoring of a photovoltaic-thermal (PVT) water collector. Sol Energy 2015;112:85–99. doi:10.1016/j.solener.2014.11.025.

[51] He W, Chow TT, Ji J, Lu J, Pei G, Chan LS. Hybrid photovoltaic and thermal solar-collector designed for natural circulation of water. Appl Energy 2006;83:199–210. doi:10.1016/j.apenergy.2005.02.007.

[52] Qu M, Chen J, Nie L, Li F, Yu Q, Wang T. Experimental study on the operating characteristics of a novel photovoltaic/thermal integrated dual-source heat pump

water heating system. Appl Therm Eng 2016;94:819–26. doi:10.1016/j.applthermaleng.2015.10.126.

[53] Kazem HA, Al-Waeli AHA, Chaichan MT, Al-Waeli KH, Al-Aasam AB, Sopian K. Evaluation and comparison of different flow configurations PVT systems in Oman: A numerical and experimental investigation. Sol Energy 2020;208:58–88. doi:10.1016/j.solener.2020.07.078.

[54] Abdullah AL, Misha S, Tamaldin N, Rosli MAM, Sachit FA. Theoretical study and indoor experimental validation of performance of the new photovoltaic thermal solar collector (PVT) based water system. Case Stud Therm Eng 2020;18:100595. doi:10.1016/j.csite.2020.100595.

[55] Yu Y, Yang H, Peng J, Long E. Performance comparisons of two flat-plate photovoltaic thermal collectors with different channel configurations. Energy 2019;175:300–8. doi:10.1016/j.energy.2019.03.054.

[56] Barone G, Buonomano A, Forzano C, Palombo A, Panagopoulos O. Photovoltaic thermal collectors: Experimental analysis and simulation model of an innovative low-cost water-based prototype. Energy 2019;179:502–16. doi:10.1016/j.energy.2019.04.140.

[57] Hossain MS, Pandey AK, Selvaraj J, Abd Rahim N, Rivai A, Tyagi V V. Thermal performance analysis of parallel serpentine flow based photovoltaic/thermal (PV/T)system under composite climate of Malaysia. Appl Therm Eng 2019;153:861–71. doi:10.1016/j.applthermaleng.2019.01.007.

[58] Wu S-Y, Chen C, Xiao L. Heat transfer characteristics and performance evaluation of water-cooled PV/T system with cooling channel above PV panel. Renew Energy 2018;125:936–46. doi:10.1016/j.renene.2018.03.023.

[59] Aste N, Del Pero C, Leonforte F, Manfren M. Performance monitoring and modeling of an uncovered photovoltaic-thermal (PVT) water collector. Sol Energy 2016;135:551–68. doi:10.1016/j.solener.2016.06.029.

[60] Yazdanifard F, Ebrahimnia-Bajestan E, Ameri M. Investigating the performance of a water-based photovoltaic/thermal (PV/T) collector in laminar and turbulent flow regime. Renew Energy 2016;99:295–306. doi:10.1016/j.renene.2016.07.004.

[61] Bombarda P, Di Marcoberardino G, Lucchini A, Leva S, Manzolini G, Molinaroli L, et al. Thermal and electric performances of roll-bond flat plate applied to conventional PV modules for heat recovery. Appl Therm Eng 2016;105:304–13. doi:10.1016/j.applthermaleng.2016.05.172.

[62] Nižetić S, Čoko D, Yadav A, Grubišić-Čabo F. Water spray cooling technique applied

on a photovoltaic panel: The performance response. Energy Convers Manag 2016;108:287–96. doi:10.1016/j.enconman.2015.10.079.

[63] Yazdanpanahi J, Sarhaddi F, Mahdavi Adeli M. Experimental investigation of exergy efficiency of a solar photovoltaic thermal (PVT) water collector based on exergy losses. Sol Energy 2015;118:197–208. doi:10.1016/j.solener.2015.04.038.

[64] Liang R, Zhang J, Ma L, Li Y. Performance evaluation of new type hybrid photovoltaic/thermal solar collector by experimental study. Appl Therm Eng 2015;75:487–92. doi:10.1016/j.applthermaleng.2014.09.075.

[65] Baloch AAB, Bahaidarah HMS, Gandhidasan P, Al-Sulaiman FA. Experimental and numerical performance analysis of a converging channel heat exchanger for PV cooling. Energy Convers Manag 2015;103:14–27. doi:10.1016/j.enconman.2015.06.018.

[66] Alami AH. Effects of evaporative cooling on efficiency of photovoltaic modules. Energy Convers Manag 2014;77:668–79. doi:10.1016/j.enconman.2013.10.019.

[67] Fudholi A, Sopian K, Yazdi MH, Ruslan MH, Ibrahim A, Kazem HA. Performance analysis of photovoltaic thermal (PVT) water collectors. Energy Convers Manag 2014;78:641–51. doi:10.1016/j.enconman.2013.11.017.

[68] Hussain F, Othman MYH, Sopian K, Yatim B, Ruslan H, Othman H. Design development and performance evaluation of photovoltaic/thermal (PV/T) air base solar collector. Renew Sustain Energy Rev 2013;25:431–41. doi:10.1016/j.rser.2013.04.014.

[69] Mojumder JC, Chong WT, Ong HC, Leong KY, Abdullah-Al-Mamoon. An experimental investigation on performance analysis of air type photovoltaic thermal collector system integrated with cooling fins design. Energy Build 2016;130:272–85. doi:10.1016/j.enbuild.2016.08.040.

[70] Kumar R, Rosen MA. Performance evaluation of a double pass PV/T solar air heater with and without fins. Appl Therm Eng 2011;31:1402–10. doi:10.1016/j.applthermaleng.2010.12.037.

[71] Brideau SA, Collins MR. Experimental model validation of a hybrid PV/thermal air based collector with impinging jets. Energy Procedia 2012;30:44–54. doi:10.1016/j.egypro.2012.11.007.

[72] Popovici CG, Hudişteanu SV, Mateescu TD, Cherecheş N-C. Efficiency Improvement of Photovoltaic Panels by Using Air Cooled Heat Sinks. Energy Procedia 2016;85:425–32. doi:10.1016/j.egypro.2015.12.223.

[73] Abene A, Dubois V, Le Ray M, Ouagued A. Study of a solar air flat plate collector: use

of obstacles and application for the drying of grape. J Food Eng 2004;65:15–22. doi:https://doi.org/10.1016/j.jfoodeng.2003.11.002.

[74] Mojumder JC, Chong WT, Ong HC, Leong KY, Abdullah-Al-Mamoon. An experimental investigation on performance analysis of air type photovoltaic thermal collector system integrated with cooling fins design. Energy Build 2016;130:272–85. doi:https://doi.org/10.1016/j.enbuild.2016.08.040.

[75] Tonui JK, Tripanagnostopoulos Y. Improved PV/T solar collectors with heat extraction by forced or natural air circulation. Renew Energy 2007;32:623–37. doi:10.1016/j.renene.2006.03.006.

[76] Tonui JK, Tripanagnostopoulos Y. Performance improvement of PV/T solar collectors with natural air flow operation. Sol Energy 2008;82:1–12. doi:https://doi.org/10.1016/j.solener.2007.06.004.

[77] Belusko M, Saman W, Bruno F. Performance of jet impingement in unglazed air collectors. Sol Energy 2008;82:389–98. doi:10.1016/j.solener.2007.10.005.

[78] Özakin AN, Kaya F. Effect on the exergy of the PVT system of fins added to an air-cooled channel: A study on temperature and air velocity with ANSYS Fluent. Sol Energy 2019;184:561–9. doi:10.1016/j.solener.2019.03.100.

[79] Fan W, Kokogiannakis G, Ma Z. Optimisation of life cycle performance of a double-pass photovoltaic thermal-solar air heater with heat pipes. Renew Energy 2019;138:90–105. doi:10.1016/j.renene.2019.01.078.

[80] Gupta A, Das B, Mondol JD. Experimental and theoretical performance analysis of a hybrid photovoltaic-thermal (PVT) solar air dryer for green chillies. Int J Ambient Energy 2020;0:1–9. doi:10.1080/01430750.2020.1734658.

[81] Shahsavar A, Rajabi Y. Exergoeconomic and enviroeconomic study of an air based building integrated photovoltaic/thermal (BIPV/T) system. Energy 2018;144:877–86. doi:10.1016/j.energy.2017.12.056.

[82] Amanlou Y, Tavakoli Hashjin T, Ghobadian B, Najafi G. Air cooling low concentrated photovoltaic/thermal (LCPV/T) solar collector to approach uniform temperature distribution on the PV plate. Appl Therm Eng 2018;141:413–21. doi:10.1016/j.applthermaleng.2018.05.070.

[83] Slimani MEA, Amirat M, Kurucz I, Bahria S, Hamidat A, Chaouch WB. A detailed thermal-electrical model of three photovoltaic/thermal (PV/T) hybrid air collectors and photovoltaic (PV) module: Comparative study under Algiers climatic conditions. Energy Convers Manag 2017;133:458–76. doi:10.1016/j.enconman.2016.10.066.

[84] Ahmed OK, Mohammed ZA. Influence of porous media on the performance of hybrid PV/Thermal collector. Renew Energy 2017;112:378–87. doi:10.1016/j.renene.2017.05.061.

[85] Hussain F, Othman MYH, Yatim B, Ruslan H, Sopian K, Anuar Z, et al. An improved design of photovoltaic/thermal solar collector. Sol Energy 2015;122:885–91. doi:10.1016/j.solener.2015.10.008.

[86] Bambrook SM, Sproul AB. Maximising the energy output of a PVT air system. Sol Energy 2012;86:1857–71. doi:10.1016/j.solener.2012.02.038.

[87] Teo HG, Lee PS, Hawlader MNA. An active cooling system for photovoltaic modules. Appl Energy 2012;90:309–15. doi:10.1016/j.apenergy.2011.01.017.

[88] Shahsavar A, Ameri M. Experimental investigation and modeling of a direct-coupled PV/T air collector. Sol Energy 2010;84:1938–58. doi:10.1016/j.solener.2010.07.010.

[89] Joshi AS, Tiwari A. Energy and exergy efficiencies of a hybrid photovoltaic-thermal (PV/T) air collector. Renew Energy 2007;32:2223–41. doi:10.1016/j.renene.2006.11.013.

[90] Lane G. Solar heat storage: latent heat materials. CRC Press; 1985.

[91] Pielichowska K, Pielichowski K. Phase change materials for thermal energy storage. Prog Mater Sci 2014;65:67–123. doi:10.1016/j.pmatsci.2014.03.005.

[92] Farid MM, Khudhair AM, Razack SAK, Al-Hallaj S. A review on phase change energy storage: Materials and applications. Energy Convers Manag 2004;45:1597–615. doi:10.1016/j.enconman.2003.09.015.

[93] M. R, S. L, S. R, H. A, A. D. Experimental investigation on the abasement of operating temperature in solar photovoltaic panel using PCM and aluminium. Sol Energy 2019;188:327–38. doi:10.1016/j.solener.2019.05.067.

[94] Hasan A, Sarwar J, Alnoman H, Abdelbaqi S. Yearly energy performance of a photovoltaic-phase change material (PV-PCM) system in hot climate. Sol Energy 2017;146:417–29. doi:10.1016/j.solener.2017.01.070.

[95] Abdelrahman HE, Wahba MH, Refaey HA, Moawad M, Berbish NS. Performance enhancement of photovoltaic cells by changing configuration and using PCM (RT35HC) with nanoparticles Al 2 O 3. Sol Energy 2019;177:665–71. doi:10.1016/j.solener.2018.11.022.

[96] Simón-Allué R, Guedea I, Villén R, Brun G. Experimental study of Phase Change Material influence on different models of Photovoltaic-Thermal collectors. Sol Energy 2019;190:1–9. doi:10.1016/j.solener.2019.08.005.

[97] Hossain MS, Pandey AK, Selvaraj J, Rahim NA, Islam MM, Tyagi V V. Two side

serpentine flow based photovoltaic-thermal-phase change materials (PVT-PCM) system: Energy, exergy and economic analysis. Renew Energy 2019;136:1320–36. doi:10.1016/j.renene.2018.10.097.

[98] Luo Z, Huang Z, Xie N, Gao X, Xu T, Fang Y, et al. Numerical and experimental study on temperature control of solar panels with form-stable paraffin/expanded graphite composite PCM. Energy Convers Manag 2017;149:416–23. doi:10.1016/j.enconman.2017.07.046.

[99] Huang MJ, Eames PC, Norton B, Hewitt NJ. Natural convection in an internally finned phase change material heat sink for the thermal management of photovoltaics. Sol Energy Mater Sol Cells 2011;95:1598–603. doi:10.1016/j.solmat.2011.01.008.

[100] Kılkış B. Development of a composite PVT panel with PCM embodiment, TEG modules, flat-plate solar collector, and thermally pulsing heat pipes. Sol Energy 2020;200:89–107. doi:https://doi.org/10.1016/j.solener.2019.10.075.

[101] Rajaee F, Rad MAV, Kasaeian A, Mahian O, Yan WM. Experimental analysis of a photovoltaic/thermoelectric generator using cobalt oxide nanofluid and phase change material heat sink. Energy Convers Manag 2020;212:112780. doi:10.1016/j.enconman.2020.112780.

[102] Sittisart P, Farid MM. Fire retardants for phase change materials. Appl Energy 2011;88:3140–5. doi:10.1016/j.apenergy.2011.02.005.

[103] Inaba H, Tu P. Evaluation of thermophysical characteristics on shape-stabilized paraffin as a solid-liquid phase change material. Heat Mass Transf und Stoffuebertragung 1997;32:307–12. doi:10.1007/s002310050126.

[104] Hong Y, Xin-shi G. Preparation of polyethylene-paraffin compound as a form-stable solid-liquid phase change material. Sol Energy Mater Sol Cells 2000;64:37–44. doi:10.1016/S0927-0248(00)00041-6.

[105] Wan Y chao, Chen Y, Cui Z xing, Ding H, Gao S feng, Han Z, et al. A promising form-stable phase change material prepared using cost effective pinecone biochar as the matrix of palmitic acid for thermal energy storage. Sci Rep 2019;9:1–10. doi:10.1038/s41598-019-47877-z.

[106] Wen R, Zhang X, Huang Z, Fang M, Liu Y, Wu X, et al. Preparation and thermal properties of fatty acid/diatomite form-stable composite phase change material for thermal energy storage. Sol Energy Mater Sol Cells 2018;178:273–9. doi:10.1016/j.solmat.2018.01.032.

[107] Li C, Yu H, Song Y, Zhao M. Synthesis and characterization of PEG/ZSM-5 composite

phase change materials for latent heat storage. Renew Energy 2018;121:45–52. doi:10.1016/j.renene.2017.12.089.

[108] Liang J, Zhimeng L, Ye Y, Yanjun W, Jingxin L, Changlin Z. Fabrication and characterization of fatty acid/wood-flour composites as novel form-stable phase change materials for thermal energy storage. Energy Build 2018;171:88–99. doi:10.1016/j.enbuild.2018.04.044.

[109] Sarı A, Bicer A, Al-Sulaiman FA, Karaipekli A, Tyagi V V. Diatomite/CNTs/PEG composite PCMs with shape-stabilized and improved thermal conductivity: Preparation and thermal energy storage properties. Energy Build 2018;164:166–75. doi:10.1016/j.enbuild.2018.01.009.

[110] Hossain MS, Pandey AK, Selvaraj J, Rahim NA, Islam MM, Tyagi V V. Two side serpentine flow based photovoltaic-thermal-phase change materials (PVT-PCM) system: Energy, exergy and economic analysis. Renew Energy 2019;136:1320–36. doi:https://doi.org/10.1016/j.renene.2018.10.097.

[111] Preet S, Bhushan B, Mahajan T. Experimental investigation of water based photovoltaic/thermal (PV/T) system with and without phase change material (PCM). Sol Energy 2017;155:1104–20. doi:10.1016/j.solener.2017.07.040.

[112] Browne MC, Norton B, McCormack SJ. Heat retention of a photovoltaic/thermal collector with PCM. Sol Energy 2016;133:533–48. doi:10.1016/j.solener.2016.04.024.

[113] Park J, Kim T, Leigh SB. Application of a phase-change material to improve the electrical performance of vertical-building-added photovoltaics considering the annual weather conditions. Sol Energy 2014;105:561–74. doi:10.1016/j.solener.2014.04.020.

[114] Atkin P, Farid MM. Improving the efficiency of photovoltaic cells using PCM infused graphite and aluminium fins. Sol Energy 2015;114:217–28. doi:10.1016/j.solener.2015.01.037.

[115] Hasan A, McCormack SJ, Huang MJ, Sarwar J, Norton B. Increased photovoltaic performance through temperature regulation by phase change materials: Materials comparison in different climates. Sol Energy 2015;115:264–76. doi:10.1016/j.solener.2015.02.003.

[116] Maiti S, Banerjee S, Vyas K, Patel P, Ghosh PK. Self regulation of photovoltaic module temperature in V-trough using a metal-wax composite phase change matrix. Sol Energy 2011;85:1805–16. doi:10.1016/j.solener.2011.04.021.

[117] Michael JJ, Iniyan S. Performance analysis of a copper sheet laminated photovoltaic

thermal collector using copper oxide - water nanofluid. Sol Energy 2015;119:439–51. doi:10.1016/j.solener.2015.06.028.

[118] Molina GJ, Aktaruzzaman F, Stregles W, Soloiu V, Rahman M. Jet-impingement effects of alumina-nanofluid on aluminum and copper. Adv Tribol 2014;2014. doi:10.1155/2014/476175.

[119] Yazdanifard F, Ameri M, Ebrahimnia-Bajestan E. Performance of nanofluid-based photovoltaic/thermal systems: A review. Renew Sustain Energy Rev 2017;76:323–52. doi:10.1016/j.rser.2017.03.025.

[120] Al-Waeli AHA, Sopian K, Chaichan MT, Kazem HA, Hasan HA, Al-Shamani AN. An experimental investigation of SiC nanofluid as a base-fluid for a photovoltaic thermal PV/T system. Energy Convers Manag 2017;142:547–58. doi:10.1016/j.enconman.2017.03.076.

[121] Al-Waeli AHA, Kazem HA, Sopian K, Chaichan MT. Techno-economical assessment of grid connected PV/T using nanoparticles and water as base-fluid systems in Malaysia. Int J Sustain Energy 2017;0:1–18. doi:10.1080/14786451.2017.1323900.

[122] Palmer KF, Williams D. Optical properties of water in the near infrared*. J Opt Soc Am 1974;64:1107. doi:10.1364/JOSA.64.001107.

[123] Hassani S, Taylor RA, Mekhilef S, Saidur R. A cascade nanofluid-based PV/T system with optimized optical and thermal properties. Energy 2016;112:963–75. doi:10.1016/j.energy.2016.06.142.

[124] Hassani. MATHEMATICAL MODELING OF OPTICAL AND. University of Malaya, 2017.

[125] Crisostomo F, Hjerrild N, Mesgari S, Li Q, Taylor RA. A hybrid PV/T collector using spectrally selective absorbing nanofluids. Appl Energy 2017;193:1–14. doi:10.1016/j.apenergy.2017.02.028.

[126] Hjerrild NE, Mesgari S, Crisostomo F, Scott JA, Amal R, Taylor RA. Hybrid PV/T enhancement using selectively absorbing Ag-SiO2/carbon nanofluids. Sol Energy Mater Sol Cells 2016;147:281–7. doi:10.1016/j.solmat.2015.12.010.

[127] Drew, DA, Passman S. Theory of Multicomponent Fluids. Springer; 1999.

[128] Brinkman HC. The Viscosity of Concentrated Suspensions and Solutions. J Chem Phys 1952;20:571–571. doi:10.1063/1.1700493.

[129] Yang, SM, Tao W. Heat Transfer. 3rd ed. Higher Education Press,Bejing, China; 1998.

[130] Hamilton RL. Thermal conductivity of heterogeneous two-component systems. Ind Eng Chem Fundam 1962;1:187–91. doi:10.1021/i160003a005.

[131] Aberoumand S, Ghamari S, Shabani B. Energy and exergy analysis of a photovoltaic thermal (PV/T) system using nanofluids: An experimental study. Sol Energy 2018;165:167–77. doi:10.1016/j.solener.2018.03.028.

[132] Hasan HA, Sopian K, Jaaz AH, Al-Shamani AN. Experimental investigation of jet array nanofluids impingement in photovoltaic/thermal collector. Sol Energy 2017;144:321–34. doi:10.1016/j.solener.2017.01.036.

[133] Al-Waeli AHA, Chaichan MT, Kazem HA, Sopian K. Comparative study to use nano-(Al 2 O 3 , CuO, and SiC) with water to enhance photovoltaic thermal PV/T collectors. Energy Convers Manag 2017;148:963–73. doi:10.1016/j.enconman.2017.06.072.

[134] Al-Shamani AN, Sopian K, Mat S, Hasan HA, Abed AM, Ruslan MH. Experimental studies of rectangular tube absorber photovoltaic thermal collector with various types of nanofluids under the tropical climate conditions. Energy Convers Manag 2016;124:528–42. doi:10.1016/j.enconman.2016.07.052.

[135] Karami N, Rahimi M. Heat transfer enhancement in a hybrid microchannel-photovoltaic cell using Boehmite nanofluid. Int Commun Heat Mass Transf 2014;55:45–52. doi:10.1016/j.icheatmasstransfer.2014.04.009.

[136] Sardarabadi M, Passandideh-Fard M, Zeinali Heris S. Experimental investigation of the effects of silica/water nanofluid onPV/T (photovoltaic thermal units). Energy 2014;66:264–72. doi:10.1016/j.energy.2014.01.102.

[137] Ladjevardi SM, Asnaghi A, Izadkhast PS, Kashani AH. Applicability of graphite nanofluids in direct solar energy absorption. Sol Energy 2013;94:327–34. doi:10.1016/j.solener.2013.05.012.

[138] Gang P, Huide F, Huijuan Z, Jie J. Performance study and parametric analysis of a novel heat pipe PV/T system. Energy 2012;37:384–95. doi:10.1016/j.energy.2011.11.017.

[139] Hammad M. EXPERIMENTAL STUDY OF THE PERFORMANCE OF A SOLAR COLLECTOR COOLED BY HEAT PIPES. Renew Energy 1995;6:11–5.

[140] Moradgholi M, Nowee SM, Abrishamchi I. Application of heat pipe in an experimental investigation on a novel photovoltaic/thermal (PV/T) system. Sol Energy 2014;107:82–8. doi:10.1016/j.solener.2014.05.018.

[141] Wu SY, Zhang QL, Xiao L, Guo FH. A heat pipe photovoltaic/thermal (PV/T) hybrid system and its performance evaluation. Energy Build 2011;43:3558–67. doi:10.1016/j.enbuild.2011.09.017.

[142] Wang Z, Qiu F, Yang W, Zhao X, Mei S. Experimental investigation of the thermal and electrical performance of the heat pipe BIPV/T system with metal wires. Appl Energy 2016;170:314–23. doi:10.1016/j.apenergy.2016.02.140.

[143] Jouhara H, Szulgowska-Zgrzywa M, Sayegh MA, Milko J, Danielewicz J, Nannou TK, et al. The performance of a heat pipe based solar PV/T roof collector and its potential contribution in district heating applications. Energy 2015;136:117–25. doi:10.1016/j.energy.2016.04.070.

[144] Gang P, Huide F, Jie J, Tin-Tai C, Tao Z. Annual analysis of heat pipe PV/T systems for domestic hot water and electricity production. Energy Convers Manag 2012;56:8–21. doi:10.1016/j.enconman.2011.11.011.

[145] Chen H, Zhang L, Jie P, Xiong Y, Xu P, Zhai H. Performance study of heat-pipe solar photovoltaic/thermal heat pump system. Appl Energy 2017;190:960–80. doi:10.1016/j.apenergy.2016.12.145.

[146] SUNSYSTEM. Hybrid photo-thermal collector SUNSYSTEM PVT 240 n.d. http://www.sunsystem.bg/en/fotovoltaika/PV-T/.

[147] DUALSUN. DUALSUN, THE REVOLUTIONARY HYBRID SOLAR PANEL n.d. https://dualsun.fr/en/product/2-in-1-solar/ (toegang verkry 28 September 2017).

[148] Conserval Engineering. SolarWall n.d. http://solarwall.com/en/home.php (toegang verkry 28 September 2017).

[149] SolarVenti D. Solar air collectors with high reliable performance n.d. http://www.solarventi.com/index.php/manuals-and-instructions/why-chose-solarventi.

[150] Solimpeks Solar Corp. Powervolt n.d. http://www.solimpeks.com/product/volther-powervolt/ (toegang verkry 28 September 2017).

[151] SunDrum Solar. SDM100 Collector n.d. http://www.sundrumsolar.com/index.php/products (toegang verkry 28 September 2017).

[152] Solar E. PVT 240,NES - New Energy System - Sunsystem n.d. https://www.enfsolar.com/pv/panel-datasheet/Polycrystalline/12159.

[153] Goldwind Americas. Innovative Energy Solutions 2016;5:2–4.

[154] FotoTherm_moduli___tehnicni_list.pdf n.d.

[155] FAFCO. CoolPV n.d. http://coolpvsolar.com/ (toegang verkry 28 September 2017).

[156] Technology 2Power. One module for everything, Generate power from sunlight and collect heat n.d. http://www.2power-hybrid.com/en/2power-modul (toegang

verkry 28 September 2017).

[157] International Clean Energy Consortium. Hybrid Solar n.d. http://www.icec.ch/en/hybride.htm.

[158] Lombardo T. Photovoltaic Thermal System Achieves 86% Efficiency n.d. http://www.engineering.com/ElectronicsDesign/ElectronicsDesignArticles/ArticleID/6123/Photovoltaic-Thermal-System-Achieves-86-Efficiency.aspx (toegang verkry 28 September 2017).

[159] Duran Sahin A, Dincer I, Rosen MA. Thermodynamic analysis of solar photovoltaic cell systems. Sol Energy Mater Sol Cells 2007;91:153–9. doi:10.1016/j.solmat.2006.07.015.

[160] Tiwari A, Dubey S, Sandhu GS, Sodha MS, Anwar SI. Exergy analysis of integrated photovoltaic thermal solar water heater under constant flow rate and constant collection temperature modes. Appl Energy 2009;86:2592–7. doi:10.1016/j.apenergy.2009.04.004.

[161] Vats K, Tiwari GN. Energy and exergy analysis of a building integrated semitransparent photovoltaic thermal (BISPVT) system. Appl Energy 2012;96:409–16. doi:10.1016/j.apenergy.2012.02.079.

[162] Koroneos C, Tsarouhis M. Exergy analysis and life cycle assessment of solar heating and cooling systems in the building environment. J Clean Prod 2012;32:52–60. doi:10.1016/j.jclepro.2012.03.012.

[163] Evola G, Marletta L. Exergy and thermoeconomic optimization of a water-cooled glazed hybrid photovoltaic/thermal (PVT) collector. Sol Energy 2014;107:12–25. doi:10.1016/j.solener.2014.05.041.

[164] Sobhnamayan F, Sarhaddi F, Alavi MA, Farahat S, Yazdanpanahi J. Optimization of a solar photovoltaic thermal (PV / T) water collector based on exergy concept. Renew Energy 2014;68:356–65. doi:10.1016/j.renene.2014.01.048.

[165] Yazdanpanahi J, Sarhaddi F, Mahdavi Adeli M. Experimental investigation of exergy efficiency of a solar photovoltaic thermal (PVT) water collector based on exergy losses. Sol Energy 2015;118:197–208. doi:10.1016/j.solener.2015.04.038.

[166] Dubey S, Solanki SC, Tiwari A. Energy and exergy analysis of PV/T air collectors connected in series. Energy Build 2009;41:863–70. doi:10.1016/j.enbuild.2009.03.010.

[167] Gholampour M, Ameri M. Energy and exergy analyses of Photovoltaic/Thermal flat transpired collectors: Experimental and theoretical study. Appl Energy 2016;164:837–56. doi:10.1016/j.apenergy.2015.12.042.

[168] Hazami M, Riahi A, Mehdaoui F, Nouicer O, Farhat A. Energetic and exergetic performances analysis of a PV/T (photovoltaic thermal) solar system tested and simulated under to Tunisian (North Africa) climatic conditions. Energy 2016;107:78–94. doi:10.1016/j.energy.2016.03.134.

[169] Tiwari S, Tiwari GN. Energy and exergy analysis of a mixed-mode greenhouse-type solar dryer, integrated with partially covered N-PVT air collector. Energy 2017;128:183–95. doi:10.1016/j.energy.2017.04.022.

[170] Dincer I, Ratlamwala TAH. Importance of exergy for analysis, improvement, design, and assessment. Wiley Interdiscip Rev Energy Environ 2013;2:335–49. doi:10.1002/wene.63.

[171] Kalogirou SA, Karellas S, Braimakis K, Stanciu C, Badescu V. Exergy analysis of solar thermal collectors and processes. Prog Energy Combust Sci 2016;56:106–37. doi:10.1016/j.pecs.2016.05.002.

[172] Tiwari A, Sodha MS. Performance evaluation of solar PV/T system: An experimental validation. Sol Energy 2006;80:751–9. doi:10.1016/j.solener.2005.07.006.

[173] Joshi AS, Dincer I, Reddy B V. Thermodynamic assessment of photovoltaic systems. Sol Energy 2009;83:1139–49. doi:10.1016/j.solener.2009.01.011.

[174] Fujisawa T, Tani T. Annual exergy evaluation on photovoltaic-thermal hybrid collector. Sol Energy Mater Sol Cells 1997;47:135–48. doi:https://doi.org/10.1016/S0927-0248(97)00034-2.

[175] Bosanac M, Sørensen B, Katic I, Sørensen H, Nielsen B, Badran J. Final Report EFP project 1713 / 00-0014 Photovoltaic / Thermal Solar Collectors and Their Potential in Denmark. 2003.

[176] Celik AN, Acikgoz N. Modelling and experimental verification of the operating current of mono-crystalline photovoltaic modules using four- and five-parameter models. Appl Energy 2007;84:1–15. doi:10.1016/j.apenergy.2006.04.007.

[177] Saloux E, Teyssedou A, Sorin M. Analysis of photovoltaic (PV) and photovoltaic/thermal (PV/T) systems using the exergy method. Energy Build 2013;67:275–85. doi:10.1016/j.enbuild.2013.08.012.

[178] Jones AD, Underwood CP. A thermal model for photovoltaic systems. Sol Energy 2001;70:349–59. doi:10.1016/S0038-092X(00)00149-3.

[179] Raghuraman P. Analytical Predictions of Liquid and Air Photovoltaic / Thermal , 2016;103.

[180] Chow TT. Performance analysis of photovoltaic-thermal collector by explicit dynamic

model. Sol Energy 2003;75:143–52. doi:10.1016/j.solener.2003.07.001.

[181] Tiwari GN, Mishra RK, Solanki SC. Photovoltaic modules and their applications: A review on thermal modelling. Appl Energy 2011;88:2287–304. doi:10.1016/j.apenergy.2011.01.005.

[182] Rajoria CS, Agrawal S, Tiwari GN. Overall thermal energy and exergy analysis of hybrid photovoltaic thermal array. Sol Energy 2012;86:1531–8. doi:10.1016/j.solener.2012.02.014.

[183] Mishra RK, Tiwari GN. Energy and exergy analysis of hybrid photovoltaic thermal water collector for constant collection temperature mode. Sol Energy 2013;90:58–67. doi:10.1016/j.solener.2012.12.022.

[184] Shyam, Tiwari GN, Al-Helal IM. Analytical expression of temperature dependent electrical efficiency of N-PVT water collectors connected in series. Sol Energy 2015;114:61–76. doi:10.1016/j.solener.2015.01.026.

[185] Dubey S, Tiwari GN. Thermal modeling of a combined system of photovoltaic thermal (PV/T) solar water heater. Sol Energy 2008;82:602–12. doi:10.1016/j.solener.2008.02.005.

[186] Skoplaki E, Palyvos JA. On the temperature dependence of photovoltaic module electrical performance: A review of efficiency/power correlations. Sol Energy 2009;83:614–24. doi:10.1016/j.solener.2008.10.008.

[187] Torres-lobera D, Valkealahti S. ScienceDirect Inclusive dynamic thermal and electric simulation model of solar PV systems under varying atmospheric conditions. Sol Energy 2014;105:632–47. doi:10.1016/j.solener.2014.04.018.

[188] Bambrook SM, Sproul AB. A solvable thermal circuit for modelling PVT air collectors. Sol Energy 2016;138:77–87. doi:10.1016/j.solener.2016.09.007.

[189] Slimani MEA, Amirat M, Bahria S, Kurucz I, Aouli M, Sellami R. Study and modeling of energy performance of a hybrid photovoltaic/thermal solar collector: Configuration suitable for an indirect solar dryer. Energy Convers Manag 2016;125:209–21. doi:10.1016/j.enconman.2016.03.059.

[190] Amori KE, Taqi Al-Najjar HM. Analysis of thermal and electrical performance of a hybrid (PV/T) air based solar collector for Iraq. Appl Energy 2012;98:384–95. doi:10.1016/j.apenergy.2012.03.061.

[191] Khelifa A, Touafek K, Ben Moussa H, Tabet I. Modeling and detailed study of hybrid photovoltaic thermal (PV/T) solar collector. Sol Energy 2016;135:169–76. doi:10.1016/j.solener.2016.05.048.

[192] Huide F, Xuxin Z, Lei M, Tao Z, Qixing W, Hongyuan S. A comparative study on three types of solar utilization technologies for buildings: Photovoltaic, solar thermal and hybrid photovoltaic/thermal systems. Energy Convers Manag 2017;140:1–13. doi:10.1016/j.enconman.2017.02.059.

[193] Simonetti R, Molinaroli L, Manzolini G. Development and validation of a comprehensive dynamic mathematical model for hybrid PV/T solar collectors. Appl Therm Eng 2018;133:543–54. doi:10.1016/j.applthermaleng.2018.01.093.

[194] Paradis PL, Rousse DR, Lamarche L, Nesreddine H. A hybrid PV/T solar evaporator using CO2: Numerical heat transfer model and simulation results. Sol Energy 2018;170:1118–29. doi:10.1016/j.solener.2018.06.015.

[195] Modjinou M, Ji J, Li J, Yuan W, Zhou F. A numerical and experimental study of micro-channel heat pipe solar photovoltaics thermal system. Appl Energy 2017;206:708–22. doi:10.1016/j.apenergy.2017.08.221.

[196] Rejeb O, Gaillard L, Giroux-Julien S, Ghenai C, Jemni A, Bettayeb M, et al. Novel solar PV/Thermal collector design for the enhancement of thermal and electrical performances. Renew Energy 2020;146:610–27. doi:10.1016/j.renene.2019.06.158.

[197] Yu Q, Hu M, Li J, Wang Y, Pei G. Development of a 2D temperature-irradiance coupling model for performance characterizations of the flat-plate photovoltaic/thermal (PV/T) collector. Renew Energy 2020;153:404–19. doi:10.1016/j.renene.2020.01.143.

[198] Rajoria CS, Agrawal S, Tiwari GN, Chaursia GS. Exergetic and enviroeconomic analysis of semitransparent PVT array based on optimum air flow configuration and its comparative study. Sol Energy 2015;122:1138–45. doi:10.1016/j.solener.2015.10.020.

[199] Raman V, Tiwari GN. Life cycle cost analysis of HPVT air collector under different Indian climatic conditions. Energy Policy 2008;36:603–11. doi:10.1016/j.enpol.2007.08.031.

[200] Buonomano A, Calise F, Palombo A, Vicidomini M. BIPVT systems for residential applications: An energy and economic analysis for European climates. Appl Energy 2016;184:1411–31. doi:10.1016/j.apenergy.2016.02.145.

[201] Bianchini A, Guzzini A, Pellegrini M, Saccani C. Photovoltaic/thermal (PV/T) solar system: Experimental measurements, performance analysis and economic assessment. Renew Energy 2017;111:543–55. doi:10.1016/j.renene.2017.04.051.

[202] Tse K-K, Chow T-T, Su Y. Performance evaluation and economic analysis of a full scale water-based photovoltaic/thermal (PV/T) system in an office building. Energy

Build 2016;122:42–52. doi:10.1016/j.enbuild.2016.04.014.

[203] Nayak S, Naaz Z, Yadav P, Chaudhary R. Economic Analysis of Hybrid Photovoltaic-Thermal (PVT) Integrated Solar Dryer 2008;1:21–7.

[204] Buker MS, Mempouo B, Riffat SB. Performance evaluation and techno-economic analysis of a novel building integrated PV/T roof collector: An experimental validation. Energy Build 2014;76:164–75. doi:10.1016/j.enbuild.2014.02.078.

[205] Nikoofard S, Ugursal VI, Beausoleil-Morrison I. Economic Analysis of Energy Upgrades Based on Tolerable Capital Cost. J Energy Eng 2015;141:1–6. doi:10.1061/(ASCE)EY.1943-7897.0000203.

[206] Asaee SR, Nikoofard S, Ugursal VI, Beausoleil-Morrison I. Techno-economic assessment of photovoltaic (PV) and building integrated photovoltaic/thermal (BIPV/T) system retrofits in the Canadian housing stock. Energy Build 2017;152:667–79. doi:10.1016/j.enbuild.2017.06.071.

[207] Master Bond. Thermally Conductive Epoxy Adhesives n.d. https://www.masterbond.com/properties/thermally-conductive-epoxy-adhesives#:~:text=Thermal conductivity of a typical,thermal conductivity of the product.

[208] Zhou J, Ke H, Deng X. Experimental and CFD investigation on temperature distribution of a serpentine tube type photovoltaic/thermal collector. Sol Energy 2018;174:735–42. doi:10.1016/j.solener.2018.09.063.

[209] Adamo F, Attivissimo F, Di Nisio A, Spadavecchia M. Characterization and testing of a tool for photovoltaic panel modeling. IEEE Trans Instrum Meas 2011;60:1613–22. doi:10.1109/TIM.2011.2105051.

[210] Plag F, Haas F, Ramspeck K, Nagel H, Albert H, Nevas S, et al. Comprehensive Analysis of a Pulsed Solar Simulator To Determine Measurement Uncertainty Components n.d.

[211] Plyta F. Optical design of a fully LED-based solar simulator 2015.

[212] Irwan YM, Leow WZ, Irwanto M, Fareq M, Amelia AR, Gomesh N, et al. Indoor Test Performance of PV Panel through Water Cooling Method. vol. 79. Elsevier B.V.; 2015. doi:10.1016/j.egypro.2015.11.540.

[213] Meng Q, Wang Y, Zhang L. Irradiance characteristics and optimization design of a large-scale solar simulator. Sol Energy 2011;85:1758–67. doi:10.1016/j.solener.2011.04.014.

[214] Solanki SC, Dubey S, Tiwari A. Indoor simulation and testing of photovoltaic thermal

(PV/T) air collectors. Appl Energy 2009;86:2421–8. doi:10.1016/j.apenergy.2009.03.013.

[215] Yu Y, Long E, Chen X, Yang H. Testing and modelling an unglazed photovoltaic thermal collector for application in Sichuan Basin. Appl Energy 2019;242:931–41. doi:10.1016/j.apenergy.2019.03.114.

[216] Krusi P, Schmid R. The CSI 1000 W lamp as a source for solar radiation simulation. Sol Energy 1983;30:455–62. doi:10.1016/0038-092X(83)90116-0.

[217] Bickler D. The simulation of solar radiation. Sol Energy 1962;6:64–8. doi:10.1016/0038-092X(62)90006-3.

[218] Esen V, Sağlam Ş, Oral B. Light sources of solar simulators for photovoltaic devices: A review. Renew Sustain Energy Rev 2017;77:1240–50. doi:10.1016/j.rser.2017.03.062.

[219] Kohraku S, Kurokawa K. A fundamental experiment for discrete-wavelength LED solar simulator. Sol Energy Mater Sol Cells 2006;90:3364–70. doi:10.1016/j.solmat.2005.09.024.

[220] Bliss M, Betts TR, Gottschalg R. Advantages in using LEDs as the main light source in solar simulators for measuring PV device characteristics. Reliab Photovolt Cells, Modul Components, Syst 2008;7048:704807. doi:10.1117/12.795428.

[221] Kolberg D, Schubert F, Lontke N, Zwigart A, Spinner DM. Development of tunable close match LED solar simulator with extended spectral range to UV and IR. Energy Procedia 2011;8:100–5. doi:10.1016/j.egypro.2011.06.109.

[222] Jang SH, Shin MW. Fabrication and thermal optimization of LED solar cell simulator. Curr Appl Phys 2010;10:537–9. doi:10.1016/j.cap.2010.02.035.

[223] Leary G, Switzer G, Kuntz G, Kaiser T. Comparison of xenon lamp-based and led-based solar simulators. 2017 IEEE 44th Photovolt Spec Conf PVSC 2017 2018:1–6. doi:10.1109/PVSC.2017.8366725.

[224] Lighting W. Halogen lamp spectrum - 10 reasons to buy. Waris Light n.d. http://warisanlighting.com/halogen-lamp-spectrum.html.

[225] Gibson JH. UVB Radiation 2004:10.

[226] López-Fraguas E, Sánchez-Pena JM, Vergaz R. A Low-Cost LED-Based Solar Simulator. IEEE Trans Instrum Meas 2019;68:4913–23. doi:10.1109/TIM.2019.2899513.

[227] Esen V, Sağlam Ş, Oral B, Esen ÖC. Spectrum measurement of variable irradiance controlled LED-based solar simulator. Int J Renew Energy Res 2020;10:109–16.

[228] Standard I. International Standard 2004;2004.

[229] ASTM International. Standard Am0 and Am1.5 Spectra 2003.

[230] E927 AS. Solar Simulation for Photovoltaic Testing 1. Annu B ASTM Stand 2015;91:5–9. doi:10.1520/E0927-10.2.

[231] Polly SJ, Bittner ZS, Bennett MF, Raffaelle RP, Hubbard SM. Development of a multi-source solar simulator for spatial uniformity and close spectral matching to AM0 and AM1.5. Conf Rec IEEE Photovolt Spec Conf 2011:001739–43. doi:10.1109/PVSC.2011.6186290.

[232] Shrotriya V, Li G, Yao Y, Moriarty T, Emery K, Yang Y. Accurate measurement and characterization of organic solar cells. Adv Funct Mater 2006;16:2016–23. doi:10.1002/adfm.200600489.

[233] Fanney AH, Davis MW, Dougherty BP, King DL, Boyson WE, Kratochvil JA. Comparison of Photovoltaic Module Performance Measurements. J Sol Energy Eng 2006;128:152. doi:10.1115/1.2192559.

[234] Salvatore Castello e Anna De Lillo, Salvatore Guastella FP. National Survey Report of PV Power Applications in Italy. Co-op Program Photovolt 2010:1–21. doi:10.1007/s00432-012-1268-1.

[235] Das D, Bordoloi U, Muigai HH, Kalita P. A novel form stable PCM based bio composite material for solar thermal energy storage applications. J Energy Storage 2020;30:101403. doi:https://doi.org/10.1016/j.est.2020.101403.

[236] Qian T, Li J, Min X, Deng Y, Guan W, Ning L. Diatomite: A promising natural candidate as carrier material for low, middle and high temperature phase change material. Energy Convers Manag 2015;98:34–45. doi:10.1016/j.enconman.2015.03.071.

[237] Sari A, Karaipekli A. Preparation, thermal properties and thermal reliability of palmitic acid/expanded graphite composite as form-stable PCM for thermal energy storage. Sol Energy Mater Sol Cells 2009;93:571–6. doi:10.1016/j.solmat.2008.11.057.

[238] Liu C, Yuan Y, Zhang N, Cao X, Yang X. A novel PCM of lauric-myristic-stearic acid/expanded graphite composite for thermal energy storage. Mater Lett 2014;120:43–6. doi:10.1016/j.matlet.2014.01.051.

[239] Reichardt C, Utgenannt S, Stahmann KP, Klepel O, Barig S. Highly stable adsorptive and covalent immobilization of Thermomyces lanuginosus lipase on tailor-made porous carbon material. Biochem Eng J 2018;138:63–73. doi:10.1016/j.bej.2018.07.003.

[240] Atinafu DG, Jin Chang S, Kim KH, Kim S. Tuning surface functionality of standard biochars and the resulting uplift capacity of loading/energy storage for organic phase change materials. Chem Eng J 2020;394:125049. doi:10.1016/j.cej.2020.125049.

[241] Tao M, Zhenpeng L, Jiaxin Z. Photovoltaic panel integrated with phase change

materials (PV-PCM): technology overview and materials selection. Renew Sustain Energy Rev 2019;116:109406. doi:10.1016/j.rser.2019.109406.

[242] Material PC. savE ® - OM 35 n.d.

[243] González-Peña D, Alonso-deMiguel I, Díez-Mediavilla M, Alonso-Tristán C. Experimental analysis of a novel PV/T panel with PCM and heat pipes. Sustain 2020;12. doi:10.3390/su12051710.

[244] Pluss Polymers. Technical Data Sheet of Save ® OM35 PLUSS ® Encapsulation 2018:1–2.

[245] Liu WJ, Jiang H, Yu HQ. Emerging applications of biochar-based materials for energy storage and conversion. Energy Environ Sci 2019;12:1751–79. doi:10.1039/c9ee00206e.

[246] Thi Nguyen TH, Boets P, Lock K, Damanik Ambarita MN, Forio MAE, Sasha P, et al. Habitat suitability of the invasive water hyacinth and its relation to water quality and macroinvertebrate diversity in a tropical reservoir. Limnologica 2015;52:67–74. doi:10.1016/j.limno.2015.03.006.

[247] McVea C, Boyd CE. Effects of Waterhyacinth Cover on Water Chemistry, Phytoplankton, and Fish in Ponds1. J Environ Qual 1975;4:375. doi:10.2134/jeq1975.00472425000400030020x.

[248] Malik A. Environmental challenge vis a vis opportunity: The case of water hyacinth. Environ Int 2007;33:122–38. doi:10.1016/j.envint.2006.08.004.

[249] Pluss Advanced Technologies. TECHNICAL DATA SHEET – savE® OM 35. 2015.

[250] Namjoo A, Sarhaddi F, Sobhnamayan F, Alavi MA, Mahdavi Adeli M, Farahat S. Exergy performance analysis of solar photovoltaic thermal (PV/T) air collectors in terms of exergy losses. J Energy Inst 2011;84:132–45. doi:10.1179/174396711x12992532689177.

[251] Radziemska E. Performance analysis of a photovoltaic-thermal integrated system. Int J Photoenergy 2009;2009. doi:10.1155/2009/732093.

[252] Aberoumand S, Ghamari S, Shabani B. Energy and exergy analysis of a photovoltaic thermal (PV/T) system using nanofluids: An experimental study. Sol Energy 2018;165:167–77. doi:10.1016/j.solener.2018.03.028.

[253] Arslan E, Aktaş M, Can ÖF. Experimental and numerical investigation of a novel photovoltaic thermal (PV/T) collector with the energy and exergy analysis. J Clean Prod 2020;276. doi:10.1016/j.jclepro.2020.123255.

[254] Yousef MS, Hassan H. Energy payback time, exergoeconomic and enviroeconomic analyses of using thermal energy storage system with a solar desalination system: An

experimental study. J Clean Prod 2020;270:122082. doi:10.1016/j.jclepro.2020.122082.

[255] Gholampour M, Ameri M. Energy and Exergy Study of Effective Parameters on Performance of Photovoltaic/Thermal Natural Air Collectors. J Sol Energy Eng 2014;136:031001. doi:10.1115/1.4026250.

[256] Gupta N, Tiwari A, Tiwari GN. Exergy analysis of building integrated semitransparent photovoltaic thermal (BiSPVT) system. Eng Sci Technol an Int J 2017;20:41–50. doi:10.1016/j.jestch.2016.09.013.

[257] Macrotrends. India Inflation Rate 1960-2020 2020. https://www.macrotrends.net/countries/IND/india/inflation-rate-cpi (toegang verkry 11 Oktober 2020).

[258] Mittal ML. Estimates of Emissions from Coal Fired Thermal Power Plants in India. 2012 Int. Emiss. Invent. Conf. "Emission Invent. - Meet. Challenges Posed by Emerg. Glob. Natl. Reg. Local Air Qual. Issues, vol. 39, 2010, bl 1–22.

[259] Gaur A, Tiwari GN. Exergoeconomic and Enviroeconomic Analysis of Photovoltaic Modules of Different Solar Cells. J Sol Energy 2014;2014:1–8. doi:10.1155/2014/719424.

[260] Mantelli M, Yovanovicht M. 16 Thermal Contact Resistance. Spacecr. Therm. Control Handb. Vol. I Fundam. Technol., 2002, bl 599–638.

[261] Loveday DL, Taki AH. Convective heat transfer coefficients at a plane surface on a full-scale building facade. Int J Heat Mass Transf 1996;39:1729–42. doi:10.1016/0017-9310(95)00268-5.

[262] Eicker U. Solar Technologies for Buildings. John Wiley & Sons Inc.; 2003.

[263] Incropera FP, DeWitt DP, Bergman TL, Lavine AS. Introduction to Conduction. 2007. doi:10.1016/j.applthermaleng.2011.03.022.

[264] Incropera, Frank P. DPD. Fundamentals of heat and mass transfer. New York: J. Wiley; 2002.

[265] Balasubramanian G, Puri IK. Heat conduction across a solid-solid interface: Understanding nanoscale interfacial effects on thermal resistance. Appl Phys Lett 2011;99:97–100. doi:10.1063/1.3607477.

[266] Liu D, Zhang J. Numerical simulation of high-temperature thermal contact resistance and its reduction mechanism. PLoS One 2018;13:1–21. doi:10.1371/journal.pone.0194483.

[267] Rejeb O, Dhaou H, Jemni A. Parameters effect analysis of a photovoltaic thermal collector : Case study for climatic conditions of Monastir , Tunisia. Energy Convers

Manag 2015;89:409–19. doi:10.1016/j.enconman.2014.10.018.

[268] Barroso JCS, Barth N, Correia JPM, Ahzi S, Khaleel MA. Solar Energy Materials & Solar Cells A computational analysis of coupled thermal and electrical behavior of PV panels. Sol Energy Mater Sol Cells 2016;148:73–86. doi:10.1016/j.solmat.2015.09.004.

[269] Kant K, Shukla A, Sharma A, Biwole PH. Heat transfer studies of photovoltaic panel coupled with phase change material. Sol Energy 2016;140:151–61. doi:10.1016/j.solener.2016.11.006.

[270] Paper W. Solar P . V . Module Lamination Membranes 2016.

[271] Zheng J, Li Y, Wang L, Tan H. An improved thermal contact resistance model for pressed contacts and its application analysis of bonded joints. Cryogenics (Guildf) 2014;61:133–42. doi:10.1016/j.cryogenics.2013.11.002.

[272] Yovanovich MM, Culham JR, Teertstra P. Calculating interface resistance. Electron Cool 1997:1–9. doi:http://www.mhtlab.uwaterloo.ca/pdf_papers/mhtl97-4.pdf.

[273] Savija I., Culham J.R. YMM. Review of Thermal Conductance Models for Joints Incorporating Enhancement Materials. J Thermophys Heat Transf 2003;17:43–52. doi:https://doi.org/10.2514/2.6732.

[274] Yeh LT. Review of Heat Transfer Technologies in Electronic Equipment. J Electron Packag 1995;117:333. doi:10.1115/1.2792113.

[275] Mikic BB. Thermal contact conductance; theoretical considerations. Int J Heat Mass Transf 1974;17:205–14. doi:10.1016/0017-9310(74)90082-9.

[276] Lorenz A, Strauch T, Demant M, Fellmeth T, Barnes Hofmeister T, Linse M, et al. Impact of texture roughness on the front-side metallization of stencil-printed silicon solar cells. IEEE J Photovoltaics 2015;5:1237–44. doi:10.1109/JPHOTOV.2015.2416916.

[277] Antonetti VW, Whittle TD, Simons RE. An Approximate Thermal Contact V ^ ol. vol. 115. 1993.

[278] Yalçin L, Öztürk R. Performance comparison of c-Si, mc-Si and a-Si thin film PV by PVsyst simulation. J Optoelectron Adv Mater 2013;15:326–34. doi:10.1002/pip.

[279] Eitner U, Kajari-Schröder S, Köntges M, Altenbach H. Thermal Stress and Strain of Solar Cells in Photovoltaic Modules. Altenbach H., Eremeyev V. Shell-like Struct. Adv. Struct. Mater. vol 15. Springer, Berlin, Heidelb., Springer, Berlin, Heidelberg; 2011, bl 453–68. doi:10.1007/978-3-642-21855-2_29.

[280] Cooper PI, Christie EA, Dunkle R V. A method of measuring sky temperature. Sol Energy 1981;26:153–9. doi:10.1016/0038-092X(81)90079-7.

[281] Das D, Kalita P, Roy O. Flat plate hybrid photovoltaic- thermal (PV/T) system: A

review on design and development. Renew Sustain Energy Rev 2018;84:111–30. doi:10.1016/j.rser.2018.01.002.

[282] Dubey S, Sarvaiya JN, Seshadri B. Temperature dependent photovoltaic (PV) efficiency and its effect on PV production in the world - A review. Energy Procedia 2013;33:311–21. doi:10.1016/j.egypro.2013.05.072.

[283] Joy B, Philip J, Zachariah R. Investigations on serpentine tube type solar photovoltaic/thermal collector with different heat transfer fluids: Experiment and numerical analysis. Sol Energy 2016;140:12–20. doi:10.1016/j.solener.2016.10.045.

[284] Michael JJ, Selvarasan I, Goic R. Fabrication, experimental study and testing of a novel photovoltaic module for photovoltaic thermal applications. Renew Energy 2016;90:95–104. doi:10.1016/j.renene.2015.12.064.

[285] Jakhar S, Soni MS. Experimental and theoretical analysis of glazed tube-and-sheet photovoltaic/thermal system with earth water heat exchanger cooling. Energy Convers Manag 2017;153:576–88. doi:10.1016/j.enconman.2017.10.037.

[286] Bigorajski J, Chwieduk D. Analysis of a micro photovoltaic/thermal - PV/T system operation in moderate climate. Renew Energy 2018:1–10. doi:10.1016/j.renene.2018.01.116.

[287] Policy C, Health M, Care S, Services R, Approved D, Effective D. Resident Bathing and Safe Water Temperatures 2020.

[288] Muigai HH, Bordoloi U, Hussain R, Ravi K, Moholkar VS, Kalita P. A comparative study on synthesis and characterization of biochars derived from lignocellulosic biomass for their candidacy in agronomy and energy applications. Int J Energy Res 2020:1–17. doi:10.1002/er.6092.

[289] Lei H, Fu C, Zou Y, Guo S, Huo J. A thermal energy storage composite with sensing function and its thermal conductivity and thermal effusivity enhancement. J Mater Chem A 2019;7:6720–9. doi:10.1039/c8ta11753e.

[290] American Elements. Aluminum Powder 2020. https://www.americanelements.com/aluminum-powder-7429-90-5.

[291] Das D, Kalita P, Dewan A, Tanweer S. Development of a novel thermal model for a PV/T collector and its experimental analysis. Sol Energy 2019;188:631–43. doi:https://doi.org/10.1016/j.solener.2019.06.005.

APPENDICES

Appendix I

Equipment's used for the experimental study

List of equipment's used in the experimental study is presented in **Table I.1**. The instrument details and its application in the experimental setup is mentioned in the table.

Table I.1 Instruments used for data collection

Name of the instrument	Make and model	Parameter measured	Uncertainty	Position in the experimental setup
Pyranometer	Apogee Instruments, MP-100	Solar irradiance	± 5 W/m^2	Adjacent to the PV/T module with a tilt angle equal to that of the module.
Thermocouple and data acquisition (DAQ) system	Keysight 34970A data acquisition	Fluid inlet temperature Fluid outlet temperature PV/T surface temperature Absorber temperature Ambient temperature	± 0.75%	Fluid inlet, fluid outlet, PV/T top surface.
PV Analyzer I-V curve tracer	Solmetric, PVA-1000S	Maximum voltage Maximum current	± 0.5%	PV/T output.
Temperature gun	Testo 835-T2	Surface temperature	± 0.5%	---
Thermal imager	Testo 835-T2	Surface temperature profile		
Flowmeter	--	Flow rate	± 2.5%	Fluid inlet

Appendix II

Uncertainty analysis

Uncertainty of measurement is doubt about the validity of the result of a measurement. The uncertainty ε_R is calculated as a function of independent variables $X_1, X_2 ..... X_n$ while $\varepsilon_1, \varepsilon_2 ..... \varepsilon_n$ represents the uncertainty in the results. The uncertainty can be expressed as;

$$\varepsilon_R = \sqrt{\left(\frac{\partial R}{\partial X_1}\varepsilon_1\right)^2 + \left(\frac{\partial R}{\partial X_2}\varepsilon_2\right)^2 + ... + \left(\frac{\partial R}{\partial X_n}\varepsilon_n\right)^2}$$

In this work electrical, thermal, energy and exergy efficiencies have been calculated. These efficiency parameters are functions of various independent variables as mentioned in **Table II.1**.

Table II.1 Variables involved in performance parameters

Efficiency	**Variables involved**
Electrical	V_m, I_m, A_c, G
Thermal	$\dot{m}, T_{fi}, T_{fo}, A_c, G$
Energy	$V_m, I_m, \dot{m}, T_{fi}, T_{fo}, G, A_c$
Exergy	$V_m, I_m, \dot{m}, T_{fi}, T_{fo}, T_a G, A_c$

Appendix III

Experimental datasets

Selected climatic and system parameters measured during the experimental study at different stages of the study are presented in **Table III.1**. and **Table III.2**.

Table III.1 Experimental results for tube only vertical oscillating (M1) and sheet-tube vertical oscillating (M2) PV/T collectors

Date	Time	G (W/m²)	T_a (°C)	RH (%)	v_w (m/s)	T_{fi} (°C)	$T_{fo,M1}$ (°C)	$T_{fo,M2}$ (°C)	P_{M1} (W)	P_{M2} (W)	P_{PV} (W)
September 8, 2018	09:00	470	30.8	78	2.4	29.2	31.8	31.2	36.7	39	33
	09:30	505	31.5	76	2.4	29.5	32.5	32.1	40.2	42.8	37.5
	10:00	570	31.5	76	1.9	30.2	33.8	33	46	48.1	40
	10:30	680	32.1	75	2.7	31	35.5	34.5	55	58	46
	11:00	788	33.1	75	2.4	31.5	37.4	35.8	64	69	62
	11:30	870	33.6	72	1.8	32.3	39	37.8	71.2	74.3	66
	12:00	940	34.6	70	1.9	33.5	41	39.8	77.5	79.2	70
	12:30	911	34.8	69	2.9	33.8	40	39.9	69.68	74.16	65.1
	13:00	900	33.5	68	3.2	33.5	39.5	39.2	68.1	71	64.42
	13:30	780	33.4	67	4.4	33.4	38.5	38.2	59	63	51.8
	14:00	760	33.2	67	4.4	33.1	37.8	36.5	57	61	50
	14:30	655	33.2	65	3.9	32	36	34.8	50	52.1	46
	15:00	618	33	62	2.2	31.8	35	34	47	49	42
	15:30	520	31.8	63	2.8	31.3	33.6	32.8	39	41.2	35
	16:00	380	31.1	63	1.9	31	32.5	32	28	30	24.6
October 24, 2018	09:00	550	26.5	73	0.6	24.5	27.1	27	41	41.8	34
	09:30	612	27.5	72	0.3	24.5	27.7	27.5	46	47.9	39
	10:00	660	28	72	0.6	24.8	28.5	28.1	50	52.5	43
	10:30	685	29	69	0.4	24.4	29.5	29.2	54	55	45
	11:00	900	29.9	68	0.8	27.5	33.8	33.5	64	67.8	58
	11:30	924	30.2	66	1	30.1	37	35.8	70	73	62
	12:00	890	30.5	66	1	30.5	37.5	37	69	71.2	60.5
	12:30	870	31	65	1	31.9	38	37.5	66.7	69.4	60
	13:00	801	31.1	63	1	34	39.5	38.2	63	64.5	55
	13:30	740	32	61	1	35.7	40.5	39.1	55	59	50
	14:00	678	31.8	59	0.7	35.1	39.2	38.2	51	54	45
	14:30	524	31.7	56	1.3	33.6	36.6	35.9	40.5	41.6	33
	15:00	430	21	56	1.5	32.5	34.5	34	32.5	34	28
	15:30	255	30.8	59	1	31.1	32.2	32	19	20	16
	16:00	120	30.5	62	0.9	31	31.5	31.4	8	8.1	7.5

October 26. 2018	09:00	645	27.5	74	1.4	24.8	28	27.6	44	45.5	40.8
	09:30	766	28	73	1.1	24.6	28.5	29.6	52	53.5	49.2
	10:00	890	28	72	0.9	26.5	31.2	30	66.53	68.7	61
	10:30	910	28.3	72	1.7	27.1	32.5	31	68.6	70	61.8
	11:00	930	28.7	71	2	27.5	34.1	33	71.15	72	63.5
	11:30	950	29.2	67	1.8	28.5	35.6	34.5	73.1	75.2	64.1
	12:00	930	29.4	62	2.1	30.15	37.4	36	72	73.8	66
	12:30	890	30.3	61	2.4	31.7	38.2	37.5	70	71.8	64
	13:00	840	31.1	57	2.6	34	40	39.6	65.2	67	58.1
	13:30	760	31.5	55	2.3	35.6	40.8	40	57	59.3	52.7
	14:00	650	31.7	55	2.6	36.34	40.5	39.8	48.6	50.2	45.1
	14:30	540	32	56	2.4	34.62	38	37.6	40.8	42.5	38.1
	15:00	390	31.8	56	2.7	33.4	35.7	35.5	29	30.36	27.6
	15:30	285	31.8	56	2.5	33	34.6	34	21.1	22	20.1
	16:00	130	31.6	57	2.5	31.2	31.8	31.5	9	9.6	8.5
October 30, 2018	09:00	672	26.7	77	0.7	24.2	27.2	27	51.6	53	44
	09:30	855	27	76	0.8	25	30	29.5	64.5	66	57
	10:00	905	27.3	77	1.6	25.9	32.1	32	68.8	71.5	60.6
	10:30	920	28.3	74	1.7	26	33	32.2	69.52	72.3	62
	11:00	922	28.5	70	1.1	26.37	34	32.3	72.1	74.57	65.5
	11:30	943	29.3	65	2	28.1	35.5	34.5	73.6	75.1	67
	12:00	905	30.8	63	1.6	31.2	37.5	36.5	69	71	64
	12:30	900	31	62	1.8	33.5	39.5	38.9	66.2	69	59.8
	13:00	850	32.1	59	2.7	33.4	40	38.5	63.8	66	55.9
	13:30	780	32.5	59	2.7	35.1	39.5	38.5	57	58.7	51.1
	14:00	635	31.4	58	1.9	34.2	38	37	48.7	50	44.5
	14:30	567	31.2	57	1.9	32.6	35.5	34.6	39.6	42	35.5
	15:00	410	31.1	56	2	32.2	34.4	33.5	31.1	32	27
	15:30	270	30.9	59	1.6	31.9	33.1	32.8	20.1	21	17.7
	16:00	165	29.9	60	2.3	31.5	32.2	32	12	12.5	11
November 24, 2018	09:00	250	25.8	69	0.6	25	26.4	26.1	19	19.1	15.5
	09:30	320	26.4	69	0.3	25.1	27	26.6	26	27.5	21
	10:00	383	27	67	0.6	25.3	27.9	27.2	31.8	33	26
	10:30	448	27.6	66	0.4	25.5	28.7	27.8	37.2	38.5	31
	11:00	550	28.5	65	0.8	26	30	29	47	48.1	40
	11:30	638	29	65	1	26.1	30.8	29.8	57	58.5	47
	12:00	615	28.8	63	1	27	31.5	30.5	54	56	42
	12:30	601	28.5	62	1	27.2	31	30.2	51.5	53	41
	13:00	583	28.4	61	1.1	27.2	30.7	30	48	50.2	39
	13:30	512	28.1	61	0.7	27.5	30.5	29.8	44	44.5	33.5
	14:00	483	27.9	60	1.3	27.1	29.8	29.2	40.5	41.8	33
	14:30	433	27.9	56	1.5	27	29.2	28.5	36	37.2	29
	15:00	385	27.5	57	1	26.8	28.6	28	32	32.6	25
	15:30	240	27.2	59	0.9	26.5	27.5	27.4	18.7	19	16
	16:00	109	26	59	0.6	26	26.3	26.3	8.2	8.5	7

December 25, 2018	09:00	121	20.8	68	0	20	20.6	20.5	9.2	10.2	9
	09:30	144	21.2	68	0	20.5	21.3	21	12	12.5	11
	10:00	193	21.8	67	0.1	21	22.1	21.9	16.5	16.8	15
	10:30	427	23	67	0.3	21.6	24.1	23.8	36.6	37.8	33.8
	11:00	440	23.3	66	0.2	22.5	25.5	25.1	38	40	35
	11:30	460	24.1	65	0.7	22.8	26.2	25.5	40.5	42	37
	12:00	455	24.5	62	1.2	23	26	25.6	40	41.5	36
	12:30	444	24.9	59	1.4	23.1	26.1	25.4	38.5	39.6	34.5
	13:00	416	25.1	58	1.4	23.5	26.2	25.6	36	37	32
	13:30	370	25.2	57	1	23.5	25.8	25.4	32	32.5	28
	14:00	326	25.5	59	2	24.1	26	25.5	27.5	28	24.5
	14:30	261	24.2	60	1.5	22.2	23.5	23.2	22.2	22.4	19.4
	15:00	179	24	61	1.5	21.5	22.5	22	15	15.3	13
	15:30	95	23.8	61	1.1	21	21.4	21.2	7.6	7.5	6.8
	16:00	62	23.5	62	0.5	20.8	21	20.9	4.5	4.8	4.4

Table III.2 Experimental results for tube only rectangular spiral (M3) and horizontal oscillating (M4) transparent PV/T collectors

Date	Time	G	T_a (^oC)	v_w (m/s)	T_{fi} (^oC)	$T_{fo,M1}$ (^oC)	$T_{fo,M2}$ (^oC)	P_{M1} (W)	P_{M2} (W)	P_{PV} (W)
October 11, 2019	09:00	828	27.6	1.3	29.2	33.5	34.2	61.2	57.2	54
	09:30	885	28.9	1	29.5	35.1	36.2	67.3	61.5	56.2
	10:00	923	29.1	1.5	30.2	35.8	36.77	72.56	67	63
	10:30	926	29.9	1.3	31	36.1	37.8	78.47	74.2	67.56
	11:00	942	29.6	2	31.5	37.2	37.5	81.2	76	70.03
	11:30	979	29.8	2.2	32.3	39.3	41.3	83.28	78.1	71.88
	12:00	967	30.5	2	33.5	40.5	41.6	79.52	75.8	68.8
	12:30	916	30.6	1.2	33.8	42	42.1	74.81	70.84	66.27
	13:00	866	30.6	2.4	33.5	40.5	41.6	73.49	70.4	66.1
	13:30	836	31	1.1	33.4	38.9	39.6	68.06	64.9	60.06
	14:00	796	31.2	0.5	33.1	36.8	38.1	56.88	53.54	50
	14:30	772	31	1.7	32	36.2	37.1	56.88	50.1	40.26
	15:00	715	30.5	3.1	31.8	34.8	35.5	44.37	40.1	39.1
	15:30	621	30.1	2.4	31.3	33.9	34.33	42.9	39.2	35.1
	16:00	527	30	2.1	31	32.7	33	36.2	34.5	31
October 14, 2019	09:00	772	28.4	1	24.5	31.6	32.1	61.1	57.7	55.68
	09:30	899	29.5	0.8	24.5	32.42	34.17	70.76	64.14	60.16
	10:00	923	30.3	0.7	24.8	35.86	38.17	72.66	69.5	63.68
	10:30	943	31.3	0.9	24.4	36.15	37.6	75.22	71.08	65.78
	11:00	964	31.7	1.4	27.5	40.46	41.8	77.1	73.83	67.15
	11:30	975	31.8	2	30.1	40.9	42	75.32	72.66	66.25
	12:00	974	32	2.9	30.5	42.5	42.8	71.56	72.38	63

12:30	947	32.6	1.8	31.9	42.66	43.1	70.8	68.07	62.3
13:00	772	32.8	2.2	34	41	41.4	62	60	59.7
13:30	768	33.5	2	35.7	39	39.17	60.5	59	57.02
14:00	763	32.8	1.5	35.1	38.2	38.6	58	55.7	54
14:30	747	31	2.3	33.6	37.1	37.44	55.2	52.6	48.07
15:00	62	30.5	2	32.5	35.4	36	45.5	42.8	42.33
15:30	617	30.2	1.6	31.1	34.1	34.4	36.7	34.1	33.1
16:00	489	30	1.4	31	32.5	32.7	29	27	24

Appendix IV

Photographs of experimental setup

This section presents few selected photographs of the experimental setups. **Figures IV.1, IV.2, IV.3 and IV.4** show outdoor experimental setup, pyranometer installation, developed indoor testing facility and PV/T collector with novel PCM-biochar composite.

Figure IV.1. Outdoor experimental setup

Figure IV.2. Pyranometer

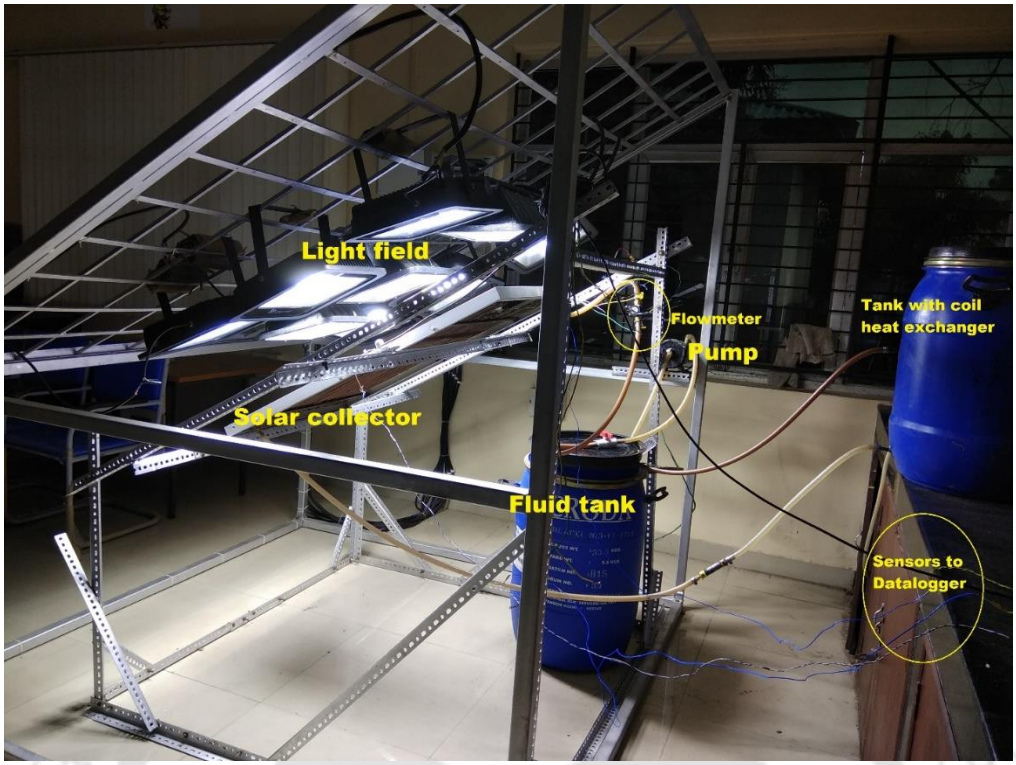

Figure IV.3. Indoor collector testing facility

Figure IV.4. PV/T collector with novel PCM-biochar composite

List of publications and awards

Journals

1. **Das, D.,** Bordoloi, U., Muigai, H., Kamble, A.D., Kalita, P. Performance investigation of a rectangular spiral flow PV/T collector with a novel form stable composite material, ***Applied Thermal Engineering***, 182, 116035, 2021. (https://doi.org/10.1016/j.applthermaleng.2020.116035)
2. **Das, D**., Kamble, A.D., Kalita, P. Outdoor experimental investigation of transparent PV/T's with horizontal oscillating and rectangular spiral tube only absorbers, ***International Journal of Energy Research***, 2020. (https://doi.org/10.1002/er.6298)
3. **Das, D**., Bordoloi, U., Muigai, H., Kalita, P. A novel form stable PCM based bio composite material for solar thermal energy storage applications, ***Journal of Energy Storage***, 30, 101403, 2020. (https://doi.org/10.1016/j.est.2020.101403)
4. **Das, D**., Kalita, P. Experimental analysis of photovoltaic-thermal collectors with closely spaced tubes, ***Energy Sources, Part A: Recovery, Utilization, and Environmental Effects***, 2020. (https://doi.org/10.1080/15567036.2020.1814904)
5. **Das, D.,** Kalita, P., Dewan, A., Tanweer, S. Development of a novel thermal model for a PV/T collector and its experimental analysis, ***Solar Energy***, 188, 631-643, 2019. (https://doi.org/10.1016/j.solener.2019.06.005)
6. **Das, D.,** Kalita, P., Roy, O. Flat plate hybrid photovoltaic- thermal (PV/T) system: A review on design and development, ***Renewable and Sustainable Energy Reviews***, 84, 111-130, 2018. (https://doi.org/10.1016/j.rser.2018.01.002)
7. **Das, D.,** Bordoloi, U., Kalita, P., Boehm, R., Kamble, A.D. Solar still distillate enhancement techniques and recent developments, ***Groundwater for Sustainable Development,*** 10, 100360, 2020. (https://doi.org/10.1016/j.gsd.2020.100360)
8. Kalita, P., Das, S., **Das, D.,** Bor Gohain, P., Dewan, A. Feasibility study of MW level grid connected solar photovoltaic power plant installation for northeastern region of India, ***Sadhana,*** 44,9,1-24, 2019. (https://doi.org/10.1007/s12046-019-1192-z)

9. **Das, D**., Bordoloi, U., Muigai, H., Das, S., Kalita, P., Bora, P., Kashyap, D. Preparation and characterization of form-stable phase change green composites with biochar as supporting matrix for thermal management of PV/T, *In preparation*.

Book chapters

1. **Das, D.,** Kalita, P. Performance improvement of a novel flat plate photovoltaic thermal (PV/T) system using copper oxide nanoparticle- water as coolant, ***Nanotechnology for Energy and Water, Springer Proceedings in Energy,*** 97-104, 2018. (https://doi.org/10.1007/978-3-319-63085-4_14)
2. **Das, D.,** Kalita, P. Feasibility Study of Photovoltaic-Thermal (PV/T), Collector in Assam (India) Using Polysun, ***Advances in Mechanical Engineering, Springer***, 1331-1337, 2020. (https://doi.org/10.1007/978-981-15-0124-1_117)

Conferences

1. **Das, D.,** Kalita, P., Kamble, A.D. Experimental study and performance evaluation of PV/T's with novel absorber designs, ***International Conference on Sustainable Energy and Green Technology 2019 (SEGT 2019),*** Bangkok, Thailand, 11-14 December, 2019.
2. **Das, D.,** Kalita, P., Experimental evaluation of a rectangular spiral tube only PV/T collector, ***International Conference on Future Aspects of Sustainable Technology (FAST 2019),*** Central Institute of Kokrajhar, 11-12 November 2019.
3. **Das, D.,** Kalita, P. Experimental evaluation of tube PV/T collector, ***12th International Conference on Sustainable Energy & Environmental Protection (SEEP 2019),*** University of Sharjah, UAE, 18 - 21 August, 2019.
4. **Das, D.,** Kalita, P. Development of a tube and sheet type PV/T collector: Experimental study and performance evaluation**,** ***National Conference on Waste to Energy 2018***, National Institute of Technology Mizoram, 28-29 December 2018.

Awards and achievements

1. **Best paper award,** ***International Conference on Sustainable Energy and Green Technology 2019 (SEGT 2019),*** Bangkok, Thailand, 11-14 December, 2019.
2. Completed ***Bhaskara Adavanced Solar Energy (BASE) Fellowship*** sponsored by Dept. of Science and Technology, Govt. of India (DST) and Indo-US Science and Technology Forum (IUSSTF), 2019.
3. **Best Poster Award** at ***Research Conclave 2017***, IIT Guwahati.